Author:
Sheldon, Derek F

Title:
A study of the stability of a plate-like load towed beneath a helicopter

UNIVERSITY OF BRISTOL

DEPARTMENT OF AERONAUTICAL ENGINEERING

A STUDY OF THE STABILITY OF A PLATE-LIKE LOAD TOWED BENEATH A HELICOPTER

by

Derek F. Sheldon, Dip.Tech.(Eng.), Grad. R.Ae.S.
Grad. I.Mech.E.

A Thesis submitted for the Degree of Doctor of Philosophy in the Faculty of Engineering of the University of Bristol

March 1968

MEMORANDUM

This research entitled "A study of the stability of a plate-like load towed beneath a helicopter" was carried out in the Department of Aeronautical Engineering at the University of Bristol from October 1964 to September 1967. Supervision was by Dr. A. Simpson, Lecturer in Aeronautical Engineering at the University of Bristol.

This dissertation has not previously been submitted, in part or in whole, for a degree or diploma, of any other University or examining body. All the work described herein, except where stated otherwise, is that of the author.

Derek F. Sheldon

D.F. Sheldon

CONTENTS

PREFACE

Recent experience has shown that a plate-type load, suspended by a single cable beneath a helicopter moving in horizontal flight, has unstable characteristics in a large regime of forward speeds. These findings have prompted a theoretical analysis with a view to obtaining a stable system. Investigations are made into the original single upper cable suspension arrangement of the plate, together with two different forms of bifilar suspension, namely, (a) a twin strop arrangement and (b) a trapezoidal arrangement.

Although the problem is strictly non-linear, the well known 'small perturbation' theory is adopted to obtain 'linearised' equations of motion. These equations are then found to be separable into symmetric and antisymmetric forms for the three arrangements investigated.

The aerodynamic derivative data required for these equations are derived, whenever possible, for the appropriate ranges of Strouhal and Reynolds' numbers. For the majority of derivatives, there is a paucity of available information and experimental static and dynamic wind tunnel techniques are therefore used to obtain certain terms. In addition, 'lifting line' theory is adopted for the remaining derivative

terms. As an aid to representing this derivative information, a curve fitting method is used to facilitate their use in the stability investigations.

Stability equations (with the complete aerodynamic derivative information) for the three systems are set up and solved on a digital computer, to give a direct indication of a stable or unstable system for a variety of physical parameters. Furthermore, the modal forms corresponding to each mode of oscillation are obtained, together with an estimation of the important derivative terms pertaining to each mode.

The adoption of either bifilar suspension would appear to confer stability on certain modes, which were found to be unstable with the single cable arrangement. Indeed, the trapezoidal suspension arrangement of a plate-like load is found to be stable at all practical forward speeds of the helicopter.

ACKNOWLEDGEMENTS

The author would like to express his appreciation to the following:-

Dr. Alan Simpson for his excellent supervision and enthusiasm throughout the period of the research.

Mr. R. Austin of Westland Aircraft Ltd for his help and continued interest.

The Science Research Council who have financially supported this research.

Miss Eileen Watkins for her assistance with the immense amount of computer programming.

Mr. T. Everett, to whom I am greatly indebted for the time spent on computer operating.

Mr. T.M. Cook and the workshop staff of the Aeronautical Engineering Workshops for the ideas and varying skills which were so willingly given.

Miss Molly Gibbs and Mrs. Pam Packham who have shown patience, understanding and skill in the typing of this thesis.

My fellow postgraduates for their suggestions and criticisms throughout this work.

My wife, Shirley, for her continued encouragement and quiet endurance.

LIST OF SYMBOLS

x, y, z	Co-ordinates of body axis system (right handed) with the origin set at the centre of gravity of the body.
m_1	Mass of lifting hook or bar, slugs.
m_2	Mass of pallet, slugs.
d_1	Length of upper attachment strops, ft.
d_2	Normal length between the pallet and lifting bar centres of gravity for the single and twin strop configurations. Also strop length for trapezoidal configuration, ft.
d_3	Length of lower strop of trapezoidal configuration.
$2a$	Length of lifting bar, ft.
S	Area of pallet, ft^2.
c	Chord of pallet, ft.
$2b$	Span of pallet, ft.
d	Thickness of pallet, ft.
Θ, Φ	Steady state strop angles w.r.t. vertical, rads.
x_1, y_1, z_1	Incremental displacements of the lifting hook or bar, ft.
x_2, y_2, z_2	Incremental displacements of the pallet, ft.
$\theta_1, \bar{\theta}_1, \phi_1, \psi_1, \eta$	Incremental rotations of the lifting bar, rads.
$\theta_2, \bar{\theta}_2, \phi_2, \psi_2, \xi, \nu$	Incremental rotations of the pallet, rads.

α_1, α_2	Steady state angles of the upper and lower strop arrangements w.r.t. vertical, rads.
u, v, w	Linear incremental velocity components along body axes, ft/sec.
p, q, r	Angular incremental velocity components along body axes, ft/sec.
V	Forward horizontal velocity of the helicopter and pallet, ft/sec.
$\underline{U}$, $\underline{V}$, $\underline{W}$	Body axis steady state components of V for the pallet and lifting bar, ft/sec.
$\underset{\sim}{V}$	Potential Energy, ft. lbs.
X, Y, Z	Aerodynamic forces, lbs.
L, M, N	Aerodynamic moments, lb.ft.
$\bar{A}$, $\bar{B}$, $\bar{C}$	Moments of inertia of the pallet and lifting hook about body axes, slugs ft^2.
$\bar{D}$, $\bar{E}$, $\bar{F}$	Products of inertia of the pallet and lifting hook about body axes, slugs ft^2.
ΔX, ΔM, ΔN	Incremental changes due to gravitational and steady state forces and moments.
$\Delta\tilde{X}$, $\Delta\tilde{M}$, $\Delta\tilde{N}$	Incremental changes due to a change in the aerodynamic forces and moments.
∇X, ∇Z, ∇M	Incremental changes in forces and moments used in the displacement method.
T_a, T_b, T_c, T_d	Steady state forces in the strops.
∇T_a, ∇T_b, ∇T_c, ∇T_d	Incremental changes in the above strop forces.
X_θ, Z_θ, M_θ Y_ϕ, L_ψ, N_ϕ	Dimensional aerodynamic stiffness derivatives

X_u, Z_w, M_q
Y_v, L_r, N_p — Dimensional aerodynamic damping derivatives.

C_L, C_D — Lift and Drag coefficients i.e. $\frac{\text{Drag force}}{\frac{1}{2}\rho V^2 S}$

x_θ, z_θ, m_θ
y_ϕ, l_ψ, n_ϕ — Non-dimensional stiffness derivatives

i.e. $x_\theta = \frac{X_\theta}{\frac{1}{2}\rho V^2 S}$ $\quad m_\theta = \frac{M_\theta}{\frac{1}{2}\rho V^2 Sc}$

$y_\phi = \frac{Y_\phi}{\frac{1}{2}\rho V^2 S}$ $\quad l_\psi = \frac{L_\psi}{\rho V^2 Sb}$

x_u, z_w, m_q
y_v, l_r, n_p — Non-dimensional damping derivatives

i.e. $x_u = \frac{X_u}{\rho V S}$, $m_q = \frac{M_q}{\rho V S c^2}$, $y_v = \frac{Y_v}{\rho V S}$, $n_p = \frac{N_p}{4\rho V S b^2}$

t — Time, secs.

τ — Non-dimensional time.

μ_1 — Relative density parameter.

F — Froude number.

R — Reynolds' number.

ρ — Air density.

λ — Root of a polynomial equation.

r_1, r_2, r_3 — Non-dimensional damping factor.

s_1, s_2, s_3 — Non-dimensional frequency parameter.

Vcrit — Forward velocity when r_1 or r_2 or $r_3 = 0$.

Subscripts

1 and 2 — Refer to the lifting bar and pallet respectively.

S — Longitudinal (symmetric) analyses.

A — Lateral (anti-symmetric) analyses.

CHAPTER I

INTRODUCTION

1.1 Background

In the last twenty years a number of philosophies on air transport have gradually evolved. One concept that has emerged is the desirability of the use of the helicopter for military and civilian roles to which it is peculiarly suited. This is apparent from the increase in military undertakings alone. For example, in Vietnam the helicopter has become an important integral part of the fighting operations. The tasks performed by this machine include combatant duties, the transport of troops, artillery, tanks and trucks, together with medical evacuation, reconnaissance, courier services, guard duty and supply services for ships at sea. Such is the importance of the helicopter that between 1961 and 1965, United States helicopters made over one million sorties, which included the transportation of more than 84 million pounds of cargo and more than 1·5 million troops. Furthermore, by the year 1968, it is estimated that more than 7,000 machines will be in use in Vietnam. Similar trends are very apparent on a smaller scale in the British, French and German armed forces.

Civilian operations, in comparison, are still on a small, but increasing scale. Because of its versatility, the helicopter is used in a number of important peaceful ways, only a few of which we have space to mention. A valuable commercial use of the helicopter is the transportation of equipment and workers to remote jungle or mountain areas (and less rugged locations), which would either take months to reach or are completely inaccessible by other means. For example, a Canadian company, Okanagan Helicopters Ltd, operate a fleet of 60 machines which are used to convey prefabricated buildings and powerline towers and are also employed in the laying of electrical transmission cables. Nearer home, the helicopter has been used in the construction of the prefabricated spire on Coventry Cathedral and has proved to be invaluable in large scale agricultural organisations (using the advantage of rotor downwash effects) to carry out crop spraying, dusting and seeding. Quite recently helicopters have been used, both by police and motoring organisations, on the reconnaissance of main roads where traffic jams are likely. The motorists can then be advised promptly of alternative routes.

The use of the helicopter in the transportation of passengers has, however, not proved to be a very worthwhile economic proposition, either in the U.S.A. or Britain. As

a result there are only two regular helicopter services in this country, one of which is the B.E.A. route between Penzance and the Scilly Isles (which has to be subsidised) and the other is the Westland Heliport in London.

In addition to the above tasks, one unusual but serious case came to the attention of the author quite recently. This concerned the use of a helicopter for the singular purpose of carrying a coffin (containing the body of an American governess) from Lahinch, Co. Clare, to the island of Inishmann. After a few minutes in the air, the suspended coffin had to be jettisoned into the sea because it began to swing (in a lateral sense) quite violently beneath the fuselage. This particular illustration does, in fact, have quite a bearing on the work investigated here, as will be discussed later.

In the present work particular interest is shown in the transportation of cargo as a practical and economic proposition for both military and commercial operations. At the present time, three basic methods of load carrying are in existence:-

i) Using the conventional helicopter internally loaded.

ii) Using a special crane helicopter.

iii) Using the conventional helicopter with the load suspended beneath the fuselage.

The first method is usually found to be adequate only when the cargo is small, both in quantity and size and/or when the loading and unloading time is considered to be unimportant. With the field of work of the helicopter continually increasing, this unfortunately places a severe limitation on the versatility of the conventional machine. Therefore, other methods of transportation are desired for the bulky loads and where the improvement on 'turn-round' time is extremely important.

In the U.S.A. and U.S.S.R. in particular, the above problem has been solved by developing a special crane helicopter (see ref. 8.2) in which the conventional fuselage is replaced by a rigid frame. This frame is so designed that it will rigidly support a pallet on which bulky cargo (e.g. a bus) can be safely mounted. If, therefore, the pallet can be pre-loaded with cargo whilst on the ground, it is quite an easy matter to land the helicopter, lock the pallet to the loaded frame and become airborne in a few minutes. Whilst these helicopters are familiar in the U.S.A. and U.S.S.R. for special operations, the vast percentage of machines used throughout the world are of the usual conventional type. Hence, for the latter type of machine, bulky cargo must be carried externally, suspended with the aid of a cable (strop) from the helicopter.

As with the crane helicopter, the external loading of conventional helicopters has one distinct advantage over internal carriage. The loading and unloading times of the former are clearly much smaller because the load can be winched to the ground and unhooked, without the necessity of landing the helicopter. This could possibly reduce the turn-round time from, say, 30 to 3 minutes, and would not necessitate the use of much handling equipment. Therefore more flying time would be available and what is at present an unprofitable operation could be transformed into a profitable mission. Because many types of cargo would be most conveniently transported on a pallet (in the form of a flat plate) suspended by cables (strops) from a helicopter, this form of transportation is investigated further in this work.

Westland Aircraft developed a great interest in this new field of freight transportation and carried out a series of full scale tests on the single strop suspension (see fig. 3.1) of an unloaded pallet. (At this stage it must be appreciated that the profile and weight of the freight on the pallet vary considerably. Thus the initial full scale dynamic stability investigations were made with the unloaded pallet). It appears in practice that the recommended size of pallet should be in the order of 12 ft. span, 6 ft. chord, 3 inches

depth and a weight of 150 lbs. (as laid down by the armed services). Also, it was considered necessary to suspend the pallet at least 50 ft. below the helicopter in order that rotor downwash effects were not a potential source of instability. Hence, with the system as described above, full scale tests were carried out and rather alarming results were obtained. These showed the pallet to be consistently unstable at speeds of horizontal flight between five and sixty knots. Invariably the pallet diverged very quickly into a combined longitudinal-lateral motion and was jettisoned before the helicopter became uncontrollable. (Similar tests were also carried out on a single strop suspension of a rectangular box-shaped load and these resulted in laterally unstable motions. Presumably this was the type of instability experienced by the suspended coffin).

With the instability developing so rapidly, it proved to be impossible to formulate any reasonable conclusions as to why the pallet was unstable. It was therefore necessary to resort to wind tunnel tests on a suspended model plate. These are fully discussed in Chapter 11, together with similar preliminary work carried out by the author. For reasons given in this Chapter, it is shown that the wind tunnel tests are not truly representative of the full scale tests and the results have only a very limited applicability.

Except for carrying out more expensive full scale tests on the suspended pallet (in the hope that the variations of certain physical parameters would furnish a stable system), it was apparent that the only alternative was to pursue an analytical course aimed at the study of the dynamic stability of the helicopter and suspended pallet.

1.2 The Formulation of the Problem

The majority of work carried out by the author has centred on the analytical investigation of the pallet stability only. This is because it became apparent, after a brief consideration of the problem, that the analysis of the pallet suspension system would, in itself, prove extremely lengthy. Therefore, the additional helicopter stability considerations would clearly make the analysis unmanageable - at least for a first treatment.

The aspects of the current problem are later shown to render it unique, although this analytical investigation is not the first in the field of towed bodies. For example, in 1915, Bairstow, Relf and Jones (ref. 1.1) carried out a 'linearised' mathematical investigation to ascertain the dynamic stability of captive observation balloons. Unfortunately, immense computational difficulties thwarted their efforts and a practical use has not been found for this work in its original form.

A great deal of analytical work has been carried out since then for the general case of a body towed by a single wire. This is in connection with the towing of radio aerials, aerodynamic instruments, kites and gliders used in military activities (see refs. 1.2 .... 1.7). On a more recent commercial basis, lateral investigations have been made on the suspension of a bomb-shaped bucket towed by a helicopter (ref. 1.6) and, in addition to this, two very recent reports (refs. 1.9 and 1.10) have again considered the general case in a similar manner to Glauert (ref. 1.3). In all cases it has been necessary to resort to an analytical scheme, following broadly the lines of G.H. Bryan's 'linearised' approach to aeroplane stability work. Certain of the reports make sensible assumptions, such that the action of the wind on the cable(s) or the weight of the cables are ignored, and in all cases the cables are assumed to hold the same form in the disturbed and steady state positions.

Although these reports have proved useful whilst becoming acquainted with the problem considered here, their results and conclusions are completely inadequate for the present purposes. This is because the towed bodies are either aerodynamically non-lifting and intrinsically more stable than the pallet (e.g. a glider), or because their physical dimensions cannot be compared with those of the pallet (e.g.

kites - box type). Hence, a unique analytical investigation into the stability of a suspended pallet is warranted.

So far very little has been mentioned about the physical arrangement of the subject under investigation. Clearly the pallet can be suspended from the helicopter by various strop arrangements and in addition could be flying under normal conditions with, for example, gusts prevalent and rotor down-wash impinging on the pallet in a yawed position. A theoretical investigation would then be virtually unmanageable. Hence, for the investigations made here, it is necessary to limit the scope of the analyses. This is achieved by assuming the pallet to be towed in a horizontal forward flight path whilst in a position of equilibrium. Also, because the pallet could assume an infinite number of shapes, it is necessary to consider a pallet of similar form to that used in the full scale tests, i.e. a flat rectangular pallet (or plate) having square edges and a 12 ft. span, 6 ft. chord and 3 inch thick-ness. The pallet is considered to hang from a lifting hook or bar by means of four strops attached to the corners of the pallet and finally the lifting hook or bar is connected to the fuselage of the helicopter by one or two upper strops.

Strictly speaking, the rotor downwash effects should be considered in the stability investigations, as these could have a direct effect on the pallet stability. However, for

reasons given in Chapter 8, these are ignored in the present investigations.

Two distinct analytical approaches to the problem are possible: i) To study more fully the mechanism of the instability encountered with the single strop configuration, or ii) To investigate the practicability of other suspension arrangements with a view to obtaining a 'flight envelope' if a reasonably stable configuration can be found. A compromise between these two lines of approach has been adopted, however, and stability investigations are initially carried out for the single strop arrangement (see fig. 3.1) of the pallet. In the light of the instabilities encountered with this arrangement (according to the analysis), further investigations are then made into two alternative suspension arrangements. These are the twin strop (bifilar) and trapezoidal strop arrangements (figs. 3.2 and 3.3). Both configurations replace the hook and upper strop of the single strop system with a lifting bar and two equal length strops respectively. Clearly, these are considered in the hope that the instabilities of the single strop system can be alleviated.

It could be argued that the addition of aerodynamic devices to the pallet might prove to be a better proposition for obtaining a stable system, but from practical considerations, this would over-complicate the shape of the pallet.

The theoretical investigations of the three systems mentioned above are described in Chapter 2. Here a system of moving axes is employed and a resultant set of governing equations is derived, based on Newtonian Laws of motion. The procedure is essentially similar to that used in aircraft stability work. The equations of motion are, of course, 'linearised' using the classical 'small perturbation' theory (refs. 1.1 - 1.10 for aircraft work) and only the incipient instability is considered here. The 'linearised' equations are further extended to a general form in Chapter 3 (applicable to the three strop configurations) and are shown to be separable into longitudinal and lateral form. In all cases the aerodynamic data are assumed to be expressible in a linear static and dynamic aerodynamic derivative form.

In Chapters 4 and 5, the longitudinal and lateral equations for the three strop configurations are developed in a non-dimensional form suitable for general solution.

The above final sets of equations are assumed to have exponential forms of solution and in Chapter 6 the various stability investigations are discussed. These include the solution of quartic and sextic polynomial equations for the longitudinal and lateral equations respectively. In addition to this, the modal forms pertaining to each root are obtained, together with an approximate estimation of the important

aerodynamic derivatives (for each mode of oscillation) appearing in the theory.

A detailed discussion of the aerodynamic derivatives is given in Chapter 7. As is usual for stability investigations in aeronautical engineering, the derivation of the derivative data proves here to be the stumbling block to progress because of the scarcity of information on low aspect ratio rectangular flat plates, or wings. This is overcome by sensibly ignoring certain derivatives, whilst the remaining terms, required for the longitudinal and lateral analyses, are determined both by theoretical (i.e. lifting line theory) and experimental (static and dynamic) techniques.

As a continuation of the study of the aerodynamic effects on the pallet, it is necessary to discuss briefly the rotor downwash effects, since these have been ignored in the present investigations. An appraisal of the importance of these effects is given in Chapter 8.

Further to the discussions of Chapter 7 on the stability derivatives, Chapter 9 discusses the extensive experimental wind tunnel work carried out (on an aspect ratio 2 flat plate) to obtain the aerodynamic derivative data. Similarly, Chapter 10 comprises discussions of further wind tunnel tests to obtain certain important dynamic stability derivatives which cannot be estimated with confidence by theoretical methods.

Because the majority of previous investigations on the suspended pallet have been in the form of model tests in a wind tunnel, Chapter 11 is devoted to a brief discussion of the merits of these tests, in addition to the preliminary tests carried out by the author.

In conclusion, Chapter 12 covers the experimental static and dynamic wind tunnel results pertaining to the derivative data, whilst Chapter 13 consists of the results obtained from the stability investigations on the three strop configurations. Chapter 14 comments on the results obtained and, finally, Chapter 15 discusses further extensions to the work investigated here.

CHAPTER 2

FORMATION OF THE GOVERNING EQUATIONS

From full scale and wind tunnel investigations into the stability of a suspended pallet beneath a helicopter, it is found that either the pallet becomes unstable so rapidly such that the destabilising forces cannot be observed, or else the tunnel tests give an inadequate representation of full scale conditions (see chapter 11). Analytical methods are therefore resorted to in order to investigate the stability of three different suspension arrangements of the pallet; namely, the single, twin and trapezoidal configurations (see fig. 3.1, 3.2, 3.3). Although it is known from full scale tests that the single strop arrangement is unstable, it is hoped that progress will be made towards obtaining a stable system with the latter two configurations.

The investigation of the stability of the helicopter and the suspended pallet requires the setting up of equations (similar to aircraft stability equations given in reference 2.1) which represent the motion of the system based on the Newtonian laws. A theoretical analysis of the complete arrangement (helicopter plus pallet) however would be beyond the scope of this initial investigation. Also because most helicopter

control systems are designed only for the helicopter stability and are not adequate to compensate for external loading instabilities, it is justifiable to consider only the stability of the pallet and the suspension configuration.

In the following analysis the governing equations of motion are developed using a system of moving orthogonal axes set in the pallet (the governing equations are later shown to be applicable to the lifting hook or bar (m_1) in chapters 3.0, 4.0 and 5.0). Moving axes are advantageous compared with fixed axes (i.e. earth axes) because the coefficients of inertia of the pallet do not change with disturbances of the axes.

Most dynamical systems are of a non-linear form and the suspended pallet arrangements will be shown to be no exception. In their original non-linear form, the equations of motion are intractable. (Theoretical methods for dealing with multi-degree of freedom systems with non-linearities are still in the development stage, though analogue simulation is always a possibility). As a first approach to the solution of these equations, they are 'linearised' using the classical 'small perturbation' method, usually adopted in aircraft stability investigations (see ref. 2.1). Further discussions on the adequacy of this method are given in chapter 6.0.

'Linearisation' of the equations involves the following assumptions:-

(i) Disturbance angles about the mean position are assumed small ($\pm 5^{o}$) such that $\cos\theta \simeq 1$ and $\sin\theta = \theta$.

(ii) With the deviations small, their time rates of change are assumed to be so small that their products and squares can be neglected.

2.1 Deviations of the Moving Axes

To develop the acceleration terms of the moving axes for the application of Newton's laws of motion, i.e. mass x accoleration = force, it is necessary to determine the position of the disturbed axes (set in the pallet) with respect to fixed earth axes.

Consider now the pallet, per se, (i.e. remove the strops and allow the pallet to be carried forward at a steady horizontal velocity in an unyawed position) and assume that a set of orthogonal axes x, y, z (moving axes) is rigidly set in the pallet with its origin at the pallet centre of gravity. Similarly consider a set of orthogonal axes x_o, y_o, z_o fixed to earth, such that for the present, the origins of both sets of axis O and O_o are coincident.

In the undisturbed motion, the moving axes are orientated so that they are coincident with the fixed axes. In the disturbed position it is necessary to refer the moving axes to the earth axes by specifying three rotations ϕ, θ and ψ (see section 9.1) respectively. The order in which these

rotations are made is given because finite rotations are not usually commutative; although it is well known that the order is immaterial for small rotations.

Take $\bar{i}$, $\bar{j}$, $\bar{k}$ to be unit vectors in the x, y, z directions where the subscripts (shown below) indicate the order of rotations. The x, y, z axes are first rotated by a small clockwise positive angle ϕ about the Ox axis to give the first 'carried' position of the moving axes, i.e. x_1, y_1, z_1. (All positive rotations are in the clockwise sense about the respective axes). This can be represented by the matrix transformation:-

$$\begin{bmatrix} \bar{i}_1 \\ \bar{j}_1 \\ \bar{k}_1 \end{bmatrix} = \begin{bmatrix} 1 & 0 & 0 \\ 0 & \cos\phi & \sin\phi \\ 0 & -\sin\phi & \cos\phi \end{bmatrix} \begin{bmatrix} \bar{i}_0 \\ \bar{j}_0 \\ \bar{k}_0 \end{bmatrix} = [\chi_1] \begin{bmatrix} \bar{i}_0 \\ \bar{j}_0 \\ \bar{k}_0 \end{bmatrix} \quad \ldots\ldots\ldots (2.1)$$

Secondly the carried xyz axes are rotated about the Oy carried axis through a small positive angle θ to give the second carried axes, i.e. x_2, y_2, z_2. Hence

$$\begin{bmatrix} \bar{i}_2 \\ \bar{j}_2 \\ \bar{k}_2 \end{bmatrix} = \begin{bmatrix} \cos\theta & 0 & -\sin\theta \\ 0 & 1 & 0 \\ \sin\theta & 0 & \cos\theta \end{bmatrix} \begin{bmatrix} \bar{i}_1 \\ \bar{j}_1 \\ \bar{k}_1 \end{bmatrix} = [\chi_2] \begin{bmatrix} \bar{i}_1 \\ \bar{j}_1 \\ \bar{k}_1 \end{bmatrix} \quad \ldots\ldots\ldots (2.2)$$

Finally the second 'carried' axes are given a small positive rotation ψ about the carried Oz axis to give the third carried axes. It is now assumed that this is the final position of the disturbed moving axes x, y, z. Hence

$$\begin{bmatrix}\bar{i}_3\\ \bar{j}_3\\ \bar{k}_3\end{bmatrix} \equiv \begin{bmatrix}\bar{i}\\ \bar{j}\\ \bar{k}\end{bmatrix} = \begin{bmatrix}\cos\psi & \sin\psi & 0\\ -\sin\psi & \cos\psi & 0\\ 0 & 0 & 1\end{bmatrix}\begin{bmatrix}\bar{i}_2\\ \bar{j}_2\\ \bar{k}_2\end{bmatrix} = [\chi_3]\begin{bmatrix}\bar{i}_2\\ \bar{j}_2\\ \bar{k}_2\end{bmatrix} \quad \ldots\ldots (2.3)$$

and the final disturbed position of the moving x, y, z axes relative to the fixed earth axes x_o, y_o, z_o can be specified by the relation

$$\{\bar{i}, \bar{j}, \bar{k}\} = \chi_3\ \chi_2\ \chi_1\ \{\bar{i}_o, \bar{j}_o, \bar{k}_o\} = \chi\ \{\bar{i}_o, \bar{j}_o, \bar{k}_o\} \quad \ldots (2.4)$$

$$[\chi] = \begin{bmatrix}\cos\psi\cos\theta, & \sin\psi\cos\phi+\cos\psi\sin\theta\sin\phi, & \sin\psi\sin\phi-\cos\psi\sin\theta\cos\phi\\ -\sin\psi\cos\theta, & \cos\psi\cos\phi-\sin\psi\sin\theta\sin\phi, & \cos\psi\sin\phi+\sin\psi\sin\theta\cos\phi\\ \sin\theta\ , & -\cos\theta\sin\phi\ , & \cos\theta\cos\phi\end{bmatrix}$$

Since the above square matrices are orthogonal, the inverse of each matrix is its transpose, thus

$$\chi^{-1} = \chi_1^{-1}.\chi_2^{-1}.\chi_3^{-1} = \chi_1'.\chi_2'.\chi_3' = \chi'.$$

With equation 2.4 given, it is now possible to determine the velocity and acceleration deviation components of the pallet. Denote by $\underline{\xi}_o$ and $\underline{\xi}$ the co-ordinate vectors of a point P in the pallet (which for generality is assumed flexible) relative to the fixed and moving axes respectively - where, for the present, the origins of both sets of co-ordinates are taken as being coincident.

Then we have $\underline{\xi} = \chi\ \underline{\xi}_o$ . . . . . (2.5)

If the origin of the moving axes is displaced by $\underline{\eta}_o$ from that of the fixed axes then

$$\underline{\xi} = \chi\ (\underline{\xi}_o - \underline{\eta}_o) \text{ or } \chi\ \underline{\xi}_o = \chi\ \underline{\eta}_o + \underline{\xi} \quad \ldots\ldots\ldots (2.6)$$

Differentiation of both sides with respect to time (t) gives

$$\chi \dot{\underline{\xi}}_o = \dot{\chi} (\underline{\eta}_o - \underline{\xi}_o) + \chi \dot{\underline{\eta}}_o + \dot{\underline{\xi}}$$

but since $\underline{\xi}_o = \underline{\eta}_o + \chi' \underline{\xi}$ since $\chi^{-1} = \chi'$

we have $\chi \dot{\underline{\xi}}_o = - \dot{\chi} \chi' \underline{\xi} + \dot{\underline{\xi}} + \chi \dot{\underline{\eta}}_o$ . . . . . (2.7)

Now $\chi\chi^{-1} = I$

Therefore $\dot{\chi}\chi^{-1} + \chi \frac{d}{dt} (\chi^{-1}) = 0$

Thus $\dot{\chi}\chi^{-1} = - \chi \frac{d\chi^{-1}}{dt} = - \bar{\omega}$ (say)

Then $\bar{\omega} = \chi \frac{d\chi^{-1}}{dt} = \chi_3\chi_2\chi_1(\dot{\chi}_1'\chi_2'\chi_3' + \chi_1'\dot{\chi}_2'\chi_3' + \chi_1'\chi_2'\dot{\chi}_3')$

$$= (\chi_3\chi_2)(\chi_1\dot{\chi}_1')(\chi_3\chi_2)' + \chi_3(\chi_2\dot{\chi}_2')\chi_3' + \chi_3\dot{\chi}_3' \quad . \quad . \quad . \quad (2.8)$$

but $\chi_1\dot{\chi}_1' = \begin{bmatrix} 0 & 0 & 0 \\ 0 & 0 & -1 \\ 0 & 1 & 0 \end{bmatrix} \dot{\phi}$, $\chi_2\dot{\chi}_2' = \begin{bmatrix} 0 & 0 & 1 \\ 0 & 0 & 0 \\ -1 & 0 & 0 \end{bmatrix} \dot{\theta}$

and $\chi_3\dot{\chi}_3' = \begin{bmatrix} 0 & -1 & 0 \\ 1 & 0 & 0 \\ 0 & 0 & 0 \end{bmatrix} \dot{\psi}$

Thus it can be shown that

$$\bar{\omega} = \begin{bmatrix} 0 & , & -\dot{\phi}\sin\theta - \dot{\psi} & , & -\dot{\phi}\sin\psi\cos\theta + \dot{\theta}\cos\psi \\ \dot{\phi}\sin\theta + \dot{\psi} & , & 0 & , & -\dot{\phi}\cos\psi\cos\theta + \dot{\theta}\sin\psi \\ \dot{\phi}\sin\psi\cos\theta - \dot{\theta}\cos\psi & , & \dot{\phi}\cos\psi\cos\theta + \dot{\theta}\sin\psi & , & 0 \end{bmatrix} . \quad (2.9)$$

and with deviations assumed small (i.e. $\cos\theta = 1$, $\sin\theta = \theta$)

$$\bar{\omega} = \begin{bmatrix} 0 & -r & q \\ r & 0 & -p \\ -q & p & 0 \end{bmatrix} \quad . \quad . \quad . \quad . \quad . \quad . \quad . \quad . \quad . \quad . \quad . \quad . \quad . \quad . \quad . \quad . \quad . \quad . \quad . \quad (2.10)$$

where $\dot{\theta} = q$, $\dot{\phi} = p$ and $\dot{\psi} = r$

Equation 2.7 now becomes

$$\chi \dot{\underline{\xi}}_o = (ID + \bar{\omega})\underline{\xi} + \chi \dot{\underline{\eta}}_o = (ID + \bar{\omega})(\underline{\xi} + \chi \underline{\eta}_o)$$

$$\text{or } \bar{v} = v_o + (ID + \bar{\omega})\underline{\xi} \quad \ldots\ldots\ldots\ldots\ldots\ldots\ldots\ldots (2.11)$$

in view of the properties of $\bar{\omega}$.

$\bar{v}$ is the absolute velocity of P, $v_o = \chi \dot{\eta}_o = (ID+\bar{\omega})\chi \underline{\eta}_o$ is the absolute velocity of the origin and $(ID + \bar{\omega})\underline{\xi}$ is the velocity of P relative to the origin of the moving axes - all, of course, being measured along the instantaneous directions of the moving axes.

By induction we also have

$$\bar{\alpha} = \chi \ddot{\underline{\xi}}_o = (ID + \bar{\omega})(v_o + (ID + \bar{\omega})\underline{\xi})$$

$$= (ID + \bar{\omega})\bar{v}_o + (D\bar{\omega} + \bar{\omega})^2\underline{\xi} \quad \ldots\ldots\ldots\ldots (2.12)$$

where $\bar{\alpha}$ is the absolute acceleration of P, $(\bar{\omega} + ID)v_o$ is the absolute acceleration of the origin and $(D\bar{\omega} + \bar{\omega})^2\underline{\xi}$ is the acceleration of P with respect to the moving axes - all measured along the instantaneous directions of the moving axes.

For the particular case of a rigid pallet

$$\bar{v} = v_o + \omega\underline{\xi}$$

$$\bar{\alpha} = (ID + \bar{\omega})v_o + (D\bar{\omega} + \bar{\omega}^2)\underline{\xi} \quad \ldots\ldots\ldots\ldots (2.13)$$

With the pallet travelling of a uniform velocity,

$v_o = \{\underline{U}, \underline{V}, \underline{W}\}$, where $\underline{U}$, $\underline{V}$ and $\underline{W}$ are the velocity components of the pallet centre of gravity and

$\underline{\xi} = \{x, y, z\}$ where x, y, z are the linear co-ordinates of P measured relative and parallel to the moving axes.

Now $\{\alpha_x, \alpha_y, \alpha_z\} = (ID + \bar{\omega})\{\underline{U}, \underline{V}, \underline{W}\} + (D\bar{\omega})\{x, y, z\}$ . . . (2.14)

when second order terms are ignored.

Equation 2.4 can thus be given by

$$\begin{bmatrix}\alpha_x\\ \alpha_y\\ \alpha_z\end{bmatrix} = \begin{bmatrix}D & -r & q\\ r & D & -p\\ -q & p & D\end{bmatrix}\begin{bmatrix}\underline{U}\\ \underline{V}\\ \underline{W}\end{bmatrix} + \begin{bmatrix}0 & z & -y\\ -z & 0 & x\\ y & -x & 0\end{bmatrix}\begin{bmatrix}p\\ q\\ r\end{bmatrix} \quad \ldots\ldots\ldots (2.15)$$

2.2 Formation of the Equations of Motion

The equations of motion of the pallet are derived in the manner adopted in aircraft work (see ref. 2.1). If the point P has mass δm, the

$$\Sigma\, \bar{F}_m = \Sigma\, (\delta m.\bar{\alpha}) \quad \ldots\ldots\ldots\ldots\ldots\ldots\ldots\ldots (2.16)$$

where $\bar{F}_m$ indicates the external forces acting on P and the summation extends over particles in the rigid pallet.

Similarly the resultant zero couples acting about the moving axes are shown to be (see ref. 2.1)

$$\begin{bmatrix}0 & -z & y\\ z & 0 & -x\\ -y & x & 0\end{bmatrix}[\Sigma\, (\bar{F}_m - \delta m\, \bar{\alpha})] = \begin{matrix}0\\ 0\\ 0\end{matrix} \quad \ldots\ldots\ldots\ldots (2.17)$$

With the origin of the moving axes at the pallet centre of gravity $\quad \Sigma\, \delta m.x = \Sigma\, \delta m.y = \Sigma\, \delta m.z = 0$

Also the external forces and moments acting on the pallet can be reduced to forces X, Y, Z acting at O (i.e. the pallet centre of gravity), parallel to the moving axes and moments L, M, N acting about Ox, Oy, Oz respectively. Hence from equations 2.16 and 2.17

$$[\Sigma\ \overline{F}_m] = [\Sigma\ (\delta m\ \overline{\alpha})] = \begin{bmatrix} X \\ Y \\ Z \end{bmatrix}$$

and $\begin{bmatrix} 0 & -z & y \\ z & 0 & -x \\ -y & x & 0 \end{bmatrix} [\Sigma\ \overline{F}_m] = \begin{bmatrix} 0 & -z & y \\ z & 0 & -x \\ -y & x & 0 \end{bmatrix} [\Sigma\ (\delta m\ \overline{\alpha})] = \begin{bmatrix} L \\ M \\ N \end{bmatrix}$ . . (2.18)

To simplify the final equations of motion

$\Sigma\ \delta m = m_2$ = Total mass of the pallet

$\overline{A} = \Sigma\ (y^2 + z^2)\delta m$ = moment of inertia about Ox

$\overline{B} = \Sigma\ (z^2 + x^2)\delta m$ = moment of inertia about Oy

$\overline{C} = \Sigma\ (x^2 + y^2)\delta m$ = moment of inertia about Oz . . . . (2.19)

$\overline{D} = \Sigma\ yz\ \delta m$ = product of inertia about Oy and Oz

$\overline{E} = \Sigma\ zx\ \delta m$ = product of inertia about Oz and Ox

$\overline{F} = \Sigma\ xy\ \delta m$ = product of inertia about Ox and Oy

The substitution of equation 2.15 into 2.18 now gives the equations of motion

$$\begin{bmatrix} X \\ Y \\ Z \end{bmatrix} = m_2 \begin{bmatrix} D & -r & q \\ r & D & -p \\ -q & p & D \end{bmatrix} \begin{bmatrix} \underline{U} \\ \underline{V} \\ \underline{W} \end{bmatrix} \quad \ldots\ldots\ldots\ldots\ldots\ldots\ldots\ldots (2.20)$$

and

$$\begin{bmatrix} L \\ M \\ N \end{bmatrix} = \begin{bmatrix} \overline{A} & -\overline{F} & -\overline{E} \\ -\overline{F} & \overline{B} & -\overline{D} \\ -\overline{E} & -\overline{D} & \overline{C} \end{bmatrix} \begin{bmatrix} \dot{p} \\ \dot{q} \\ \dot{r} \end{bmatrix} \quad \ldots\ldots\ldots\ldots\ldots\ldots\ldots\ldots (2.21)$$

While the above equations relate to the rigid pallet only, they will be used in chapters 3.0, 4.0 and 5.0 to deal with the lifting hook or bar (m_1) also.

In this chapter the rigid pallet has been considered to move under the influence of external forces and moments. These terms are further discussed in the following chapters and shown to consist of structural constraining and aerodynamic forces and moments.

View From Above.

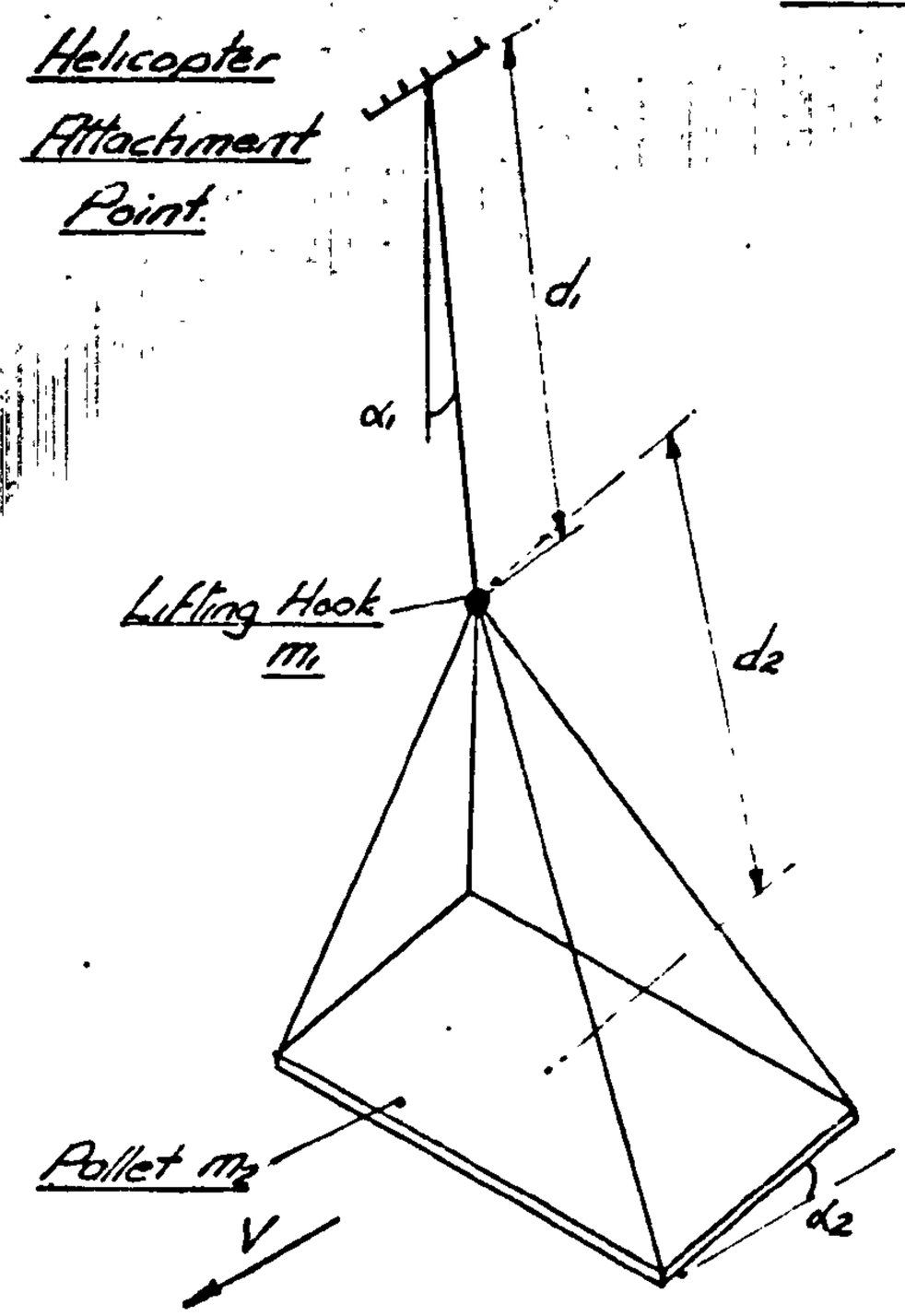

Fig. 3.1.

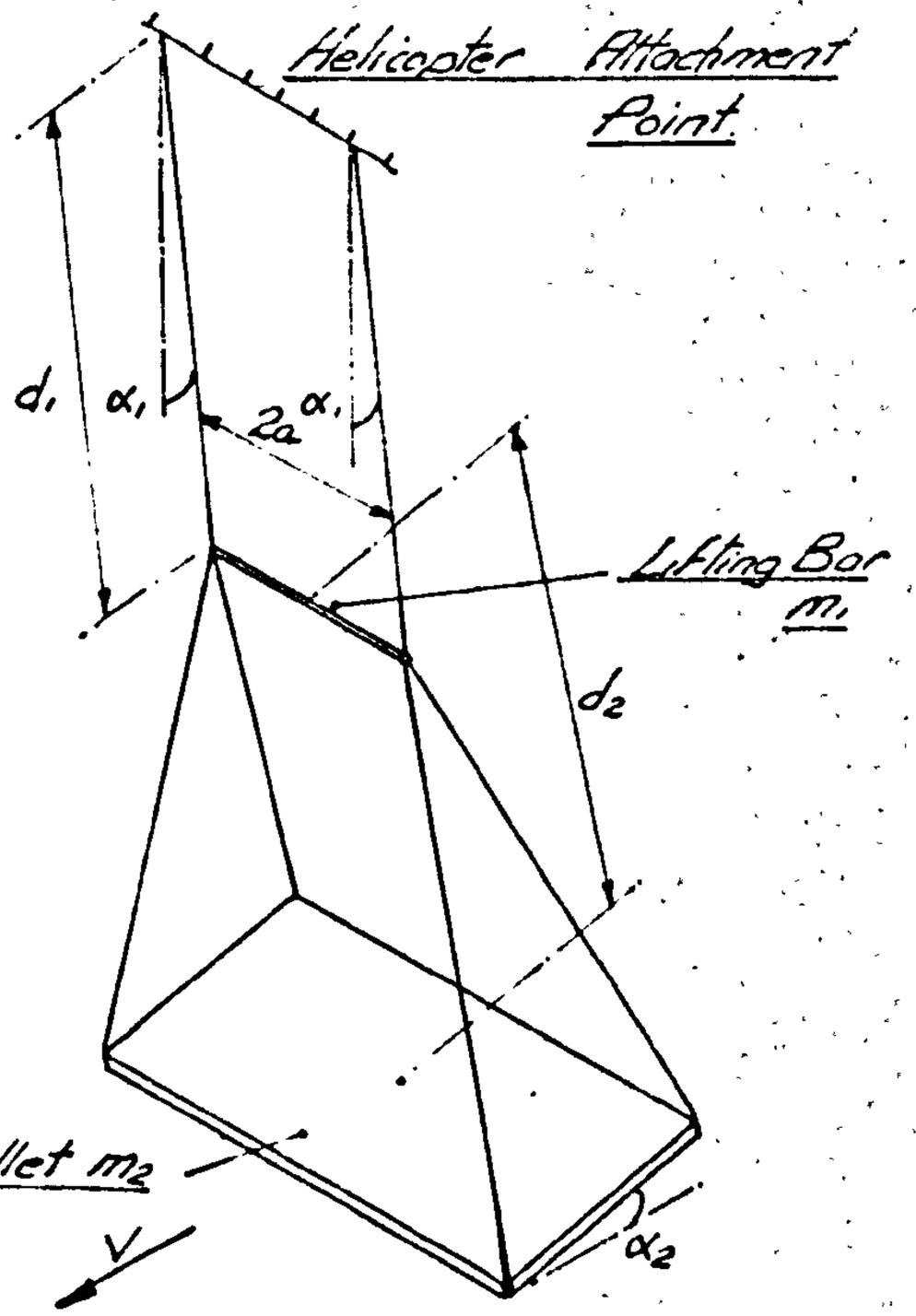

Fig. 3.2

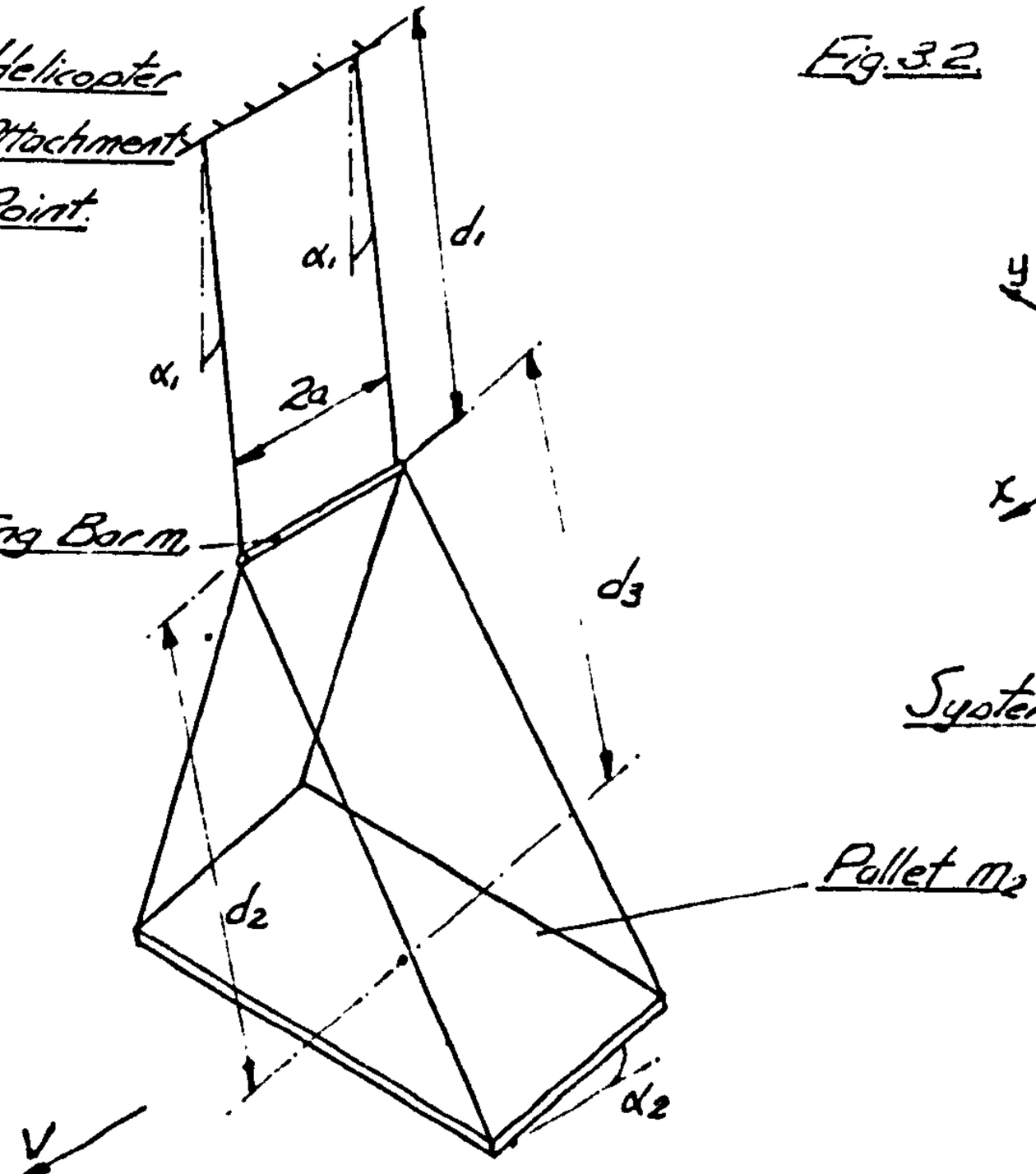

Fig. 3.3.

General Pallet Dimensions:

Span - 2b

Chord - c

Thickness d.

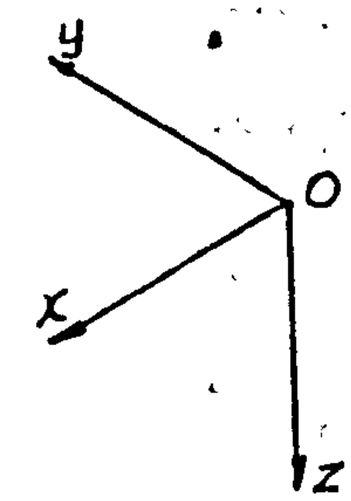

System of Orthogonal Axes.

THREE STEOP ARRANGEMENTS.

CHAPTER 3

A GENERAL THEORY FOR THREE SUSPENSION ARRANGEMENTS OF A PALLET

A general theory applicable to the single, twin and trapezoidal suspension arrangements of the pallet is developed from the governing equations of motion given in section 2.2. Extensions to this theory, pertaining to the individual systems, are given in Chapters 4.0 and 5.0. Whenever possible, the Lagrange equations of motion are used to justify the correctness of the above 'linearised' equations of motion.

Figs. 3.1, 3.2 and 3.3 show that the usual load suspension arrangements consist of two sections:- (a) An upper section (one or more strops) tethered to the helicopter attachment point/s and carrying a hook or bar at its lower end. (b) A lower section (four strops) connecting the hook or bar to the rectangular rigid pallet (2b x c x d). All joints are assumed to have negligible frictional constraining forces.

The structural constraining forces imposed on both the pallet and the lifting hook are difficult to represent accurately in the disturbed positions and it is therefore necessary to make certain sensible assumptions in order that the final equations of motion can be thrown into a manageable form. We therefore assume that the strops are inextensible,

massless and straight at all times. This last assumption is open to criticism for the pallets of smaller weight (i.e. <50 lbs), because the strops would not remain straight when exposed to a moderate wind loading. Nevertheless, ref. 3.1 shows this assumption to be valid in a wide range of cases. Alternatively, if the above assumptions were not made and the cables were assumed flexible, the complete suspension arrangement would have an infinite number of degrees of freedom and the resulting infinite number of equations would prove intractable.

The equations of motion given in section 2.2 are derived for the pallet (m_2) only. Similar equations could, however, be derived for the lifting hook or bar (m_1). In the following analyses governing equations are given for both masses, where the equations are based on orthogonal Ox_1, Oy_1, Oz_1 axes set in the lifting bar and Ox_2, Oy_2, Oz_2 in the pallet. The origins of both sets of axes are assumed to be at the centre of gravity of the masses and the Ox, Oz axes set in the planes of symmetry.

In the steady state position, the pallet and lifting bar are assumed to move at a horizontal velocity V in unyawed positions. Also, the pallet must be considered to be set at an incidence α_2 for a forward velocity V, and as a result of the steady state aerodynamic forces acting on the pallet, the

upper strop section will subtend an angle α_1 to the vertical (see fig. 3.1). Because the axes are set in the planes of symmetry of both masses, the velocity components of V measured along Ox and Oz for m_1 and m_2 are denoted by $\underline{U}_1$, $\underline{W}_1$ and $\underline{U}_2$, $\underline{W}_2$ respectively. (See section 2.1). $\underline{V}_1$ and $\underline{V}_2$ are zero, together with the angular velocities p, q and r in the unyawed steady state position.

The steady state external forces and moments (X, Y, Z, L, M, N) measured on both sets of axes consist of gravitational forces and the aerodynamic forces and moments acting on the pallet. The aerodynamic forces acting on the lifting bar are assumed negligible in these investigations.

In the disturbed condition, the steady state incidence, displacement, velocity and force terms change by small amounts and α_1 and α_2 change to $\alpha_1 - \bar{\theta}_1$ and $\alpha_2 - \bar{\theta}_2$ say, respectively. Angular displacements ϕ and ψ also occur about the Ox and Oz axes. Alternatively, the angular displacements can be given by linear displacements x, y, z (measured parallel to the new positions of the orthogonal axes). The generalised velocities $\underline{U}$, $\underline{V}$, $\underline{W}$ also change to $\underline{U}$ + u, $\underline{V}$ + v, $\underline{W}$ + w and p, q, r act about the Ox, Oy, Oz axes respectively. Finally, the external forces and moments imposed on the masses m_1 and m_2 have increments $\Delta X \cdots\cdots \Delta N$ and $\Delta\tilde{X} \cdots\cdots \Delta\tilde{N}$, where, for example, ΔX is the change in force X due to the gravitational and steady

state aerodynamic forces and $\Delta\tilde{X}$ is the change in force X due to the changes in the aerodynamic forces. The aerodynamic forces acting on the strops are sensibly ignored as these are difficult to represent adequately and would be small in comparison to the aerodynamic forces acting on the pallet.

The governing equations 2.22 and 2.23 with their second order terms neglected, can now be written

$$\begin{bmatrix} D & -r_1 & q_1 & 0 & 0 & 0 \\ r_1 & D & -p_1 & 0 & 0 & 0 \\ -q_1 & p_1 & D & 0 & 0 & 0 \\ 0 & 0 & 0 & D & -r_2 & q_2 \\ 0 & 0 & 0 & r_2 & D & -p_2 \\ 0 & 0 & 0 & -q_2 & p_2 & D \end{bmatrix} \begin{bmatrix} m_1u_1 \\ m_1v_1 \\ m_1w_1 \\ m_2u_2 \\ m_2v_2 \\ m_2w_2 \end{bmatrix} = \begin{bmatrix} \Delta X_1 \\ \Delta Y_1 \\ \Delta Z_1 \\ \Delta X_2 \\ \Delta Y_2 \\ \Delta Z_2 \end{bmatrix} + \begin{bmatrix} 0 \\ 0 \\ 0 \\ \Delta\tilde{X}_2 \\ \Delta\tilde{Y}_2 \\ \Delta\tilde{Z}_2 \end{bmatrix} \quad \ldots\ldots (3.1)$$

and

$$\begin{bmatrix} \Delta L_1 \\ \Delta M_1 \\ \Delta N_1 \\ \Delta L_2 + \Delta\tilde{L}_2 \\ \Delta M_2 + \Delta\tilde{M}_2 \\ \Delta N_2 + \Delta\tilde{N}_2 \end{bmatrix} = \begin{bmatrix} \bar{A}_1 & -\bar{F}_1 & -\bar{E}_1 & 0 & 0 & 0 \\ -\bar{F}_1 & \bar{B}_1 & -\bar{D}_1 & 0 & 0 & 0 \\ -\bar{E}_1 & -\bar{D}_1 & \bar{C}_1 & 0 & 0 & 0 \\ 0 & 0 & 0 & \bar{A}_2 & -\bar{F}_2 & -\bar{E}_2 \\ 0 & 0 & 0 & -\bar{F}_2 & \bar{B}_2 & -\bar{D}_2 \\ 0 & 0 & 0 & -\bar{E}_2 & -\bar{D}_2 & \bar{C}_2 \end{bmatrix} \begin{bmatrix} \dot{p}_1 \\ \dot{q}_1 \\ \dot{r}_1 \\ \dot{p}_2 \\ \dot{q}_2 \\ \dot{r}_2 \end{bmatrix} \quad \ldots\ldots (3.2)$$

The subscripts 1 and 2 indicate the incremental changes with respect to the lifting bar (m_1) and the pallet (m_2) respectively. Also the $\Delta\tilde{X}_2$ .....$\Delta\tilde{N}_2$ terms are later extended

in a linear series form and represented by aerodynamic derivatives.

At this stage the equations 3.1 and 3.2 are simplified because with the Oxz_1 and Oxz_2 axes set on the longitudinal planes of symmetry of both masses, the mass distributions will be symmetric about these planes and the product of inertia terms $\bar{D}_1$, $\bar{F}_1$, $\bar{D}_2$, $\bar{F}_2$ are therefore zero. $\bar{E}_1$ and $\bar{E}_2$ are not necessarily zero in the steady state condition unless the above axes are set on the principal axes of inertia of both masses. In the individual analyses for the three strop configurations, the axes are set on both types of axes, depending on their suitability for each analysis.

The incremental changes in the aerodynamic forces and moments (included in equations 3.1 and 3.2), which are assumed to act solely on the pallet, are not conservative and depend strictly on the complete history of motion of the pallet. These forces and moments are represented by a set of derivatives given in a method introduced by Bryan (ref. 3.2) in 1911. Great success has been obtained with this method in the majority of aircraft stability work.

This method assumes the incremental changes in the aerodynamic components to be linearly dependent on the small deviations x, y, z, θ etc. and their time derivatives. Although this is an approximate method, it is the only form available, except for the similar aerodynamic transfer

function technique (see ref. 3.3), whereby the incremental changes in the aerodynamic terms can be represented.

Each aerodynamic term is usually expressed in the form of a Taylor series of the variables. Therefore, with second order terms, as usual, neglected:-

$$\Delta\tilde{X}_2 = \frac{\partial X}{\partial \theta}.\theta + \frac{\partial X}{\partial u}.u. + \frac{\partial X}{\partial \dot{w}}.\dot{w} + \frac{\partial X}{\partial q}.q + \frac{\partial X}{\partial v}.v. + \frac{\partial X}{\partial p}.p \text{ etc. } \ldots(3.3)$$

where the terms $\frac{\partial X}{\partial u}$ etc. are partial derivatives evaluated at the steady state conditions and normally expressed by Xu etc. From equation 3.3 it can be seen that force in the longitudinal sense is dependent on disturbances in both the longitudinal and lateral senses (i.e. q and v respectively).

Because the Oxz_2 axes are taken in the longitudinal (symmetric) plane of the pallet, it is implied that the derivatives $\frac{\partial X}{\partial v}$, $\frac{\partial X}{\partial p}$ etc. (usually named cross-coupling derivatives) are even functions which have zero values at the steady state condition. This is necessarily so because, for example, the X force is always positive regardless of whether v is positive or negative in magnitude. Hence, for small perturbation theory, the cross coupling derivatives are ignored, and the aerodynamic forces and moments can be expressed in two groups (see ref. 2.1)

$$\begin{bmatrix}\Delta\tilde{X}_2\\ \Delta\tilde{Z}_2\\ \Delta\tilde{M}_2\end{bmatrix} = \begin{bmatrix}0 & 0 & X_\theta\\ 0 & 0 & Z_\theta\\ 0 & 0 & M_\theta\end{bmatrix}\begin{bmatrix}x_2\\ z_2\\ \theta_2\end{bmatrix} + \begin{bmatrix}Xu & Xw & Xq\\ Zu & Zw & Zq\\ Mu & Mw & Mq\end{bmatrix}\begin{bmatrix}\dot{x}_2\\ \dot{z}_2\\ \dot{\theta}_2\end{bmatrix} + \begin{bmatrix}X\dot{u} & X\dot{w} & X\dot{q}\\ Z\dot{u} & Z\dot{w} & Z\dot{q}\\ M\dot{u} & M\dot{w} & M\dot{q}\end{bmatrix}\begin{bmatrix}\ddot{x}_2\\ \ddot{z}_2\\ \ddot{\theta}_2\end{bmatrix}$$

$$\text{i.e.} = [\tilde{R}_S]\,[\theta] + [\tilde{S}_S]\,[\dot{\theta}] + [\tilde{R}_S]\,[\ddot{\theta}] \quad \ldots\ldots\ldots\ldots (3.4)$$

$$\begin{bmatrix} \Delta\tilde{Y}_a \\ \Delta\tilde{L}_a \\ \Delta\tilde{N}_a \end{bmatrix} = \begin{bmatrix} 0 & Y_\phi & Y_\psi \\ 0 & L_\phi & L_\psi \\ 0 & N_\phi & N_\psi \end{bmatrix} \begin{bmatrix} y_a \\ \phi_a \\ \psi_a \end{bmatrix} + \begin{bmatrix} Y_v & Y_p & Y_r \\ L_v & L_p & L_r \\ N_v & N_p & N_r \end{bmatrix} \begin{bmatrix} \dot{y}_a \\ \dot{\phi}_a \\ \dot{\psi}_a \end{bmatrix} + \begin{bmatrix} Y_{\dot{v}} & Y_{\dot{p}} & Y_{\dot{r}} \\ L_{\dot{v}} & L_{\dot{p}} & L_{\dot{r}} \\ N_{\dot{v}} & N_{\dot{p}} & N_{\dot{r}} \end{bmatrix} \begin{bmatrix} \ddot{y}_a \\ \ddot{\phi}_a \\ \ddot{\psi}_a \end{bmatrix}$$

$$\text{i.e.} = [\tilde{R}_A]\,[\phi] + [\tilde{S}_A]\,[\dot{\phi}] + [\tilde{P}_A]\,[\ddot{\phi}] \quad \ldots\ldots\ldots\ldots\ldots\ldots \quad (3.5)$$

where the first, second and third 3 x 3 matrices contain stiffness, damping and acceleration derivatives respectively. The latter are usually small in comparison with the structural inertias of a system and are ignored (see chapter 7.0). Also the X_q, Y_p and Y_r derivatives are assumed small enough to be neglected because they have insignificant effects on the stability of system in comparison with the other damping derivatives.

As a result of the assumptions made in applying the governing equations to the three systems and representing the aerodynamic terms by the above method, it is possible to divide the governing equations into two exclusive groups (see ref. 2.1), where the structural constraining terms can be separated in a like manner. (This is shown to be possible in sections 4.0 and 5.0). The one group of equations is dependent on the longitudinal co-ordinates x, z, θ, u, w, q and are called the longitudinal (symmetric) equations, whilst the other group of equations is dependent on the lateral co-ordinates y, ϕ, ψ, v, p, r and are called the lateral (antisymmetric) equations.

Because these equations can be separated (to the first order of approximation), it is implied that unless the deviations are large, a pure longitudinal oscillation will not induce a lateral oscillation, or vice-versa. It is possible that coupling will occur, however, for large amplitude oscillations, as experienced in the full scale tests on the single strop suspension of a pallet. Alternatively, coupled small oscillations could occur in the accelerated flight of the helicopter (see Ref. 3.4). In both cases we then have to return to the non-linear form of equations 2.20 and 2.21 for complete stability investigations. However, for the present analyses, the two groups of equations are given by longitudinal equations

$$\begin{bmatrix} m_1(\dot{u}_1 + q_1\underline{W}_1) \\ m_1(\dot{w}_1 - q_1\underline{U}_1) \\ \bar{B}_1\dot{q}_1 \\ m_2(\dot{u}_2 + q_2\underline{W}_2) \\ m_2(\dot{w}_2 - q_2\underline{U}_2) \\ \bar{B}_2\dot{q}_2 \end{bmatrix} = \begin{bmatrix} \Delta X_1 \\ \Delta Z_1 \\ \Delta M_1 \\ \Delta X_2 \\ \Delta Z_2 \\ \Delta M_2 \end{bmatrix} + \begin{bmatrix} 0 \\ 0 \\ 0 \\ \Delta\tilde{X}_2 \\ \Delta\tilde{Z}_2 \\ \Delta\tilde{M}_2 \end{bmatrix} \quad \ldots\ldots\ldots\ldots (3.6)$$

and the lateral equations

$$\begin{bmatrix} m_1(\dot{v}_1 - p_1\underline{W}_1 + r_1\underline{U}_1) \\ \bar{A}_1\dot{p}_1 - \bar{E}_1\dot{r}_1 \\ -\bar{E}_1\dot{p}_1 + \bar{C}_1\dot{r}_1 \\ m_2(\dot{v}_2 - p_2\underline{W}_2 + r_2\underline{U}_2) \\ \bar{A}_2\dot{p}_2 - \bar{E}_2\dot{r}_2 \\ -\bar{E}_2\dot{p}_2 + \bar{C}_2\dot{r}_2 \end{bmatrix} = \begin{bmatrix} \Delta Y_1 \\ \Delta L_1 \\ \Delta N_1 \\ \Delta Y_2 \\ \Delta L_2 \\ \Delta N_2 \end{bmatrix} + \begin{bmatrix} 0 \\ 0 \\ 0 \\ \Delta\tilde{Y}_2 \\ \Delta\tilde{L}_2 \\ \Delta\tilde{N}_2 \end{bmatrix} \quad \ldots\ldots (3.7)$$

3.1 The Longitudinal Equations

The Longitudinal equations given by equation 3.6 are in the general form applicable to the three strop arrangements. They can also be expressed in concise form as follows:-

$$[A_S][\ddot{\theta}] + [B_S][\dot{\theta}] = [\Delta F_S] + [\tilde{C}_S][\theta] + [\tilde{B}_S][\dot{\theta}] \quad \ldots\ldots (3.8)$$

where $[\theta] = \{x_1, z_1, \theta_1, x_2, z_2, \theta_2\}$, $[\Delta F_S] = \{\Delta X_1, \Delta Z_1 \ldots \Delta M_2\}$,

$$[A_S] = \begin{bmatrix} m_1 & & & & & \\ & m_1 & & & & \\ & & \bar{B}_1 & & & \\ & & & m_2 & & \\ & & & & m_2 & \\ & & & & & \bar{B}_2 \end{bmatrix}, \quad [B_S] = \begin{bmatrix} 0 & 0 & m_1\underline{W}_1 & 0 & 0 & 0 \\ 0 & 0 & -m_1\underline{U}_1 & 0 & 0 & 0 \\ 0 & 0 & 0 & 0 & 0 & 0 \\ 0 & 0 & 0 & 0 & 0 & m_2\underline{W}_2 \\ 0 & 0 & 0 & 0 & 0 & -m_2\underline{U}_2 \\ 0 & 0 & 0 & 0 & 0 & 0 \end{bmatrix}$$

The 6 x 6 matrix

$$[\tilde{B}_S] = \begin{bmatrix} 0 & & 0 & \\ & X_u & X_w & X_q \\ 0 & Z_u & Z_w & Z_q \\ & M_u & M_w & M_q \end{bmatrix}$$

and $[\tilde{C}_S]$ is null since moving axes are being used.

It can be seen that $[B_S]$ contains gyroscopic-inertia terms which are dependent on forward velocity. These are centrifugal force terms which occur when the masses are disturbed in an angular sense (i.e. q) whilst moving forward at a steady horizontal velocity V.

From a consideration of Figs. 3.1, 3.2 and 3.3, it can be seen that for pure longitudinal disturbances, the three suspension arrangements have individually two degrees of freedom, and thus any deviation can be indicated by the increments x_1, z_1, θ_1, x_2, z_2, θ_2, or more conveniently $\bar{\theta}_1$ and $\bar{\theta}_2$. Similarly, the incremental changes in the forces and moments of a system can be represented adequately by two generalised moments - the one is measured about the helicopter attachment point(s) and the other about the pallet centre of gravity. Therefore, the six longitudinal force and moment equations given by eqn. 3.8 can be transformed to two moment equations with co-ordinates $\bar{\theta}_1$ and $\bar{\theta}_2$.

Now a relationship may be obtained for each suspension arrangement of the form

$$\{x_1, z_1, \theta_1, x_2, z_2, \theta_2\} = [T_S]\{\bar{\theta}_1, \bar{\theta}_2\} \quad \ldots\ldots\ldots \quad (3.9)$$

where $[T_S]$ is a 6 x 2 transformation matrix between the two sets of co-ordinates. In the simple case under consideration this is a linear relationship because the second and higher order terms are neglected. Similarly the matrices $[T_S]$ and $[T_{S_1}]$ (see chapter 4.0) are found to govern the relationship between the time derivatives of the two columns matrices in equation 3.9.

By the principle of virtual work, the eqn. 3.8 can now be transformed to two linearized moment equations as follows:-

$$[T_S]'[A_S][T_S][\ddot{\bar{\theta}}] + [T_S]'[B_S][T_S][\dot{\bar{\theta}}] = [T_S]'[\Delta F_S] + [T_S]'[\tilde{C}_S][T_S][\bar{\theta}]$$
$$+[T_S]'[A_S][T_{S_1}][\dot{\bar{\theta}}] + [T_S]'[B_S][T_{S_1}][\bar{\theta}] \qquad +[T_S]'[\tilde{B}_S][T_S][\dot{\bar{\theta}}] \quad \ldots(3.10)$$

where $\{\bar{\theta}_1, \bar{\theta}_2\}$ is denoted by $[\bar{\theta}]$ and the $[\tilde{C}_S]$ and $[\tilde{B}_S]$ matrices contain stiffness and damping derivatives respectively, now defined on fixed axes.

The $[T_S]$, $[T_{S_1}]$ matrices, together with the $[T_S]'[\Delta F_S]$ matrix (which denotes the gravitational and aerodynamic steady state terms) are developed in chapter 4 for each strop configuration.

3.2 The Lateral Equations

In a similar manner to eqn. 3.8, the lateral equations of motion are given in a general form applicable to the three suspension arrangements as follows:-

$$[A_A]\,[\ddot{\phi}] + [B_A]\,[\dot{\phi}] = [\Delta F_A] + [\tilde{C}_A]\,[\phi] + [\tilde{B}_A]\,[\dot{\phi}] \quad \ldots\ldots \quad (3.11)$$

where $[\phi] = \{y_1, \phi_1, \psi_1, y_2, \phi_2, \psi_2\}$, $[\Delta F_A] = \{\Delta Y_1, \Delta L_1, \ldots \Delta N_2\}$,

$$[A_A] = \begin{bmatrix} m_1 & 0 & 0 & 0 & 0 & 0 \\ 0 & \bar{A}_1 & -\bar{E}_1 & 0 & 0 & 0 \\ 0 & -\bar{E}_1 & \bar{C}_1 & 0 & 0 & 0 \\ 0 & 0 & 0 & m_2 & 0 & 0 \\ 0 & 0 & 0 & 0 & \bar{A}_2 & -\bar{E}_2 \\ 0 & 0 & 0 & 0 & -\bar{E}_2 & -\bar{C}_2 \end{bmatrix}, \quad [B_A] = \begin{bmatrix} 0 & -m_1\underline{W}_1 & m_1\underline{U}_1 & 0 & 0 & 0 \\ 0 & 0 & 0 & 0 & 0 & 0 \\ 0 & 0 & 0 & 0 & 0 & 0 \\ 0 & 0 & 0 & 0 & -m_2\underline{W}_2 & m_2\underline{U}_2 \\ 0 & 0 & 0 & 0 & 0 & 0 \\ 0 & 0 & 0 & 0 & 0 & 0 \end{bmatrix}$$

$$[\tilde{B}_A] = \begin{bmatrix} 0 & & 0 & \\ & Y_v & Y_p & Y_r \\ 0 & L_v & L_p & L_r \\ & N_v & N_p & N_r \end{bmatrix}$$

and $[\tilde{C}_A]$ is zero since moving axes are being used.

The matrix $[B_A]$ has similar properties to $[B_S]$ in that it represents the centrifugal forces acting on m_1 and m_2 when disturbed by the small angular velocities p, r whilst moving forward at a horizontal velocity V.

As in section 3.1, the six lateral force and moment equations are reduced (by the action of the strop constraints) to three generalised moment equations based on the co-ordinate system η, ξ, ν (see Figs. 3.1, 3.2 and 3.3). This transformation is brought about by using the 6 x 3 transformation matrix $[T_A]$ defined by

$$\{y_1, \phi_1, \psi_1, y_2, \phi_2, \psi_2\} = [T_A]\{\eta, \xi, \nu\} \quad \ldots\ldots\ldots (3.12)$$

Similarly, $[T_A]$ & $[T_{A_1}]$ are found to apply between the time derivatives of the displacements (see chapter 5).

By using the principle of virtual work, equation 3.11 becomes, when linearised,

$$[T_A]'[A_A][T_A][\ddot{\bar{\eta}}] + [T_A]'[B_A][T_A][\dot{\bar{\eta}}] = [T_A]'[\Delta F_A] + [T_A]'[\breve{C}_A][T_A][\bar{\eta}]$$

$$+[T_A]'[A_A][T_{A_1}][\dot{\bar{\eta}}] + [T_A]'[B_A][T_{A_1}][\bar{\eta}] \quad .+[T_A]'[\tilde{B}_A][T_A][\dot{\bar{\eta}}] \ldots(3.13)$$

$[\tilde{C}_A]$ & $[\tilde{B}_A]$ contain stiffness and damping derivatives respectively, now defined on fixed axes.

The matrices $[T_A]$, $[T_{A_1}]$ and $[T_A]'[\Delta F_A]$ are derived for the three strop arrangements under consideration in chapter 5.

3.3 The Non-Dimensionalised Equations

In order that the longitudinal and lateral equations of motion, 3.10 and 3.13 respectively, can be used for comparing two similar suspension arrangements with different overall scale factors, it is convenient to non-dimensionalise

these equations for all the stability investigations.

Therefore, when the equations 3.10 and 3.13 are fully developed for each suspension arrangement in sections 4.0 and 5.0, they are non-dimensionalised using the following parameters:-

$t = \frac{m_2}{\rho V S}\tau$ where τ is non-dimensionalised time,

$\mu_1 = \frac{m_2}{\rho S d_2}$ = relative density parameter,

$\frac{V^2}{d_2 g}$ = Froude number,

$\frac{d\theta}{dt} = \frac{\rho V S}{m_2}\frac{d\theta}{d\tau}$ and $\frac{d^2\theta}{dt^2} = \left(\frac{\rho V S}{m_2}\right)^2 \frac{d^2\theta}{d\tau^2}$

The final equations of motion are then given in an appropriate non-dimensional form, amenable to stability investigations.

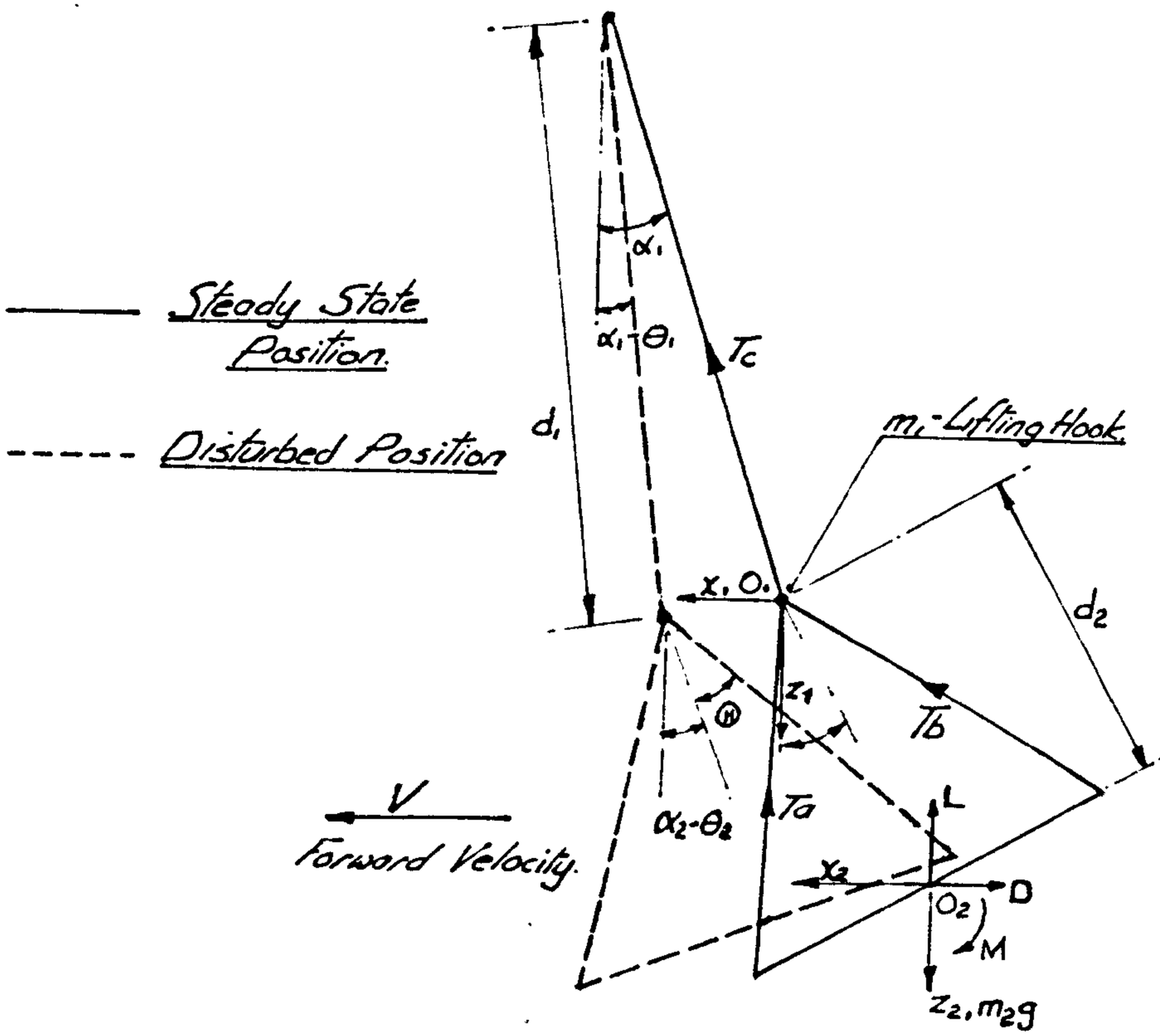

Fig. 4.1. The Single and Twin Strop Configurations.

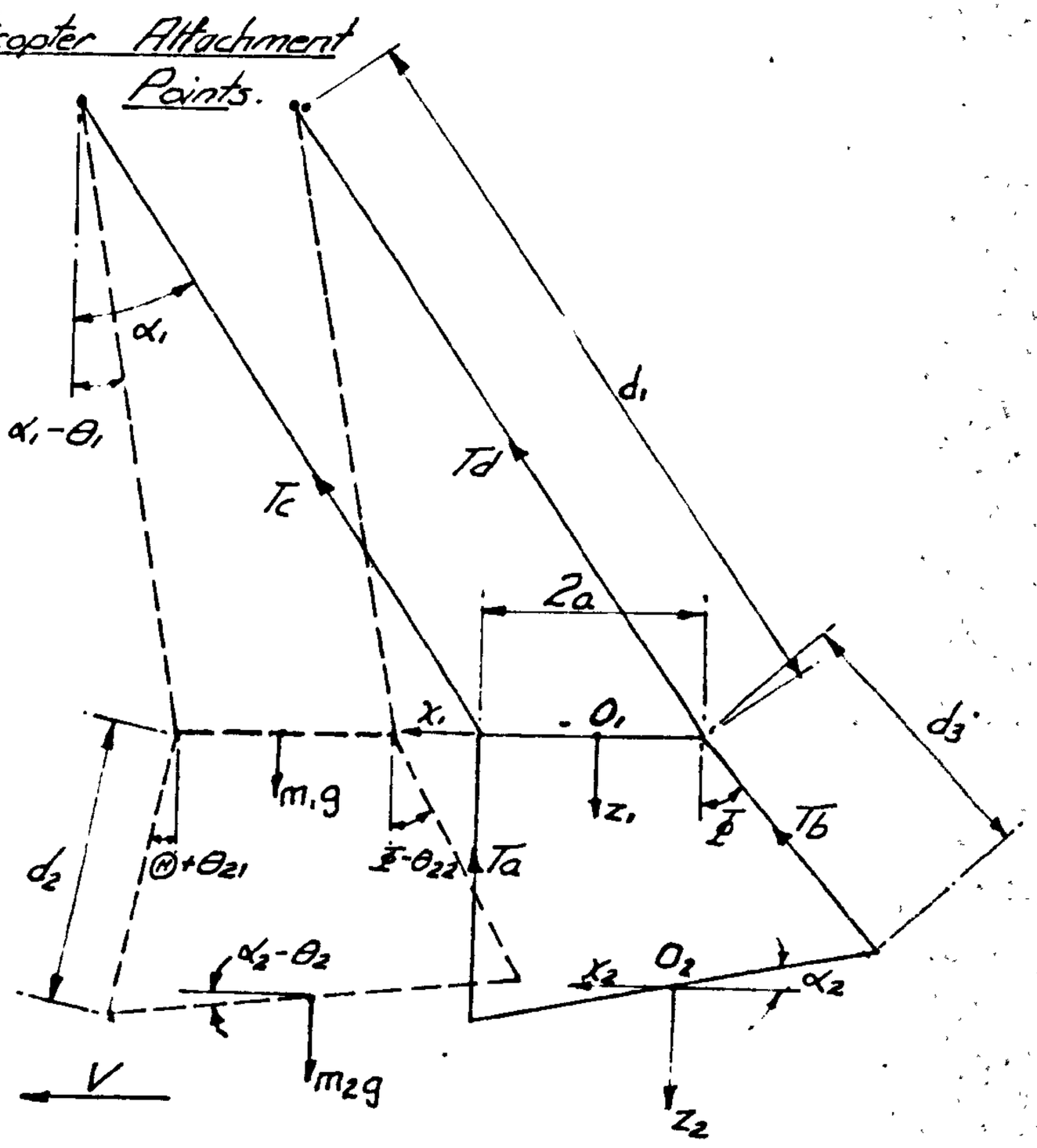

Fig. 4.2. The Trapezoidal Configuration.

THE LONGITUDINAL COORDINATE SYSTEMS

CHAPTER 4

THE LONGITUDINAL ANALYSES OF THE SUSPENSION ARRANGEMENTS

It is shown in chapter 3.0 that separate longitudinal and lateral investigations can be made for small disturbances of the three strop arrangements (shown in fig. 3.1, 3.2 and 3.3). Since the longitudinal equations (equation 3.10) are in a general form applicable to the three systems considered, it is only necessary to determine the $[T_S]$, $[T_{S_1}]$ and $[T_S]'[\Delta F_S]$ matrices. These are now considered in fuller detail for the single, twin and trapezoidal strop arrangements.

4.1 The Single Strop Configuration

For the longitudinal (symmetric) motions it is adequate to represent the single strop arrangement in a simpler form. The upper strop remains the same, but the lower four strops are considered schematically as two support strops attached on the plane of symmetry of the pallet (see fig. 4.1). The upper strop length is denoted by d_1 and the normal distance between the centres of gravity of the hook and pallet is given by d_2. In the equilibrium (steady state) position, the angles α_1 and α_2 give the position of the arrangement with respect to vertical and horizontal datum lines respectively.

4.1.1 The Transformation Matrix

In the steady state position the Oxz_1 and Oxz_2 axes of the hook and pallet respectively are set on wind axes for this analysis (i.e. with the x axes set parallel to the horizontal forward movement). In the disturbed position, however, it can be shown (with second and higher order terms neglected, $\cos\theta \simeq 1-\frac{\theta^2}{2}$ and $\sin\theta \simeq \theta$) that

$$\begin{bmatrix} x_1 \\ z_1 \\ \theta_1 \\ x_2 \\ z_2 \\ \theta_2 \end{bmatrix} = \begin{bmatrix} d_1\cos\alpha_1, & 0 \\ d_1\sin\alpha_1, & 0 \\ 1, & 0 \\ d_1\cos\alpha_1, & d_2\cos\alpha_2 \\ d_1\sin\alpha_1, & d_2\sin\alpha_2 \\ 0 & 1 \end{bmatrix} \begin{bmatrix} \bar{\theta}_1 \\ \bar{\theta}_2 \end{bmatrix}, \quad [T_{S_1}] = \begin{bmatrix} -\underset{\sim}{W}_1 & 0 \\ \underset{\sim}{U}_1 & 0 \\ 0 & 0 \\ 0 & -\underset{\sim}{W}_2 \\ 0 & \underset{\sim}{U}_2 \\ 0 & 0 \end{bmatrix}$$

$$[\theta] = [T_S][\bar{\theta}], \quad [\dot{\theta}] = [T_S][\dot{\bar{\theta}}]+[T_{S_1}][\bar{\theta}] \text{ and } [\ddot{\theta}] = [T_S][\ddot{\bar{\theta}}] +[T_{S_1}][\dot{\bar{\theta}}] \quad \ldots\ldots 4.1$$

where, for example,

$$x_2 = d_1\sin(\alpha_1+\bar{\theta}_2)+d_2\sin(\alpha_2+\bar{\theta}_2)-d_1\sin(\alpha_1+\bar{\theta}_2-\bar{\theta}_1)-d_2\sin\alpha_2$$

$$= d_1\cos\alpha_1\,\bar{\theta}_1 + d_2\cos\alpha_2\,\bar{\theta}_2 + \text{second order terms}$$

4.1.2 The Constraining Forces and Moments

These structural constraining terms denoted by $[T_S]'[\Delta F_S]$, include only the gravitational and steady state aerodynamic forces and moments acting on m_1 and m_2, because the incremental changes in the aerodynamic terms due to $\bar{\theta}_1$ and $\bar{\theta}_2$ are accounted for by the 2 x 2 matrix $[T_S]'[\tilde{C}_S][T_S][\bar{\theta}]$.

The usual procedure of displacing the generalised co-ordinates $\bar{\theta}_1$, $\bar{\theta}_2$ is used to obtain the incremental constraining terms. Therefore with the aid of fig. 4.1, it can be shown $\nabla X_{S_2} = (T_a + \nabla T_a)\sin(\alpha_2 - \bar{\theta}_2 - \Theta) + (T_b + \nabla T_b)\sin(\alpha_2 - \bar{\theta}_2 + \Theta)$

$$-T_a\sin(\alpha_2 - \Theta) - T_b\sin(\alpha_2 + \Theta)$$

where ∇T_a, ∇T_b, ∇T_c are the change in the strop tensions, or more completely,

$$\begin{bmatrix} \nabla X_{S_1} \\ \nabla Z_{S_1} \\ \nabla M_{S_1} \\ \nabla X_{S_2} \\ \nabla Z_{S_2} \\ \nabla M_{S_2} \end{bmatrix} = \begin{bmatrix} 0 & 0 & \sin\alpha_1 & -T_c\cos\alpha_1 & 0 \\ 0 & 0 & -\cos\alpha_1 & -T_c\sin\alpha_1 & 0 \\ 0 & 0 & 0 & -d_1(L'\cos\alpha_1 - D\sin\alpha_1) & 0 \\ \sin(\alpha_2-\Theta) & \sin(\alpha_2+\Theta) & 0 & 0 & 0 \\ -\cos(\alpha_2-\Theta) & -\cos(\alpha_2+\Theta) & 0 & 0 & \begin{pmatrix} +T_b\cos(\alpha_2+\Theta) \\ -T_a\cos(\alpha_2-\Theta) \end{pmatrix} \\ \frac{c}{2}\cos\Theta & -\frac{c}{2}\cos\Theta & 0 & 0 & \begin{pmatrix} T_b\sin(\alpha_2+\Theta) \\ -T_a\sin(\alpha_2-\Theta) \end{pmatrix} \end{bmatrix} \begin{bmatrix} \nabla T_a \\ \nabla T_b \\ \nabla T_c \\ \bar{\theta}_1 \\ \bar{\theta}_2 \end{bmatrix}$$

. . . . . 4.2

where $L' = (m_1 + m_2)g - L$ and ∇X_{S_1} .... ∇M_{S_2} are the incremental changes in the force and moment components measured along the Ox and Oz axes.

As the column vector $\{\nabla T_a$ .... $\bar{\theta}_1, \bar{\theta}_2\}$ contains only the generalised displacements $\bar{\theta}_1$ and $\bar{\theta}_2$, it is sufficient to determine only ∇M_{S_1} and ∇M_{S_2} corresponding to these. The forces ∇X_{S_1}, ∇Z_{S_1}, ∇X_{S_2}, ∇Z_{S_2} may then be set to zero.

Therefore

$$\begin{bmatrix} 0 \\ 0 \end{bmatrix} = \begin{bmatrix} \sin(\alpha_2-\Theta), & \sin(\alpha_2+\Theta) \\ -\cos(\alpha_2-\Theta), & -\cos(\alpha_2+\Theta) \end{bmatrix} \begin{bmatrix} \nabla T_a \\ \nabla T_b \end{bmatrix} + \begin{bmatrix} 0, & (T_b\cos(\alpha_2+\Theta) - T_a\cos(\alpha_2-\Theta)) \\ 0, & (T_b\sin(\alpha_2+\Theta) - T_a\sin(\alpha_2-\Theta)) \end{bmatrix} \begin{bmatrix} \overline{\theta}_1 \\ \overline{\theta}_2 \end{bmatrix} \quad . . 4.3$$

$$\text{and } \begin{bmatrix} \nabla M_{S_1} \\ \nabla M_{S_2} \end{bmatrix} = \begin{bmatrix} 0 & , & 0 \\ \frac{c}{2}\cos\Theta, & - & \frac{c}{2}\cos\Theta \end{bmatrix} \begin{bmatrix} \nabla T_a \\ \nabla T_b \end{bmatrix} + \begin{bmatrix} -d_1(L'\cos\alpha_1 - D\sin\alpha_1), & 0 \\ 0 & , & 0 \end{bmatrix} \begin{bmatrix} \overline{\theta}_1 \\ \overline{\theta}_2 \end{bmatrix} \quad . . 4.4$$

Elimination of $\{\nabla T_a, \nabla T_b\}$ between equations 4.3 and 4.4 gives on simplification

$$\begin{bmatrix} \nabla M_{S_1} \\ \nabla M_{S_2} \end{bmatrix} = \begin{bmatrix} -d_1 \sec\alpha_1 \{(m_1+m_2)g-L\}, & 0 \\ 0 & -d_2\{(m_2g-L)\cos\alpha_2 + D\sin\alpha_2\} \end{bmatrix} \begin{bmatrix} \overline{\theta}_1 \\ \overline{\theta}_2 \end{bmatrix} \quad . . 4.5$$

Finally $[T_S]'\{\nabla X_{S_1}, \nabla Z_{S_1}, \nabla M_{S_1}, \nabla X_{S_2}, \nabla Z_{S_2}, \nabla M_{S_2}\}$

$= [T_S]'\{0, 0, \nabla M_{S_1}, 0, 0, \nabla M_{S_2}\} = \{\nabla \overline{M}_{S_1}, \nabla \overline{M}_{S_2}\}$

where the bar indicates the moments are in the same frame of reference as the co-ordinates $\overline{\theta}_1$ and $\overline{\theta}_2$.

As a result,

$$[T_S]'[\Delta F_S] = \begin{bmatrix} -d_1 \sec\alpha_1 \{(m_1+m_2)g-L\}, & 0 \\ 0 & -d_2\{(m_2g-L)\cos\alpha_2 + D\sin\alpha_2\} \end{bmatrix} \begin{bmatrix} \overline{\theta}_1 \\ \overline{\theta}_2 \end{bmatrix} \quad . . 4.6$$

Before the general equation 3.10 is reduced to its final form for the single strop configuration, two simplifications are now made. Whilst the pallet (m_2) has a moment of inertia $B_2 = m_2k_1^2$ (where k_1 is the radius of gyration about the

Oy_2 axis), the moment of inertia ($\bar{B}_1$) of the lifting hook (m_1) is assumed to be small enough to be neglected. Also because 'wind' axes have been adopted for the steady state condition, the resultant components of velocity of both masses along their corresponding axes are $U_1 = U_2 = V$ and $W_1 = W_2 = 0$.

It can now be shown with $[T_S]$ and $[T_S]'[\Delta F_S]$ substituted in the general longitudinal equation 3.10, the resulting non-dimensional equation is

$$[\underline{A}_S]\,[\ddot{\theta}] + [\underline{B}_S]\,[\dot{\theta}] + [\underline{C}_S] = 0 \qquad \ldots\ldots 4.7$$

where $\underline{A}_{S_{11}} = \frac{1}{\mu_1}\left(\frac{m_1 + m_2}{m_2}\right)\left(\frac{d_1}{d_2}\right)^2$, $\underline{A}_{S_{12}} = \underline{A}_{S_{21}} = \frac{d_1}{d_2}\,\frac{\cos(\alpha_2 - \alpha_1)}{\mu_1}$

$$\underline{A}_{S_{22}} = \frac{1}{\mu_1}\left\{1 + \left(\frac{k_1}{d_2}\right)^2\right\}$$

$$\underline{B}_{S_{11}} = -\left(\frac{d_1}{d_2}\right)^2 \frac{1}{\mu_1}\left\{\cos\alpha_1(\cos\alpha_1 . x_u + \sin\alpha_1 . z_u) + \sin\alpha_1(\cos\alpha_1 . x_w + \sin\alpha_1 . z_w)\right\}$$

$$\underline{B}_{S_{12}} = -\frac{d_1}{d_2}\cdot\frac{1}{\mu_1}\left\{\begin{array}{l}\cos\alpha_2(\cos\alpha_1 . x_u + \sin\alpha_1 . z_u) + \sin\alpha_2(\cos\alpha_1 . x_w + \sin\alpha_1 . z_w) \\ -\frac{c}{d_2}(\cos\alpha_1 . x_q + \sin\alpha_1 . z_q)\end{array}\right.$$

$$\underline{B}_{S_{21}} = -\frac{d_1}{d_2}\cdot\frac{1}{\mu_1}\left\{\begin{array}{l}\cos\alpha_1(\cos\alpha_2 . x_u + \sin\alpha_2 . z_u) + \sin\alpha_1(\cos\alpha_2 . x_w + \sin\alpha_2 . z_w) \\ -\frac{c}{d_2}(\cos\alpha_1 . m_u + \sin\alpha_1 . m_w)\end{array}\right.$$

$$\underline{B}_{S_{22}} = -\frac{1}{\mu_1}\left\{\begin{array}{l}\cos\alpha_2(\cos\alpha_2.x_u+\sin\alpha_2.z_u)+\sin\alpha_2(\cos\alpha_2 x_w+\sin\alpha_2.z_w)\\ +\left(\frac{c}{d_2}\right)^2 m_q + \frac{c}{d_2}\left(\cos\alpha_2(m_u + x_q) + \sin\alpha_2(m_w + z_q)\right)\end{array}\right\}$$

$$\underline{C}_{S_{11}} = \frac{d_1}{d_2}\left\{\frac{(m_1 + m_2) - \frac{L}{g}}{m_2 F}\right\}\mu_1 \sec\alpha_1$$

$$\underline{C}_{S_{12}} = -\frac{1}{2}\frac{d_1}{d_2}\left(\cos\alpha_1.x_\theta + \sin\alpha_1.z_\theta\right) \qquad \underline{C}_{S_{21}} = 0$$

$$\underline{C}_{S_{22}} = \frac{\mu_1}{F}\frac{\cos\alpha_2}{m_2.g}\left\{m_2 g - L + \tan\alpha_2.D\right\} - \frac{1}{2}\left\{\cos\alpha_2.x_\theta + \frac{c}{d_2}.m_\theta + \sin\alpha_2.z_\theta\right\}$$

and x_u .... m_q are the non-dimensionalised aerodynamic derivatives.

4.2 The Twin Strop (Bifilar) Configuration

From a consideration of the twin strop configuration given in fig. 3.2, it is apparent that identical schematic representations of both the single and twin strop configurations can be made. Therefore the required longitudinal equations of motion for the bifilar configuration are given by equation 4.7.

4.3 The Trapezoidal Configuration

The trapezoidal suspension arrangement shown in fig. 3.3 can, for these symmetric considerations, be adequately represented by fig. 4.2. The upper strops remain the same, but the four lower strops are substituted with two strops of lengths d_2 and d_3. These are assumed to support the pallet on its

plane of symmetry from the lifting bar. The strops d_2 and d_3 are always considered of unequal length such that a wind off incidence of α_2 is impressed on the pallet.

4.3.1 The Transformation Matrix

In the equilibrium position the axes Oxz_1 and Oxz_2 are considered as 'wind' axes. Therefore in the disturbed position it can be shown (with x_1, z_1, x_2, z_2, measured along the new position of the axes and ignoring second order terms) that

$$\begin{bmatrix} x_1 \\ z_1 \\ \theta_1 \\ x_2 \\ z_2 \\ \theta_2 \end{bmatrix} = \begin{bmatrix} d_1 \cos\alpha_1, & 0 \\ d_1 \sin\alpha_1, & 0 \\ 0, & 0 \\ d_1 \cos\alpha_1, & G \\ d_1 \sin\alpha_1, & H \\ 0 & 1 \end{bmatrix} \begin{bmatrix} \bar{\theta}_1 \\ \bar{\theta}_2 \end{bmatrix}, \quad [T_{S_1}] = \begin{bmatrix} -W_1 & 0 \\ U_1 & 0 \\ 0 & 0 \\ 0 & -W_2 \\ 0 & U_2 \\ 0 & 0 \end{bmatrix}$$

$$[\theta] = [T_S][\bar{\theta}], \quad [\dot{\theta}] = [T_S][\dot{\bar{\theta}}] + [T_{S_1}][\bar{\theta}] \text{ and } [\ddot{\theta}] = [T_S][\ddot{\bar{\theta}}] + [T_{S_1}][\dot{\bar{\theta}}] \quad \ldots 4.8$$

where, for example,

$$x_2 = d_1 \sin(\alpha_1 + \bar{\theta}_2) - d_1 \sin(\alpha_1 - \bar{\theta}_1 + \bar{\theta}_2) + \frac{1}{2}\left\{\begin{matrix} d_1 \cos\Theta\, \bar{\theta}_{21} + d_3 \cos\Phi\, \bar{\theta}_{22} \\ + d_2 \sin\Theta \left(\frac{\bar{\theta}_{21}}{2}\right)^2 - d_3 \sin\Phi \left(\frac{\bar{\theta}_{22}}{2}\right)^2 \end{matrix}\right\}$$

$$= d_1 \cos\alpha_1\, \bar{\theta}_1 + G\bar{\theta}_2 + \text{second order terms}$$

$$G = \frac{d_2 \cos\Theta A + d_3 \cos\Phi B}{2}, \qquad H = \frac{d_3 \sin\Phi B - d_2 \sin\Theta A}{2}$$

$$A = \frac{\bar{\theta}_{21}}{\bar{\theta}_2} = \frac{c \cos(\alpha_2 - \Phi)}{d_2 \sin(\Phi + \Theta)} \quad \text{and} \quad B = \frac{\bar{\theta}_{22}}{\bar{\theta}_2} = \frac{c \cos(\alpha_2 + \Theta)}{d_3 \sin(\Phi + \Theta)}$$

when second and higher order terms are neglected.

4.3.2. The Constraining Forces and Moments

The structural constraining forces and moments denoted by $[T_S]'[\Delta F_S]$ in equation 3.10 are similar to those given in section 4.1.2 because they consist only of gravitational and steady state aerodynamic terms. They are also similarly derived on the $\bar{\theta}_1$, $\bar{\theta}_2$ frame of reference using the usual displacement method. Hence with the aid of fig. 4.2 it can be shown, for example, that

$$\nabla X_{S_2} = -(T_a + \nabla T_a)\sin(\Theta + \bar{\theta}_{21}) + (T_b + \nabla T_b)\sin(\Phi - \bar{\theta}_{22}) + T_a \sin\Theta - T_b \sin\Phi$$
$$= -\sin\Theta \nabla T_a + \sin\Phi \nabla T_b - \{T_b \cos\Phi B + T_a \cos\Theta A\}\bar{\theta}_2 + \text{second order terms.}$$

In the complete linear form

$$\begin{bmatrix} \nabla X_{S_1} \\ \nabla Z_{S_1} \\ \nabla M_{S_1} \\ \nabla X_{S_2} \\ \nabla Z_{S_2} \\ \nabla M_{S_2} \end{bmatrix} = \begin{bmatrix} 0 & 0 & \sin\alpha_1 & \sin\alpha_1 & -(T_c + T_d)\cos\alpha_1 & 0 \\ 0 & 0 & -\cos\alpha_1 & -\cos\alpha_1 & -(T_c + T_d)\sin\alpha_1 & 0 \\ d_1\sin(\alpha_1+\Theta) & d_1\sin(\alpha_1-\Phi) & 0 & 0 & -d_1\begin{Bmatrix} m_1 g\cos\alpha_1 \\ +T_a\cos(\alpha_1+\Theta) \\ +T_b\cos(\alpha_1-\Phi) \end{Bmatrix} & \begin{Bmatrix} T_a\cos(\alpha_1+\Theta).Ad_1 \\ +T_b\cos(\alpha_1-\Phi)Bd_1 \end{Bmatrix} \\ -\sin\Theta & \sin\Phi & 0 & 0 & 0 & -\begin{Bmatrix} T_b\cos\Phi.B \\ +T_a\cos\Theta.A \end{Bmatrix} \\ -\cos\Theta & -\cos\Phi & 0 & 0 & 0 & \begin{Bmatrix} T_a\sin\Theta.A \\ -T_b\sin\Phi.B \end{Bmatrix} \\ \frac{c}{2}\cos(\Theta+\alpha_2) & -\frac{c}{2}\cos(\Phi-\alpha_2) & 0 & 0 & 0 & \frac{c}{2}\begin{Bmatrix} T_a\sin(\Theta+\alpha_2)(1-A) \\ +T_b\sin(\Phi-\alpha_2)(1-B) \end{Bmatrix} \end{bmatrix} \begin{bmatrix} \nabla T_a \\ \nabla T_b \\ \nabla T_c \\ \nabla T_d \\ \bar{\theta}_1 \\ \bar{\theta}_2 \end{bmatrix}$$

. . . . . 4.9

Hence proceeding in the manner shown in section 4.1.2. we obtain

$$[T_S]'[\Delta F_S] = \begin{bmatrix} -d_1\{(m_1 + m_2)g-L\}\sec\alpha_1 & 0 \\ 0 & \frac{c}{2}\begin{Bmatrix} T_a\sin(\Theta+\alpha_2)(1-A) + T_b\sin(\Phi-\alpha_2)(1-B) \\ +\cos(\Theta+\alpha_2)J - \cos(\Phi-\alpha_2)K \end{Bmatrix} \end{bmatrix} \begin{bmatrix} \dot{\bar{\theta}}_1 \\ \dot{\bar{\theta}}_2 \end{bmatrix}$$

. . . . . 4.10

where $T_a = \left\{\dfrac{\cos\alpha_2\ (m_2.g-L) + \sin\alpha_2.D}{2} - \dfrac{M}{c}\right\}\sec(\Theta + \alpha_2)$

$T_b = \left\{\dfrac{\cos\alpha_2\ (m_2\ g-L) + \sin\alpha_2.D}{2} + \dfrac{M}{c}\right\}\sec(\Phi - \alpha_2)$

$$J = \frac{1}{\sin(\Theta+\Phi)} \{-T_b.B - T_a.A \cos(\Phi+\Theta)\}$$

$$K = \frac{1}{\sin(\Theta+\Phi)} \{-T_b.B \cos(\Phi+\Theta) - T_a.A\}$$

With 'wind' axes chosen for the two sets of axes Oxz_1 and Oxz_2, $U_1 = U_2 = V$ and $W_1 = W_2 = 0$. Also the moment of inertia of the pallet about the Oy_2 axis is given by $\bar{B}_2 = m_2 k_1^2$, whilst $\bar{B}_1$ is not required because of the structural constraint imposed on the lifting bar m_1. Therefore on the substitution of equations 4.8 and 4.10 into the general equations 3.10, the final non-dimensionalised longitudinal equations for the trapezoidal configuration are given by

$$[\underline{A}_S] [\ddot{\bar{\theta}}] + [\underline{B}_S] [\dot{\bar{\theta}}] + [\underline{C}_S] [\bar{\theta}] = 0 \quad \ldots\ldots\ldots\ldots\ldots\ldots\ldots\ldots 4.11$$

where $\underline{A}S_{11} = \left(\frac{d_1}{d_2}\right)^2 \left(\frac{m_1 + m_2}{m_2}\right) \frac{1}{\mu_1}$, $\underline{A}S_{12} = \underline{A}S_{21} = \frac{d_1}{d_2^2 \mu_1} \{\cos \alpha_1.G + \sin \alpha_1.H\}$

$$\underline{A}S_{22} = \frac{1}{d_2^2 \mu_1} \{(G^2 + H^2) + k_1^2\}$$

$$\underline{B}S_{11} = -\left(\frac{d_1}{d_2}\right)^2 \frac{1}{\mu_1} \{\cos \alpha_1 (\cos \alpha_1.x_u + \sin \alpha_1.z_u) + \sin \alpha_1 (\cos \alpha_1.x_w + \sin \alpha_1.z_w)\}$$

$$\underline{B}S_{12} = -\frac{d_1}{d_2^2 \mu_1} \left\{ \begin{array}{l} G (\cos \alpha_1.x_u + \sin \alpha_1.z_u) + H (\cos \alpha_1.x_w + \sin \alpha_1.z_w) \\ + c (\cos \alpha_1.x_q + \sin \alpha_1.z_q) \end{array} \right\}$$

$$\underline{B}S_{21} = -\frac{d_1}{d_2^{\,2}\mu_1}\{\cos\alpha_1\ (G.x_u + H.z_u + c.m_u) + \sin\alpha_1\ (G.x_w + H.z_w + c.m_w)\}$$

$$\underline{B}S_{22} = \frac{-1}{\mu_1 d_2^{\,2}}\left\{\begin{matrix} G\ (G.x_u + H.z_u + c.m_u) + H\ (G.x_w + H.z_w + c.m_w) \\ + c\ (G.x_q + H.z_q + c.m_q)\end{matrix}\right\}$$

$$\underline{C}S_{11} = \frac{d_1\ \sec\alpha_1\ \mu_1}{d_2\quad m_2\quad F}\left\{(m_1 + m_2) - \frac{L}{g}\right\}, \qquad \underline{C}S_{21} = 0$$

$$\underline{C}S_{12} = -\frac{d_1}{2d_2}\ \{\cos\alpha_1.x_\theta + \sin\alpha_1.z_\theta\}$$

$$\underline{C}S_{22} = -\frac{c}{2d_2\ F\ m_2 g}\left\{\begin{matrix} T_a \sin(\Theta+\alpha_2)\ (1-A) + T_b \sin(\Phi-\alpha_2)(1-B) \\ + \cos(\Theta+\alpha_2)J - \cos(\Phi-\alpha_2)K\end{matrix}\right\} -\frac{1}{2}\left\{G.x_\theta + H.z_\theta - \frac{c}{d_2}.m_\theta\right\}$$

Equations 4.7 and 4.11 are now in a form amenable to the stability investigations.

THE LATERAL COORDINATE SYSTEMS.

Single Strop Suspension.

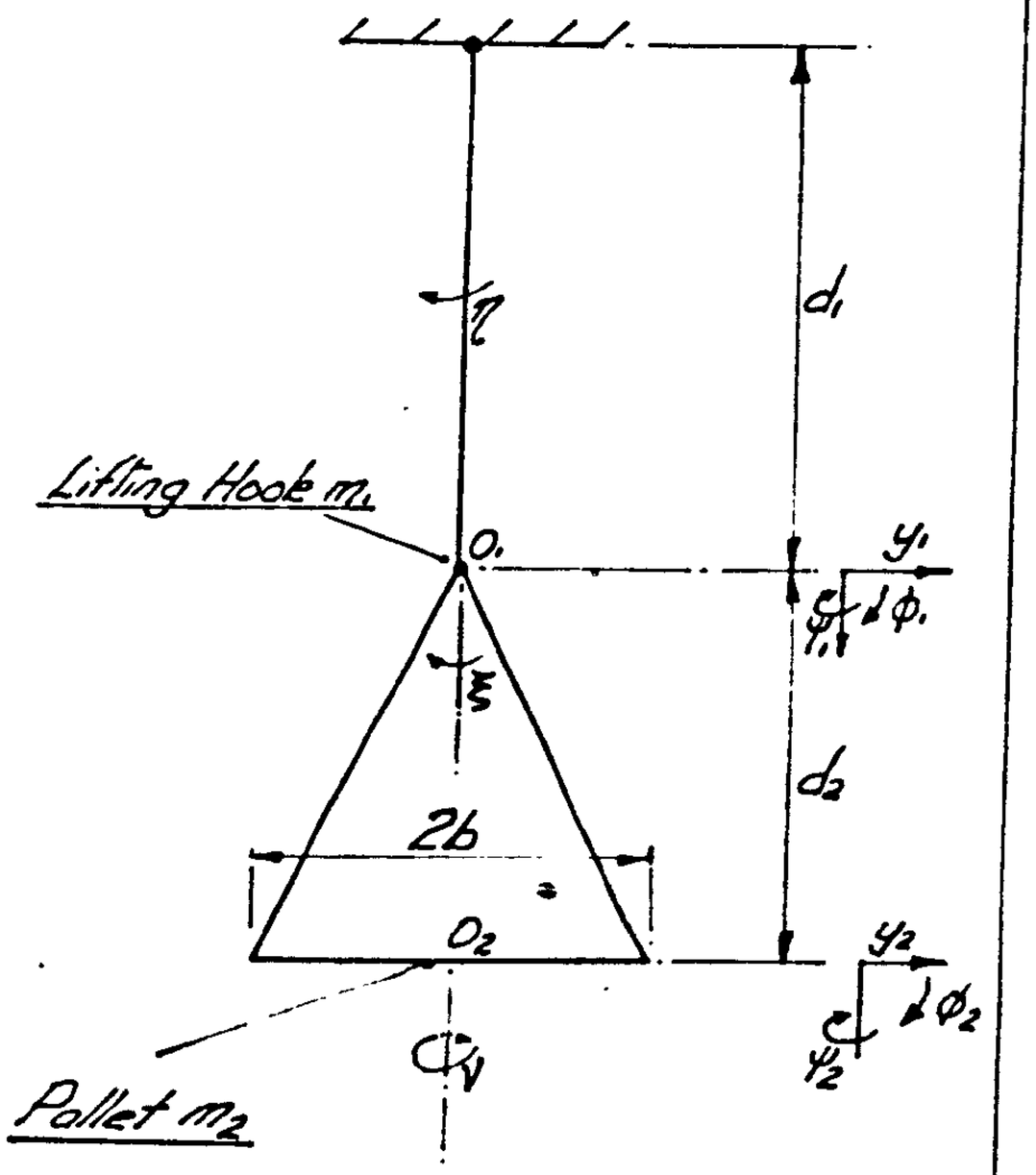

$d_1, \eta, y_1, \phi_1, \psi_1$ are measured on a plane defined by incidence α_1.

$d_2, \xi, \nu, y_2, \phi_2, \psi_2$ are measured on a plane defined by incidence α_2.

Fig. 5.1.

Twin Strop Suspension.

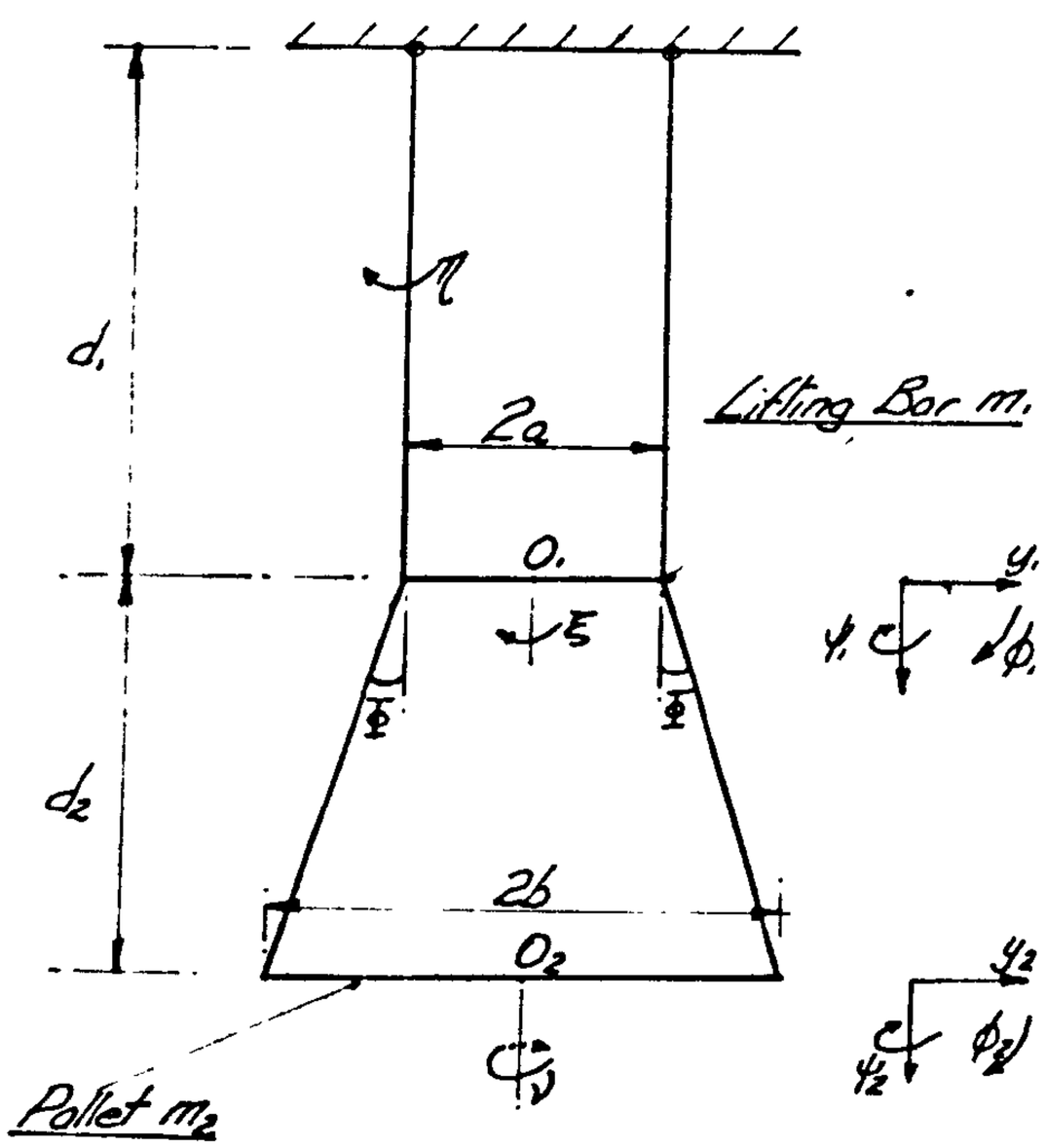

$d_1, \eta, y_1, \phi_1, \psi_1$ are measured on a plane defined by incidence α_1.

$d_2, \xi, \nu, y_2, \phi_2, \psi_2$ are measured on a plane defined by incidence α_2.

Fig. 5.2.

Trapezoidal Suspension

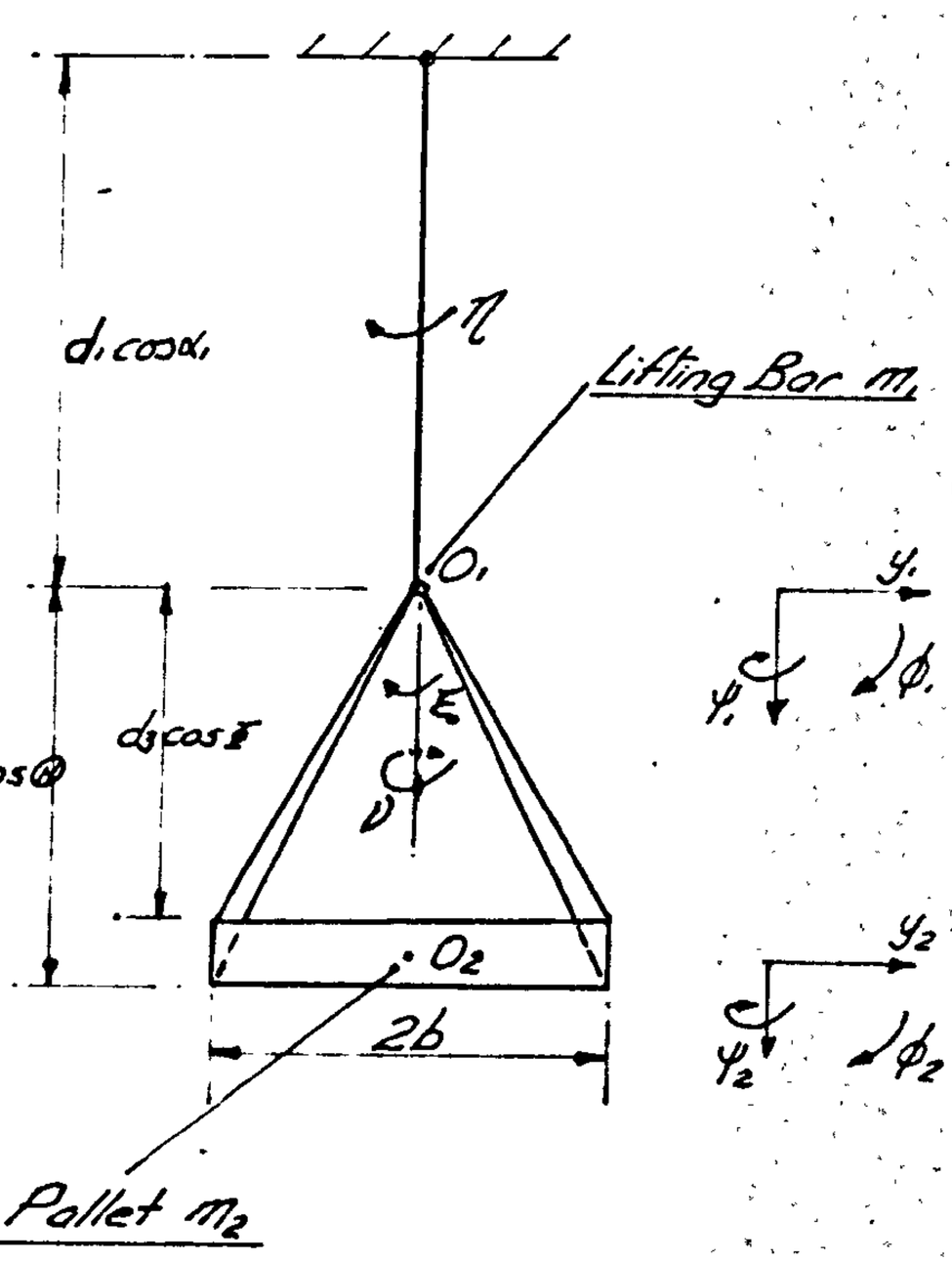

All coordinates are measured on vertical or horizontal axes

Fig 5.3.

CHAPTER 5

LATERAL ANALYSES OF THE STROP ARRANGEMENTS

The final lateral equations of motion for the single, twin and trapezoidal suspension arrangements can be developed by a similar technique to that adopted in section 4.0. With the general equation of motion given by equation 3.11, it is only necessary to determine the transformation matrices $[T_A]$, $[T_{A_1}]$ and the structural constraints matrix $[T_A]'[\Delta F_A]$ for each suspension arrangement.

5.1 The Single Strop Configuration

The single strop suspension arrangement of the pallet can be represented by the schematic diagram fig. 5.1. This is similar to the figure used for the longitudinal case, except the η, ξ, ν co-ordinate system is adopted when the arrangement is disturbed in its three degrees of freedom from the steady state (equilibrium) position.

5.1.1 The Transformation Matrix

In the equilibrium position, defined by the incidences α_1 and α_2, the axes $Oxyz_1$ and $Oxyz_2$ are set on the principal axes of the lifting hook (m_1) and pallet (m_2) respectively. Therefore in the disturbed position it can be shown that with the disturbances measured with respect to the principal axes and second order terms neglected,

$$\begin{bmatrix} y_1 \\ \phi_1 \\ \psi_1 \\ y_2 \\ \phi_2 \\ \psi_2 \end{bmatrix} = \begin{bmatrix} -d_1 & 0 & 0 \\ 1 & 0 & 0 \\ 0 & 0 & 0 \\ -d_1 & -d_2 & 0 \\ 0 & 1 & 0 \\ 0 & 0 & 1 \end{bmatrix} \begin{bmatrix} \eta \\ \xi \\ \nu \end{bmatrix}, \quad [T_{A_1}] = \begin{bmatrix} \underline{W}_1 & 0 & 0 \\ 0 & 0 & 0 \\ 0 & 0 & 0 \\ 0 & \underline{W}_2 & -\underline{U}_2 \\ 0 & 0 & 0 \\ 0 & 0 & 0 \end{bmatrix}$$

i.e. $[\bar{\phi}] = [T_A]\,[\bar{\eta}]$ 5.1

where, for example, $y_2 = -d_1 \sin \xi + d_1 \sin (\xi-\eta) - d_2 \sin \xi$

$= -d_1 \eta - d_2 \xi +$ second order terms

Also $[\dot{\bar{\phi}}] = [T_A]\,[\dot{\bar{\eta}}] + [T_{A_1}][\bar{\eta}]$ and $[\ddot{\bar{\phi}}] = [T_A][\ddot{\bar{\eta}}] + [T_{A_1}][\dot{\bar{\eta}}]$

5.1.2 The Constraining Forces and Moments

The structural constraining forces and moments acting on the lifting hook and the pallet when disturbed from the equilibrium position, are similar to those mentioned in section 4.1.2. Hence they consist of the changes in the gravitational forces and the steady state aerodynamic forces and moments when based on the y, ϕ, ψ frame of reference. However to comply with the general equation 3.11, it is necessary to obtain the constraining terms in the form of three moments based on the η, ξ, ν frame of reference (i.e. $[T_A]'[\Delta F_A]$). These moments are resolved about the helicopter attachment point and the lifting bar as rolling moments and about the pallet centre of gravity as a yawing moment.

As an alternative to the displacement method given in section 4.1.2, the energy method is used here. In this, the partial differential of the potential energy $\underset{\sim}{V}$ with respect to the co-ordinates η, ξ, ν can be shown to give the required $+[T_A]'[\Delta F_A]$ matrix (see ref. 2.2). We consider the change in potential energy of m_1 and m_2 and the steady state aerodynamic forces, for the incremental displacements η, ξ, ν. With the aid of fig. 5.1 and $\cos\eta \simeq 1 - \frac{\eta^2}{2}$ and $\sin\eta \simeq \eta$, it can be shown that

$$\underset{\sim}{V} = \{(m_1 + m_2)g-L\}\, d_1 \cos\alpha_1 .\frac{\eta^2}{2} + D\, d_1 \sin\alpha_1 \frac{\eta^2}{2}$$
$$+ (m_2g-L)\, d_2 \cos\alpha_2 .\frac{\xi^2}{2} + D\, d_2 \sin\alpha_2 \frac{\xi^2}{2} \quad \ldots\ldots\ldots 5.2$$

as it is necessary to consider the second order displacements only when obtaining a linear stiffness matrix. Thus

$$[T_A]'[\Delta F_A] = -\begin{bmatrix} \frac{\partial V}{\partial \eta} \\ \frac{\partial V}{\partial \xi} \\ \frac{\partial V}{\partial \nu} \end{bmatrix} = \begin{bmatrix} -\{(m_1+m_2)-L\}d_1\cos\alpha_1 \\ -D\, d_1 \sin\alpha_1 & 0 & 0 \\ 0 & -\{(m_2g-L)d_2\cos\alpha_2 \\ & +D\, d_2 \sin\alpha_2\} & 0 \\ 0 & 0 & 0 \end{bmatrix} \begin{bmatrix} \eta \\ \xi \\ \nu \end{bmatrix} \quad \ldots\ldots 5.3$$

Before the general equation 3.11 is reduced to its final form, certain simplifications can be made. As a result of principal axes being chosen for the single strop configuration, the product of inertia terms $\bar{E}_1$ and $\bar{E}_2$ are zero whilst $\underset{\sim}{U}_1 = V\cos\alpha_1$, $\underset{\sim}{U}_2 = V\cos\alpha_2$, $\underset{\sim}{W}_1 = -V\sin\alpha_1$ and $\underset{\sim}{W}_2 = -V\sin\alpha_2$.

Also $\bar{A}_2$ and $\bar{C}_2$ are denoted by $m_2k_4^2$ and $m_2k_2^2$ respectively and $\bar{C}_1$ is ignored because the lifting hook (m_1) is assumed not to displace in yaw. Finally $\bar{A}_1$ is assumed small enough to be neglected.

It can now be shown that with equations 5.2 and 5.3 substituted in equation 3.11, the following non-dimensional equation is formed.

$$[\underline{A}_A]\,[\ddot{\bar{\eta}}] + [\underline{B}_A]\,[\dot{\bar{\eta}}] + [\underline{C}_A]\,[\bar{\eta}] = 0 \quad \ldots\ldots\ldots 5.4$$

where $\underline{A}_{A_{11}} = \frac{1}{\mu_1}\left(\frac{d_1}{d_2}\right)^2\left(\frac{m_1+m_2}{m_2}\right)$, $\underline{A}_{A_{12}} = \underline{A}_{A_{21}} = \frac{d_1}{\mu_1 d_2}$,

$\underline{A}_{A_{13}} = \underline{A}_{A_{31}} = 0$, $\underline{A}_{A_{22}} = \frac{1}{\mu_1}\left\{1 + \left(\frac{k_4}{d_2}\right)^2\right\}$,

$\underline{A}_{A_{23}} = \underline{A}_{A_{32}} = 0$, $\underline{A}_{A_{33}} = \frac{1}{\mu_1}\left(\frac{k_2}{d_2}\right)^2$,

$\underline{B}_{A_{11}} = -\frac{d_1}{d_2}\left\{\frac{d_1}{d_2}\,\frac{y_v}{\mu_1}\right\}$, $\underline{B}_{A_{12}} = \frac{d_1}{d_2}\left\{\frac{2b}{d_2}\,\frac{y_p}{\mu_1} - \frac{y_v}{\mu_1}\right\}$

$\underline{B}_{A_{13}} = \frac{d_1}{d_2}\left\{\frac{2b}{d_2}\cdot\frac{y_r}{\mu_1}\right\}$, $\underline{B}_{A_{21}} = \frac{d_1}{\mu_1 d_2}\left\{\frac{2bl_v}{d_2} - y_v\right\}$

$\underline{B}_{A_{22}} = \frac{1}{\mu_1}\left\{\frac{2b}{d_2}\,(y_p+l_v) - y_v - \frac{4b^2}{d_2^2}\cdot l_p\right\}$

$\underline{B}_{A_{23}} = \frac{2b}{d_2\mu_1}\left\{y_r - \frac{2bl_r}{d_2}\right\}$

$\underline{B}_{A_{31}} = \frac{d_1}{d_2^2}\cdot\frac{2b}{\mu_1}\,n_v$, $\underline{B}_{A_{32}} = \frac{2b}{\mu_1 d_2}\left\{n_v - \frac{2b}{d_2}\,n_p\right\}$, $\underline{B}_{A_{33}} = \frac{-4b^2}{\mu_1 d_2^2}\,n_r$,

$\underline{C}_{A_{11}} = \frac{d_1}{d_2}\,\frac{\mu_1}{F\cdot m_2}\left\{\left(m_1+m_2-\frac{L}{g}\right)\cos\alpha_1 + \frac{D}{g}\,\sin\alpha_1\right\}$, $\underline{C}_{A_{12}} = \frac{d_1}{2d_2}\cdot y_\phi$,

$\underline{C}_{A_{13}} = \frac{d_1}{2d_2}\,y_\psi$, $\underline{C}_{A_{21}} = \underline{C}_{A_{31}} = 0$

$\underline{C}_{A_{22}} = \frac{\mu_1}{F\cdot m_2}\left\{(m_2-\frac{L}{g})\cos\alpha_2 + \frac{D}{g}\,\sin\alpha_2\right\} + \frac{y_\phi}{2} - \frac{b}{d_2}\,l_\phi$,

$\underline{C}_{A_{23}} = \frac{y_\psi}{2} - \frac{b}{2}\,l_\psi$, $\underline{C}_{A_{32}} = -\frac{b}{d_2}\,n_\phi$, $\underline{C}_{A_{33}} = -\frac{b}{d_2}\,n_\psi$.

5.2 The Twin Strop Configuration

The twin strop arrangement can be represented as shown in fig. 5.2. The two upper strops remain the same, but the four lower strops are simply reduced to two strops mounted on the plane of symmetry of the pallet. This representation is adequate because there is no relative movement in yaw (about an axis normal to the surface of the pallet) between the lifting bar and the pallet. Hence the configuration will have three lateral degrees of freedom as shown in fig. 5.2.

5.2.1 The Transformation Matrix

In the equilibrium position, the $Oxyz_1$ and $Oxyz_2$ axes are set on the principal axes of both masses. Again the upper and lower strops are set at incidences α_1 and α_2 respectively. In the disturbed state, the position of the twin strop arrangement is defined by the co-ordinates η, ξ, ν or y_1, ϕ_1, ψ_1, y_2, ϕ_2, ψ_2. The linear relationship between these co-ordinates is given by

$$\begin{bmatrix} y_1 \\ \phi_1 \\ \psi_1 \\ y_2 \\ \phi_2 \\ \psi_2 \end{bmatrix} = \begin{bmatrix} -d_1 & 0 & 0 \\ 0 & 0 & 0 \\ 0 & 0 & \sec(\alpha_2 - \alpha_1) \\ -d_1 & -d_2 & -d_2 \tan(\alpha_2 - \alpha_1) \\ 0 & +\frac{d_2}{b}\tan\Phi & \tan(\alpha_2 - \alpha_1) \\ 0 & 0 & 1 \end{bmatrix} \begin{bmatrix} \eta \\ \xi \\ \nu \end{bmatrix}$$

i.e. $[\bar{\phi}] = [T_A]\,[\bar{\eta}]$ 5.5

Furthermore it can be shown that

$$[T_{A_1}] = \begin{bmatrix} 0 & 0 & -\underline{U}_1 \sec(\alpha_2-\alpha_1) \\ 0 & 0 & 0 \\ 0 & 0 & 0 \\ 0 & \underline{W}_2 \frac{d_2}{b} \tan\Phi & \underline{W}_2 \tan(\alpha_2-\alpha_1) - \underline{U}_2 \\ 0 & 0 & 0 \\ 0 & 0 & 0 \end{bmatrix}$$

Also $[\dot{\overline{\phi}}] = [T_A]\,[\dot{\overline{\eta}}] + [T_{A_1}]\,[\overline{\eta}]$

and $[\ddot{\overline{\phi}}] = [T_A]\,[\ddot{\overline{\eta}}] + [T_{A_1}]\,[\dot{\overline{\eta}}]$

5.2.2 The Structural Constraining Forces and Moments

The energy method, shown previously in section 5.1.2, is again adopted to obtain the incremental constraining moments due to the displacements η, ξ, ν. Therefore with the aid of fig. 5.2 we find

the potential energy $\underset{\sim}{V} = \{(m_1 + m_2)-L\}\, d_1 \cos\alpha_1 \frac{\eta^2}{2}$

$$+ (m_2 g-L)\, d_2 \sec^2\Phi \cos\alpha_2 \left[1 - \frac{d_2 \sin^2\Phi \tan\Phi}{b}\right] \frac{\xi^2}{2}$$

$$+ \{(m_1 + m_2)g-L\} \frac{a^2}{d_1} \sec^2(\alpha_2 - \alpha_1) \sec\alpha_1 \frac{\nu^2}{2}$$

$$+ \{(m_2 g-L)\cos\alpha_2 + D\sin\alpha_2\}\, d_2 \tan^2(\alpha_2 - \alpha_1) \frac{\nu^2}{2} \quad \ldots 5.6$$

Hence

$$[T_A]'[\Delta F_A] = -\begin{bmatrix} \frac{\partial V}{\partial \eta} \\ \frac{\partial V}{\partial \xi} \\ \frac{\partial V}{\partial \nu} \end{bmatrix} = \begin{bmatrix} -\{(m_1+m_2)-L\} d_1 \cos\alpha_1 & 0 & 0 \\ 0 & -\left\{\frac{(m_2 g-L) d_2 \sec^2\Phi \cos\alpha_2 x}{1 - d_2 \sin^2\Phi \tan\Phi / b}\right\} & 0 \\ 0 & 0 & -\{(m_1+m_2)g-L\}\frac{a^2}{d_1}\sec^2(\alpha_2-\alpha_1)\sec\alpha_1 \\ & & -\{(m_2 g-L)\cos\alpha_2 + D\sin\alpha_2\} d_2 \tan^2(\alpha_2-\alpha_1) \end{bmatrix} \begin{bmatrix} \eta \\ \xi \\ \nu \end{bmatrix}$$

$$\ldots 5.7$$

With principal axes chosen for this lateral analysis, $\bar{E}_1$ and $\bar{E}_2$ are zero, together with $U_1 = V \cos \alpha_1$, $U_2 = V \cos \alpha_2$, $W_1 = - V \sin \alpha_1$ and $W_2 = - V \sin \alpha_2$. $\bar{C}_1$, $\bar{C}_2$ and $\bar{A}_2$ are also denoted by $m_1 k_3^2$, $m_2 k_2^2$ and $m_2 k_4^2$ respectively. The substitution of equations 5.6 and 5.7 into equation 3.11 can now be shown to give the following non-dimensional equation

$$[\underline{A}_A] [\ddot{\overline{\eta}}] + [\underline{B}_A] [\dot{\overline{\eta}}] + [\underline{C}_A] [\overline{\eta}] = 0 \quad \ldots\ldots\ldots\ldots\ldots\ldots\ldots\ldots \quad 5.8$$

where $\underline{A}_{A_{11}} = \left(\frac{d_1}{d_2}\right)^2 \frac{1}{\mu_1} \left(\frac{m_1 + m_2}{m_2}\right)$, $\underline{A}_{A_{12}} = \underline{A}_{A_{21}} = \left(\frac{d_1}{d_2}\right) \frac{1}{\mu_1}$,

$\underline{A}_{A_{13}} = \underline{A}_{A_{31}} = \frac{1}{\mu_1} \left(\frac{d_1}{d_2}\right) \tan (\alpha_2 - \alpha_1)$, $\underline{A}_{A_{22}} = \frac{1}{\mu_1} \left\{1 + \left(\frac{k_4}{b}\right)^2 \tan \Phi\right\}$,

$\underline{A}_{A_{23}} = \underline{A}_{A_{32}} = \frac{1}{\mu_1} \left\{\tan (\alpha_2 - \alpha_1) + \frac{k_4^2}{b d_2} \tan (\alpha_2 - \alpha_1) \tan \Phi\right\}$,

$\underline{A}_{A_{33}} = \frac{1}{\mu_1} \left\{\tan^2 (\alpha_2 - \alpha_1) \left(1 + \left(\frac{k_4}{d_2}\right)^2\right) + \left(\frac{k_2}{d_2}\right)^2 + \left(\frac{m_1}{m_2}\right) \left(\frac{k_3}{d_2}\right)^2 \sec^2 (\alpha_2 - \alpha_1)\right\}$,

$\underline{B}_{A_{11}} = -\left(\frac{d_1}{d_2}\right)^2 \frac{y_V}{\mu_1}$, $B_{A_{12}} = \left(\frac{d_1}{d_2}\right) \frac{1}{\mu_1} \left(2 \tan \Phi\, y_p - y_V\right)$,

$\underline{B}_{A_{13}} = \left(\frac{d_1}{d_2}\right)\left\{\frac{1}{\mu_1} \frac{2b}{d_2}(y_r + \tan(\alpha_2 - \alpha_1) y_p) - \tan(\alpha_2 - \alpha_1) y_V\right\}$

$\underline{B}_{A_{21}} = \left(\frac{d_1}{d_2}\right)\frac{1}{\mu_1} \left\{2 \tan \Phi\, l_V - y_V\right\}$, $\underline{B}_{A_{22}} = \frac{\tan \Phi}{\mu_1} \left(2 (y_p + l_V) - 4 \tan \Phi\, l_p - y_V\right)$

$$\underline{B}_{A_{23}} = -\frac{1}{\mu_1}\left\{\begin{array}{l}\tan(\alpha_2-\alpha_1)\left(\frac{4b}{d_2}\tan\Phi\, l_p - 2\tan\Phi\, l_V + y_V - \frac{2b}{d_2}\, y_p\right)\\ +\frac{2b}{d_2}\left(2\tan\Phi\, l_r - y_r\right)\end{array}\right\}$$

$$\underline{B}_{A_{31}} = \frac{2b\, d_1}{\mu_1 d_2^{\,2}}\left\{\tan(\alpha_2-\alpha_1)\, l_V + n_V\right\} - \frac{d_1}{\mu_1 d_2}\tan(\alpha_2-\alpha_1)\, y_V,$$

$$\underline{B}_{A_{32}} = \frac{1}{\mu_1}\left\{\begin{array}{l}\tan(\alpha_2-\alpha_1)\left(\frac{2b}{d_2}\, l_V - y_V - \frac{4b}{d_2}\tan\Phi\, l_p + 2\tan\Phi\, y_p\right)\\ -\frac{2b}{d_2}\left(2\tan\Phi\, n_p - n_V\right)\end{array}\right\}$$

$$\underline{B}_{A_{33}} = -\frac{1}{\mu_1}\left\{\begin{array}{l}\tan(\alpha_2-\alpha_1)\left(\frac{4b^2}{d_2^{\,2}}(n_p+l_r) - \frac{2b}{d_2}(n_V+y_r)\right) + \frac{4b^2}{d_2^{\,2}}\, n_r\\ +\tan^2(\alpha_2-\alpha_1)\left(y_V + \frac{4b^2}{d_2^{\,2}}\, l_p - 2b\,(l_V+y_p)\right)\end{array}\right\}$$

$$\underline{C}_{A_{11}} = \left\{(m_1+m_2) - \frac{L}{g}\right\}\frac{d_1}{d_2}\,\frac{\sec\alpha_1}{m_2}\,\frac{\mu_1}{F}, \qquad \underline{C}_{A_{12}} = \frac{d_1}{2b}\tan\Phi\, y_\phi,$$

$$\underline{C}_{A_{13}} = \frac{d_1}{2d_2}\left\{\tan(\alpha_2-\alpha_1)\, y_\phi + y_\psi\right\}, \qquad \underline{C}_{A_{21}} = \underline{C}_{A_{31}} = 0,$$

$$\underline{C}_{A_{22}} = \left\{1 - \frac{d_2}{b}\sin^2\Phi\tan\Phi\right\}\sec^2\Phi\,\frac{\mu_1}{F}\left\{\left(1 - \frac{L}{m_2 g}\right)(\cos\alpha_2 + \sin\alpha_2\tan\alpha_1) + \frac{m_1}{m_2}\sin\alpha_2\tan\alpha_1\right\},$$

$$+\frac{d_2}{b}\tan\Phi\left\{\frac{y_\phi}{2} - \tan\Phi\, l_\phi\right\}$$

$$\underline{C}_{A_{23}} = -\tan(\alpha_2 - \alpha_1)\left\{\tan\Phi\, l_\phi - \frac{y_\phi}{2}\right\} - \tan\Phi\, l_\psi + \frac{y_\psi}{2},$$

$$\underline{C}_{A_{32}} = \tan\Phi\left\{\frac{d_2}{2b}\, y_\phi \tan(\alpha_2 - \alpha_1) - n_\phi - \tan(\alpha_2 - \alpha_1)\, l_\phi\right\},$$

$$\underline{C}_{A_{33}} = \frac{\mu_1}{m_2 F}\left\{(m_1 + m_2 - \frac{L}{g})\sec^2(\alpha_2-\alpha_1)\sec\alpha_1 \frac{a^2}{d_1 d_2} + \left((m_2 - \frac{L}{g})\cos\alpha_2 + \frac{D}{g}\sin\alpha_2\right)\tan^2(\alpha_2-\alpha_1)\right\}$$

$$+ \tan^2(\alpha_2-\alpha_1)\left\{\frac{y_\phi}{2} - \frac{b}{d_2}\, l_\phi\right\} - \tan(\alpha_2-\alpha_1)\left\{\frac{b}{d_2}\left(n_\phi + l_\psi\right) + \frac{y_\psi}{2}\right\} - \frac{b}{d_2}\, n_\psi .$$

5.3 The Trapezoidal Configuration

The trapezoidal suspension arrangement of the pallet can, for lateral considerations, be adequately represented by two strops in the lower arrangement, whilst the two upper strops remain unaltered (see fig. 5.3). These two lower strops, of unequal lengths d_2 and d_3, are assumed to be mounted on the pallet mid-chord line. Hence the arrangement has three lateral degrees of freedom η, ξ and ν as shown in fig. 5.3.

5.3.1 The Transformation Matrix

The two sets of axes $Oxyz_1$ and $Cxyz_2$ are conveniently set on wind axes for the equilibrium position of m_1 and m_2, i.e. the lifting bar and pallet respectively. This is because the nature of the constraints allow a yawing degree of freedom about a vertical axis and a rolling degree of freedom about a horizontal axis for the pallet. Hence the aerodynamic forces are more conveniently represented on the wind axes of the pallet.

With the system now disturbed from the steady state position (denoted by α_1 and α_2 in the longitudinal plane), the deviations can be given by y_1, ϕ_1 ... ψ_2 or η, ξ, ν as shown in fig. 5.3. The linear relationship between the two sets of co-ordinates is then given by:-

$$\begin{bmatrix} y_1 \\ \phi_1 \\ \psi_1 \\ y_2 \\ \phi_2 \\ \psi_2 \end{bmatrix} = \begin{bmatrix} -d_1 \cos\alpha_1 & 0 & 0 \\ 1 & 0 & 0 \\ 0 & 0 & 1 \\ -d_1 \cos\alpha_1 & P & Q \\ 0 & 1 & 0 \\ 0 & 0 & 1 \end{bmatrix} \begin{bmatrix} \eta \\ \xi \\ \nu \end{bmatrix} \quad \text{and} \quad [T_{A_1}] = \begin{bmatrix} \underline{W}_1 & 0 & -\underline{U}_1 \\ 0 & 0 & 0 \\ 0 & 0 & 0 \\ 0 & \underline{W}_2 & -\underline{U}_2 \\ 0 & 0 & 0 \\ 0 & 0 & 0 \end{bmatrix}$$

where $P = \dfrac{-d_2 \cos\Theta - d_3 \cos\Phi}{2}$ and $Q = d_2 \sin\Theta + a - \dfrac{c}{2}\cos\alpha_2$

$$[\overline{\phi}] = [T_A]\,[\overline{\eta}] \quad \ldots\ldots\ldots\ldots\ldots\ldots\ldots\ldots\ldots\ldots\ldots\ldots\ldots\ldots\ldots\ldots\ldots\ldots 5.9$$

Also $[\dot{\overline{\phi}}] = [T_A]\,[\dot{\overline{\eta}}] + [T_{A_1}]\,[\overline{\eta}]$ and $[\ddot{\overline{\phi}}] = [T_A]\,[\ddot{\overline{\eta}}] + [T_{A_1}]\,[\dot{\overline{\eta}}]$

5.3.2 The Constraining Forces and Moments

By means of the energy method, the incremental change in the constraining moments due to the disturbances η, ξ, ν can now be obtained. With the aid of fig. 5.3 it can be shown that

Potential energy $\underset{\sim}{V} = \left\{(m_1 + m_2)\ g - L\right\} d_1 \cos\alpha_1 \frac{\eta^2}{2} - \frac{P}{2}(m_2 g - L)\frac{\xi^2}{2}$

$$+\left\{\left((m_1 + m_2)\ g - L\right)\cos\alpha_1 \frac{a^2}{d_1} + D\left(\sin\alpha_1 \frac{a^2}{d_1} - Q\right)\right\}\frac{\nu^2}{2} \quad \ldots\ 5.10$$

Hence in the usual manner, it can be shown that

$$[T_A]'[\Delta F_A] = -\begin{bmatrix} \frac{\partial V}{\partial \eta} \\ \frac{\partial V}{\partial \xi} \\ \frac{\partial V}{\partial \nu} \end{bmatrix} = \begin{bmatrix} -\left\{(m_1+m_2)g-L\right\}d_1\cos\alpha_1, & 0, & 0 \\ 0, & -(m_2 g - L)P, & 0 \\ 0, & 0, & -\left\{(m_1+m_2)g-L\right\}\cos\alpha_1 \frac{a^2}{d_1} \\ & & + D\left\{\sin\alpha_1 \frac{a^2}{d_1} - Q\right\} \end{bmatrix} \begin{bmatrix} \eta \\ \xi \\ \nu \end{bmatrix}$$

$\ldots\ 5.11$

Before the stiffness, damping and inertia terms are grouped together, certain terms need to be defined. For instance, with wind axes chosen for the lateral equations, $\underline{W}_1 = \underline{W}_2 = 0$ and $\underline{U}_1 = \underline{U}_2 = V$. Also the product of inertia term $\bar{E}_2$ is found to equal $\frac{m_2 \sin 2\alpha_2}{24}[c^2 - d^2]$. $\bar{E}_1$ is zero because the $Oxyz_1$ axes are principal and wind axes in the equilibrium position. Finally $\bar{C}_1$, $\bar{A}_2$ and $\bar{C}_2$ are denoted in the usual manner by $m_1 k_3^2$, $m_2 k_4^2$ and $m_2 k_2^2$ respectively.

The lateral equations for the trapezoidal configuration can now be presented in non-dimensionalised form as follows:-

$$[\underline{A}_A]\,[\ddot{\overline{\eta}}] + [\underline{B}_A]\,[\dot{\overline{\eta}}] + [\underline{C}_A]\,[\overline{\eta}] = 0 \quad \ldots\ldots\ldots\ldots\ldots\ldots\ldots\ldots 5.12$$

where $\underline{A}_{A_{11}} = \left(\frac{d_1}{d_2}\right)^2 \frac{1}{\mu_1}\left(\frac{m_1 + m_2}{m_2}\right)\cos^2\alpha_1$, $\underline{A}_{A_{12}} = \underline{A}_{A_{21}} = \frac{-d_1 P}{d_2{}^2\mu_1}\cos\alpha_1$,

$$\underline{A}_{A_{13}} = \underline{A}_{A_{31}} = -\frac{Q\,d_1\cos\alpha_1}{d_2{}^2\mu_1}, \qquad \underline{A}_{A_{22}} = \frac{P^2 + k_4{}^2}{\mu_1 d_2{}^2},$$

$$\underline{A}_{A_{23}} = \underline{A}_{A_{32}} = \frac{1}{d_2{}^2\mu_1}\left\{PQ - \frac{\sin 2\alpha_2.(c^2-d^2)}{24}\right\}, \qquad \underline{A}_{A_{33}} = \frac{1}{d_2{}^2\mu_1}\left\{k_3{}^2 + k_2{}^2 + Q^2\right\},$$

$$\underline{B}_{A_{11}} = -\left(\frac{d_1}{d_2}\right)^2 \frac{\cos^2\alpha_1}{\mu_1}\,y_v, \qquad \underline{B}_{A_{12}} = +\frac{d_1}{\mu_1 d_2{}^2}\left\{P\cos\alpha_1\,y_v + 2b\cos\alpha_1\,y_p\right\},$$

$$\underline{B}_{A_{13}} = \frac{d_1}{d_2{}^2\mu_1}\cos\alpha_1\left\{Qy_v + 2by_r\right\}$$

$$\underline{B}_{A_{21}} = \frac{d_1\cos\alpha_1}{d_2{}^2\mu_1}\left\{Py_v + 2bl_v\right\}, \qquad \underline{B}_{A_{22}} = -\frac{1}{d_2{}^2\mu_1}\left\{P^2y_v + 2bP\,(l_v+y_p) + 4b^2l_p\right\},$$

$$\underline{B}_{A_{23}} = -\frac{1}{d_2{}^2\mu_1}\left\{Q(Py_v + 2bl_v) + 2bPy_r + 4b^2l_r\right\},$$

$$\underline{B}_{A_{31}} = \frac{d_1}{d_2{}^2\mu_1}\cos\alpha_1\left\{Qy_v + 2bn_v\right\}, \qquad \underline{B}_{A_{32}} = -\frac{1}{d_2{}^2\mu_1}\left\{P(Qy_v+2bn_v) + 2bQy_p+4b^2n_p\right\},$$

$$\underline{B}_{A_{33}} = -\frac{1}{d_2{}^2\mu_1}\left\{Q(Qy_v + 2b\,(n_v + y_r) + 4b^2n_r\right\},$$

$$\underline{C}_{A_{11}} = \left\{(m_1 + m_2) - \frac{L}{g}\right\} \frac{d_1}{d_2} \frac{\cos \alpha_1 \, \mu_1}{m_2 F}, \qquad \underline{C}_{A_{12}} = \frac{d_1 \cos \alpha_1}{2d_2} y_\phi, \qquad \underline{C}_{A_{13}} = \frac{d_1 \cos \alpha_1}{2d_2} y_\psi,$$

$$\underline{C}_{A_{21}} = \underline{C}_{A_{31}} = 0, \qquad \underline{C}_{A_{22}} = - \frac{P y_\phi}{2d_2} - \frac{b l_\phi}{d_2} - \left(m_2 - \frac{L}{g}\right) \frac{\mu_1 P}{d_2 m_2 F},$$

$$\underline{C}_{A_{23}} = - \frac{P y_\psi}{2d_2} - \frac{b l_\psi}{d_2}, \qquad \underline{C}_{A_{32}} = - \frac{Q y_\phi}{2d_2} - \frac{b n_\phi}{d_2},$$

$$\underline{C}_{A_{33}} = \frac{\mu_1}{d_2 m_2 F} \left\{\left(m_1 + m_2 - \frac{L}{g}\right) \cos \alpha_1 . \frac{a^2}{d_1} + \frac{D}{g} \left(\sin \alpha_1 . \frac{a^2}{d_1} - Q\right)\right\} - \frac{Q y_\psi}{2d_2} - \frac{b n_\psi}{d_2}.$$

Equations 5.4, 5.8 and 5.12 are now in a form amenable to the stability investigations.

CHAPTER 6

THE GENERAL STABILITY INVESTIGATIONS

6.1 General Considerations

As a first approach to investigating the stability of a pallet suspended beneath a helicopter, it is necessary to 'linearise' the equations of motion (given in Chapters 3, 4 and 5) because they would be unmanageable in a non-linear form (except for simulation on an analogue computer). By using Liapunov's second method (see ref. 6.5) it may be proved, except for the case with a pure oscillatory solution, that when the 'linearised' system is 'asymptotically stable', i.e. the disturbed system tends towards the position of equilibrium as time increases, so is the non-linear system for small deviations. Alternatively, if the 'linearised' system is unstable, so then is the non-linear system.

A number of theoretical methods are available for investigating the stability of a linear system and a typical collection of these is given by Parks in ref. 6.1. From these methods a measure of the stability is obtained using a series of test functions, avoiding the task of finding the roots of the characteristic polynomial equation. In addition to the above 'stability criteria' techniques, the roots can be found and an examination of their real parts can be carried out to ascertain the nature of the motions.

On consideration of the two forms of investigation the latter method is found to be convenient, because, (a) the order of the characteristic polynomial is small and (b) with the roots for each mode of oscillation known, the modal form corresponding to each root can be found, together with the relative importance of the aerodynamic and other terms on the stability of the system. Therefore with the aid of an Elliot 503 digital computer, the latter technique is adopted for all the stability investigations. A brief outline of these investigations is now given and also a typical solution for a stability investigation is given in appendix 1.

In previous work, the non-dimensionalised linear equations of motion with constant coefficients are given in matrix form for the separated longitudinal and lateral motions. The longitudinal and lateral equations are based on the $\bar{\theta}_1$, $\bar{\theta}_2$ and η, ξ, ν respectively for the various suspension arrangements. As is normal with linear homogeneous second order differential equations with constant coefficients, solutions are assumed in the form:-

$\bar{\theta}_1 = k_1 e^{\lambda_S t}$ and $\bar{\theta}_2 = k_2 e^{\lambda_S t}$ for the longitudinal motions and

$\eta = k_3 e^{\lambda_A t}$, $\xi = k_4 e^{\lambda_A t}$ and $\nu = k_5 e^{\lambda_A t}$ for the lateral motions,

where k_1, k_2, k_3, k_4, k_5, λ_S and λ_A are constants. The non-dimensionalised equations can then be reduced to the general forms:

$$\begin{bmatrix} \underline{A}_{11}\lambda_S^2 + \underline{B}_{11}\lambda_S + \underline{C}_{11}, & \underline{A}_{12}\lambda_S^2 + \underline{B}_{12}\lambda_S + \underline{C}_{12} \\ \underline{A}_{21}\lambda_S^2 + \underline{B}_{21}\lambda_S + \underline{C}_{21}, & \underline{A}_{22}\lambda_S^2 + \underline{B}_{22}\lambda_S + \underline{C}_{22} \end{bmatrix} \begin{bmatrix} k_1 \\ k_2 \end{bmatrix} = 0$$

i.e. $[S_S]\,[k] = 0$ 6.1

for the longitudinal equations, and

$$\begin{bmatrix} \underline{A}_{11}\lambda_A^2+\underline{B}_{11}\lambda_A+\underline{C}_{11}, & \underline{A}_{12}\lambda_A^2+\underline{B}_{12}\lambda_A+\underline{C}_{12}, & \underline{A}_{13}\lambda_A^2+\underline{B}_{13}\lambda_A+\underline{C}_{13} \\ \underline{A}_{21}\lambda_A^2+\underline{B}_{21}\lambda_A+\underline{C}_{21}, & \underline{A}_{22}\lambda_A^2+\underline{B}_{22}\lambda_A+\underline{C}_{22}, & \underline{A}_{23}\lambda_A^2+\underline{B}_{23}\lambda_A+\underline{C}_{23} \\ \underline{A}_{31}\lambda_A^2+\underline{B}_{31}\lambda_A+\underline{C}_{31}, & \underline{A}_{32}\lambda_A^2+\underline{B}_{32}\lambda_A+\underline{C}_{32}, & \underline{A}_{33}\lambda_A^2+\underline{B}_{33}\lambda_A+\underline{C}_{33} \end{bmatrix} \begin{bmatrix} k_3 \\ k_4 \\ k_5 \end{bmatrix} = 0$$

i.e. $[S_A]\,[k] = 0$ 6.2

for the lateral equations.

Except for the trivial case where $k_1, k_2 = 0$ and $k_3, k_4, k_5 = 0$; which is of no particular interest, the scalar equations comprising 6.1 and 6.2 are incompatible unless $|S_S|$ and $|S_A| = 0$. Therefore the expansion of these determinants gives characteristic polynomial equations of the usual form

$$\begin{aligned} p_4\lambda_S^4 + p_3\lambda_S^3 + p_2\lambda_S^2 + p_1\lambda_S + p_0 = 0 \\ p_6\lambda_A^6 + p_5\lambda_A^5 + p_4\lambda_A^4 + p_3\lambda_A^3 + p_2\lambda_A^2 + p_1\lambda_A + p_0 = 0 \end{aligned} \quad \text{. . } 6.3$$

for the longitudinal and lateral equations respectively.

The coefficients p contain various combinations of the $\underline{A}$, $\underline{B}$ and $\underline{C}$ terms given in equation 6.1 and 6.2. Because of the effort involved in determining the p terms and the roots of both polynomial equations manually, a number of ALGOL programmes (for use on an Elliot 503 computer) are developed. These are applicable to the separate longitudinal and lateral equations of the single, twin and trapezoidal suspension arrangements.

As anticipated, almost all the roots are found to be complex conjugate pairs $r \pm is$ (on using the Bairstow method to obtain the roots of the polynomials), where r and s are the non-dimensional damping factor and frequency parameter respectively. As a result, sinusoidal oscillations with increasing or decreasing amplitudes are evident in each mode. The modes corresponding to each of the roots are determined in the following manner (see ref. 2.2).

With, for example, the root $\lambda_S = r_i \pm is_i$ substituted in equation 6.1 (with $|S_S| = 0$) the adjoint matrix $adj[S_S]$ is obtained giving a 2 x 2 matrix containing two columns of terms. The vector q_i corresponding to the root $r_i \pm is_i$ is then chosen proportional to a normalised non-vanishing column of $adj[S_S]$. By repeating this procedure with the remaining roots substituted in turn, a full set of modes is obtained.

The majority of derivative data required for the analytical work is difficult to obtain experimentally for the correct ranges of Strouhal and Reynolds numbers. Therefore theoretical methods (see chapter 7) are adopted to give values of certain derivatives. This unfortunately introduces errors into the analysis and it is therefore necessary to determine which derivatives have important effects on the stability of a system (i.e. on the damping factor terms).

Analogue simulation is a suitable means of examining the effects of derivative changes if, of course, the computer is sufficiently large to handle the equations of motion for either the longitudinal or lateral analyses. The analogue computer available was found, indeed, to be too small and an alternative analytical method was therefore sought.

A straightforward step by step method can be considered, whereby a derivative is varied and the changes of the damping factor (r_1, say) calculated. This would prove to be a rather laborious procedure for the many stability investigations undertaken in this research and is therefore not used. Instead, a method developed by Woodcock (see ref. 6.2) is used, this giving the rates of change of the roots with respect to a chosen parameter in the unsymmetric lambda matrices $[S_S]$ or $[S_A]$. (Other methods (see ref. 6.3 and 6.4) rely on the lambda matrices being symmetrical). This method is used to calculate the longitudinal and lateral stiffness and damping derivative effects on stability.

Consider, for example, the lambda matrix $S_S\ (r_1 + is_1)$. The adjoint matrix adj.$S_S\ (r_1 + is_1)$ can be shown as $\{q_S\}\ [p_S\ \ ]$ where $\{q_S\}$ is the normalised column eigenvector and $[p_S\ \ ]$ the corresponding row - both appropriate to the root $\lambda_S = r_1 + is_1$. It can then be shown, knowing p_S/S_S, $S_S q_S$ and $|S_S|$ are zero, that for a known λ_S and a variable parameter δ (i.e. a derivative value)

$$\frac{d\lambda_S}{d\delta} = \frac{-[p_S]\left[\frac{dA_S}{d\delta}.\lambda_S^2 + \frac{dB_S}{d\delta}\lambda_S + \frac{dC_S}{d\delta}\right][q_S]}{[p_S]\,[2A_S\lambda_S + B_S]\,[q_S]} \quad \ldots\ldots\ldots\ldots 6.4$$

A similar procedure is also carried out for the lateral equations of motion. In both cases $d\lambda/d\delta$ is calculated with δ taking each derivative value in turn, whilst the remaining derivatives are maintained constant. A more accurate prediction of the relative importance of each derivative can be made if $d\lambda^2/d\delta^2$ and higher derivatives are determined using the formulae given in ref. 6.2. However, since we require only qualitative results here, this procedure is not used.

In the investigations, an equal change is considered for each derivative in turn and an apparent change in a root (i.e. $r \pm is$) is obtained. The change in the root can only be accurate for small changes in the derivatives since, in most cases, the variation of $r +$ is with any derivative is non-linear. Details of these derivative effects for the unstable modes are given in chapter 13.

With the above facilities written into the ALGOL programmes for the longitudinal and lateral analyses, it is possible to obtain automatically the results for a combination of independent structural parameters. The independent structural parameters are α_2, m_1, m_2, d_1, d_2 and a for the single and twin strop configurations. For the trapezoidal configuration d_2 must be replaced by d_3.

For a completely automatic programme, it is necessary to have the derivative data in a form from which any derivative value can be obtained for a range of steady state incidences (α_2) of the pallet. This is accomplished using the least squares method to fit polynomial equations to the derivative data (see chapter 7.0).

The ALGOL programmes fall into two general groups because different techniques are required to evaluate the equilibrium positions of the three configurations. The single and twin strop equilibrium positions are easily obtained whilst the trapezoidal equilibrium position proves more difficult to ascertain.

6.2 Determination of the Positions of Equilibrium

6.2.1 The Single and Twin Strop Arrangements

With the aid of fig. 3.1 and 3.2 it can be seen that the steady state incidences (α_1 and α_2) are dependent on the aerodynamic forces (i.e. on V), the masses m_1 and m_2, the area of the pallet (2b x c) and the normal length d_2. If a steady forward velocity V is assumed initially, the incidence α_2 would have to be determined from a polynomial equation (assuming d_2, b and c known). The order of this equation would depend on the size of the polynomials representing the aerodynamic force coefficient C_L and C_D and ec (the distance of the centre of pressure measured from the pallet centre of

gravity). Therefore an alternative method is used whereby a value of α_2 is chosen. Because the derivative polynomial equations are based on α_2, together with the length ec, V can be determined from

$$V = \sqrt{\frac{2\, m_2 g\, d_2}{\rho S\left(\frac{C_D\, d_2 - C_L\, ec}{\tan \alpha_2} + C_L\, d_2 + C_D\, ec\right)}} \quad \ldots\ldots\ldots 6.5$$

Also it can be shown that

$$\alpha_1 = \tan^{-1}\left(\frac{C_D}{\frac{2\,(m_1 + m_2)g}{\rho V^2 S} - C_L}\right) \quad \ldots\ldots\ldots\ldots 6.6$$

Investigations into the stability of a pallet 12' span by 6' chord (i.e. A.R. = 2) are made for a practical range of the independent variables α_2, m_1, m_2, d_1, d_2, a. The α_2 range is limited however to pre-stall incidences (i.e. $\alpha_2 \leqslant 21^\circ$, where 21° is given in chapter 9 as the incidence at stall) because the aerodynamic forces are grossly non-linear at and above stall conditions. Therefore the values of the variables are taken as:-

α_2 = 0.25, 0.625, 1, 3, 5, 10, 15, 21°

m_1 = 0.5/g, 5.0/g, and 10.0/g slugs

m_2 = 50/g, 100/g, 200/g, 400/g, 600/g, 1000/g slugs

d_1 and d_2 = 25, 50, 100 ft.

a = 0, 3.0, 6.0 and 9.0 ft.

6.2.2 The Trapezoidal Arrangement

The equilibrium position of the trapezoidal configuration can be shown to depend on α_2 and V (independently), m_1, m_2 and d_3. Because similar difficulties to those in section 6.2.1 are encountered when attempting to calculate α_2, the only convenient method available is to choose α_2, d_3 and a for a constant pallet area (2b x c). It can then be shown that

$$\frac{1}{A'}\left\{\begin{matrix} D\ (c.\sin\alpha_2 + d_3\cos\Phi) \\ +\ (m_2g-L)(c.\cos\alpha_2-2a-d_3\sin\Phi)\end{matrix}\right\}(\cos\alpha_2+\sin\alpha_2\tan\Phi) = 0$$

$$+ 2a + d_3\sin\Phi - c\cos\alpha_2 - \tan\Phi(c\sin\alpha_2+d_3\cos\Phi) \quad \ldots 6.7$$

where $A' = (D\sin\alpha_2 - L\cos\alpha_2)(0.5-e) + 0.5\, m_2 g\cos\alpha_2$

With the aid of Newton's method and a sensible starting value of Φ, the correct value of Φ can be obtained from equation 6.7 by an iteration process included in the automatic ALGOL programme. It is then a straightforward procedure to obtain Θ and d_2 respectively from

$$\Theta = \tan^{-1}\left(\frac{c\cos\alpha_2 - 2a - d_3\sin\Phi}{c\sin\alpha_2 + d_3\cos\Phi}\right) \text{ and } d_2 = \frac{c\sin\alpha_2 + d_3\cos\Phi}{\cos\Theta}$$

$\ldots\ldots 6.8$

The equilibrium incidence α_1 can then be determined from equation 6.7 (which, of course, is applicable to all three configurations).

For a pallet size of 12' span by 6' chord, a range of independent variables (α_2, m_1, m_2 etc.) to those given in section 6.2.1 are used for the stability investigations.

However a is now chosen from 0.5, 1.5, 3.0 and 4.5 ft., d_3 replaces d_2 and V is included with the values 5, 10, 20, 40, 55, 75, 90 ft./sec.

Although Woodock's method (ref. 6.2) can be used to obtain the importance of d_1, d_2, m_1, m_2, etc. on the roots of the characteristic equations 6.3, the step by step method is used to provide more accurate results in view of the large variations in d_1, d_2, etc. studied here. These results are obtained, where necessary, in both numerical and graphical forms and a typical set of results is shown in chapter 12. Here the damping factors are plotted against forward velocity V for various combinations of the structural parameter and, whenever possible, plots are also given of critical velocity (i.e. when r = 0) against m_2. Furthermore, the relative importance of each derivative on the stability of a system is given.

CHAPTER 7

DETERMINATION OF THE AERODYNAMIC STABILITY DERIVATIVES

7.1 General

An accurate knowledge of the stiffness, damping and acceleration derivatives has proved to be the stumbling block to progress in the stability investigations. This is because research has not been carried out in the field of small aspect ratio flat rectangular plates. Furthermore, only a limited knowledge of derivatives is available for small aspect ratio rectangular wings and this is found to rely mainly on theoretical methods (i.e. lifting line or lifting surface theory), although recently a few experimental techniques have given reasonable results (see ref. 7.1).

The majority of aerodynamic derivatives are shown in refs. 7.1 and 7.2 to be generally dependent on Strouhal number, mean incidence and plan form and to a lesser extent on Reynolds' number, amplitude of oscillation and plate thickness. The art of determining most of these effects on the derivatives is still in its infancy and even now some of the derivatives are still estimated on quasi-static assumptions.

In aircraft stability work, some of the derivatives are determined on quasi-static assumptions even when the aircraft

is in unsteady motion. This is because the motion is usually considered to be in a Strouhal number range 0 - 0·1, where the changes in circulation around the disturbed aircraft are small and the trailing vortices are too weak to influence the aerodynamic forces appreciably (see ref. 2.1). Hence (as will be shown later for the pallet) some of the longitudinal and lateral stiffness and damping derivatives are obtained from static wind tunnel data on the aircraft (i.e. C_L, C_D, C_m, etc.)

Whilst these quasi-static assumptions are valid for a plate (in an unsteady motion) in the Strouhal number range 0 - 0·1, they are not considered applicable for values greater than 0·1. However, from the wind tunnel work (see chapter 11.0) it can be seen that a Strouhal number range 0·5 - 1·0 must be anticipated for the unsteady motions of the suspended pallet. Therefore it appears that quasi-static assumptions are open to criticism if used to determine the derivatives for the pallet in the present investigation.

Refs. 7.2 and 7.3 show by experimental and theoretical methods that for the non-dimensionalized damping derivative $m_{\dot{\theta}}$, based on fixed axes (known as m_q in the theory) and measured about the mid-chord line at zero incidence, quasi-static assumptions are valid for a rectangular plate or wing $\leq$ A.R.3 for the Strouhal number range 0 - 1·0. However, an increase of aspect ratio above three does bring about a

Strouhal number dependance for this particular derivative. These effects appear to be due t o the strength of the trailing vortices suppressing the flow separation over the wing of small aspect ratio. For the larger aspect ratio wing, this vortex strength is not adequate and separation occurs, the extent of the separation being dependent on the frequency of oscillation of the wing.

In addition to the constancy of $m_{\dot{\theta}}$ for a value of zero incidence, there is evidence (ref. 10.5) that extrapolated experimental values of $m_{\dot{\theta}}$ (fixed axis derivative) vary as much as 20% in a Strouhal number range 0 - 1·0 for mean incidences 8° and 10°. Similarly, there is a variation of at least 8% at zero incidence. (The state of the art of measuring derivatives is such that, at present, derivatives with a 20% error are acceptable in aircraft stability work).

Whilst mention is not made of the Z_{θ} derivative in chapter 10, it can be shown from the oscillatory experimental work (see ref. 10.5) for the correct Strouhal and Reynolds' number ranges, that this derivative is only 5% different to the quasi-static value obtained in chapter 9 for an incidence range 0 - 15°. Similar evidence for the other longitudinal derivatives (i.e. X_{θ}, M_{w}, etc.) for unsteady motions is not, however, available, although from available lateral derivative data, the stiffness and damping terms are not Strouhal

number dependent, even at high values of incidence.

Since only limited information is available on the majority of aerodynamic derivatives for small aspect ratio wings, quasi-static assumptions are made for certain derivatives. In addition, an extension of the lifting line theory is used to determine some of the lateral derivatives. (The greater accuracy of the lifting surface theory is not warranted here because the lifting line and lifting surface theories are both open to criticism at moderate incidences).

For those derivatives which are considered to be accurate on quasi-static assumptions, it is necessary to obtain static aerodynamic force and moment data for a rectangular flat plate of aspect ratio 2. Only a limited amount of data was available and it proved necessary, therefore, to carry out experimental work on the measurement of lift, drag and side forces in addition to pitching, rolling and yawing moments for a flat plate orientated in both incidence and yaw. Further details of this work are given in chapter 9.0.

From the dynamic experimental work carried out on the suspended model plate (see chapter 11), it was apparent that a longitudinal oscillatory instability occurred. This was thought to be due to a lack of rotary aerodynamic damping in the system, i.e. m_q was thought to be insufficiently large. A theoretical estimation of the m_q derivative was not

considered to be adequate and it was decided to obtain this derivative (together with z_q) from experimental oscillatory tests (see chapter 10.0). Because of the limited time available, it was not possible to determine other damping derivatives experimentally, although the above oscillatory apparatus was suitable for the measurement of the rotary lateral derivatives.

The stiffness, damping and acceleration derivatives are now discussed briefly with regard to their importance on the stability of the suspended pallet.

7.2 The Longitudinal Derivatives

7.2.1 The Stiffness Derivatives

The aerodynamic stiffness derivatives are shown in chapter 3.0 to consist of X_θ, Z_θ, and M_θ. These terms are obtained using the quasi-static approach because there is evidence that they are independent of Strouhal number. Reference 7.2 shows M_θ to be independent of Strouhal number (in the range 0 - 1·0) for zero incidence and small aspect ratio. Also it has previously been mentioned that Z_θ is only 5% different when determined from oscillatory tests or a quasi-static method. Hence from static wind tunnel tests (see chapters 9 and 12) carried out at the correct Reynolds' number, the forces X and Z and moment M are measured on wind axes for a range of incidence 0 - 45°. Because 'small

perturbation' theory is assumed in the previous analyses, it is possible to obtain the above derivatives for a mean incidence value. For example, if a graph of a load against incidence is plotted, then a number of local slopes of the curve can be obtained for corresponding values of incidence. These slopes are assumed to be linear at each point for small changes of incidence and therefore values of X_θ, Z_θ and M_θ are obtained from graphs of X, Z and M plotted against incidence (θ).

From an inspection of the X, Z and M curves against incidence (see chapter 12) it is apparent that the process of local linearization is valid only when severe changes of slope do not occur. Hence the above X_θ, Z_θ and M_θ values are only valid in the incidence range 0 - 21° (where 21° is found to be the stalling incidence) because drastic changes of slope do occur above this incidence, especially for the Z force (i.e. negative lift force). However, for a stability investigation of the suspended pallet at an equilibrium incidence between 0 - 21° the values of X_θ, Z_θ and M_θ derived on the above basis are valid.

7.2.2 The Damping Derivatives

The longitudinal damping derivatives are usually denoted by the linear and angular terms X_u, Z_u, M_u, X_w, Z_w, M_w and X_q, Z_q and M_q, as shown in chapter 3.0. These two groups are now

discussed separately in fuller detail.

The X_u .....M_w linear derivatives are usually obtained for aircraft stability work using the quasi-static assumptions. These assumptions are considered to be valid for the usual 'phugoid ' or 'short-period' motions since the Strouhal number is rarely greater than 0·1. It has been mentioned previously, however, that Strouhal numbers up to 1·0 are anticipated for the suspended pallet. Clearly, if quasi-static assumptions are to be made here, justification is required. Unfortunately, this is not possible because very little information is available on these damping derivatives for unsteady motions of finite plates or wings (A.R.2) about a mean incidence position. From ref. 7.4 it is suggested that X_u .....M_w derivatives are virtually independent of Strouhal number (in the range 0 - 0·1) for two dimensional theory. Since most derivatives are less sensitive to frequency effects in three-dimensional work, (ref. 2.1), it is reasonable to assume that the above derivatives (for the Strouhal number range 0 - 0·5*) are adequately determined with quasi-static theory for small values of mean incidence. This reasoning is supported by the work done to determine Z_θ (see section 7.2.1). Furthermore, quasi-static theory is also extended to higher value of mean incidence, although there is no information to support this procedure.

* *In the calculations described below, it is rare for the Strouhal Number to exceed 0·5.*

The linear damping derivatives can now be obtained in the usual manner, for example as described in ref. 2.1, where they are shown to depend on lift and drag coefficients and their corresponding rates of change with incidence. As a result, the linear damping derivatives are given in a non-dimensional form by

$$x_u = -C_D \qquad x_w = \frac{1}{2}\left(C_L - \frac{dC_D}{d\theta}\right)$$

$$z_u = -C_L \qquad z_w = -\frac{1}{2}\left(C_D + \frac{dC_L}{d\theta}\right) \quad \ldots\ldots 7.1$$

$$m_u = C_m \qquad m_w = \frac{1}{2}\frac{dC_m}{d\theta}$$

where the derivatives are based on the required wind axes. In a similar manner to that discussed in section 7.2.1., C_L, C_D, C_m, $\frac{dC_L}{d\theta}$, $\frac{dC_D}{d\theta}$ and $\frac{dC_m}{d\theta}$ can be obtained for various values of incidence (in the range 0 - 21°) from the static aerodynamic curves (see chapters 9 and 12). A plot of x_u, z_u, m_u, x_w, z_w and m_w can therefore be obtained against the mean incidence of the pallet. These are then in a form suitable for the longitudinal stability investigations discussed in chapter 6.0.

The non-dimensional rotary damping derivatives x_q, z_q and m_q are considered (for reasons mentioned previously) to be important in the longitudinal stability investigations of the suspended pallet. The experimental determination of these

derivatives is therefore necessary in order that accurate stability predictions may be made.

Existing information on the rotary damping derivatives for a rectangular wing shows the x_q derivative to be very small in comparison to the z_q derivative, even at stall conditions, and it is therefore neglected (see refs. 2.1 and 7.1). The z_q derivative is, however, thought to be important in the stability investigations and because previous z_q derivatives were determined assuming a uniform rate of angular velocity q (i.e. whirling arm technique - see refs. 7.5 and 7.6), it is necessary to obtain this term by the more accurate oscillatory technique.

The m_q derivative appears to have been well investigated (because of its importance in aircraft stability work), both experimentally and theoretically, for unsteady motions. However, the majority of this work is carried out at zero incidence. Because Strouhal number effects appear to occur at large incidences (ref. 10.5), it is necessary to obtain an accurate estimation of m_q for the correct Strouhal and Reynolds' numbers in the incidence range 0 - 21° (see chapter 6.0). Details of the experimental work on a freely oscillating flat plate are given in chapters 10 and 12.

7.2.3 The Acceleration Derivatives

The acceleration derivatives $X_{\dot{u}}$, $Z_{\dot{u}}$, $M_{\dot{u}}$, $X_{\dot{w}}$, $Z_{\dot{w}}$, $M_{\dot{w}}$, $X_{\dot{q}}$,

$Z_{\dot{q}}$ and $M_{\dot{q}}$ are assumed to be small for the pallet of aspect ratio 2. In this first treatment, these derivative terms are ignored as their effects on stability are also assumed to be small (see ref. 10.6). Except for the $M_{\dot{w}}$ derivative, the above derivatives are similarly assumed negligible in aircraft stability work. The $M_{\dot{w}}$ derivative is significant because "downwash lag" downstream of the wings induces lift at the tailplane, (for tailless aircraft $M_{\dot{w}}$ is thought to be negligible except at transonic speeds - see ref. 10.6). In the present application, the "downwash lag" across the chord of the plate is small and it is reasonable to assume $M_{\dot{w}}$ negligible for these low speed stability investigations. Further justification of this could be furnished, however, using the experimental technique given in ref. 7.7.

7.3 The Lateral Derivatives

7.3.1 The Stiffness Derivatives

The lateral stiffness derivatives consist of the following terms Y_ϕ, L_ϕ, N_ϕ, Y_ψ, L_ψ, N_ψ. For the lateral stability investigations, these are required on both wind and principal axes of the pallet. From the limited evidence available (see ref. 7.8), the general impression is that the derivatives are independent of Strouhal number (in the range 0 - 0.1) for incidences 0 - 30°. As there is no available evidence to the contrary for Strouhal numbers in excess of

0·12, the above derivatives are derived from static aerodynamic curves obtained from the wind tunnel tests as described in chapter 9.

In the wind tunnel tests side force (Y), rolling moment (L) and yawing moment (N) are measured on wind axes and the plate (A.R.2) can be orientated into various positions of combined incidence, θ, and yaw, ψ, (see sections 9.1 and 9.2). As a result it is necessary to transform the forces, moments and angular displacements onto both wind and principal axes of the pallet. This requires a considerable amount of manipulation of the static wind tunnel results. An ALGOL programme has been written in order to effect these transformations - details of which are given in appendices 3 and 4.

The derivatives based on principal axes are most suitable for the single and twin strop lateral stability investigations, whilst those based on wind axes are most suitable for the trapezoidal configurations. Both sets of derivative data are given in detail in chapter 12.

7.3.2 The Damping Derivatives

The lateral damping derivatives consist of the linear terms Y_v, L_v and N_v and the rotary terms Y_p, L_p, N_p, Y_r, L_r and N_r. Both sets are now considered separately because they are derived by different methods.

The Y_v, L_v and N_v are considered to have important

effects on the lateral stability of the pallet-strop arrangements considered here. A considerable amount of experimental and theoretical work has been carried out previously to obtain these derivatives, but satisfactory information is not available for a rectangular wing or flat plate of aspect ratio 2. However, it is apparent that Strouhal number effects are small in the incidence range 0 - 30° (see ref. 7.8). Therefore a quasi-static approach is made to obtain Y_v, L_v and N_v.

These derivatives with respect to sideslip velocity v are obtained simply from the static wind tunnel results given in chapter 12. For example, with the model plate yawed through an angle β on tunnel axes (such that the starboard tip moves forward), the wind velocity has a component V sin β (where $\beta = -\psi$) perpendicular to the plane of symmetry of the plate. However, with the plate assumed to move forward in the stationary air, this is equivalent to a velocity of sideslip v in the usual sense. With this procedure repeated for various angles of incidence (where forces and moments are measured at each incidence), Y_v, L_v and N_v are obtained for a range of incidences (α_2).

From chapter 9 it is apparent that the above yaw angle β followed by incidence α_2 cannot be set on the pallet because the plate arrangement allows only θ and ψ, in that order, to

be set on the principal axes of the plate. If, however, a displacement, ϕ, in roll is allowed to precede θ and ψ, the equivalent position of β and α_2 can be obtained. With the amounts of rotation known for ϕ, θ and ψ, it is then possible to transform the wind axes forces and moments Y, L, N to the correct principal axes of the plate. The Y_v, L_v and N_v derivatives can then be determined on principal axes for a range of mean incidences (α_2). These transformations are given in greater detail in appendix 3. Alternatively, Y_v, L_v and N_v are also required on wind axes and are obtained on the substitution of the above derivatives in a set of derived transformation equations given in appendix 4.

The rotary damping derivatives Y_p, L_p, N_p, Y_r, L_r and N_r have been investigated extensively in aircraft stability work. Although information is not available for a wing or flat plate of aspect ratio 2, definite conclusions on Strouhal number and incidence effects are available for wings of higher aspect ratio (see refs. 7.8 and 7.9). It is apparent, for wings approximating to a rectangular form, that Strouhal number effects are small (in the range 0 - 0·24) for an incidence range 0 - 20°. Therefore quasi-static estimations of the derivatives are considered to be adequate for these stability investigations.

The derivatives Y_p and Y_r for a wing are invariably

considered to be negligible in aircraft stability work. As there is no information available to the contrary, the same assumptions are made for the flat plate of aspect ratio 2.

Because of the limited time available, it was not possible to estimate the derivatives L_p, N_p, L_r and N_r by an oscillatory experimental method. Therefore a theoretical method is adopted to obtain these terms. From the experience of previous investigators it is assumed that the Lanchester - Prandtl theory of the finite aerofoil (lifting line theory) is adequate, at least for a first estimation of the derivatives. (The 'lifting surface' theory is not used because of the theoretical complications involved). Therefore an extension of the lifting line theory (with special reference to rectangular wings), developed by Lofts (ref. 7.11), is used to obtain an assessment of the L_p, N_p, L_r, N_r damping derivatives.

This method is considered valid for rectangular wings at small angles of incidence only, because the Fourier Series representation of circulation appears to break down at angles of incidence greater than 10° for the plate of aspect ratio 2. (See ref. 9.2). This is due to a strong vortex action at the ends of the plate.

Using Lofts' method it can be shown, after a great deal of simplification, that in a non-dimensional form

$$l_p = -0{\cdot}07 \qquad l_r = -0{\cdot}222\ C_L$$

$$n_p = -0{\cdot}01575\ C_L \qquad n_r = 0{\cdot}006\ C_L^2 - \frac{C_D}{3} \qquad \ldots\ldots\ 7.2$$

for small angles of incidence.

These terms are measured about the centre of pressure of the plate and based on wind axes. Therefore, using the static experimental results obtained in chapter 9 and a transformation matrix given in appendix 4, the derivatives are transformed to the principal axes of the plate. However, when required for the stability investigations of the trapezoidal configuration, the derivatives are simply transformed to wind axes and measured about the centre of gravity of the plate (see appendix 4).

A set of graphs derived from equation 7.2 is given in chapter 12 (based on both wind and principal axes) for an incidence range of 0 - 15°, even though the derivatives are assumed accurate only up to 10° incidence. Despite the inaccuracies incurred in the derivatives at 15° incidence, it is considered to be advantageous to have a larger field of stability investigation. If 'derivative importance' tests show a rotary damping derivative to be of great importance at this incidence, then, if necessary, other means for accurately deriving the term must be explored.

7.3.3 The Acceleration Derivatives

The lateral acceleration derivatives $Y_{\dot{v}}$, $L_{\dot{v}}$, $N_{\dot{v}}$, $Y_{\dot{p}}$, $L_{\dot{p}}$,

$N_p^{\cdot}$, $Y_r^{\cdot}$, $L_r^{\cdot}$, $N_r^{\cdot}$ are considered to be negligible in these stability investigations. These assumptions are substantiated by ref. 7.1 and are invariably made for aircraft stability investigations. Also, as far as is known, no theoretical work on such derivatives exists.

7.4 Curve Fitting the Derivative Data

To accomplish the use of low storage space in the computer when using the derivative data in the stability investigations, it is convenient to express a derivative in a general form whereby a value can be obtained automatically for any value of incidence in a given range. Furthermore, it is useful to express the static wind tunnel results in a form which will be suitable for transformation to the required stability derivatives (see section 7.3.1).

A number of methods are available to fit polynomials to data, i.e. power series, series of Chebyshev polynomials (see ref. 7.12). The least squares method is used here to fit a power series polynomial equation to the required data. This would appear to be more direct than the alternative methods, though some care must be exercised in its application.

At first the least squares method did not prove very successful because it was necessary to invert a badly

conditioned matrix (involving elements with extreme values of, say, $(10)^{20}$ and 1) of order up to 20. After a great deal of investigation, the accuracy of the inversion was improved (although not sufficiently) by using a "full pivotal" inversion method. In addition, the abscissa of each plot was transformed, for example, from the original $0<x<45^{\circ}$ to the range $-1<X<1$ using the simple equation $X = [2x - 45]/45$. This latter step led to good conditioning of the matrix to be inverted - indeed the range of the elements was reduced to about -20 - +20. With this final refinement, excellent curve fitting of all derivative data was achieved. Also, differentiation of a particular equation gave, on comparison with graphical differentiation, excellent results for such derivatives as $dC_{L/d\theta}$, obtained from the lift coefficient against incidence plot.

CHAPTER 8

DOWNWASH EFFECTS FROM THE HELICOPTER ROTOR

In the previous analyses on the pallet suspended beneath a helicopter, any 'effects' from the helicopter have been deliberately ignored. Whilst this is justified for the initial stability investigations, it is worthwhile to consider what effects the rotor downwash is likely to have. The effects of helicopter manoeuvres on the pallet stability are, however, beyond the scope of this research. A brief discussion is now given on the downwash from the rotor in both hovering and horizontal forward flight.

For most practical situations, the pallet is suspended between 25 ft. and 200 ft. below the helicopter and the suspension arrangement is attached at or near the centre of gravity of the helicopter. When the helicopter is hovering the pallet is directly beneath the rotor and the full downwash impinges on the pallet. At certain speeds of forward flight, however, the induced flow field moves away from the vicinity of the pallet. An approximate method is later used to illustrate this point.

The field of induced flow from the blades of a single rotor in hover is generally in the form of a truncated cone. A measure of this downwash is given by the induced velocity v_i through the rotor blades (normal to the tip-path plane).

However from simple momentum theory, this induced velocity increases twofold for a distance below the helicopter, equal to the rotor diameter when ground effects can be ignored. Reference 8.1 gives a good representation of this induced flow field (using an approximate theoretical method) for hovering and forward flight.

In most practical circumstances the ground effects cannot be ignored because, for example, the helicopter is rarely above 200 ft. when loading or unloading the pallet. It is then found that the induced flow field changes considerably from that discussed above. From the limited evidence available (reference 8.2 and 8.3) it can be reasonably concluded for the single rotor, that a low velocity region exists in the centre of the downwash field. As a result the downwash drag on the pallet is reduced at hover. In the full scale tests on the single strop suspension of the pallet it was apparent that the pallet remained stable whilst hovering near the ground.

There is less possibility of suspending a stable pallet beneath a tandem helicopter than a single rotor helicopter because there are two regions of small induced velocity below each rotor in hovering flight. Hence there might be a tendency for the pallet to oscillate between the two low velocity points and result in an unacceptable oscillation of the suspension arrangement.

A typical solution is now given to ascertain when the downwash effects on the pallet can be ignored in flight (ground effects are assumed negligible). Consider a single rotor Westland Whirlwind or Wessex helicopter with an average disc loading of 5.1 lb/ft^2 (aircraft weight + pallet weight/disc area) and a rotor diameter of 50 ft. It can now be shown (see reference 8.4) that the induced velocity of the air through the rotor (v_i) is equal to

$v_i = 1.2k \sqrt{\frac{P}{2\rho}}$ where P is the disc loading of 5.1 lb/ft^2

ρ is air density

and k is a factor dependent on the term $\frac{V}{\sqrt{P}}$. For an increase in the forward velocity V, k correspondingly reduces in value (see ref. 8.4).

In hovering flight therefore (where k = 1)

$$v_i = 1.2 \sqrt{\frac{5.1 \times 10^4}{2 \times 23.8}} = 39.3 \text{ ft/sec.}$$

In conjunction with ref. 8.1 the following table can be produced to give the angle (χ) of the induced flow field (with respect to a vertical axis) for a range of forward speeds V. This angle is approximately given by $\chi \simeq \tan^{-1} \left(\frac{V}{v_i}\right)$.

The Induced Flow Field Of A Typical Helicopter Rotor.

The Flow Field is obtained from ref. 8.1.

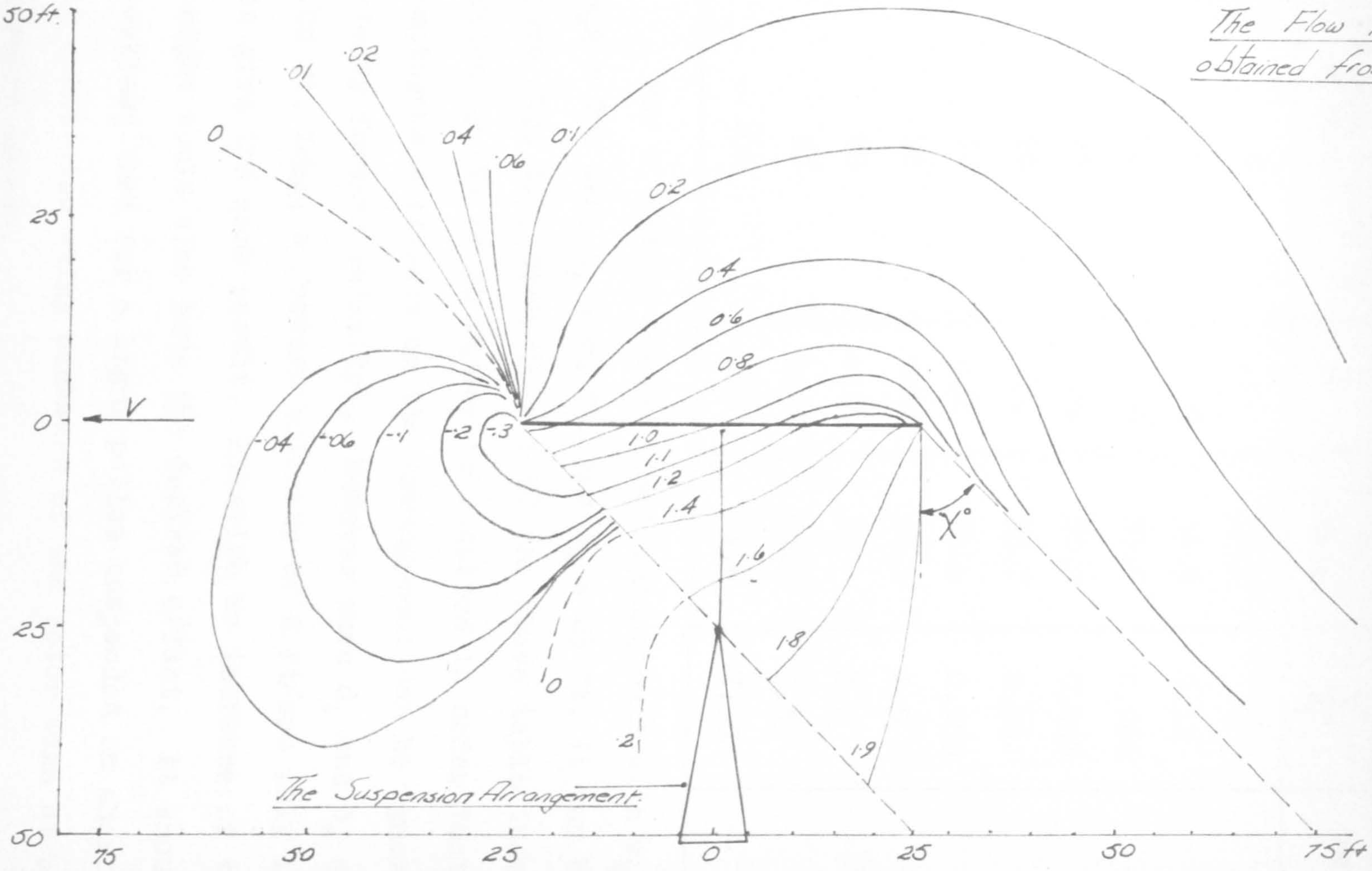

Rotor Diameter 50ft. Disc Loading 5·1 lb/ft^2 Horizontal Velocity 30 ft/sec.

0·6 denotes the induced velocity as a ratio of the induced velocity at the rotor (on the plane of symmetry of the rotor).

Fig. 8.1.

Forward Velocity V ft/sec	k	v_i ft/sec	$\frac{V}{v_i}$	$\tan^{-1}\left(\frac{V}{v_i}\right) = \chi^{o}$
0	1.0	39.3	0	0
5	0.98	38.5	0.13	7.4
10	0.96	37.6	0.266	14.9
15	0.94	36.9	0.408	22.2
20	0.91	35.7	0.56	29.3
30	0.8	31.4	0.955	43.7
40	0.68	26.7	1.5	56.4
60	0.51	20	3.0	71.6
80	0.38	14.9	5.35	79.4
100	0.32	12.6	7.95	82.8

For a typical single strop arrangement with $m_1 g$ = 5 lbs, $m_2 g$ = 200 lbs, d_1 = 25 ft. and d_2 = 25 ft. it can be shown (see fig. 8.1) with the aid of the above table that a minimum velocity (V) of 30 ft/sec is required in order that downwash impingement effects on the arrangement can be ignored (for a steady forward velocity). However when d_1 and d_2 are both 100 ft. long, a forward velocity of 2 ft/sec only is required to give the same result. Likewise an increase of the pallet weight would also have the desired effect. It should also be realised that for a light pallet suspended on short strops, it could also swing backward of the rotor wake at certain forward speeds.

From the brief discussions above it is apparent that the downwash impingement effects are important in the lower range of forward speeds of the helicopter. Whilst the full scale pallet is apparently stable near the ground (in full scale hover tests) it is difficult to judge whether it would remain stable for small forward speeds (presuming an intrinsically stable suspension arrangement of the pallet). Therefore an experimental study of downwash effects on a suspended pallet would be useful. If a stable suspension arrangement can at first be found, the inclusion of the downwash effects (from the experimental work) in the linearised analyses would then give a more adequate representation of the full scale flight conditions.

CHAPTER 9

THE WIND TUNNEL SIX COMPONENT BALANCE

In order that some of the longitudinal and lateral derivative data can be obtained for a rectangular plate of aspect ratio 2, an estimation must be made of the static and dynamic forces and moments acting on the plate when in certain positions of incidence and yaw. It was found, however, that very little previous work had been done for low aspect ratio plates, except for the usual measurements of lift, drag and pitching moment with incidence variation at zero yaw (see refs. 9.1 and 9.2). It has therefore proved necessary to carry out experimental work to obtain this data. Two separate pieces of apparatus were designed and manufactured. The first rig, explained in this chapter, was made to give adequate information required for forming both damping and stiffness derivatives x_u, z_w, x_θ, m_θ, y_ϕ, n_ψ, l_v, etc. The second rig (described in chapter 10) was designed solely to give the damping derivative m_q and z_q for a rectangular plate of aspect ratio 2.

9.1 Requirements

The purpose of the first rig is to facilitate the measurement of a full set of three static forces and three moments acting on a rigidly supported AR2 flat plate in a wind tunnel.

Therefore lift, drag and side forces, pitching, rolling and yawing moments should be obtainable for any orientation of the plate in the wind tunnel, and subsequently, quasi-static damping and stiffness derivatives, i.e. $x_w = \frac{1}{2}\left(C_L - \frac{dC_D}{d\theta}\right)$ etc. can easily be obtained.

To satisfy the geometrical and dynamical similarity between the full scale pallet and the model, the plate was manufactured on a $\frac{1}{8}$ scale, giving the dimensions 18" span, 9" chord and $\frac{3}{8}$" thickness and the Reynolds Number was 4.75×10^5 (i.e. 97 ft./sec. on the model and 12 ft./sec. on the full scale pallet). A 3' 6" diameter open jet closed circuit wind tunnel was used and it was found from experience that at wind speeds of 80 ft./sec. and 108 ft./sec. severe flow pulsations and vibrations of the tunnel structure occurred. However, these were not noticeable at a velocity of 88 ft./sec. To obtain a good degree of sensitivity in the measuring equipment, an intermediate velocity of 97 ft./sec. was therefore chosen.

Because the derivative data was required for both wind tunnel axes and plate body axes, it proved difficult at first to decide on what axes the apparatus should be designed. The wind tunnel axes were finally used because the majority of derivative data was required on these axes. Therefore, the corresponding forces and moments are read on mutually perpendicular wind axes, with their origin at the plate centre of gravity.

At this stage it is advisable to clarify the orientation of the plate with respect to each axes, because so often this is a point of argument in aircraft work (ref. 9.3). Usually the attitude of the plate in flight or in the wind tunnel is specified (w.r.t. earth axes) by imagining its normal axis OZ set initially in a vertical position OZ_o and its longitudinal axis OX set parallel to the wind direction OX_o. The plate is then given an angular displacement ψ about OZ_o, followed by θ about the new ('carried') position of the lateral body axis and finally by ϕ about the final position of the longitudinal axis OX, to give the disturbed position of the plate. However, because the suspended steady state position of the pallet is set at incidence to the direction of forward flight, a more appropriate system of rotations was used to specify the disturbed plate position. With the plate axes OZ and OX in the undisturbed positions OZ_o and OX_o, the plate is then given an angular displacement ϕ about the OX_o axis, followed by a θ rotation about the 'carried' OY body axis, followed finally by a rotation ψ about the 'carried' OZ axis (see fig. 9.1). With this system of rotations adopted in wind tunnel experimental work, it can be appreciated that it is necessary to consider only the latter two of the three rotations, since the ϕ rotation only rotates the vectors of the resultant wind axis forces and moments without altering their magnitudes.

The Angular Coordinates Of The Rigid Pallet Refereed To Fixed Earth Axes.

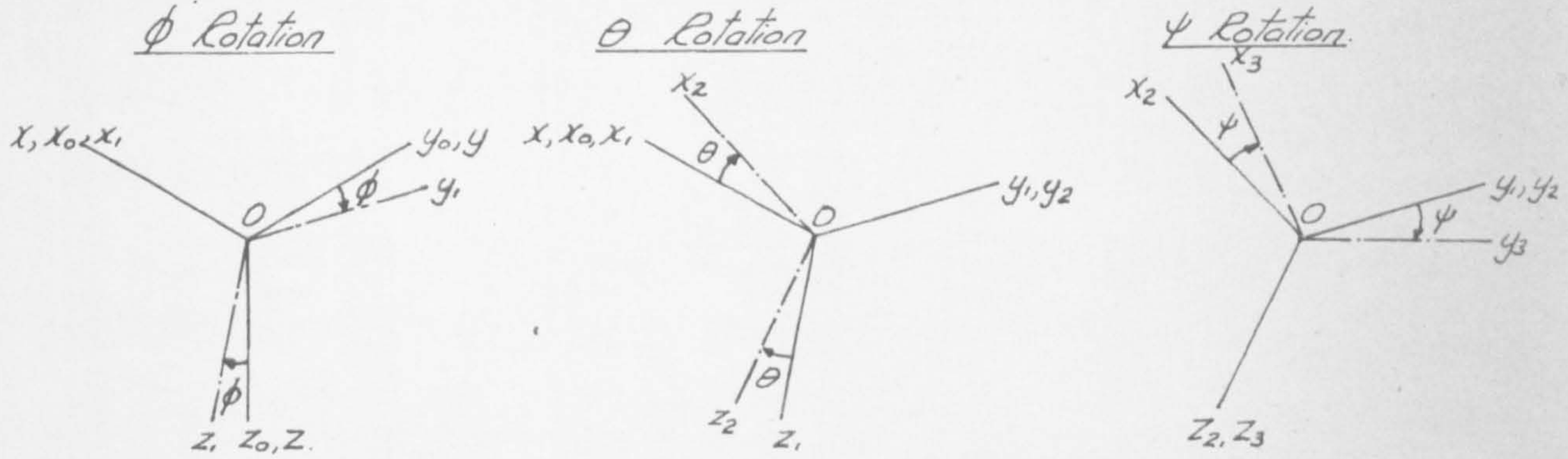

Fig. 9.1.

Two Force And Moment Measuring Systems.

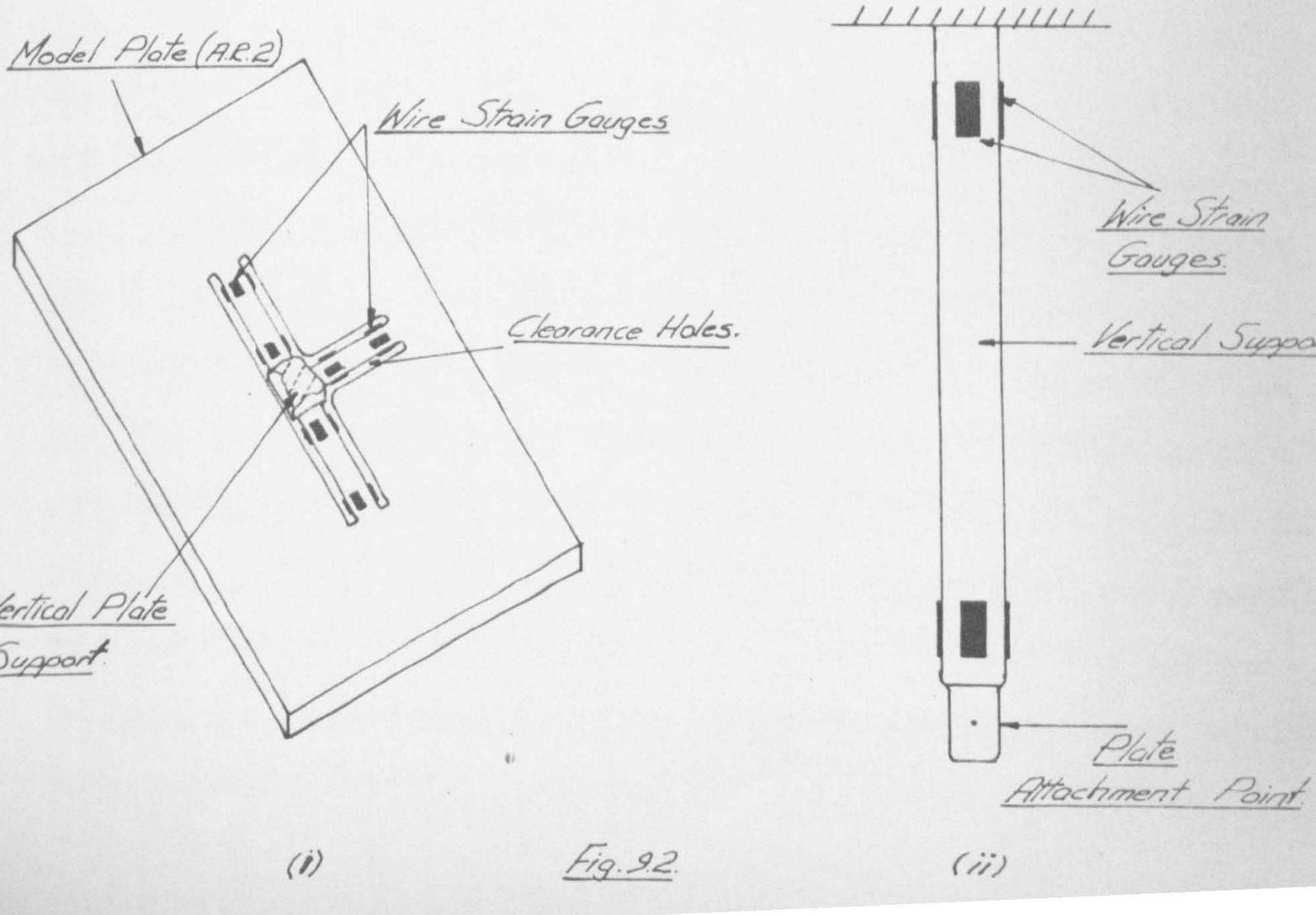

(i) Fig. 9.2. (ii)

9.2 The Plate Support Design

Very few establishments, including Bristol University, possessed apparatus to measure the required six components of force and moment acting on the supported plate in the wind tunnel. Normally most balances measure only lift, drag and pitching moment.

A pulley system was first considered as a measuring system, but this proved extremely complicated at the design stage and would have proved cumbersome in use. Hence this system was abandoned at an early stage. Subsequently two systems were envisaged whereby the forces could be measured with the aid of a strain gauge system, i.e. (i) with the strain gauges disposed on the rigidly supported plate and (ii) with the gauges disposed along the length of the plate support (see fig. 9.2). With the former system, the force and moment components would be measured on the plate body axes. This arrangement would require provision for movement in two degrees of freedom, θ and ψ, and a suitably hinged support would be necessary. The latter method however would require the provision for movements θ, ψ at the plate centre of gravity instead of on the support. Also the components of force and moment would be measured on fixed tunnel wind axes. The one advantage of the former arrangement over the latter is that the manufacture of the apparatus would be more straightforward and machining tolerances would not be so strict.

FIGURE 9.3

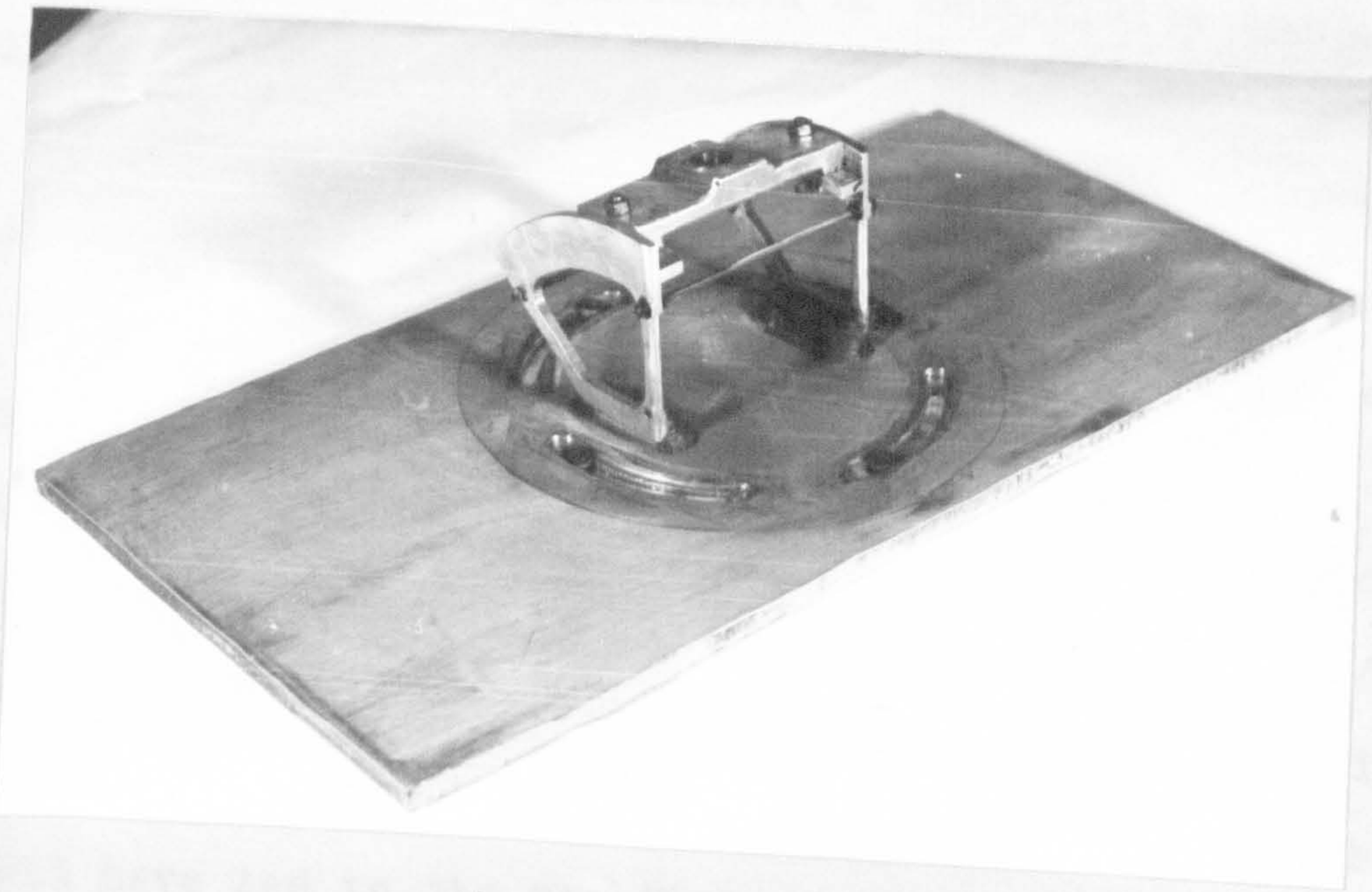

FIGURE 9.4

Before a final design was decided upon, a five component sting balance, which had previously been used in high speed subsonic work, was made available to the laboratory (see Fig. 9.3). This consisted of steel bar of length 22" varying in diameter from 0.5" to 1.75". Strain gauges were glued on 'flats' disposed along the length such that five components of force and moment could be measured. The leads from these strain gauges were passed through the sting core into a 25 way connection socket fitted on the mounting end.

After reconditioning the strain gauge wiring throughout the sting, it was found that the degree of sensitivity was limited for the side force, rolling and yawing moment components, as will be shown later in our discussion of the calibration of the sting. However, the apparatus proved to be within the minimum requirements of sensitivity and adequate as a plate support and force and moment measuring unit.

As mentioned previously, all the experimental work was carried out in a 3' 6" diameter open jet wind tunnel, on which a three component force and moment mechanical balance was mounted. Because of the dimensions of the sting, it was thought to be more practical to mount the sting rigidly on the wind tunnel balance and normal to the tunnel axis. Another possibility would have been to support the sting horizontally on a rigid bracket mounted onto the tunnel balance, but this would have led to the possibility of low frequency large amplitude vibrations. Hence with the sting mounted vertically,

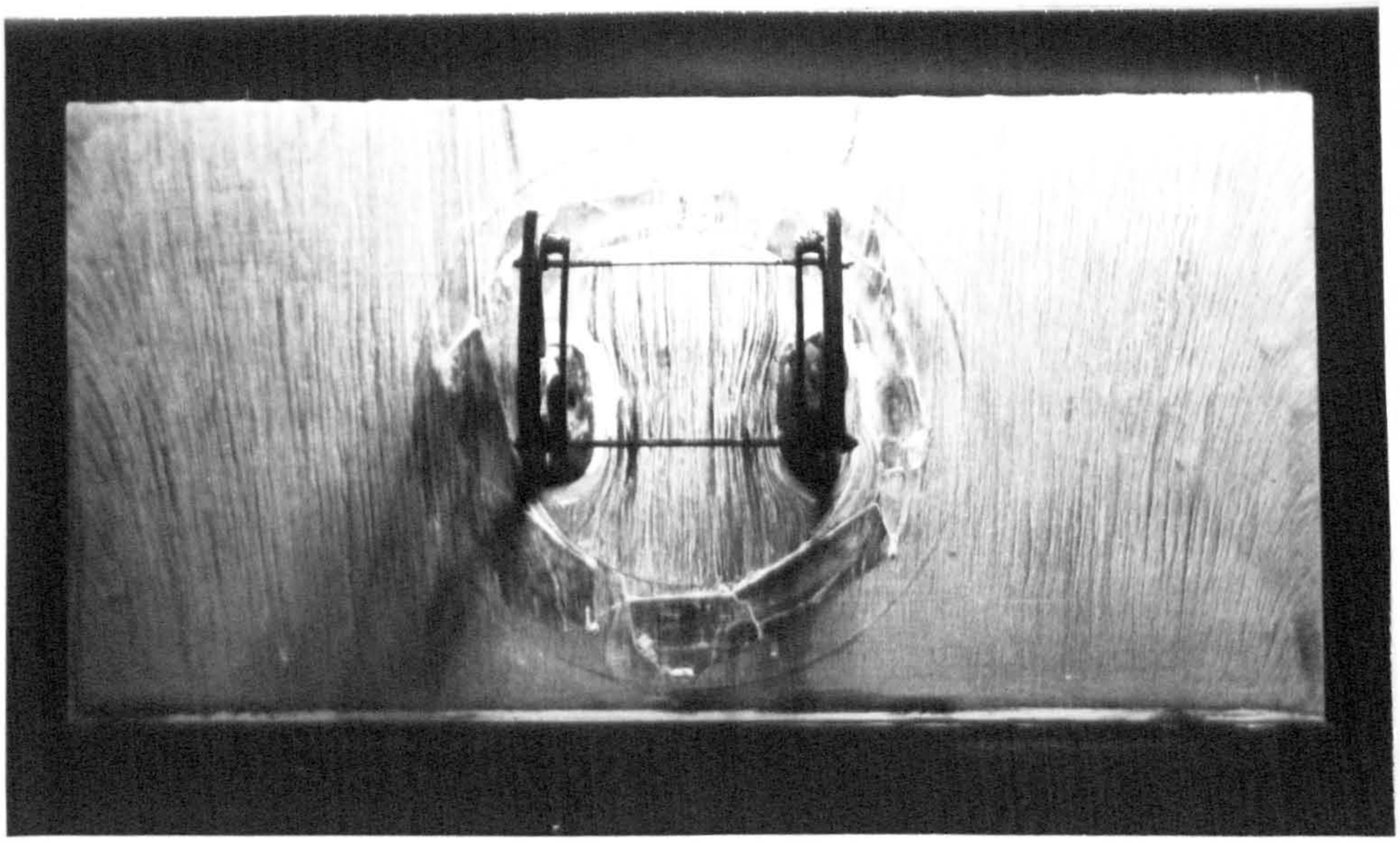

5° Incidence 0° Yaw.

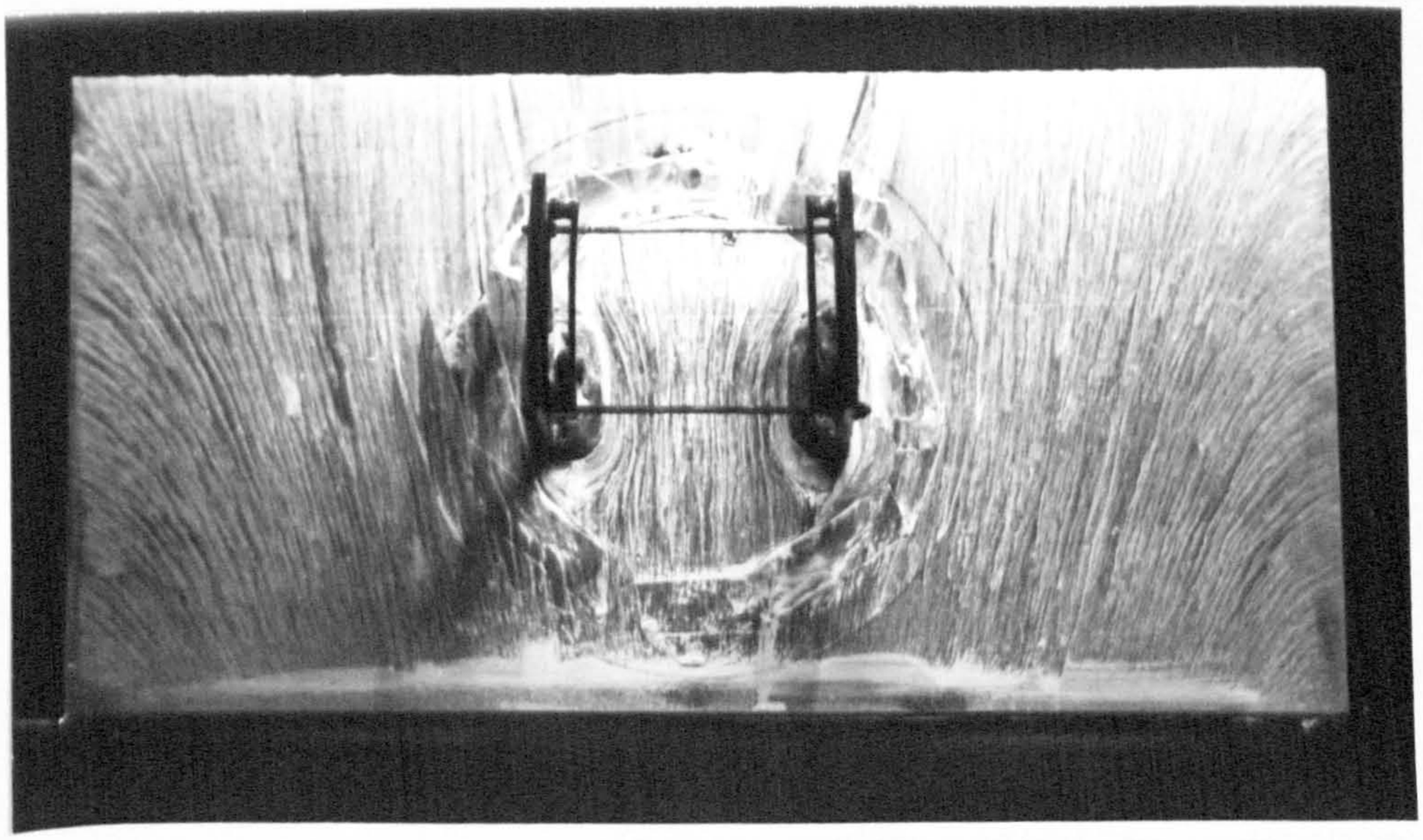

45° Incidence 0° Yaw.

FIGURE 9.5.

drag and side forces and rolling, pitching and yawing moments were measured on wind axes using the strain gauge arrangements, and the lift force was also measured on the same axes using the mechanical balance. Throughout the wind tunnel tests the sting was protected from serious damage and temperature effects by a streamline cowling fixed to the beam of the tunnel balance.

The variable orientation of the plate was accomplished by designing a bracket, which secured the plate to the sting, allowing a degree of freedom in pitch about the wind tunnel axes and a degree of freedom in yaw about the carried plate axes (i.e. the support bracket axes also), see Fig. 9.4. With this arrangement, the support bracket was always in line with the tunnel axis and therefore an out of balance component of side force, rolling or yawing moment was not experienced by the bracket. Similarly, its interference effects on the plate were small compared with those of a bracket which rotates in yaw with the plate. (See Fig. 9.5). In the special case where the plate is set at 45° incidence (nose down), with or without yaw, it was found that the bracket interference effects are still small.

In order that the plate should have a fixed position of centre (with respect to the sting axes), regardless of the plate orientation, it proved necessary to design the support bracket in the form of a quadrant whose centre of rotation was

also the plate centre of gravity. The plate could thus be positioned at incidence between 0° and 45° by clamping the quadrant arms to the support base by means of two locking setscrews shown in fig. 9.4.

The proportions of the bracket were such that loads experienced on the plate could be transmitted to the sting without distortion of the quadrant arms. However the structure was manufactured with a thin section because of the interference effects on the plate. Furthermore, since it was sometimes necessary to set the plate at large incidences, it was desirable to keep the structural inertia to a minimum to reduce the possibility of large amplitude vibrations of the sting. Therefore two aluminium quadrant arms of $^{3}/_{16}$" section were designed to support the plate on a constant 3" radius from the support base. This support base was manufactured so that it fitted tightly on the tapered end of the sting. To withstand yawing moments acting on the plate, the support base was keyed to the sting.

9.3 The Plate Design

To obtain a Reynolds Number of 4.75×10^{5} and keep interference effects on the plate small, the plate dimensions are made 18" span, 9" chord and $\frac{3}{8}$" thick ($\frac{1}{8}$ full size). Also the same design criterion has been applied to the plate as was applied to the support. That is, the weight of the plate

THE MODEL PLATE DESIGN.

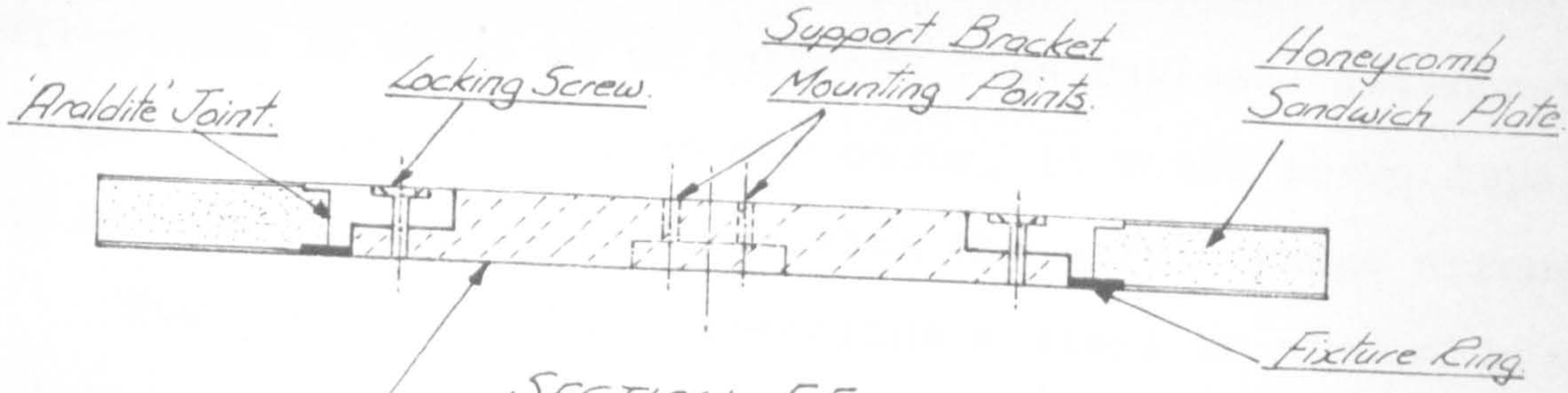

SECTION E.E.

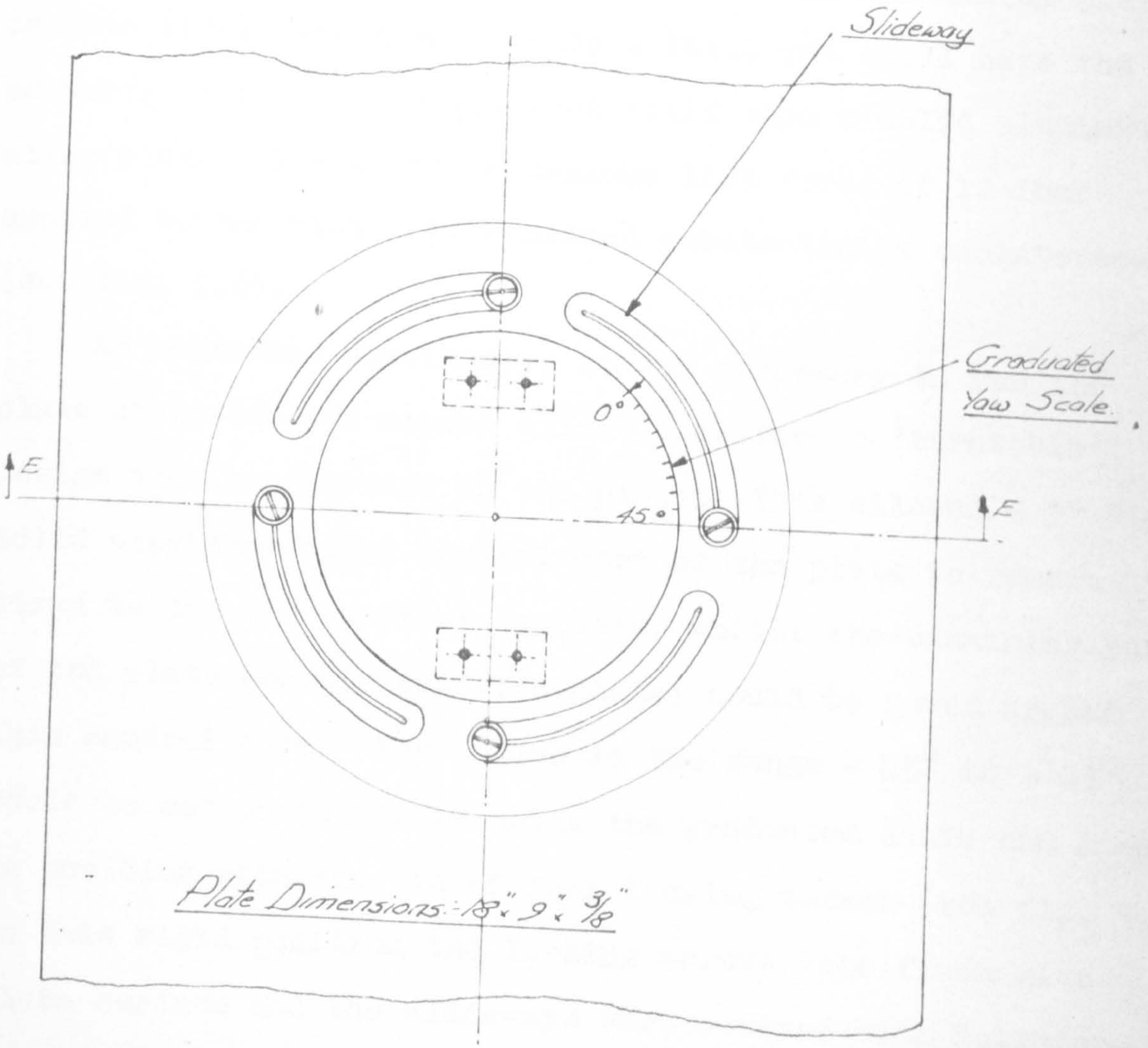

Plate Dimensions:- 8" x 9" x 3/8"

Fig. 9.6.

was kept small, to offset the tendency for large amplitude vibrations to occur in an unsteady flow regime. If, however, large amplitude vibrations did occur, it would prove impossible to measure any value of force with the strain gauge arrangement.

For the above plate dimensions a steel or aluminium alloy plate would weigh 17 or 6 lbs. respectively. It was found, however, that a sandwich plate, consisting of an aluminium hexagonal honeycomb core and clad with 1/32" aluminium plate on both sides, would weigh only 2 lbs., yet still have the property of being only 10% less stiff than a solid aluminium alloy plate. Hence with a maximum lift force of 12 lbs. applied to the plate, it remained substantially undistorted (see fig. 9.6).

As mentioned previously, it was necessary to yaw the plate about its own normal axis. Therefore a 'turntable' design was incorporated in the plate. This allowed a 5" dia. solid aluminium alloy central core of the plate to remain fixed to the two quadrant supports, whilst the remaining part of the plate (mainly sandwich plate) could be yawed around this central core. Yaw angles in the range -45° to $+45^{\circ}$ could be set on the plate using the graduated scale and locked in position with the aid of four locking screws (see fig. 9.6). In this rigid position the locking screws were flush with the plate surface and the slideways were covered with Sellotape

THE STRAIN GAUGE ARRANGEMENT ON THE STING.

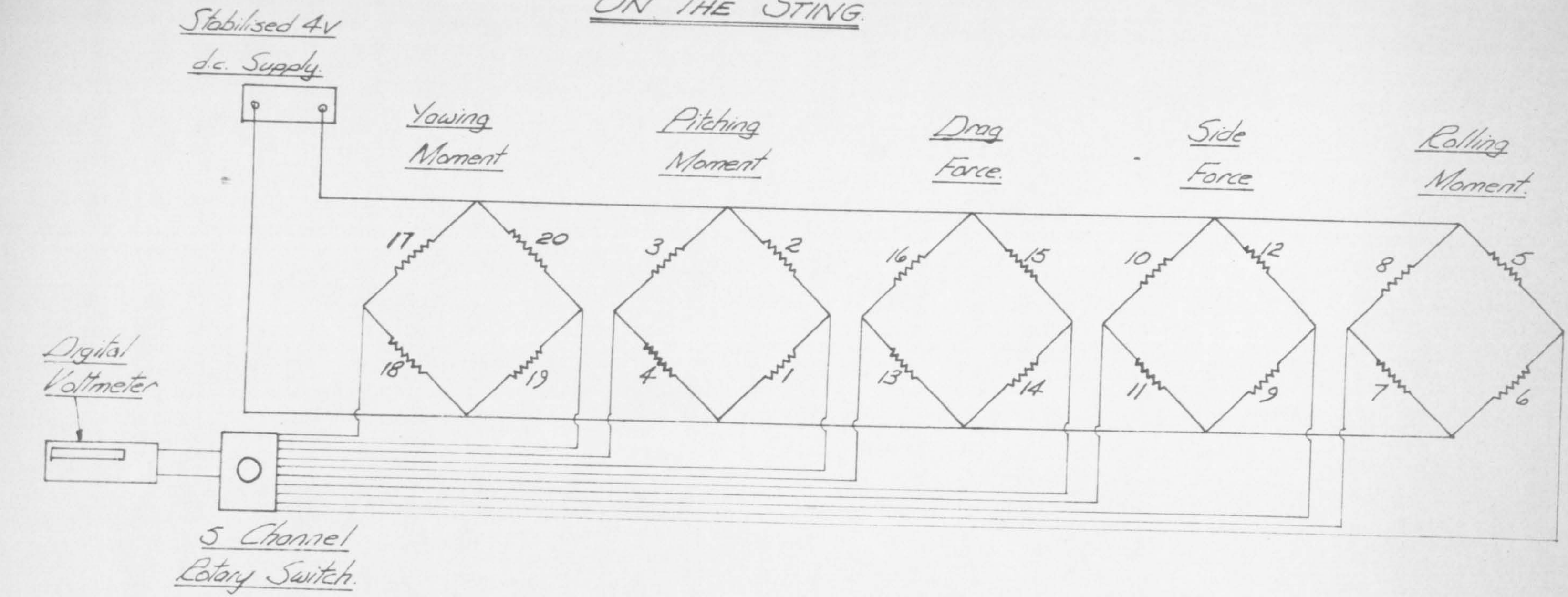

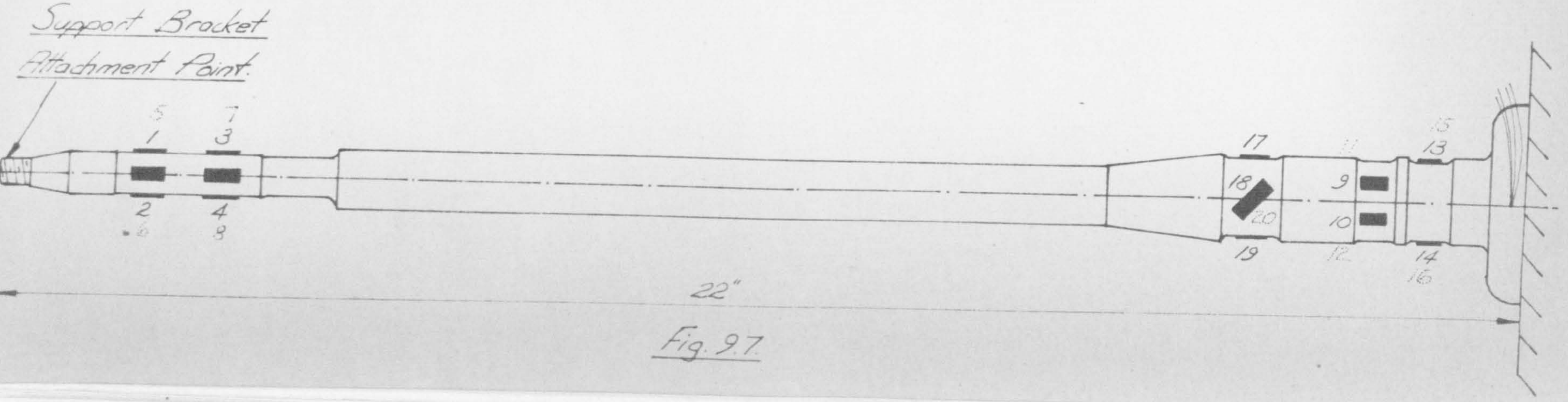

Fig. 9.7.

throughout the experimental work, to eliminate any possibility of irregular flow over the plate. Similarly, both plate mounting points on the support bracket were streamlined with 'Plasticine' to reduce the support interference effects on the plate.

9.4 Instrumentation

The components of force and moment acting on the plate were, except for the lift component, measured by means of strain gauges disposed along the length of the sting balance. These 100 Ω, 25 mA resistance strain gauges were so arranged to form a 'four active arm' Wheatstone Bridge circuit for each component of force and moment, as shown in Fig. 9.7. All five component circuits were connected in parallel to a stabilised 4 volt direct current supply, in the form of an Apt Stabiliser Unit TCU.150. The readout signal was monitored on a volt-meter and it could be measured in two ways, (i) the null method, and (ii) the displacement method. The former consisted of balancing the bridge circuit for each separate measurement and furnishing a reading which is independent of the supply voltage. Alternatively, the latter gave a direct readout of the bridge unbalance, which is clearly more expedient than the former method. Because a stabilised voltage supply was used instead of a lead acid 4V battery, both methods had the same order of readout accuracy and the displacement method was adopted in view of its convenience for stepwise readout recording.

WIND TUNNEL ARRANGEMENT

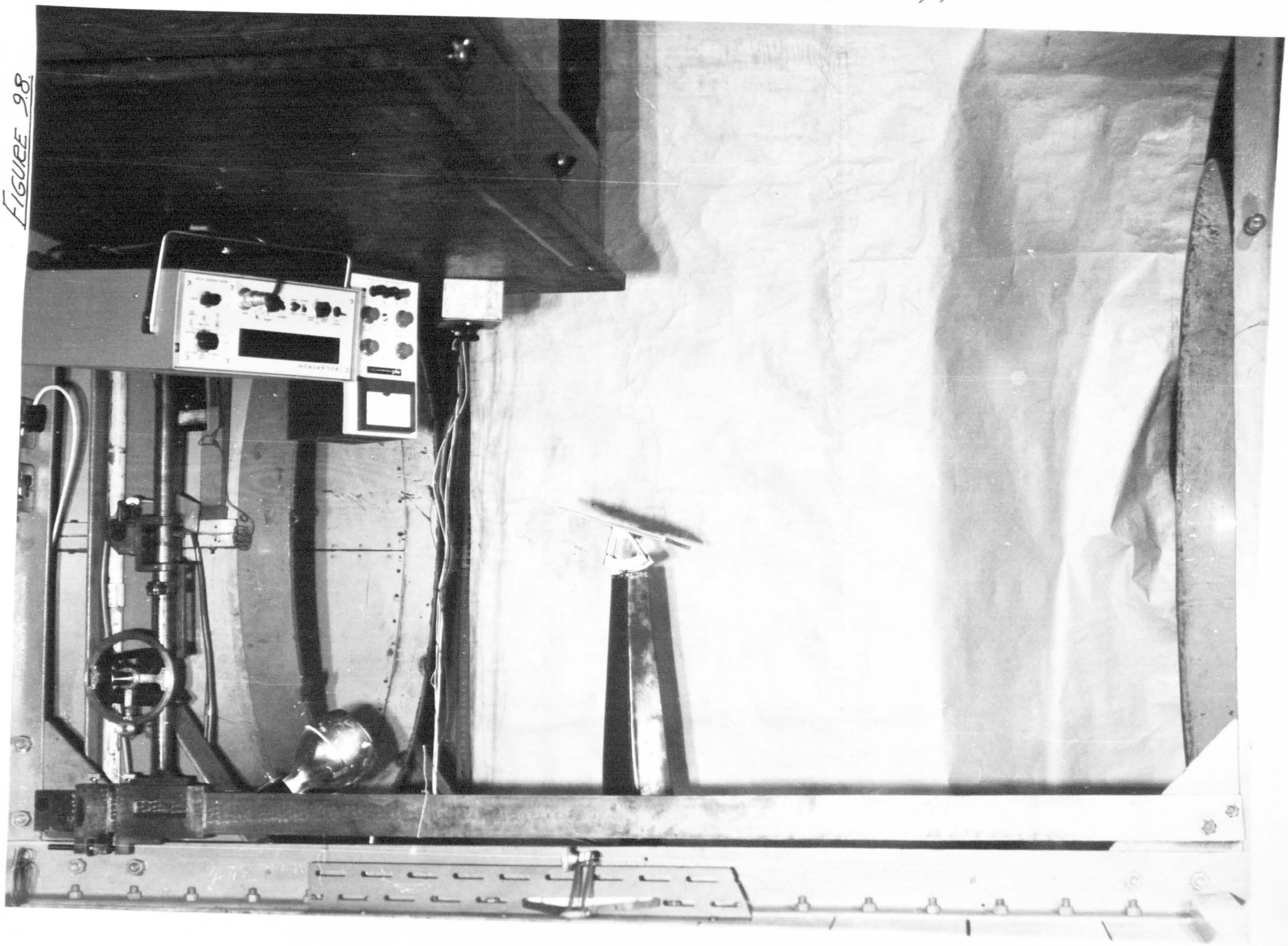

FIGURE 9.8.

In order that the five component readout signals could be monitored by a voltmeter, a Weston 10 way, 2 pole rotary selector switch (Model S.88) was incorporated in the circuit. This was a low impedence switch of contact resistance 0.007 ohms. and consequently contact resistance variation had negligible effect on the readout voltage, especially when the voltmeter internal impedence was 49 k.ohms. The voltmeter used (see fig. 9.8) was a Solartron electronic visual display digital voltmeter (type L.M. 1420) with a sensitivity of 1 μ volt on the required 0-20 m.volt range. With this direct readout on the voltmeter screen, it required approximately 30 seconds to scan the five components of force and moment. In fact the majority of measuring time was taken in measuring the lift force on the tunnel mechanical balance.

9.5 The Sting Calibration

To give relevance to the voltmeter readout values, it was necessary to carry out a set of calibration tests on the five component sting balance. (It was in a "cart before the horse" manner that these tests indicated the adequacy of the sting for the wind tunnel experiments on the flat plate.) With a more sophisticated five or six component mechanical balance, a direct reading of load could be obtained quite independently from the other components. However for a sting balance these components of force and moment are rarely measured independently

For the most accurately manufactured sting, second order interactions can occur even though the primary purpose of strain gauge balance design is to make each bridge circuit sensitive to only one component of load. These interaction effects are normally in the form of thermal and mechanical effects.

9.5.1 Thermal Effects

Thermal interaction effects are usually first order terms and in some cases second order terms. The first order interactions are due to ambient temperature effects creating uniform expansion of the sting. Fortunately the symmetrical bridge arrangements eliminated these effects. However second order effects are due to the different thermal coefficients of each gauge, or to non-uniform expansion of the sting, or finally, to temperature gradients over the length of the sting. In view of the fact that the laboratory was not temperature controlled, it proved impossible to measure these second order effects. Consequently, to minimise these effects a cowling was mounted closely around the sting (see fig. 9.8) which allowed the sting to 'breathe', but eliminated any direct wind effects on the sting. Also the calibration of the balance was carried out at temperatures very similar to those encountered in the tunnel.

9.5.2 Mechanical Effects

Mechanical interaction effects exist due to the following causes:- (i) Gauges not perfectly positioned on the sting. (ii) Unequal gauge factors. (iii) Badly machined gauge surfaces on the sting (see ref. 11.4 for less important effects). However, as the balance was available in a near working state, these design factors were beyond the author's control.

The majority of the sting calibration tests was not carried out with the sting balance in the tunnel. Instead the sting was mounted horizontally on a surface table by means of a heavy angle plate as illustrated in fig. 9.9. Also the sting was very precisely positioned in a roll position using a clinometer, so that the strain gauge surfaces were horizontal. In order that the applied calibrating forces and moments were centred on the plate centre of gravity, the test plate was removed and replaced with a loading fixture. This transmitted the loads to the balance in the same manner as the plate does in the experimental work. This fixture is illustrated in fig. 9.9 and it should be apparent that drag force, pitching moment and yawing moment were applied with the sting in the position shown, whilst side force and rolling moment were applied with the sting rotated through a right angle.

In the calibration test of the balance, loading could be applied, utilizing a hydraulic jack and load cell arrangement, or alternatively a dead weight loading arrangement. This latter technique was adopted because, with accurate weights, it was at least as accurate as the former method while being much more straightforward. Hence with the 'long arm' loading fixture mounted on the support bracket, forces were applied using cast iron disks hung on a weight pan, supported from the underside of the loading fixture by a thin cord (see fig. 9.9). Similarly with a fixed load applied, moments were also applied in increments by moving the loaded weight pan in steps along the graduated arms. Alternatively pure couples were applied using two parallel long arms in line. With the one arm loaded by means of the usual dead weight pan and the other loaded in the opposite in line direction by means of an accurately calibrated spring balance, a pure couple was applied to represent pitching yawing or rolling moment. With these means of loading available first order and second order interactions were determined. Higher order interactions were ignored as it has been found generally that these are negligible (see ref. 9.5 and 9.6).

From the tests above, interactions were determined for five components of loading, i.e. drag and side forces, pitching yawing and rolling moments. Because the lift force

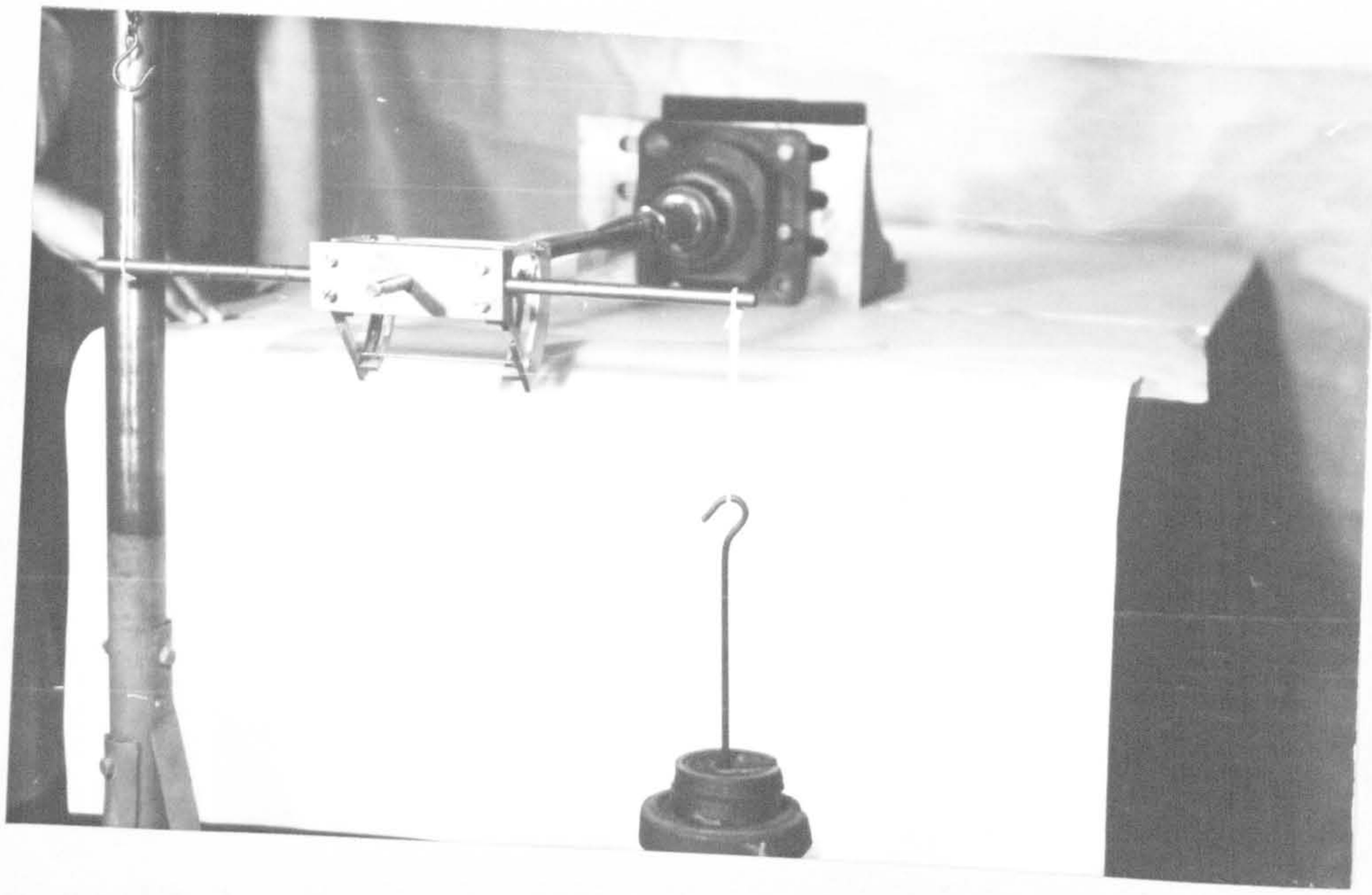

FIGURE 9.9

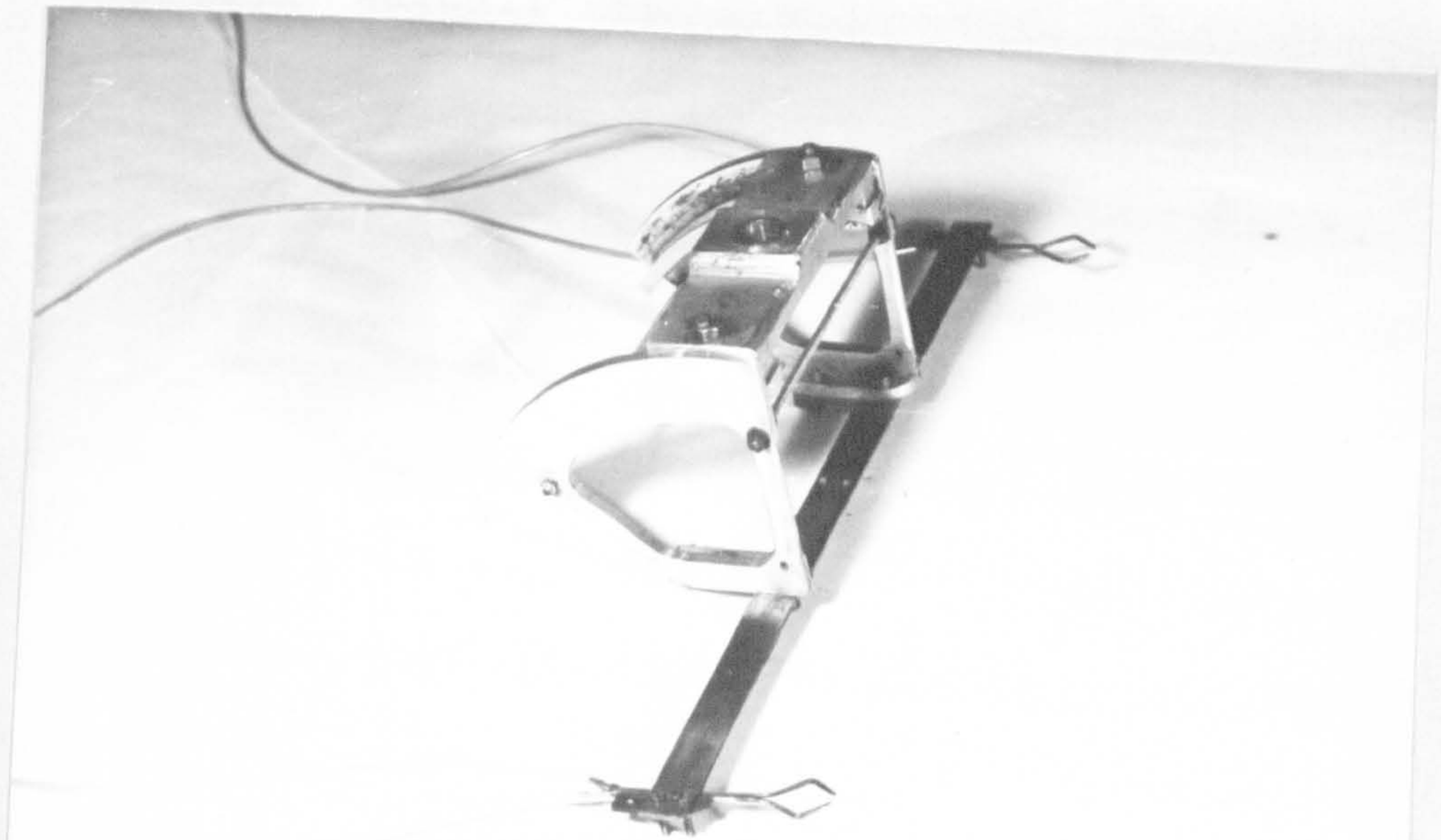

FIGURE 9.10

is measured independently on the tunnel mechanical balance, a direct reading was obtained. However, this component will interact with the other five load components. Hence in addition to the horizontal calibration set up, it is necessary to mount the sting vertically in the wind tunnel and measure the necessary interactions on the sting due to an applied lift force.

With the assumed first and second order interactions occurring between the load components, each indicated reading (R_1) of a component load will, theoretically, have 27 first and second order interactions (except for the independent lift force) of the form:-

$$R_1 = k_{1X}.X + k_{1Y}.Y + k_{1Z}.Z + k_{1L}.L + k_{1M}.M + k_{1N}.N$$
$$+k_{1X^2}.X^2 + k_{1Y^2}.Y^2 + k_{1Z^2}.Z^2 + k_{1L^2}.L^2 + k_{1M^2}.M^2 + k_{1N^2}.N^2$$
$$+k_{1XY}.X.Y + k_{1XZ}.X.Z + k_{1YZ}.Y.Z + k_{1XM}.X.M + k_{1XL}.X.L + k_{1XN}.X.N$$
$$+k_{1YM}.Y.M + k_{1YL}.Y.L + k_{1YN}.Y.N + k_{1ZM}.Z.M + k_{1ZL}.Z.L + k_{1ZN}.Z.N$$
$$+k_{1MN}.M.N + k_{1ML}.M.L + k_{1LN}.L.N$$

where k_{1X}, k_{1MN}, etc. are constant calibration coefficients.

The experimental determination of these calibration coefficients is now briefly discussed below.

Assuming the sting, loading equipment and readout equipment were set up for operation on the test bench, the first tests carried out were to obtain the linear calibration coefficients. Firstly with no load applied, all zero readings

of the five load components were measured on the 0-20 mV range (sensitivity 1 μV) of the digital voltmeter. A load of 1 lb. was then applied to the loading fixture, say in the drag force direction, and by means of the rotary switch the five apparent load components were measured. This procedure was again carried out for incremental loading, increasing to a maximum value in excess of the anticipated load experienced in the wind tunnel testing. The above procedure was repeated for the other four load components measured by the sting balance, where the maximum loadings were:-

	Maximum Loading	Allowable Sting Loading
Drag Force	9 lbs.	105 lbs.
Pitching Moment	16 lb.in.	130 lb.in.
Side Force	8 lbs.	105 lbs.
Rolling Moment	16 lb.in.	130 lb.in.
Yawing Moment	56 lb.in.	2,000 lb.in.

At a later stage of the calibration tests, the sting balance was mounted vertically in the wind tunnel and lift forces in the range 0-10 lbs. were applied using the above standard procedure. After plotting the apparent readout loads against the individual applied loads, linear relationships were obtained for all the components; giving the following calibration coefficients k_{1X} .... k_{1N} etc.

Readout Component m Volts	Applied Drag Force lbs.	Applied Lift Force lbs.	Applied Side Force lbs.	Applied Pitching Moment lb.in.	Applied Rolling Moment lb.in.	Applied Yawing Moment lb.in.
Drag Force	0.04 mV/lb.	0	+0.00083	-0.00192 mV/lb.in.	0	0
Side Force	0	0	+0.0486	0	-0.00197	0
Pitching Moment	-0.1636	-0.0011	-0.00567	+0.0377	+0.00083	0
Rolling Moment	-0.00775	-0.0013	-0.17	+0.00152	+0.0382	+0.00063
Yawing Moment	+0.00021	0	-0.00192	0	0	+0.00662

Sensitivities are measured in mV/lb. applied force or mV/lb.in. applied moment - the applied forces and moments acted in the usual directions adopted in aircraft stability work.

As a check, the same procedure was repeated and the same values of linear calibration coefficients resulted. Furthermore, since the plots of applied load against apparent load were all of linear form, it was assumed that the six second order calibration coefficients (i.e. k_{LX^2} .... k_{1N^2}, etc.) were negligible. If the above plots had been non-linear, however, additional plots of readout value/applied load against applied load would have been necessary to ascertain the second order calibration coefficients (k_{1X^2} .... k_{1N^2}).

With the above calibration coefficients determined, it only remained to determine the second order coefficients k_{1XY} .... k_{1LN} etc. Whenever possible, these were determined using a similar procedure to the one above. In this latter procedure, however, two loads are applied simultaneously to the loading fixture. With the applied load 1. kept constant, the applied load 2 was increased in increments and the five apparent load readings were recorded after each increment. Because the predominant loads acting on the balance were lift force, drag force and pitching moment in the wind tunnel tests, calibration tests were initially carried out for only the three combinations of these loads. With the results plotted in the same form as the first linear calibration tests, but now also for constant values of applied Load 1 (in all three cases) it was found on comparing the graphs for various constant values of applied load 1, that they were of the same slope and hence non-linear effects were negligible.

Because the majority of these second order effects depend solely on the flexural stiffness of the sting, it is reasonable to assume the remaining second order calibration coefficients to be negligible for the following reasons:- Under a maximum drag force of 10 lbs, the end of the sting deflected only $^{1}/_{64}$" on a 22" sting length. Secondly, the sting was used to a maximum of only 10% of the allowable working load for all components and thus, although adequate, the sting was over-

designed for this application.

If it had been found that the above second order effects were of finite value when applying incremental load 2, with applied load 1 set at constant values, a full set of graphs would have been obtained resulting in a readout value of one component/applied load 2 plotted against applied load 1. The typical calibration coefficients k_{1XY} .... k_{1LN} etc. would have been obtained.

From the calibration tests performed on the sting balance, it was concluded that the interactions of the six components of load were all of a linear nature. In Section 9.8 the linear calibration coefficients will be used in the processing of wind tunnel results.

With the sting mounted horizontally on the test bench, the loading fixture was loaded in increments of 1 lb to a maximum of 10 lbs in the drag direction. Similarly, a pitching moment was applied in increments of 2 lb.in to a maximum of 16 lb.in. In both cases the angular deflection of the loading fixture was obtained with the aid of a clinometer at each incremental stage. The following corrections could then be made to the geometric incidence set in the plate support:-

- 0.125°/ft.lb of pitching moment + 0.067°/lb Drag	increase taken as positive anticlockwise.

9.6 Sting Positioning

The setting up of the sting balance axes on the wind tunnel axes proved to be a difficult operation. This was because the actual wind direction was not known accurately. It is obvious, therefore, that the accurate calibration of the sting balance would be wasted if it were set up on an 'apparent' wind direction; for instance, normal to the tunnel effuser opening, or the drag axes of the tunnel mechanical balance. The only available sensitive apparatus for setting the balance on wind axes was the bent tube yawmater. This consisted of two pitot tubes, 3/64" diameter, as shown in fig. 9.10. With the tubes bent inwards towards each other at 45°, instead of straight and parallel, greater sensitivity to yaw was obtained. Normally, the tubes were connected to a manometer, so that the instrument alignment to the velocity direction was adjusted until both tubes of the manometer gave the same reading.

Because of the slight variation of wind direction in the wind tunnel, two yawmeters were used and supported 12" apart on a thin bar. (See fig. 9.10). This support bar was mounted accurately on the sting support bracket (instead of on the test plate) and aligned on the sting balance axes. In order that the yawmeters could be aligned correctly on the support bar, the support bracket and support bar were mounted on the axes of an 18" x 18" closed section, open circuit wind tunnel

(known for the "straightness" of its flow parallel to the tunnel axis and negligible turbulence). The two yawmeters mounted on the support bar were then connected to two 'mercury' electronic micromanometers. With the tunnel speed set at 26 ft/sec (max. speed 40 ft/sec), the yawmeters were positioned and locked on the support bar, when the micromanometers indicated a zero reading. This support arrangement was then subsequently mounted onto the sting balance and aligned in its previous position with the aid of the tapered key.

With the sting balance free only to yaw about its fixture position in the open jet wind tunnel, the wind speed was set at 97 ft/sec and the balance rotated about its yaw axis. It was found, however, that a yaw position could not be obtained where both yawmeter pressure readings balanced out simultaneously. Therefore, the balance was yawed to the position where both yawmeters gave the same out of balance reading on their respective manometers, and locked rigidly in this position. This was not an adequate check of the sting position and therefore the above procedure was repeated, but this time with the two yawmeters spaced only 6" apart on the support bar. It was found subsequently, by means of this repeat procedure, that the sting axes were lined up correctly with the mean flow direction of the wind. With the test plate accurately re-positioned on the support bracket instead of the yawmeter arrangement, the sting balance was finally in position for

measuring the load components on the test plate.

9.7 Wind Tunnel Corrections

As mentioned previously, a 3' 6" diameter open jet wind tunnel was used for static experimental work on the flat plate. With an unblocked working section, the tunnel had a wind speed range of 0 - 120 ft/sec. These tunnel speeds were measured by means of a static pressure tapping at an orifice in the side of the tunnel, upstream of the effuser section. A Betz manometer was connected to the orifice so that with a pitot-static tube mounted at the model position with the tunnel empty, the orifice manometer could be calibrated against the accurate pitot tube. However, with the sting balance and plate arrangement mounted in the wind tunnel, certain corrections have to be made when measuring the wind velocity by means of the calibrated tunnel manometer. Those corrections due to tunnel interference effects and sting interference effects on the plate are now further detailed.

9.7.1 Wind Tunnel Interference Effects

For an open jet circular section wind tunnel the effects can be subdivided into a) Blockage effects, b) Lift effects.

a) Blockage Effects

It is usually assumed that the above tunnel velocity calibration is valid with the model mounted in the working section. This would be a fair assumption with the plate mounted at 0^{o} incidence. However, with a maximum incidence

setting of 45°, definite blockage would occur; invalidating the free stream condition. Thus, for an open jet working section, the flow over the plate would be less than the free stream velocity. At the time of writing, three dimensional work on solid blockage effects in open jet wind tunnels had not been undertaken. However, certain conflicting suggestions have been made regarding solid blockage corrections. For instance, it is stated by Pankhurst and Holder (Ref. 9.7) that solid blockage effects could occur with the resultant slower velocity over the plate. In Ref. 9.8, it is suggested that for a three dimensional wing in an open jet tunnel, the solid blockage is quite negligible, even for models at appreciable angles of incidence. Because of all the uncertainty in this specialised field, it was thought necessary to carry out a brief check on the solid blockage effects.

With the tunnel already calibrated for free stream velocity (i.e. tunnel empty velocity) conditions on the tunnel manometer, a further test was made with the plate supported by the sting balance in the tunnel. An N.P.L. type pitot-static tube was also rigidly mounted two chord lengths upstream of the plate leading edge on the tunnel axis and connected to an independent manometer.

This above test was carried out with the independent manometer constant at 2.15 in. of H_2O (i.e. the required velocity 97 ft/sec), whilst the plate incidence was increased

in increments from 0 - 45° for each constant value of the plate yaw angle (i.e. 0 - 45° in steps of 5°). From the results obtained, it was shown that a discrepancy of ≃ 1% in dynamic pressure occurred with the plate set at 20° incidence. However, at a plate incidence of 45°, an error of 8% was apparent in the dynamic pressure reading. These results therefore give an indication of the blockage effects occurring for an 18" x 9" x $\frac{3}{8}$" plate set at incidence in a 3' 6" diameter working section.

It is stressed that only an indication of the effects is given, because the plate could affect the static pressure reading taken by the pitot-static tube; although with two chord lengths between the plate and tube, this would be only slight. Also, the dynamic pressure reading given by the pitot-static tube was not measured at the plate position and therefore slightly inaccurate readings were possibly recorded (owing to the lower dynamic pressures occurring at the plate compared with the tube position.)

As an alternative to the use of the above pitot-static tube, a vane type anemometer was used in the tube position. Unfortunately, this had a velocity limit of only 40 ft/sec, whereas the required tunnel velocity was 97 ft/sec. However, tests were made at 40 ft/sec with the plate set at various incidences and comparative results between the anemometer and pitot-static tube showed no difference between the readings. Unfortunately, this agreement could not be reasonably assumed

for higher speeds.

As a further alternative, a hot wire probe was manufactured, so that, when calibrated, a measure of the tunnel velocity could be made. Whilst in the process of calibrating the probe against the free stream velocity, it was found that the wind tunnel temperature increased with the duration of a test run and greatly interfered with the probe filament temperature. Therefore this form of measurement was discontinued and the pitot static tube results were relied upon.

b) Lift Effects

The lift effect on the plate is another form of wind tunnel constraint, although somewhat different from the above solid blockage effect. This is due to the fact that solid blockage effects can be ignored if the tunnel dimensions are large compared with the plate dimensions, whereas the lift effects occur always, regardless of the tunnel and plate dimensions. Lift effect corrections are made because the interference effects of the tunnel boundary constraints induce a downwash on the plate such that the measured geometrical value of incidence is greater than the effective incidence for an open jet tunnel. (See Ref. 9.7 and 9.8). This requires a correction, to be applied to incidence and drag, of the form

$$\Delta\alpha = -\frac{\delta}{2}\frac{S}{C}C_L$$

$$\Delta C_D = -\frac{\delta}{2}\frac{S}{C}C_L^2$$

where δ = 0.251 S = plate area c = plate chord

C = tunnel area D = tunnel diameter

$$\frac{S}{C} = \frac{1.125}{9.6} = 0.117$$

However, it is shown by Adamson (Ref. 9.9) that for $^{c}/_{D}$ ratio > 0.2 a further correction has to be made to allow for a further increase in downwash along the chord. The final corrections are now given as

$$\text{Effective Incidence} = \text{geometric incidence} - \frac{\delta}{2}\frac{S}{C} C_L \left(1 + 0.395 \frac{c}{D}\right)$$

$$= \underline{\text{geometric incidence} - 0.0159\, C_L \text{ (radians)}}$$

and Effective Drag = $\underline{\text{measured drag} - 0.0147\, C_L^2}$.

These corrections are shown to apply up to stall conditions in Ref. 9.9 and are applied here to pre and post stall results. The application to post stall conditions is made, however, for completeness rather than correctness, as no correction theory is available for post stall incidences.

No mention has so far been made of the constraints on the rolling moment, yawing moment and side force acting on the plate. However, very little theoretical work has been developed on asymmetric loading corrections, thus only the above effective incidence correction is applied.

9.7.2 Sting Interference Effects

With the plate supported by the sting balance and support bracket in the wind tunnel tests, the resultant forces

and moments included the interferences forces and moments of these support fixtures. It therefore proved necessary to support the plate in close proximity (i.e. $\frac{1}{64}$") to the support bracket, but without contact. Thus the plate was rigidly mounted from the ground by means of a dexion frame (having negligible blockage effects on the tunnel flow) which incorporated a degree of freedom in pitch to allow the plate to be set rigidly at incidence. Results for all six components of load were subsequently recorded with the plate in various attitudes of incidence and yaw between 0 and 45°. As was anticipated, interference effects were not measured in rolling moment, yawing moment or side force.

9.8 The Experimental Procedure

With the sting balance and plate orientated normal to the tunnel wind direction and the stabilised voltage supply, rotary selector switch and digital voltmeter connected in circuit with the five component strain gauge arrangements on the balance (see Fig. 9.7), the apparatus was then ready for wind tunnel tests.

A two hour warming up period was allowed for the stabilised voltage supply (set at 4V d.c.). Similarly, the digital voltmeter was switched on one hour before tests were made, with the 0 - 20 m. Volt range and low pass filter switched into the circuit. After this instrument was adjusted for zero, zero load readings were noted for the five components

of load. In like manner the zero load reading of lift force was noted from the tunnel mechanical balance.

At the required calibrated tunnel speed of 97 ft/sec, a set of readings was taken (for a given incidence) from the five load components using the digital voltmeter and the tunnel balance for the lift force. At this incidence the six components were also recorded for values of plate yaw angle between 0 - 45°, in increments of 5°. At each increment, the tunnel was shut down and the zero load readings checked before altering the yaw angle. In the same way, the incidence (nose down) was increased in increments of 3° between 0 - 30° and thereafter 35°, 40°, 45°. At incidences in the 20° - 30° range, difficulty was encountered in this stall region because the plate support vibrated slightly, thus giving unsteady pitching and rolling moment 'apparent' readings. Fortunately, with a low pass filter switched into the circuit, it proved possible to take a visual mean reading of both these components.

9.9 Data Processing

In this section we discuss the manipulation of the wind tunnel results into their "true" form, where tunnel and sting interference effects are accounted for. The apparent loads acting on the sting and support bracket are subtracted from the combined plate + sting apparent loads - thus giving the apparent loads (acting on the plate) in a form whereby tunnel corrections can be made.

At this stage of the processing it was necessary to convert the apparent load data (in mVolt units) into true loads (lb or lb.ft). From the sting calibration tests (see Section 9.5) it was shown that

$$R_1 = k_{1X}.X + k_{1Y}.Y + k_{1Z}.Z + k_{1M}.M + k_{1L}.L + k_{1N}.N$$

where R_1 = apparent load

k_{1X} etc. = calibration coefficients

X etc. = true loads.

This may be written in the more complete matrix form:-

$$\begin{bmatrix} X^1 \\ Y^1 \\ Z^1 \\ L^1 \\ M^1 \\ N^1 \end{bmatrix} = \begin{bmatrix} 1 & k_{XY} & k_{XZ} & k_{XL} & k_{XM} & k_{XN} \\ k_{YX} & 1 & k_{YZ} & k_{YL} & k_{YM} & k_{YN} \\ 0 & 0 & 1 & 0 & 0 & 0 \\ k_{LX} & k_{LY} & k_{LZ} & 1 & k_{LM} & k_{LN} \\ k_{MX} & k_{MY} & k_{MZ} & k_{ML} & 1 & k_{MN} \\ k_{NX} & k_{NY} & k_{NZ} & k_{NL} & k_{NM} & 1 \end{bmatrix} \begin{bmatrix} X \\ Y \\ Z \\ L \\ M \\ N \end{bmatrix}$$

i.e. $[F_A] = [A][F_T]$

X = -Drag Force L = Rolling Moment

Y = Side Force M = Pitching Moment

Z = -Lift Force N = Yawing Moment

where F_A = vector of apparent loads.

F_T = " " true "

A = matrix of calibration coefficients.

The above equation can therefore be solved to give

$$\left[F_T\right] = \left[A\right]^{-1} \left[F_A\right]$$

From the previous calibration tests it was found that

$$\left[A\right] = \begin{bmatrix} 0\cdot04 & +\cdot00083 & 0 & 0 & -\cdot00192 & 0 \\ 0 & +\cdot0486 & 0 & -\cdot00197 & 0 & 0 \\ 0 & 0 & 1 & 0 & 0 & 0 \\ -\cdot00775 & -\cdot17 & -\cdot0013 & +\cdot0382 & +\cdot00152 & +\cdot00063 \\ -\cdot1636 & -\cdot00567 & -\cdot0011 & +\cdot00083 & +\cdot0377 & 0 \\ +\cdot00021 & -\cdot00192 & 0 & 0 & 0 & +\cdot00662 \end{bmatrix}$$

With the aid of a standard inversion programme

$$\left[A\right]^{-1} = \begin{bmatrix} 31.56 & -\cdot58 & +\cdot00165 & -\cdot0649 & +1\cdot606 & +\cdot00614 \\ +\cdot0488 & +25\cdot116 & +\cdot00156 & 1\cdot294 & -\cdot0495 & -\cdot1223 \\ 0 & 0 & +1 & 0 & 0 & 0 \\ +1\cdot205 & +111\cdot58 & +\cdot0386 & 31\cdot947 & -1\cdot223 & \cdot0386 \\ +136\cdot9 & -1\cdot209 & +\cdot035 & -\cdot793 & 33\cdot516 & \cdot075 \\ -\cdot977 & +7\cdot308 & +\cdot000402 & +\cdot377 & -\cdot0648 & 151\cdot02 \end{bmatrix}$$

and the true forces and moments acting on the plate were thus obtained. The vector F_T was then modified to a non-dimensional form in order to facilitate the correction process. The inclusion of the necessary corrections with the true forces then gave

Actual C_D = True Drag Coefficient - $0\cdot01475\ C_L^2$

and Actual Incidence ^{o} =

Geometric Incidence - $1.175^{o}/C_m + 0.841^{o}/C_D + 0.858^{o}/C_L + 0.274^{o}$

where $- 1.175^{o}/C_m$ and $0.841^{o}/C_D$ - angular displacement corrections

$0.858^{o}/C_L$ - wind tunnel 'lift effect' constraint

$+ 0.274^{o}$ - measured downwash in the tunnel.

Initially, downwash of the air stream in the tunnel was not anticipated and the constant $+0.274^{o}$ was not included in the actual incidence term. However, after processing the first experimental results, it was found that with the plate in a position of zero degrees incidence and yaw, finite values of lift force and rolling moment were recorded. Subsequently swirl of the wind flow in the tunnel was found to be the cause, of which further details are given in Appendix 2. As a result of corrections made to the tunnel, a nett downwash (with zero swirl over the plate span) or effective incidence of $+ 0.274^{o}$ was measured relative to the tunnel wind axes. With the complete experimental procedure repeated, satisfactory results were finally obtained.

On reverting back to the corrections made to C_D and Incidence, it was found worthwhile to put the data processing procedure in ALGOL programme form for the Elliot 503 Computer. With an immense amount of data to process, it would have proved worthwhile using an analogue to digital converter (A.D.C.) to

obtain the digital voltmeter readings directly on eight hole computer data tape. However, for the amount of data obtained, the processing programme proved quite adequate.

CHAPTER 10

DETERMINATION OF THE OSCILLATORY DERIVATIVES

To complete the required longitudinal derivative data for a flat plate of aspect ratio 2, an estimation was required of the pitching moment damping derivative m_q and the vertical force damping derivative z_q, both with respect to angular rotation $q(\dot{\theta})$. Until quite recently these dynamic derivatives were based on 'quasi-static' theory where, for instance, m_q was calculated on a constant rate of rotation q. Alternatively, this derivative was determined experimentally using whirling arm apparatus (see Ref. 10.1 and 10.2). In neither of these techniques was the previous history of motion of the system taken into account and thus the derivative values obtained were open to criticism. Because of the apparent importance of these derivatives on the stability of the flat plate (see Section 11.2), an oscillatory technique was required to measure the m_q and z_q derivatives experimentally.

The oscillatory derivatives are normally dependent on Strouhal Number, Reynolds Number, mean incidence, amplitude of oscillation, plan form and axis of rotation and would be difficult to estimate theoretically. However, only frequency of oscillation, wind velocity and mean incidence are of prime importance because 'small perturbation' theory is assumed for

all the theoretical work. Also, only a rectangular plate of aspect ratio 2, with a degree of freedom θ about a mid chord axis is considered in the experimental work.

10.1 Requirements of the Oscillatory Apparatus

In this section consideration is given to the experimental ranges of Strouhal and Reynolds Numbers as well as mean incidence, in order that correct values of m_q and z_q can be obtained for use in the theoretical work in sections 3.0, 4.0 and 5.0. This is a new field of investigation and as such, an immense amount of information is available with respect to the above derivatives. However, because of the limited time available, only those ranges of Reynolds and Strouhal Numbers encountered in full scale work are considered.

It was mentioned previously in section 9.0 that most of the full scale tests were carried out for a Reynolds Number range of $2.8 \times 10^5 - 3.45 \times 10^6$ (i.e. 5 m.p.h. - 60 m.p.h. based on a 6 ft chord pallet). In the oscillatory experimental work, however, it is difficult to satisfy both Reynolds and Strouhal Numbers simultaneously. Since, of the two, Strouhal Number has the greater effect on the oscillatory derivatives, the experimental work is carried out for the correct Strouhal Number range.

In the estimation of a design criterion for Strouhal Number difficulties were encountered because information was not available from full-scale tests. Also, it was anticipated that

two longitudinal modes of oscillation would occur on the full scale plate; the one being a pendulum mode of low frequency and the other a flutter mode of greater frequency. Two ranges of Strouhal Number should therefore be investigated. However, it is reasonable to assume that the m_q and z_q derivatives would be of greater importance in the flutter mode than in the pendulum mode. Hence it is necessary to obtain the higher Strouhal Number range pertaining to the flutter mode. For the dynamic scale model wind tunnel experiments discussed in section 11.2, a conservative range of Strouhal Number (0.5 - 1.0) was used. Although this range was determined from strictly an unrepresentative arrangement of the suspended pallet, the theoretical results have since shown this range to be adequate.

At the time of design of the oscillatory equipment, only a 3'-6" diameter open-jet, closed circuit wind tunnel was available for the experimental work. Very little was understood about the wind tunnel interference effects on an oscillating flat plate and so the plate dimensions were kept small in comparison to the tunnel dimensions (see Ref. 10.11). Therefore, a $\frac{1}{8}$ scale plate was chosen with dimensions 18" span, 9" chord and $\frac{3}{8}$" thick.

In section 6.0 it is shown that stability investigations were made in a mean incidence range of 0 - 21° (≃ stall incidence). Therefore derivative information was required for this range. For academic reasons this range was increased to

35^{o} so that investigations of the m_q and z_q derivatives could be made in both pre and post stall conditions. With the Strouhal, Reynolds and incidence ranges in mind, the various oscillatory techniques were considered as a basis for design of the rig.

10.2 Oscillatory Techniques Available

Three basic methods were available to measure the m_q and z_q damping derivatives:- i) Inexorable Forcing technique, ii) Forcing through a Spring, iii) Decaying oscillation technique. These are discussed briefly below, (more complete details are given in Ref. 10.3). The techniques all rely on the assumption of sinusoidal motion of the oscillating plate and therefore the aerodynamic reactions can be represented in vector form, displaced by a phase angle from the displacement vector. Hence either the reaction vectors and phase angles are measured or alternatively the components of the reactions are measured in phase and quadrature with the displacement.

10.2.1 The Inexorable Forcing Technique (Rigid Drive)

This technique is the best method for determining the derivatives accurately, although the apparatus design is usually quite sophisticated. With this method the model pivots about a fixed axis and is rigidly forced through a drive link connected to a constant speed motor (see Fig. 10.1a). The force reactions and their corresponding phase angles with respect to the displacement vector can then be measured at the

Schematic Representation Of Three Oscillatory Techniques.

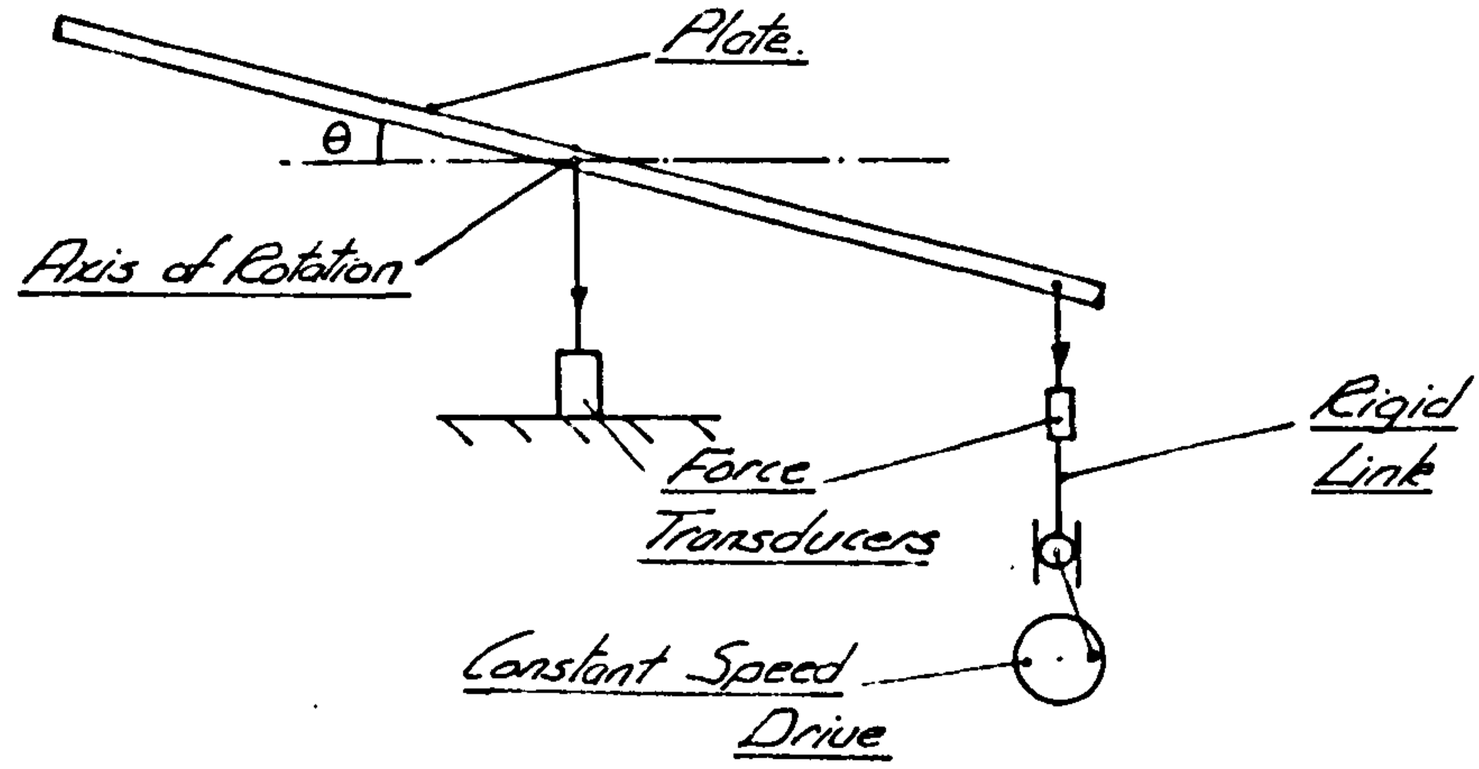

a) 'Rigid Drive'

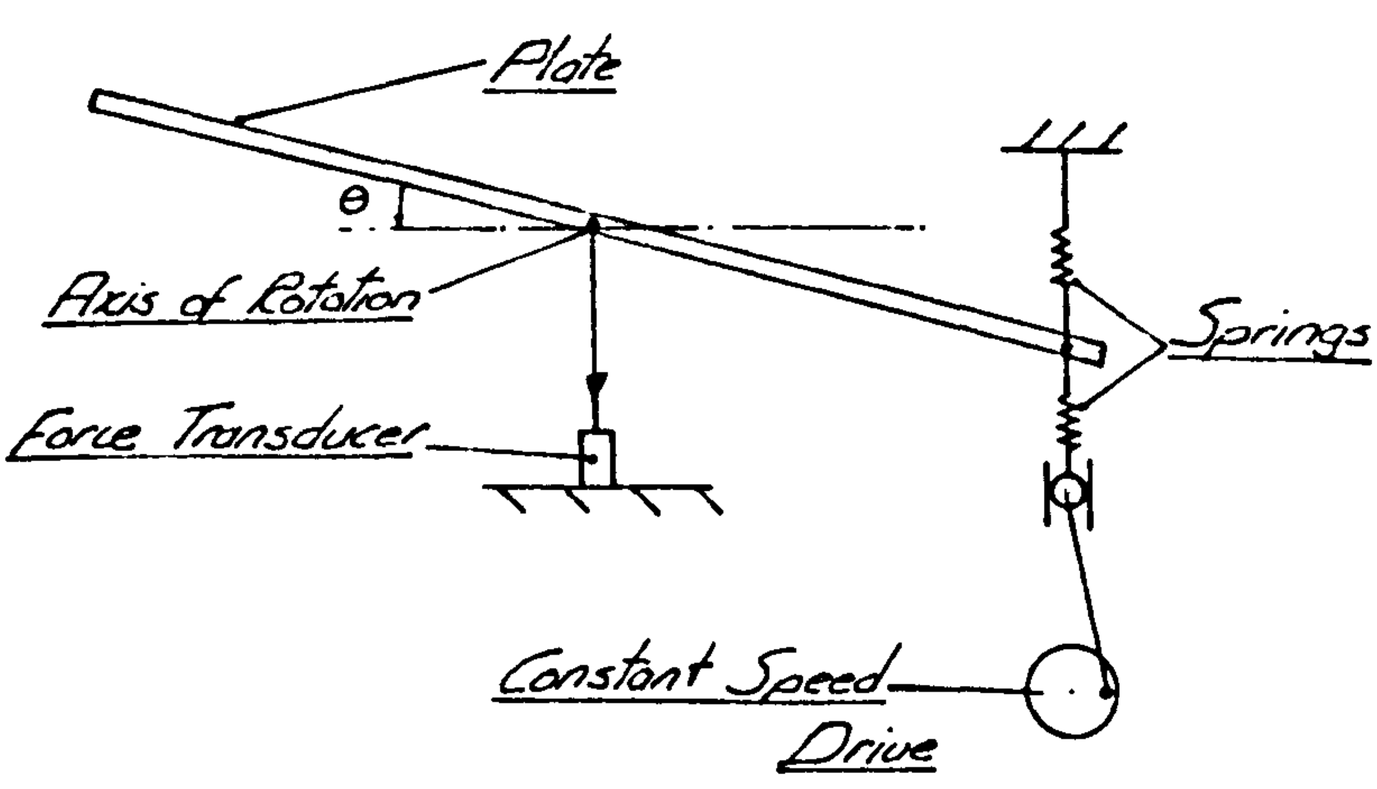

b) 'Forcing Through a Spring'

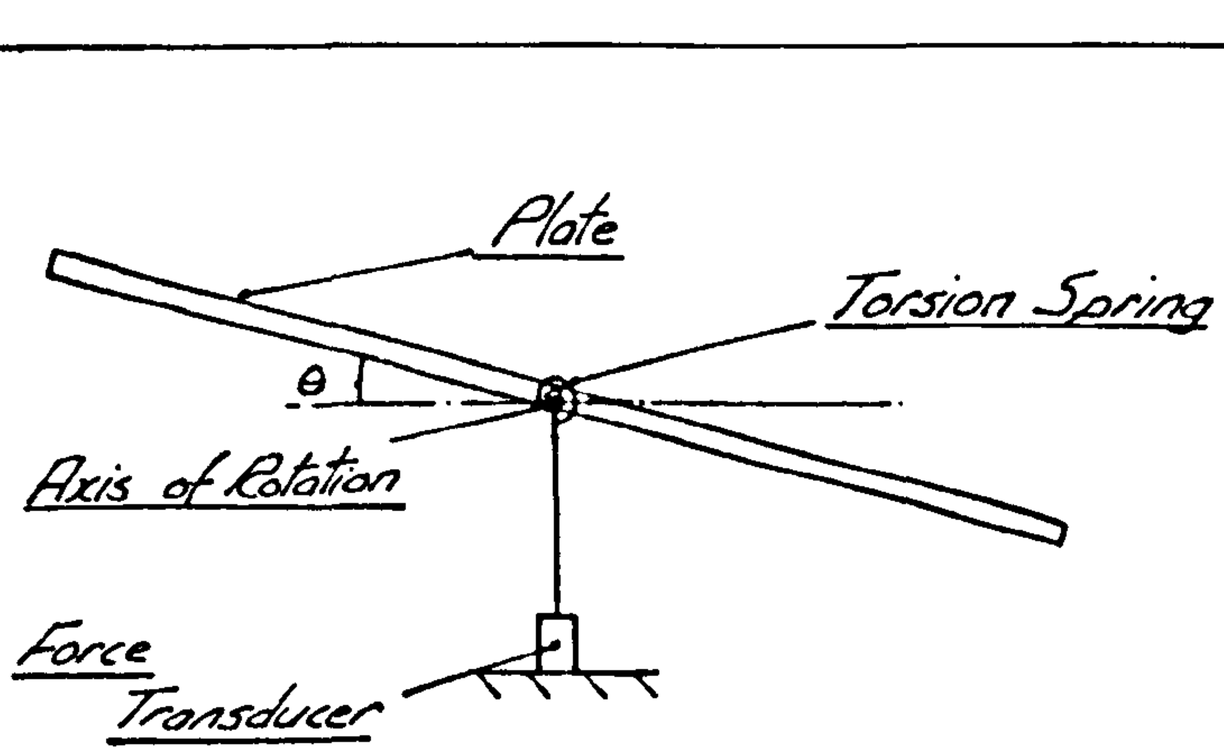

c) Free Oscillation.

Fig 10.1.

axis of rotation and the drive point to give the required m_q and z_q derivatives. This technique would prove adequate for the study of variations in frequency of oscillation, amplitude and velocity.

10.2.2 Forcing through a Spring Technique (Elastic Excitation)

The "forcing through a spring" technique is similar to the above rigid drive method, except that two springs are introduced into the system (see Fig. 10.1b). With the drive motor running at constant speed, the plate would settle down to a constant amplitude oscillation. In this condition, it would then be necessary to measure the frequency and amplitude of oscillation, as well as the phase angle between the motion of the plate and the drive motor. This method has been applied successfully to low-speed work, but the accuracy obtained is greatly dependent on the tunnel turbulence level.

10.2.3 The Decaying Oscillation Technique (Free Oscillations)

This "free motion" technique provides the simplest experimental arrangement of all the techniques. The procedure here is to displace the torsionally constrained plate and then to release it - allowing it to oscillate freely in the airstream. A force transducer, mounted at the torsional axis, then measures the lift force and its phase angle relative to the displacement (see Fig. 10.1c). From these measurements the derivatives are easily obtained. This method is valid only

if the tunnel conditions are reasonably steady with a low turbulence level.

On consideration of all three methods, the final choice was made between the 'inexorable forcing' and 'decaying oscillation' techniques. This was because the 'forcing through a spring' technique required as much instrumentation as the first method, yet the same order of accuracy is seldom obtained and the amplitude and frequency of oscillation cannot be varied to the same extent.

After consultations with Lambourne and Woodgate at the N.P.L. (Teddington), it was decided to proceed with the 'free oscillation' technique in preference to 'inexorable forcing' in view of the extremely complicated hardware associated with the latter technique. This decision led undoubtedly to a sacrifice of general accuracy, but, against this, it was possible to construct a suitable test facility in the limited time available.

The design of the 'free oscillation' apparatus is now described below.

10.3 General Design Theory

It has been mentioned previously that the arrangement employed to obtain the m_q and z_q derivatives consists simply of a plate free to oscillate about a fixed axis constrained by a torsional spring. At this stage we briefly mention the theory involved in the 'free oscillation' technique and not

the structural detail.

Assuming small ($\pm$ 3° amplitude) sinusoidal motions, it can be shown in Reference 10.3 that from 'wind on' and 'wind off' tests, using the general equation for the system (wind on)

$$I.\ddot{\theta} + C.\dot{\theta} + K.\theta = \theta.M_{\theta} + \dot{\theta}\, M_{\dot{\theta}} \quad \ldots\ldots\ldots\ldots \quad (10.1)$$

$$M_{\dot{\theta}} = \frac{2K(\mu - \mu_o)}{(po^2 + \mu_o^2)} ,$$

where I, C and K denote moment of inertia, apparatus damping and torsional stiffness respectively. Likewise μ, p and the subscript o denote the damping factor, frequency of oscillation and wind off conditions respectively.

In a similar manner it is shown in Reference 10.3 that with the lift force leading the motion by an angle ε

$$Z_{\dot{\theta}} = \frac{Z_1}{\theta_1}.e^{\frac{\mu\varepsilon}{p}} \sin \varepsilon$$

where Z_1 and θ_1 are corresponding peak values of the lift force and amplitude of oscillation.

At this stage it must be stressed that M_{θ}, Z_{θ}, $M_{\dot{\theta}}$ and $Z_{\dot{\theta}}$ (the latter two damping terms are known as M_q and Z_q in the stability investigations) are derivatives based on a fixed axis system and not on the moving axis system, normally used in aircraft stability investigations. It is shown by Duncan (Ref. 10.6) that on a transformation of M_q and Z_q to a moving axis system they become $M_q + VM_w^{\bullet}$ and similarly $Z_q + VZ_w^{\bullet}$, where $M_w^{\bullet}$ and $Z_w^{\bullet}$ are acceleration derivatives. However, the required M_q and Z_q fixed axis, non-dimensional damping derivatives are

$$m_q = \frac{2K\ (\mu - \mu o)}{\rho VSc^2(po^2 + \mu o^2)} \qquad \text{and} \qquad z_q = \frac{Z_1\ e^{\frac{\mu\varepsilon}{p}}\ \sin\varepsilon}{p\theta_1\ \rho VSc}$$

In order that the wind on and wind off tests could be compared in the above oscillatory methods, it was important that the amplitudes and frequences of oscillation for both tests were the same. The latter, however, was not strictly possible, although the wind effects on the 'wind on' frequency were very small and could be ignored. Also, it was vitally important that all inertia forces were balanced out exactly, and structural rigidity maintained in all but the required pitching degree of freedom (θ), otherwise spurious derivative values would be obtained. Finally, it is suggested by Molyneux (see Ref. 10.7) that the results might be suspect in the 'decaying oscillation' technique if the damping factor μ exceeds -0·1. This is due to the dependence of the derivatives on damping factors in excess of 0·1.

10.4 The Plate Support Structure

In this section, the design of the plate support structure is discussed in detail.

The basic oscillatory rig consisted of a large rigid frame designed to fit into the open jet wind tunnel working section.

FIGURE 10.2.

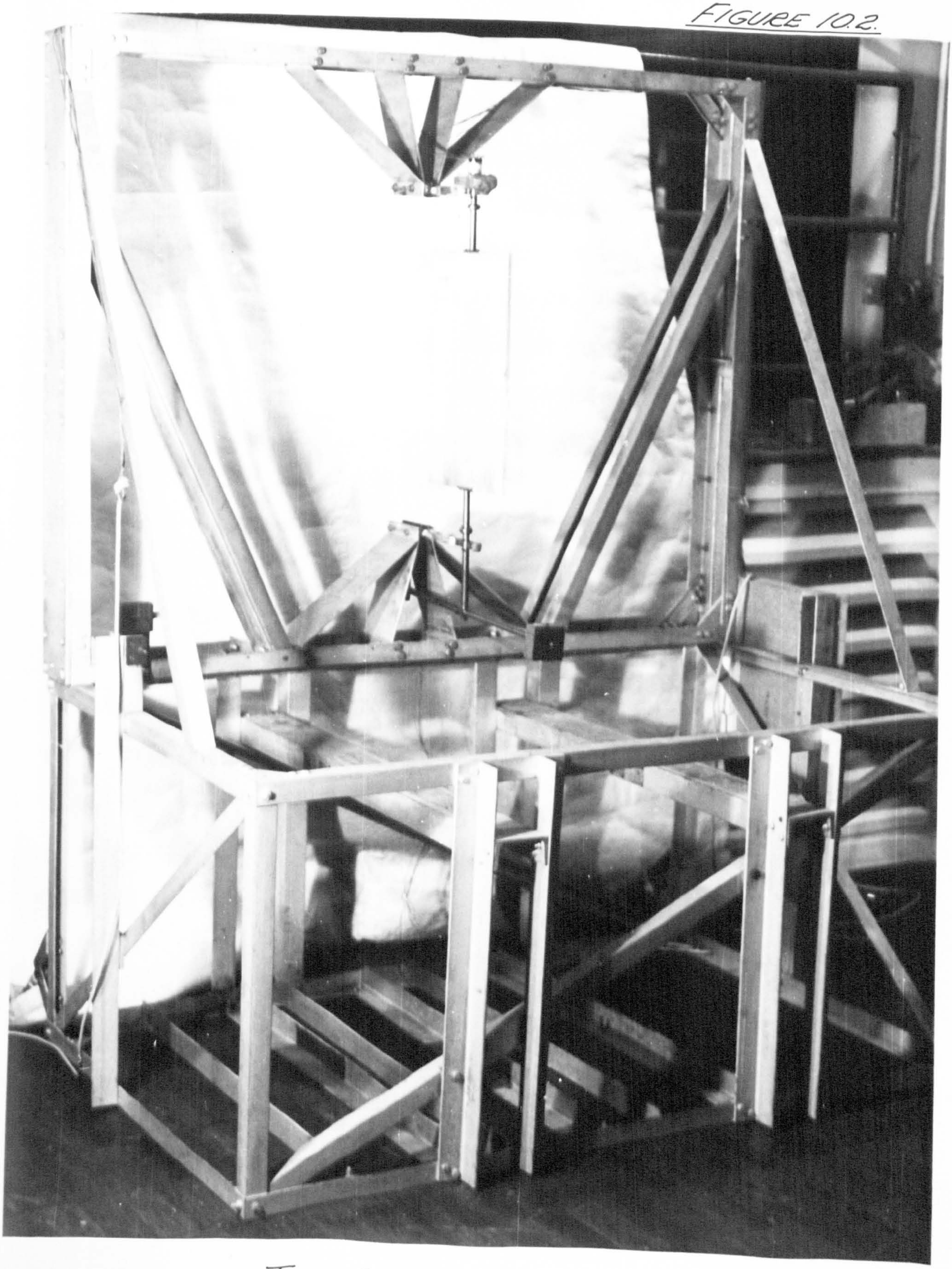

THE OSCILLATORY RIG.

Previously, the same frame had been used in similar work, but was modified for the present purposes to support the test plate rigidly in all but the pitching degree of freedom (see Fig. 10.2). This test plate, with dimensions 18" x 9" x $\frac{3}{8}$", was mounted vertically in the main frame by two support arms, designed so that the out of balance inertia forces from the inertia arms (see Fig. 10.2) were not transmitted to the plate.

The two support arms were designed to set the plate upstream of the main frame in order that aerodynamic interference effects from the frame would not affect the results. Mounted on the end of each of the above support arms were spring bearings, (devoid of frictional forces) from which the plate was supported by two end shafts. Also a strain gauge arrangement was disposed along both support arms so that the lift force could be recorded with the plate oscillating in 'wind on' conditions.

Before a more detailed description of the oscillatory apparatus is given, it is thought worthwhile to give a brief resumé of the design calculations involved in the manufacture of the oscillatory rig.

10.4.1 Typical Design Calculations

The design calculations fall into two categories:- a) the stiffness and inertia arrangement and b) the force measuring system.

10.4.1a The Stiffness and Inertia Design Calculations

In order that an oscillatory rig could be designed, it was necessary to assume a value of m_q and then determine the correct stiffness and inertia in the oscillating system such that the damping factor was ≤ -0.1. From Ref. 10.8 it was found that a theoretical estimate of the m_q derivative for an aspect ratio 2 rectangular plate at 0° mean incidence was approximately -0·1. At an assumed wind tunnel velocity of 50 ft/sec for a plate with dimensions 18" x 9" x $\frac{3}{8}$", M_q = -0·008 slugs ft²/sec. Now from the previous design theory $M_q = 2I\mu + C$ for wind on conditions. Therefore, assuming the structural damping = +0·01 and using the limiting damping factor μ = -0·1

$$I = \frac{M_q - C}{2\mu} = \underline{0{\cdot}08 \text{ slugs ft}^2}$$

Knowing $I = Mk^2$ where $k^2 = 0{\cdot}047$ ft² for the plate dimensions about a spanwise axis.

The required mass of the oscillating plate is thon ≃ 56 lbs. However, a steel plate would weigh only 17 lbs. Therefore, the extra inertia forces must be equal to 0·032 slugs ft².

By means of an inertia arm positioned on the axis of rotation (see Fig. 10.2) with two weights disposed at each end of the arm, a further 0·2 slugs ft² was provided. Assuming a Strouhal Number of 0·5 = $\frac{pc}{V}$ (see section 10.1) it can be shown that the required frequency of oscillation (p) of the plate =

$$\frac{0{\cdot}5 \times 50}{2\pi \times 0{\cdot}75} = \underline{5.3 \text{ c.p.s.}}$$

For a 'Wind Off' condition $p^2 = \frac{K}{I}$

Thus $K = (5.3 \times 2\pi)^2 \times 0.08 = \underline{1.53 \text{ lb.ft/degree}}$ (a minimum torsional stiffness)

This torsional stiffness was provided by a simple flat steel spring (encastré at both ends), built into the two support arms (see Fig. 10.3). It can then be shown by simple beam theory that the change in slope at the axis of rotation = $\frac{9ML}{48EI}$.

Hence the torsional spring stiffness $\left(\frac{\text{lb.ft}}{\text{degree}}\right) = \frac{48EI}{9L \times 57.3}$.

Assuming E for steel = $30 \times 10^6 \times 144$ lb/ft^2,

and an overall spring length L = $\frac{1}{6}$ft and spring width b = $\frac{1}{24}$ ft,

the spring thickness $d = \sqrt[3]{\frac{1.53}{2} \times \frac{12 \times 9 \times 57.3 \times 24 \times 1728}{\times\ 6 \times 48 \times 30 \times 10^6 \times 144}}$

$= \underline{0.0538 \text{ inches}}$

This thickness has since proved to be an overestimate of that used in the experimental work (0.025"). This is not surprising, however, considering the approximations made in the calculations. Other modifications were also made to the basic design at a later stage.

10.4.1b The Force Measuring System

In section 10.3, it was mentioned that a force transducer unit was required to measure lift on the axis of rotation. The Z_q derivative could then be obtained using the record of lift force. A strain gauge system was adopted on both support arms to measure this force.

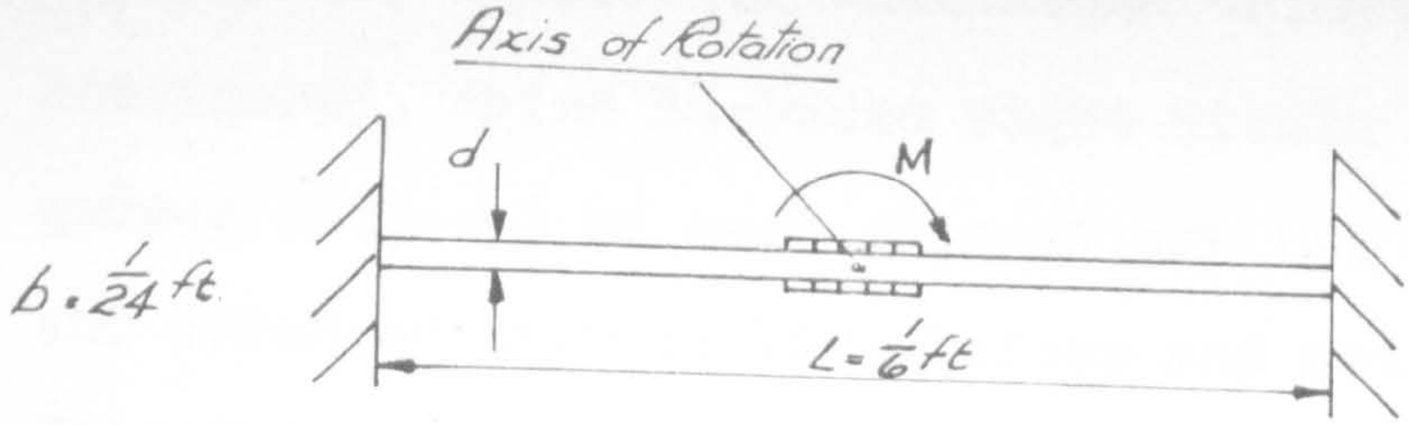

Fig. 10.3. A Simple Torsional Spring.

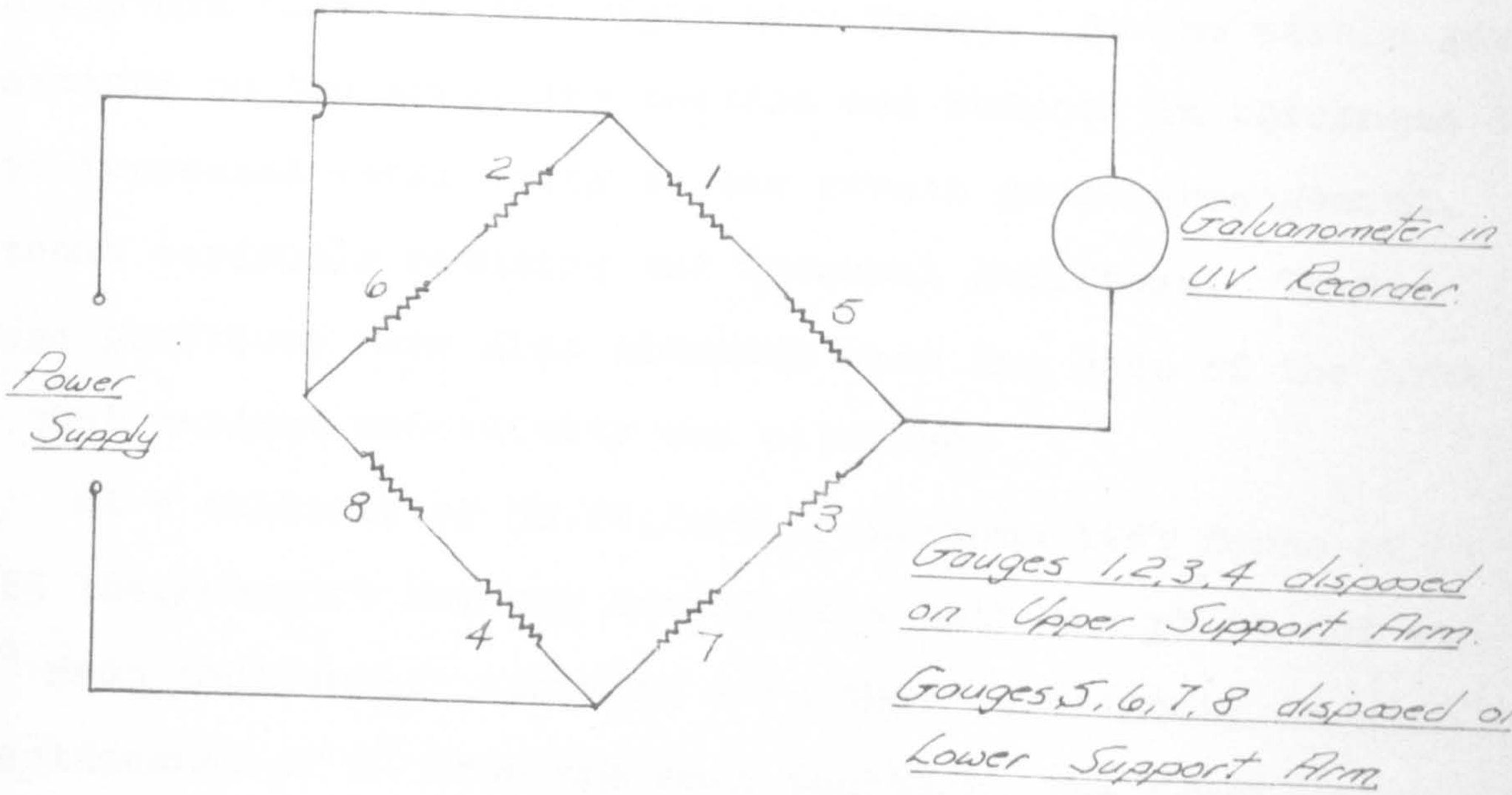

Fig. 10.4. Four Active Arm Wheatstone Bridge Circuit

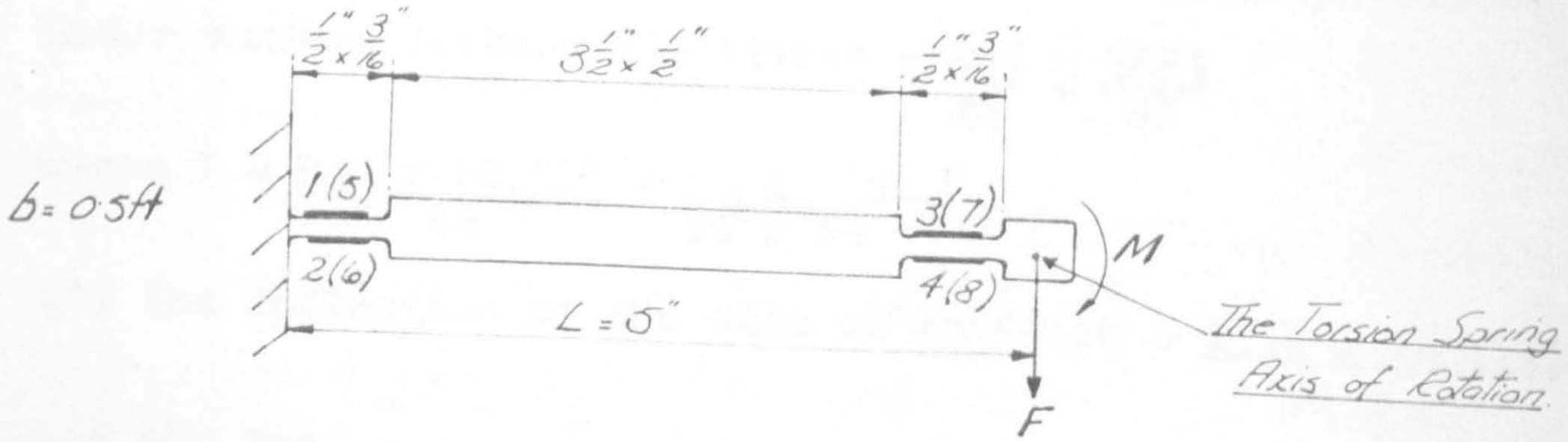

Fig. 10.5. The Support Arm Design

A four active arm Wheatstone bridge arrangement was considered, which included eight strain gauges, i.e. four gauges disposed on each support arm (as shown in Fig. 10.4) and arranged so that lift forces and not moments were recorded. This ordered arrangement is discussed further in ref. 9.4.

A typical design calculation is now given for the support arms, where it is reasonably assumed that the supports act as cantilevers fixed to the rigid main frame. At the strain gauge positions on the arms, the section was reduced in thickness to give increased sensitivity to the strain gauge arrangement, without seriously reducing the flexural stiffness. These gauge positions were also situated near the ends of the arms so that maximum sensitivity was attained.

At a velocity of 50 ft./sec. a maximum lift force of 1.25 lbs./support arm was anticipated with the plate set at 20° mean incidence. Assuming a further oscillatory angular displacement of 2° from the mean position, the torsional moment becomes 1.53 lb. ft./support arm. It can be shown using the moment-area method, that the lateral flexural displacement under maximum loading conditions $= \frac{254}{EI} + \frac{1663}{EI}$

where $I = \frac{0.5 \times (0.5)^3}{12} = \frac{1}{16 \times 12}$ in.^{4}

$\therefore$ the deflection at the axis of rotation $= \frac{1917 \times 16 \times 12}{30 \times 10^6}$

$= \underline{\underline{0.012 \text{ ins}}}$.

Similarly the change in slope (i.e. angular rotation at the axis of rotation) under maximum loading conditions is

$$\frac{63.2}{2.EI} + \frac{738}{2.EI} = \frac{400.6}{EI} = 0.0026 \text{ rads.}$$

In comparison with the 'apparent' plate angle of rotation, a maximum error of 7% would occur if the above change in slope is not accounted for in the true angle of plate rotation. This correction can be incorporated in the calibration tests of the rig (see section 10.5).

With the strain gauge arrangement as shown in fig. 10.5 it is possible to determine the maximum stress under a resistance strain gauge for a direct lift force of 1.25 lbs. (maximum) per support arm, i.e. with M = $4\frac{1}{2}$ x 1.25 lb. in.,

$$f = \frac{6M}{bd^2} = 1920 \text{ lb./in.}^2.$$

With an allowable working stress of 40,000 lb./in.^{2} only $^1/_{20}$th of the maximum sensitivity of the strain gauge arrangement is used. This sensitivity could be increased with a reduction in the section thickness of the support arm. However, the flexural deflections would, as a result, increase and coupling between the angular and flexural displacements would occur.

In addition to the brief description of the oscillating rig and the above design calculations, it is now necessary to give a fuller account of the structural design (see fig. 10.2).

From the design calculations, the suggested mild steel test plate 18" span, 9" chord and $\frac{3}{8}$" thickness was used for all the experimental work. The end shafts supporting the test plate between the two support arms were made of $\frac{1}{2}$" diameter mild steel, reducing to $\frac{3}{8}$" at the plate edges. For a shaft less than $\frac{1}{2}$" diameter, the distortions would have proved too large to ignore in the calibration tests.

With the end shafts mounted rigidly in the torsional spring units, it would have been difficult to set the plate at a mean incidence by fixing the support arms to a quadrant. Therefore with the support arms each positioned 4" away from the plate edge, a coupling was provided in each shaft to accommodate the setting of mean incidence to the plate, without disturbing the supports. A coupling was designed with slots in one flange such that a mean incidence setting between 0-35° could be held by three inset locking screws clamping both flanges together (see fig. 10.2). Graduations were marked on the one flange of a coupling, so that the mean incidence could be positioned accurately.

The support arms were designed basically as suggested in the previous calculations (see fig. 10.6) and were mounted horizontally in the main support assembly by means of four $\frac{1}{8}$" thick plates bolted to each arm. Both arms protruded 7" upstream of these support plates.

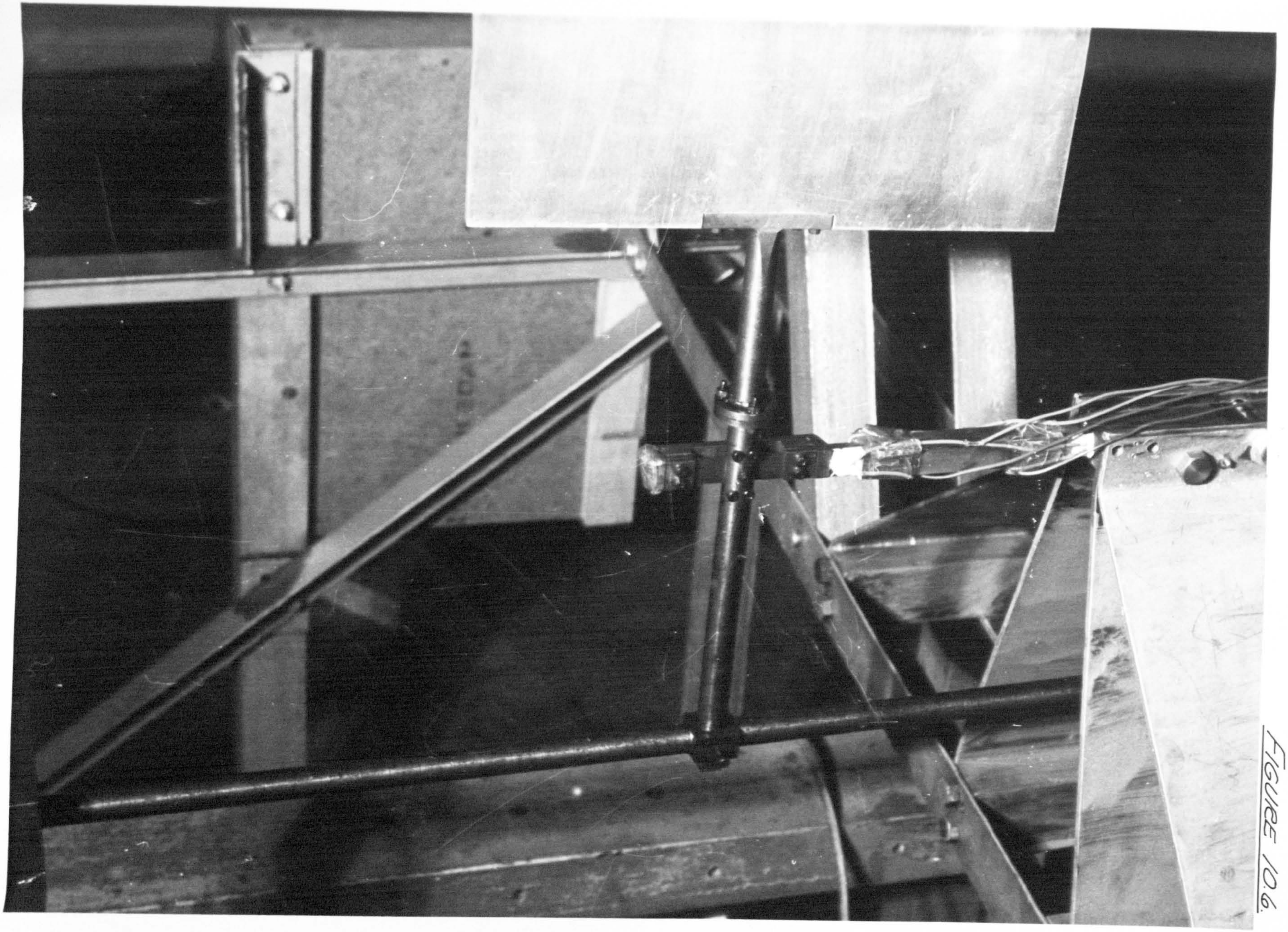

FIGURE 10.6.

THE SUPPORT ARM ARRANGEMENT.

The strain gauge arrangement was as shown in fig. 10.4. The gauges used were Hawker Siddeley HNR/200/0125/E with gauge factor 1.83, nominal resistance 200 ohms ± 2½% and physical dimensions 0.35" x 0.15".

To ease the difficulty in aligning the gauges on the reduced sections of the support arms, gauge centre lines were scribed around the gauge areas on the reduced sections. The surfaces, to which the gauges were to be fixed, were slightly roughened and thoroughly cleaned with acetone. The gauges were then cemented to the surfaces with the recommended adhesive, 'Durofix'. Great care was taken at this stage to align the gauges correctly in position and simultaneously to press them hard against the surfaces. Although this was only a five minute procedure for each gauge, it was still necessary to cure each one under a heating lamp for 24 hours. As a means of protection against humidity and accidental knocks, a very low modulus silicone rubber coating was liberally pasted over each gauge.

Integral with the above strain gauge units on each support arm were mounted the flat spring stiffness assemblies (see fig. 10.6). Each flat spring was found to be adequate with dimensions 2½" x ½" x 0.025" although twice this thickness was estimated in the design calculations. Both springs were positioned on U-shaped formers and clamped to them using

packing pieces and setscrews. By varying the lengths of the springs (i.e. by altering the lengths of the packing pieces), the frequency of oscillation of the plate could be set at any desired value within a specified range.

In order that the torsional spring action could be transmitted to the test plate, it was necessary to clamp both end shafts to the two flat springs. This was achieved (as shown in fig. 10.6) by producing a $\frac{1}{2}$" wide groove in the end shafts, four inches from the test plate. Each flat spring was then locked in a groove by a clamping piece located by two setscrews and a taper pin, to eliminate any frictional movement of the spring relative to the shaft.

One principal requirement of the oscillatory rig is that the angular displacement of the test plate should be recorded. This was achieved using a Sperry A.C. Rotary Pickoff mounted on the upper support arm. This device was compact, accurate and produced negligible frictional damping as well as an output signal directly proportional to shaft rotation and it proved ideal for this application. With this transducer located in the end of the upper shaft, direct angular displacement readings could be obtained.

From the design calculations, it was shown that additional inertia was required in the oscillating system, so that the damping factor $\mu > -0.1$. Therefore an inertia arm $\frac{1}{2}$" diameter

SCHEMATIC DIAGRAM OF INSTRUMENTATION.

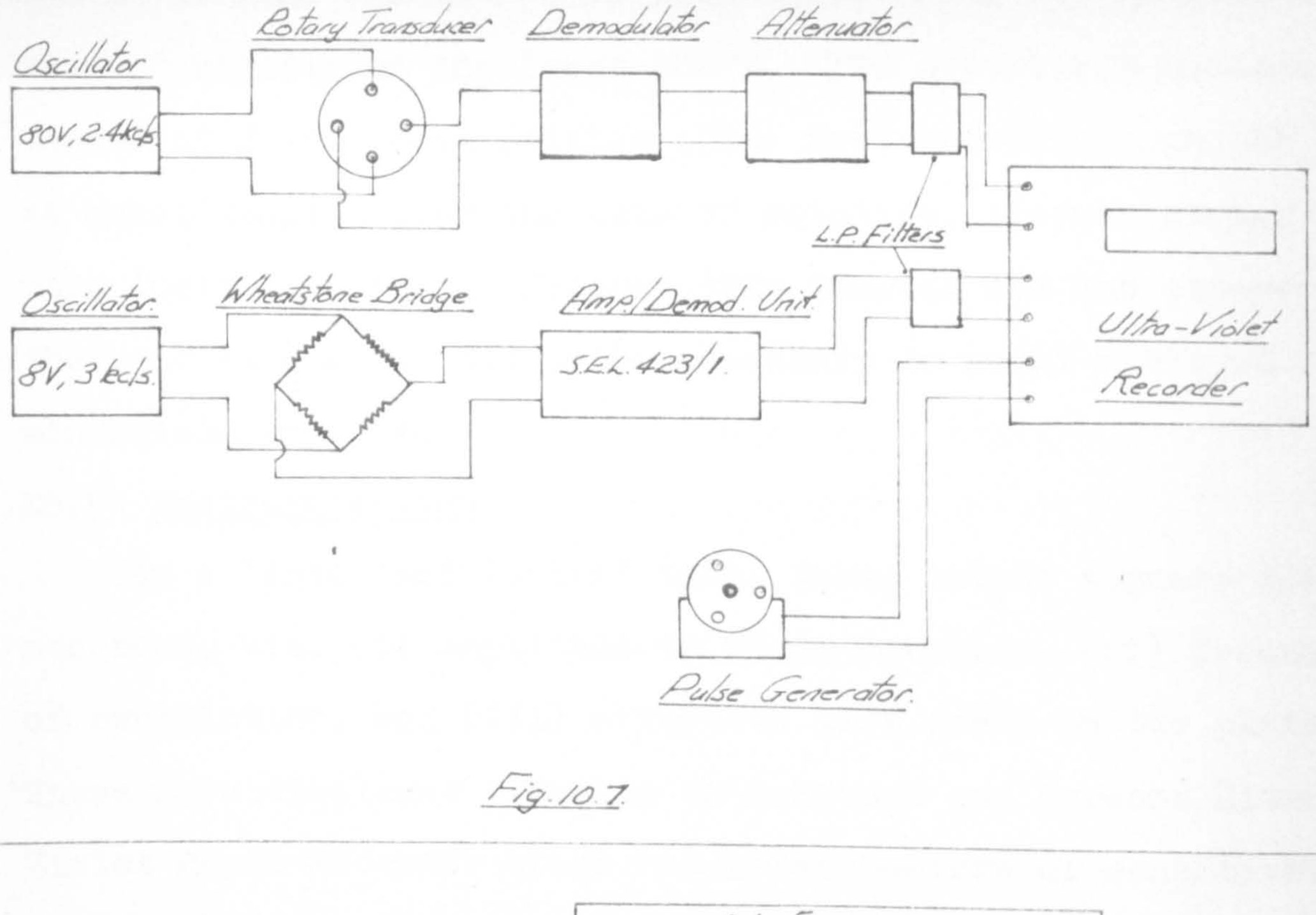

Fig. 10.7.

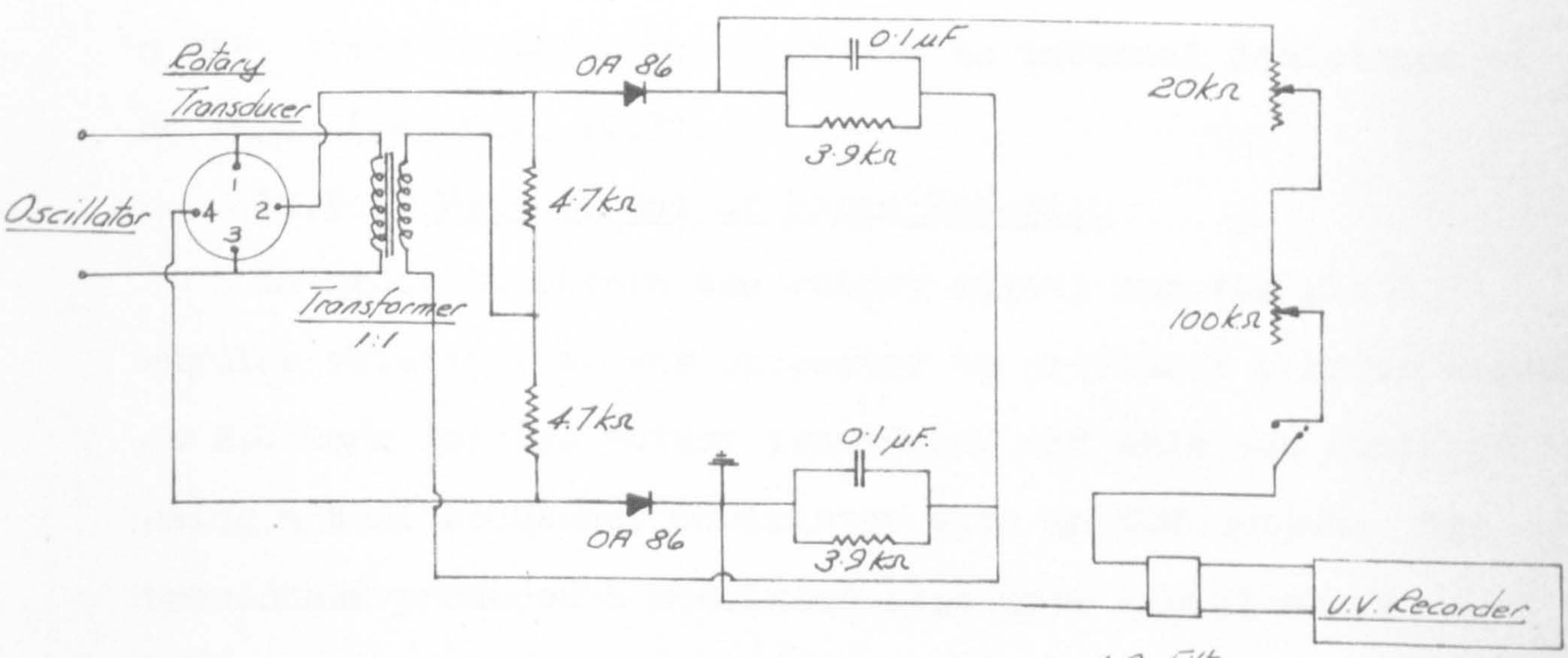

DEMODULATOR AND ATTENUATOR CIRCUIT.

Fig. 10.8.

and 2 ft. long (graduated in inch units along its length) was mounted rigidly on the lower shaft. Two accurately machined masses of 3 lbs. each (within .01%) were positioned on the arm at equal lengths from the axis of rotation, thereby giving a pure inertial torque. Because this inertia arm was exposed to the wind stream, it did prove necessary to mount a curved windshield over it.

10.5 Instrumentation

In a 'free oscillation' test, three output signals were recorded, viz. (i) amplitude of plate rotation, (ii) frequency of oscillation, and (iii) effective lift force on the plate. These were displayed visually on a Savage and Parsons Ultra-Violet Paper Recorder which had galvanometers of sensitivity 0.055, 3 and 10 mA/cm movement and an internal resistance of 80 ohms. (see fig. 10.7).

10.5.1 Measurement of Plate Rotation

In order to obtain the output signal for the plate angular rotation, it was necessary to provide a carrier signal at 2.4 kc/s for the rotary transducer and this was achieved by using a Beat Frequency Oscillator with an 80V output. The transducer produced a modulated sine wave signal whose amplitude was directly proportional to the angle of rotation and whose frequency was equal to the plate frequency. To obtain maximum sensitivity of the transducer it was necessary

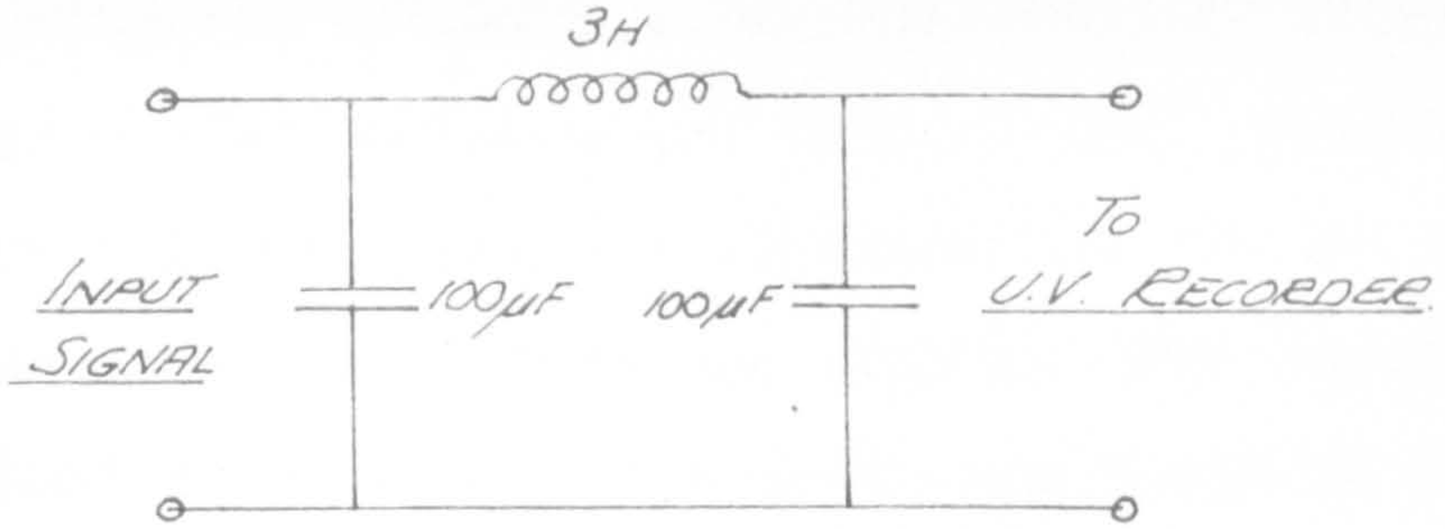

$$\text{Cut Off Frequency} = \frac{1}{\pi\sqrt{2LC}} \simeq 8 \text{ c.p.s.}$$

LOW-PASS FILTER

Fig. 10.9

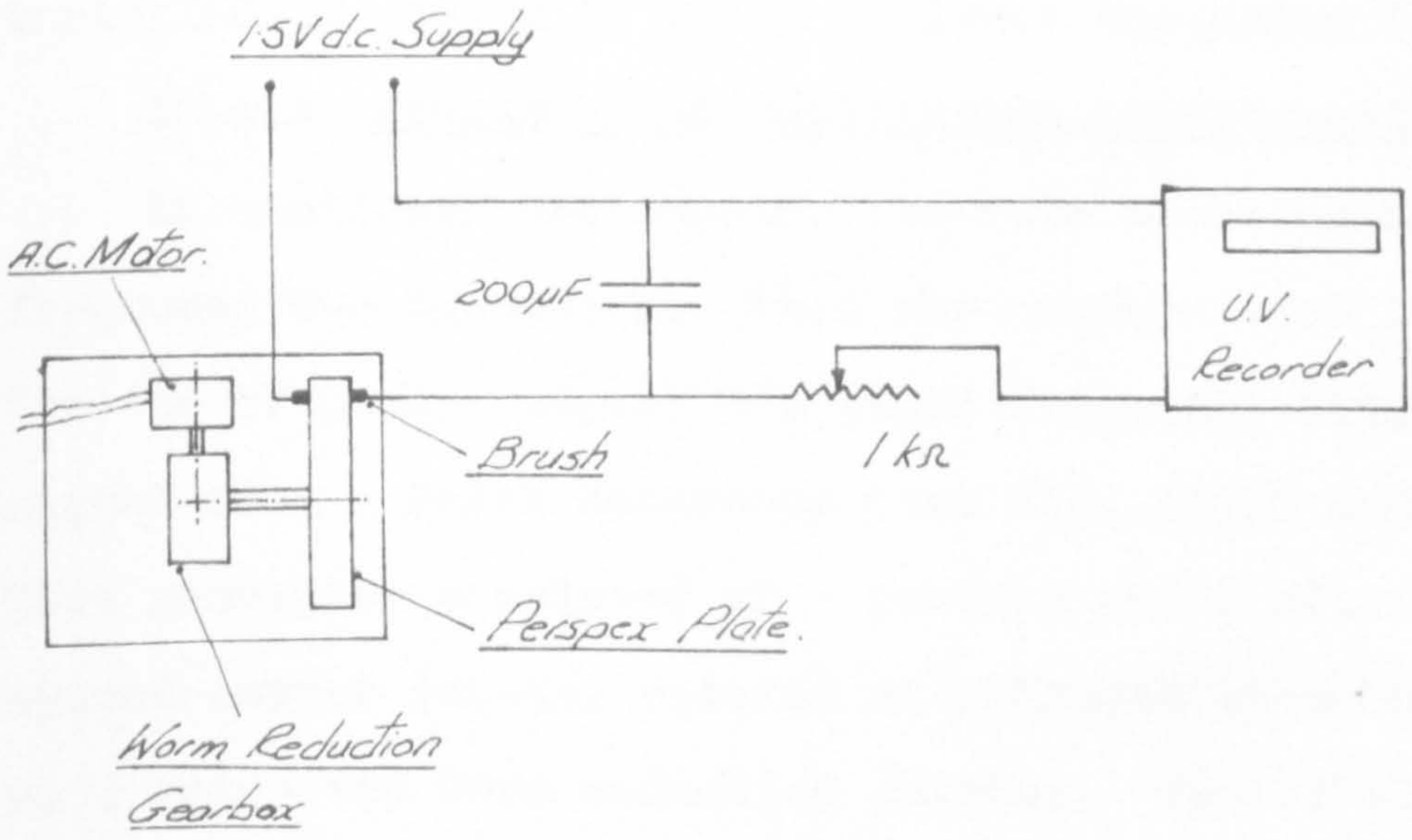

THE PULSE GENERATOR CIRCUIT.

Fig. 10.10.

to zero its spindle position with respect to its field windings. This was effected by using a special spanner which rotated the transducer casing on the upper support arm. Before the transducer output signal could be monitored on the UV recorder, it was necessary to demodulate the signal. The demodulator unit already installed on the main frame was found to be quite adequate and further details of this RC network are given in ref. 10.9. Similarly the attenuator previously installed on the frame by Birdsall (see ref. 10.9) was found to be adequate in limiting the current through a 0.055 mA/cm sensitive galvanometer of the UV recorder (see fig. 10.8). Before the signal was finally transmitted to the UV recorder, however, a simple low-pass filter (cut off frequency 8 c.p.s.) was installed in series in order to limit the noise (see fig. 10.9).

10.5.2 Frequency of Oscillation Measurement

As mentioned previously, accurate measurement of plate frequency was necessary. This was accomplished by comparing (on the UV paper output) the plate frequency with that of a signal from a Pulse Generator (see fig. 10.10 and 10.11). This generator consisted of a perspex plate with three equally spaced copper insets, rotated at constant speed by a small a.c. motor and worm reduction gearbox. Two brushes completed the electrical circuit to a 200 μF capacitor and 1½ volt d.c. supply. Each time a copper insert passed between the two brushes, a pulse (varied in magnitude by a potentiometer)

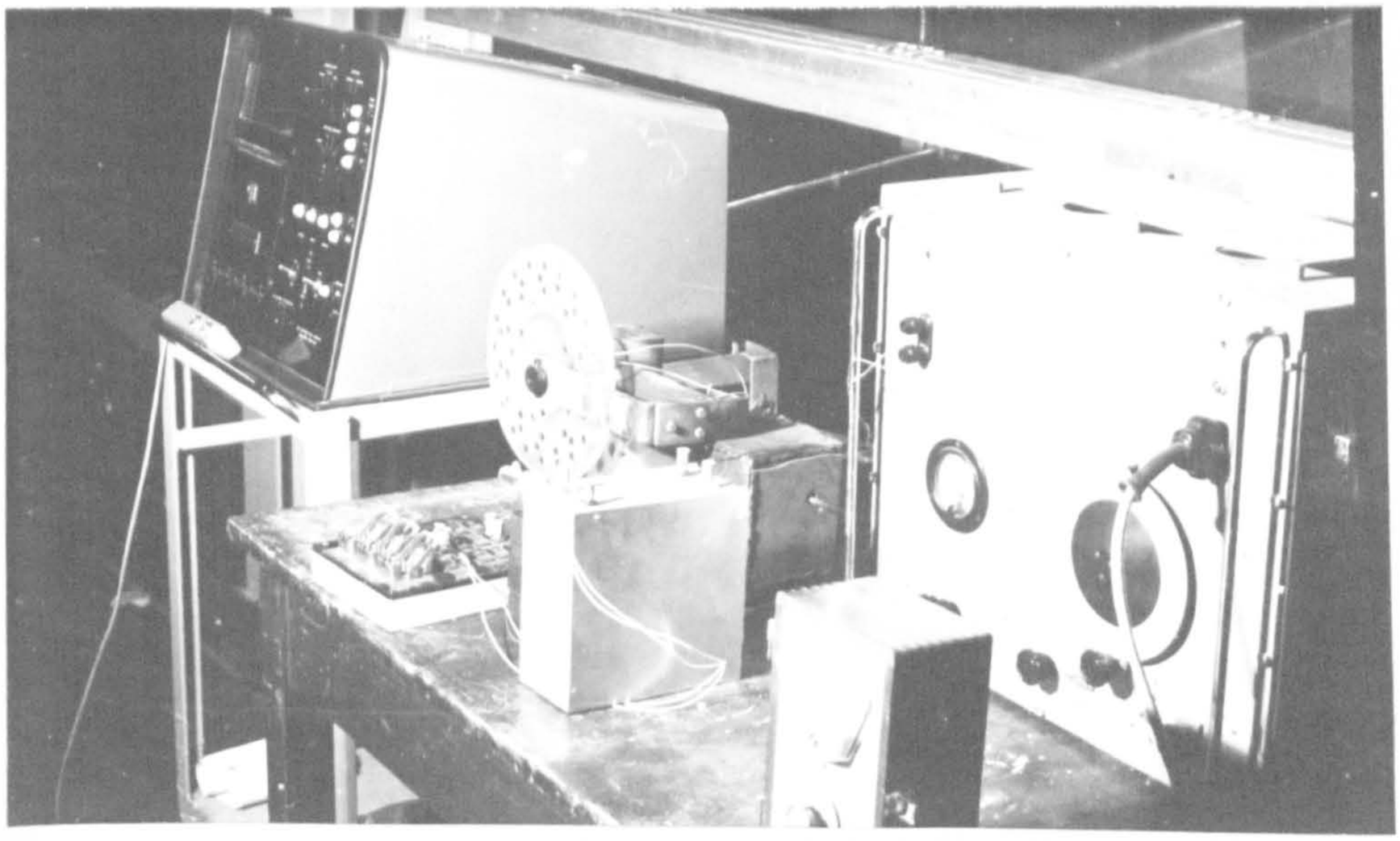

Fig. 10.11

Logarithmic Distorting Circuit

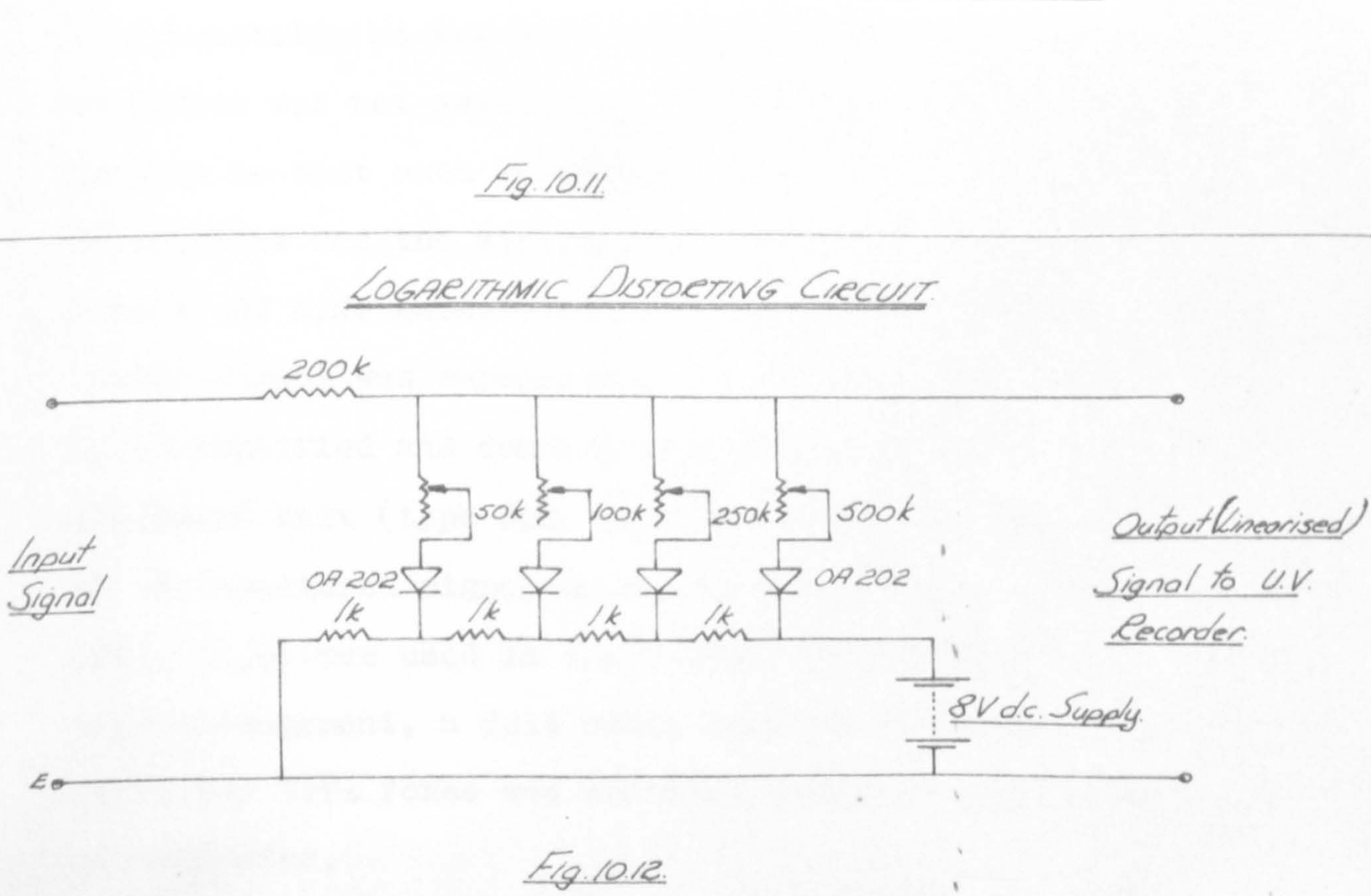

Fig. 10.12.

was monitored through a 3 mA/cm sensitive galvanometer on to the UV recorder screen (see ref. 10.10). This proved more suitable than the 50 c.p.s. marker in the recorder, as the latter obliterated the transducer signals.

10.5.3 Measurement of Effective Lift Force

The resistance strain gauge arrangement designed to measure the lift force, could be used with a d.c. or a.c. power supply. For 200 Ω, 30 mA type gauges a 24 volt d.c. power supply could be used with the 'four active arm' wheatstone bridge arrangement (see fig. 10.4). It can be shown, however, that for a 2 lb. lift force applied to the plate, a d.c. system would produce a 0.5 cm deflection on the UV recorder using the most sensitive 0.055 mA/cm galvanometer. Unfortunately, at the time of the experiments a stable d.c. amplifier was not available. Therefore, an a.c. arrangement, similar to that used in section 10.5.1, was used as an alternative and the strain gauge arrangement was excited by a 3 kc/s, 8V S.E. Labs. Oscillator (type S.E. 511/S). The output signal was superimposed on an a.c. carrier, and it had to be amplified and demodulated using a standard S.E. Labs. Amp/Demod Unit (type S.E. 423/1). To reduce the noise level of the monitored signal on the UV recorder, a low-pass filter (fig. 10.9) was used in the circuit (see fig. 10.11). With this arrangement, a full scale deflection of the calibrated effective lift force was obtained using a 0.055 mA/cm galvanometer.

10.5.4 Measurement of Phase Angle

In order to estimate the Z_q derivative, it was necessary to obtain the phase angle by which the lift force leads the angular displacement. Three attempts were made to measure this angle accurately:- (a) by using a phase comparator, (b) by Lissajous figures on an oscilloscope, (c) by direct estimation from the recorded trace histories.

10.5.4a The Phase Comparitor

A Muirhead phase comparitor was at first used to obtain the phase angle. This apparatus made a direct comparison of both the effective lift and displacement vectors. However, it was found that constant amplitude oscillations were required from both signals to give a direct reading of the phase angle. This of course was not possible with a decaying oscillation technique and as a result this method was discontinued.

10.5.4b Lissajous Figures

As an alternative to the above method, the lift and displacement signals were fed onto the X and Y plates respectively of an oscilloscope. The one signal was fed in via an adjustable calibrated phase-shift unit, such that the usual Lissajous figure could then be transformed to a straight line by adjustment. It was found that both signals required amplification to register a figure on the oscilloscope. Because stable d.c. amplifiers were not available, a further alternative was required.

10.5.4c Direct Estimation from Trace Histories

The simplest but most laborious method of direct estimation from the UV paper records was finally used. This involved recording the trace histories of both signals over a five second period, with a UV paper speed of 5 inches/sec. For one condition of plate frequency, mean incidence and tunnel wind speed, this procedure was usually repeated four times.

With the aid of an accurate UV paper reader it proved quite easy to measure the phase angle between the two superimposed signals. Hence for four sets of five second trace histories, approximately 60 phase shifts (of good repeatability) were measured and averaged to give the phase angle for one condition of the oscillating plate.

An unexpected inconsistency in the effective lift sine curve did occur at mean incidence positions between 20-25°. From the static tests it was found that the plate stalled between 20-22°. It was therefore anticipated that the lift force would change sign in the above range of incidence. Although the flow separation over the plate resulted in an unsteady oscillatory lift force of greatly reduced amplitude compared with smaller angles of incidence, the force did not change sign. In view of these unsteady flow effects, measurements of phase angle were discontinued above a mean

incidence of 15^{o}. The above inconsistencies appear to be due to no fault of the rig design, but more so to wind tunnel interference effects. At present, however, very little is known about wind tunnel effects on oscillating three dimensional wings or plates, especially for open-jet wind tunnels (see ref. 10.11).

10.5.5 Wind Tunnel Interference Effects

To confirm the existence of wind tunnel interference effects, similar tests were carried out with the same oscillatory rig mounted in the return section of a 7' x 5' closed section wind tunnel. The return section dimensions were 18' by 12' and thus the tunnel effects on the plate were assumed negligible. For the M_q derivative values obtained in the open-jet tunnel, it was found on comparison with results in the larger tunnel that the interference effects in the 3' 6" open-jet tunnel were very pronounced, especially near and above stall conditions (see Chapter 12). At the time of these latter tests, the necessary equipment required to obtain Z_q was not available. However interference effects would also be apparent in the Z_q derivative.

10.6 Instrument Calibration

This section deals with the necessary calibrations of the rotary transducer, the strain gauge arrangement and the torsional stiffness in the oscillatory system. A check was

also made on the intrinsic instrument phase lag between the effective lift force and angular displacement signals in 'wind off' conditions.

The calibration of the plate angular displacement was made with the Sperry rotary transducer connected in the circuit shown in fig. 10.7. With the plate displaced through a small angular rotation on the pickup, it was also necessary to account for the angular distortion of the support arms (see section 10.4.1b for further details). Dial indicators mounted on the leading and trailing edges of the vertical plate, and supported from the main frame, were found to be adequate for measurement of the actual angular displacement under a torque applied by a weight pulley system. Simultaneously a comparison was made between the true rotation and the rotation recorded by the rotary transducer on the UV recorder. This was found to give a linear relationship between the two rotations such that a calibration of 0.25 degrees/cm movement on the UV paper was obtained for displacements between $\pm 3^{o}$.

Before a calibration test was carried out on the lift force measuring arrangement, a check was made to determine the possible applied moment interaction effects on the lift sensing strain gauge arrangement. This was carried out independently on both support arms with the plate oscillating

in 'wind off' conditions. The upper support arm proved to be completely free from any interactions, even when measured at a higher amplification than was normally used. However interactions did occur on the lower support arm. These were thought to be due to an incorrectly positioned strain gauge. It was therefore decided to use the upper support arm arrangement only to measure the lift force. With this arrangement connected to the 8V a.c. supply, the test plate was loaded at the axis of rotation in the force direction. From the corresponding recording obtained on the UV paper, a linear calibration of 0.1803 lbs/cm trace movement was obtained.

With the angular rotation of the test plate previously calibrated, an accurate calibration of the torsional stiffness was obtained by applying a pure couple to the plate and measuring the true angular displacement on the UV recorder. A linear calibration of 80.7 lb. ft./rad. was finally obtained for the torsional stiffness.

Use of a.c. circuits to measure both the effective lift force and angular displacement implied inherent phase lags in the measuring instruments. This had to be accounted for from 'wind off' tests so that the required aerodynamic phase lag was determined between the two components in 'wind on' tests. A 'wind off' test was then made on the oscillating plate with

a light spring arrangement attached to the plate to simulate the lift force varying with incidence. The spring stiffness was small so that the frequency of oscillation was not seriously affected. After analysing the lift force and displacement traces, the inherent instrument phase lag was such that the angular displacement lead the effective force vector by 319.3^{o}. Since the frequency of oscillation for 'wind off' test and 'wind on' tests varied less than 0.5%, the above phase lag was assumed for 'wind on' tests.

10.7 The Experimental Procedure

Throughout the experimental work, the oscillatory rig and the measuring instruments remained as shown in fig. 10.6 and 10.7. Similarly the torsional stiffness and inertia remained constant, although the tunnel velocity was varied for tests in both the open jet and closed section wind tunnels.

Before each set of tests the instrumentation was allowed a 'warming up' period of an hour, after which all the power supplies proved quite stable. With the rig set normal to the open jet tunnel axis and the plate mean incidence set at 0^{o}, a 'wind off' test was performed on the plate. This involved the manual 'bonking' of the plate and the recording of the free decaying oscillation (from amplitudes of approximately 3^{o}) on the UV recorder at a paper speed of 50 inches/min. Simultaneously a pulse was generated with which to compare

the recorded frequency of oscillation of the plate. This 'wind off' procedure was repeated three times to check the repeatability of the results.

The previous procedure was then repeated for 'wind on' tests at 0° mean incidence in the 3' 6" open jet tunnel at a wind velocity of 38.6 ft./sec. A resultant Strouhal number and Reynold number in the order of 0.4 and 1.81×10^{5} respectively were obtained for these tests. Both parameters were outside the design range, but the resulting derivatives were still considered adequate for use in the theoretical analyses.

In the 'wind on' tests, ultra-violet paper recordings were made at two speeds. With a speed of 50 inches/min., the decaying sinusoidal traces of displacement and lift force were recorded along with the frequency comparison pulse. Hence the frequency and rate of decay of oscillation could be accurately obtained. However, to obtain an accurate value of the phase angle (see section 10.6) between the components of lift force and angular displacement the paper speed was set at 5 in./sec. At both paper speeds it was necessary to repeat the 'wind on' tests three or four times to obtain an average value of frequency of oscillation, rate of decay and phase angle. The variability was due to wind tunnel turbulence level and other unsteady effects varying slightly from one test

to another. However the above parameters were always within a scatter range of ± 5% for each test.

To provide a complete picture, both 'wind off' and 'wind on' tests were carried out for mean incidence values of $2\frac{1}{2}$, 5, $7\frac{1}{2}$, 10, $12\frac{1}{2}$, 15, 20, 25, 30 and 35° and in all of these the trace reading measurements were only considered in the range $|\theta| = 1.5^{\circ} - 0.5^{\circ}$.

Similar dynamic tests were also carried out in the 18' x 12' return section of a 7' x 5' closed section wind tunnel, to determine the tunnel interference effects on M_q (see section 10.5.5). Because the maximum tunnel velocity was only 30 ft./sec., the resultant M_q derivatives were obtained at a Reynolds number of 1.4×10^5 and an approximate Strouhal number of 0.5.

In all cases it proved to be quite straightforward to determine the frequency of oscillation by comparison with the pulse trace. Similarly the phase angle was easily obtained in the first section of experimental work by the method discussed in section 10.5.4c. However a rather laborious procedure was involved when determining the rates of decay of the angular displacement oscillations between $|\theta| = 1.5^{\circ}$ and 0.5°. (A function generator was made in order that the exponential trace could be distorted to a calibrated linear trace, but no success was obtained with the method (see

fig. 10.12)). This involved drawing an exponential envelope over the peaks of a decaying, sinusoidal amplitude of oscillation trace.

Now $\theta = e^{\mu t}$ where μ = the required damping factor

and $\log_{10}\theta = 0.4343\ \mu t$

Hence, from the drawn envelope, a graph of $\log_{10}$ (amplitude) against time usually gave a linear slope = $0.4343\ \mu$ and the damping factor μ was obtained directly. This procedure was repeated for all trace recordings in both 'wind on' and 'wind off' tests and the ensuing results for m_q and z_q are given in section 12.

CHAPTER 11

SCALE MODEL DYNAMIC WIND TUNNEL WORK

Full scale tests on a single strop suspension of a pallet (flat plate) towed by a helicopter did not prove very satisfactory for a study of the pallet stability. This was because the pallet diverged quickly from an equilibrium position and was promptly jettisoned before the helicopter became uncontrollable.

In an attempt to reproduce the full scale instabilities, Austin and Flower (ref. 11.1) subsequently carried out scale model wind tunnel tests on a 12" x 6" flat plate suspended in a 3' 6" open-jet wind tunnel. Conclusions were drawn from both single and twin strop suspension arrangements of the plate. However the majority of these were open to criticism because dynamically similar conditions were not obtained for the model and full scale pallet. Also wind tunnel interference effects on the model plate were thought to be appreciable, especially with confirmation of these effects in the oscillatory derivative work (see 10.5.5). Similar experimental work was carried out by Kitchen and Thomas (ref. 11.2) in the same tunnel, and this is also open to the above criticisms.

To obtain a fuller understanding of the modes of oscillation encountered by the previous investigators, in the absence of tunnel constraints, the author carried out tests on three

different suspension arrangements of a flat plate. These tests were performed in the 18' x 12' return section of a 7' x 5' closed section wind tunnel, and a 16 m.m. film was taken to illustrate the different modes of oscillation.

11.1 Dynamic Similarity between the Model and Full Scale Pallet

In order to obtain similarity in behaviour between a model and a full scale pallet, it is necessary that the geometric and dynamic scales should be the same.

A typical resultant force F, acting at the centre of gravity of the pallet, can be shown to be a function of the following parameters:-

$V,\ g,\ \rho_p,\ \rho_a,\ c,\ E,\ N,\ \alpha,\ \eta,\ \delta,\ b$

where

ρ_p = plate density, ρ_a = air density,

E = Young's Modulus of Elasticity, N = Frequency of Oscillation,

α = Mean Incidence, δ = Structural Damping,

the remaining terms being well known.

Using the Buckingham π theorem, it was deduced that the following non-dimensional parameters must have the same value for the model and the full scale pallet:-

(i) α = Incidence parameter

(ii) $\frac{\rho_a}{\rho_p}$ = Relative density parameter

(iii) $\frac{V^2}{cg}$ = Froude No.

(iv) $\frac{E}{\rho_a V^2}$ = Collar No.

(v) $\frac{Nc}{V}$ = Strouhal No.

(vi) $\frac{\rho_a Vc}{\eta}$ = Reynolds No.

(vii) $\frac{b}{c}$ = Geometric parameter

(viii) δ_s = Structural damping parameter

The simultaneous satisfaction of similarity based on the eight non-dimensional parameters is obviously impossible and therefore parameters of second order importance are ignored. Because only rigid modes of oscillation are considered and structural damping is assumed very small, Collar No. and the Structural damping parameter are ignored. Similarly, although Reynolds No. effect should be taken into account it is of second order importance in comparison with the remaining parameters.

It is found on consideration of the remaining five parameters that it is impossible to eliminate another parameter without seriously upsetting the similarity

conditions. In the model tests carried out by the previous investigators only Froude No., Density parameter and Geometric parameter were considered, Incidence parameter and Strouhal Number being ignored. For convenience, the Froude No. and Density parameter were combined to give a resulting Aerodynamic Force/Gravitational Force similarity criterion:

$$\left(\frac{SV^2}{M}\right)_m = \left(\frac{SV^2}{M}\right)_f \quad \ldots\ldots (11.1)$$

where S = Plate Area, M = Mass of Plate

m indicates model and f indicates full scale pallet.

Equation 11.1 was also assumed to satisfy the "incidence condition", because incidence is a function of aerodynamic and gravitational forces. Using the above parameter along with the geometrical parameter as similarity criteria, similarity is assumed between the model plate and the full scale pallet. A typical example is now given, however, to indicate the error in the assumed similarity above.

With a geometric parameter of two, a linear scale factor of 12 (i.e. $^1/_{12}$ scale model of a 12' x 6' full scale pallet) a pallet mass of 200/g slugs and a model mass of 0.0715/g slugs, a mean incidence α of 15^o was obtained for a full scale wind velocity of 94 ft./sec. (in the theoretical stability results). Substitution of the above data in equation 11.1 gives

$$\frac{M_m}{V_m^2} = \frac{S_m}{S_f} \times \frac{M_f}{V_f^2} = \frac{200}{144 \times g \times 94^2} = \frac{1}{6400g}$$

Hence $V_m = \sqrt{6400 \times 0.0715} = \underline{21.4 \text{ ft./sec.}}$

It was found from wind tunnel model tests that for a velocity of 21.4 ft./sec., the mean incidence of the plate was approximately 45°. In fact it is impossible to obtain similarity when considering the combined relative density and Froude No. parameters together with the geometrical parameter and the mean incidence parameter. Moreover the above discrepancy in mean incidence, does increase as large mean incidences are considered.

If the three parameters, Froude No., relative density and geometric parameters had been considered separately, the model plate would have been made from the same material as the full scale pallet (i.e. steel). A Froude No. comparison for geometrically similar plates would then result in the opposite effect to above, i.e. actual wind tunnel plate mean incidence would have been less than the calculated value. Hence for either of the above methods, similarity conditions are greatly in error because of the discrepancy in the mean incidences.

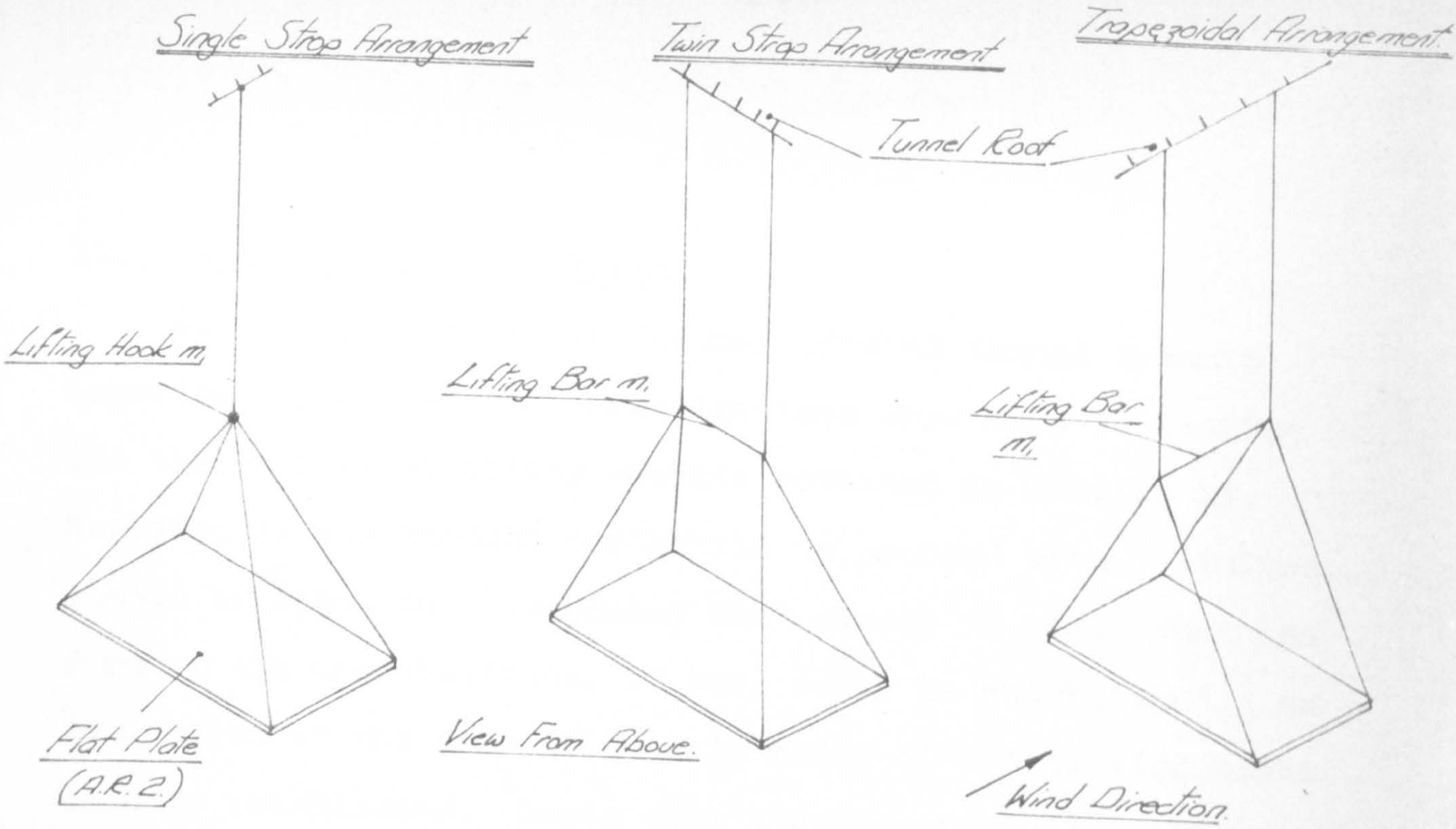

WIND TUNNEL MODELS.

Fig. 11.1.

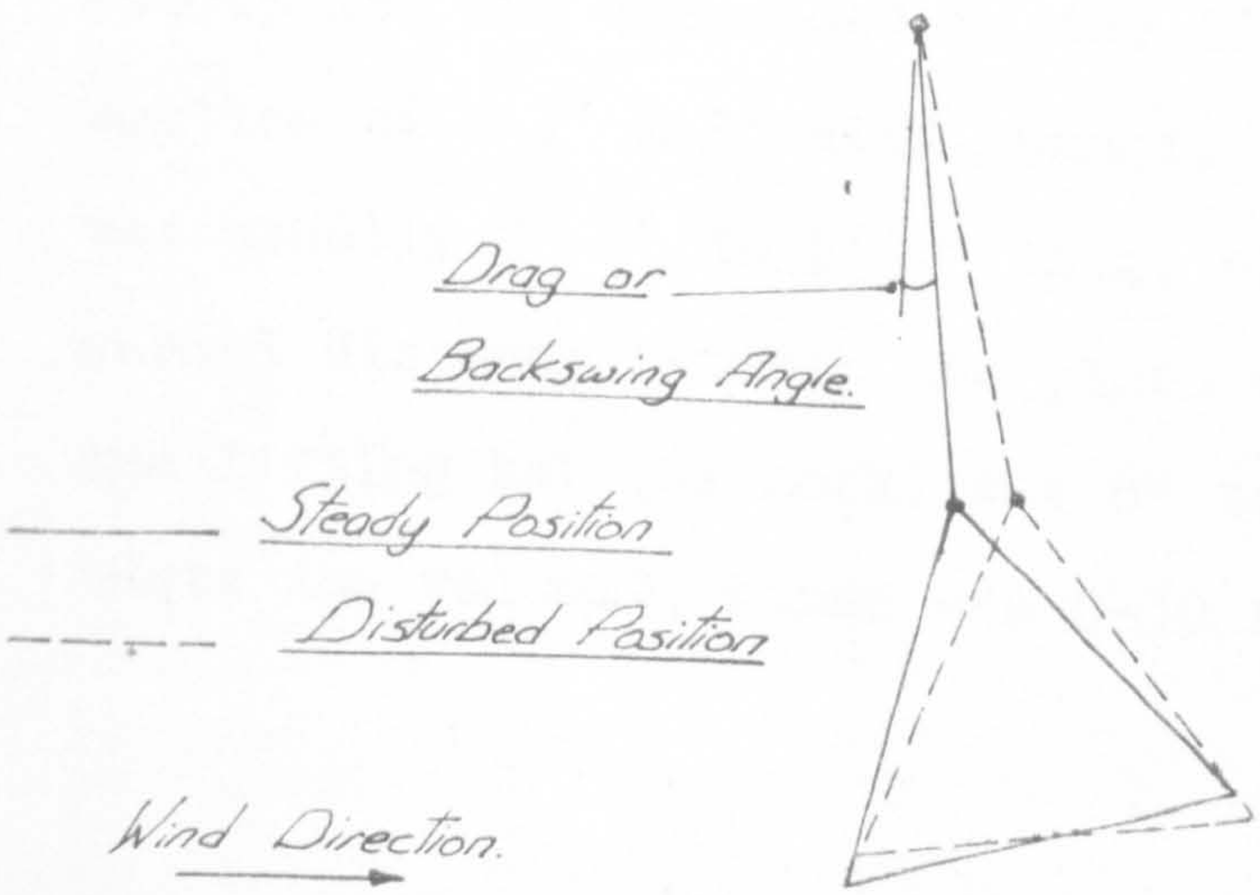

A LONGITUDINAL FLUTTER MODE OF OSCILLATION.

Fig. 11.2.

11.2 Wind Tunnel Model Tests

As a result of the inadequacy of wind tunnel dynamic experiments, no serious investigations were made to confirm the theoretical stability results obtained in Chapter 13. However, it was thought worthwhile to proceed with a limited number of tests on a suspended flat plate, in order that the form of the instabilities, if any, could be established. An indication of the true full scale modes of oscillation might then be established. Tests were thus carried out on the following forms of plate suspension:-

(1) Single Strop, (2) Twin Strop (bifilar), and (3) Trapezoidal as shown in fig. 11.1. A flat plate with dimensions 12" span, 6" chord and $\frac{1}{4}$" thick and weight 0.0715 lbs was suspended in the 18' x 12' closed working section of a 7' x 5' wind tunnel. The upper strop length was usually 2' 6" to 3' 0" long, whilst the corresponding normal distance between the plate centre of gravity and the lifting bar (or hook) was 6" to 1' 0". For all the tests the velocity range was 0-30 ft./sec.

11.2.1 The Single Strop Suspension

The results obtained from these tests were the same regardless of the strop length variations. For velocities of 7 ft./sec. and less, the plate remained in a steady position. An increase in velocity above 7 ft./sec. resulted in a longitudinal flutter mode which increased in severity and frequency (approx. 6 c.p.s.) until a velocity of 13 ft./sec. was reached. This flutter mode consisted of a rotary oscillation about the plate centre of gravity together with a small translational movement (see fig. 11.2). At this stage the drag or backswing angle was approximately 20°. Above 13 ft./sec. however, a definite transition to a pure autorotational oscillation about the plate longitudinal axis occurred (approx. 3 c.p.s.). Oscillations continued in the mode up to 17 ft./sec., whereupon a further transition to a pure yawing mode occurred (approx. 2 c.p.s.) at an approximate drag angle of 30°. Occasionally in this mode the plate yawed quite severely and as a result diverged into the wind, whereupon it 'flipped' over at the zero incidence position.

11.2.2 Twin Strop Suspension (bifilar)

Similar tests to those mentioned above were also carried out with a bifilar suspension of the flat plate (see fig. 11.1). As anticipated the flutter mode occurred in a similar range of velocity as the single strop arrangement. The upper end of

this range was extended to approximately 22 ft./sec. The drag angle at this speed was approximately 40°. Above this velocity a transition to a pure low frequency, yawing mode occurred. With short (2") lifting bars, the mode was particularly severe, but amplitudes were reduced considerably as the lifting bar length was increased. (This, of course, is what we should have expected since an increase in the lifting bar length increases the torsional restoring moment in yaw). These lateral oscillations were not, however, obtained from the theoretical results in chapter 13, because lateral stability was predicted for nearly all the configurations.

11.2.3 Trapezoidal Suspension

With the above suspension arrangements, a strong longitudinal flutter oscillation was encountered (for small angles of mean incidence of the pallet), in both the theoretical and wind tunnel work. In order to eliminate this instability without making additions to the basic arrangement (i.e. using a droque chute), an additional structural constraint was imposed on the plate using the suspension shown in fig. 11.1. With this suspension arrangement it was found necessary to set an initial negative incidence to the suspended plate (with the wind off) so that vertical gusts did not cause the plate to 'flip' over.

From the wind tunnel tests carried out with this arrangement, in a velocity range 0-30 ft./sec., it was found at all speeds that the arrangement remained completely steady in the airstream, even for a lifting bar length of 2". However, below this length there was an indication of the flutter mode experienced in the two other suspension arrangements. Also in comparison with the previous suspension arrangements the backswing or drag angle was greatly reduced. From these tests it appeared that a stable arrangement for suspending the pallet has been found. Subsequent theoretical results have also indicated the plate to be completely stable for certain configurations.

CHAPTER 12

THE EXPERIMENTAL RESULTS AND DERIVATIVE INFORMATION

12.1 General

A series of results are given here for a flat plate of rectangular planform (with square edges) and aspect ratio 2. These results include information from both static and dynamic wind tunnel experiments, together with aerodynamic derivative data obtained from 'lifting line' theory. For convenience, the static wind tunnel results leading to certain derivative terms are discussed initially and the dynamic wind tunnel results are later included with the required set of longitudinal and lateral aerodynamic derivative information.

12.2 The Static Wind Tunnel Results

A comprehensive set of results is given in figures 12.1 .... 12.7 which includes the six components of force and moment acting on a flat plate (of aspect ratio 2) for a wide range of incidence and yaw angles. The variation in both angles is rather excessive (0 - 40°) in comparison to the information required, i.e. incidence range of 0 - 21° and yaw angle range 0 - 10°. However, because of the paucity of information on flat plates of low aspect ratio, together with

FIGURE 12.1.

GRAPH OF LIFT COEFFICIENT AGAINST INCIDENCE FOR VARIOUS YAW ANGLES.

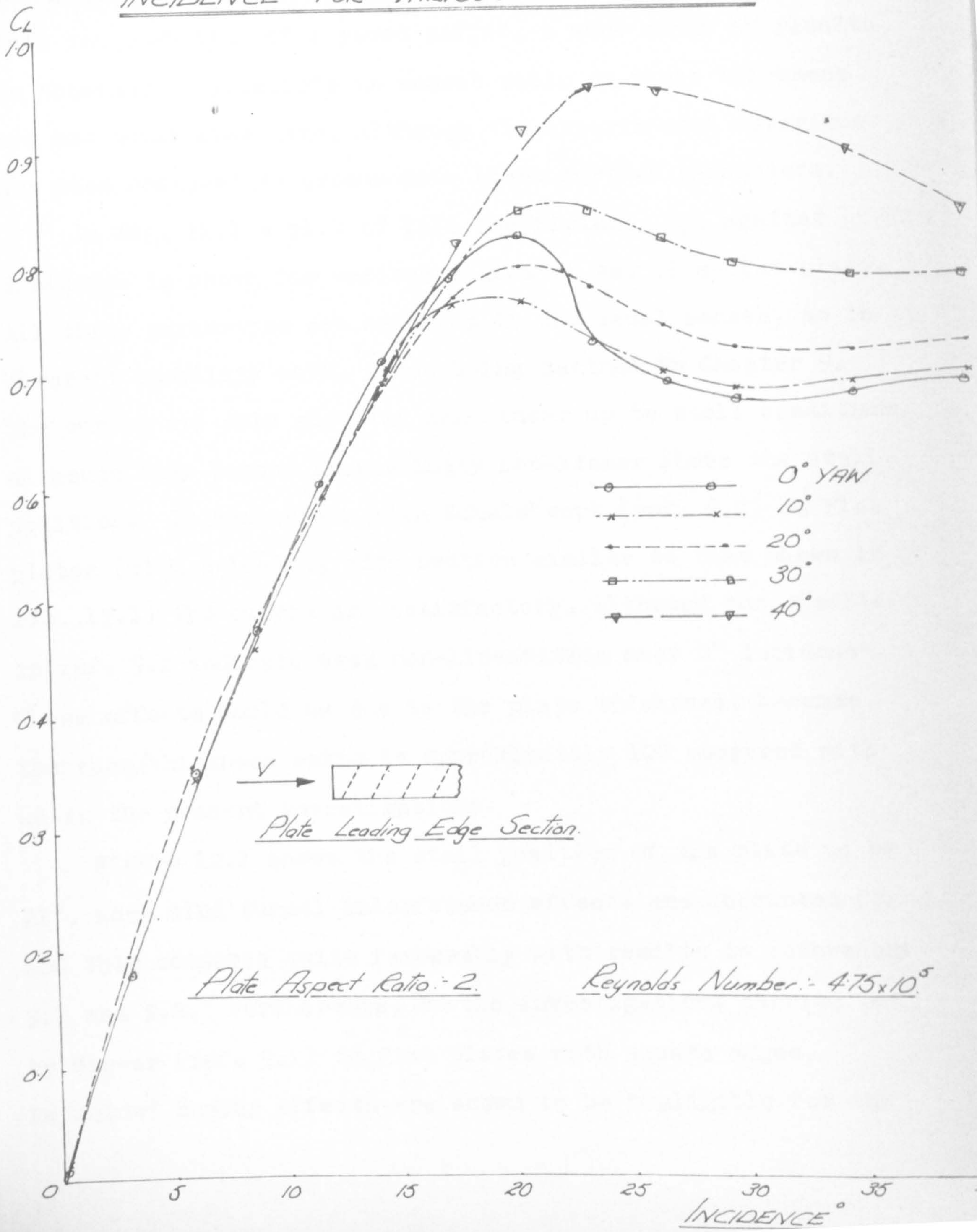

the requirements of data suitable for further investigations into the stability of a yawed pallet, a wide range of results is obtained. Variations in aspect ratio or plate thickness are not considered here, although the experimental apparatus has been designed to accommodate these further parameters.

In fig. 12.1 a plot of lift coefficient, C_L, against incidence is shown for various angles of yaw of a flat plate. All three parameters are measured in the usual senses, as in aircraft stability work, these being defined in Chapter 9. The curves are only slightly non-linear up to stall conditions, although they become increasingly non-linear above the stall position. In comparison with Scholz' work (ref. 9.2) on flat plates (with a leading edge section similar to that shown in fig. 12.1) the curves are satisfactory, although the results in ref. 9.2 indicate weak non-linearities near 0° incidence. These effects would be due to the plate thickness, because the span/thickness ratio is approximately 100 compared with 48 in the present investigations.

Figure 12.1 shows the stall position of the plate to be 21°, when wind tunnel interference effects are accounted for and this compares quite favourably with results in references 9.1 and 9.2. Furthermore, in the investigations carried out by Winter (ref. 9.1) on flat plates with square edges, Reynolds' number effects are shown to be negligible for the

FIGURE 12.2.

GRAPH OF DRAG COEFFICIENT AGAINST INCIDENCE FOR VARIOUS YAW ANGLES.

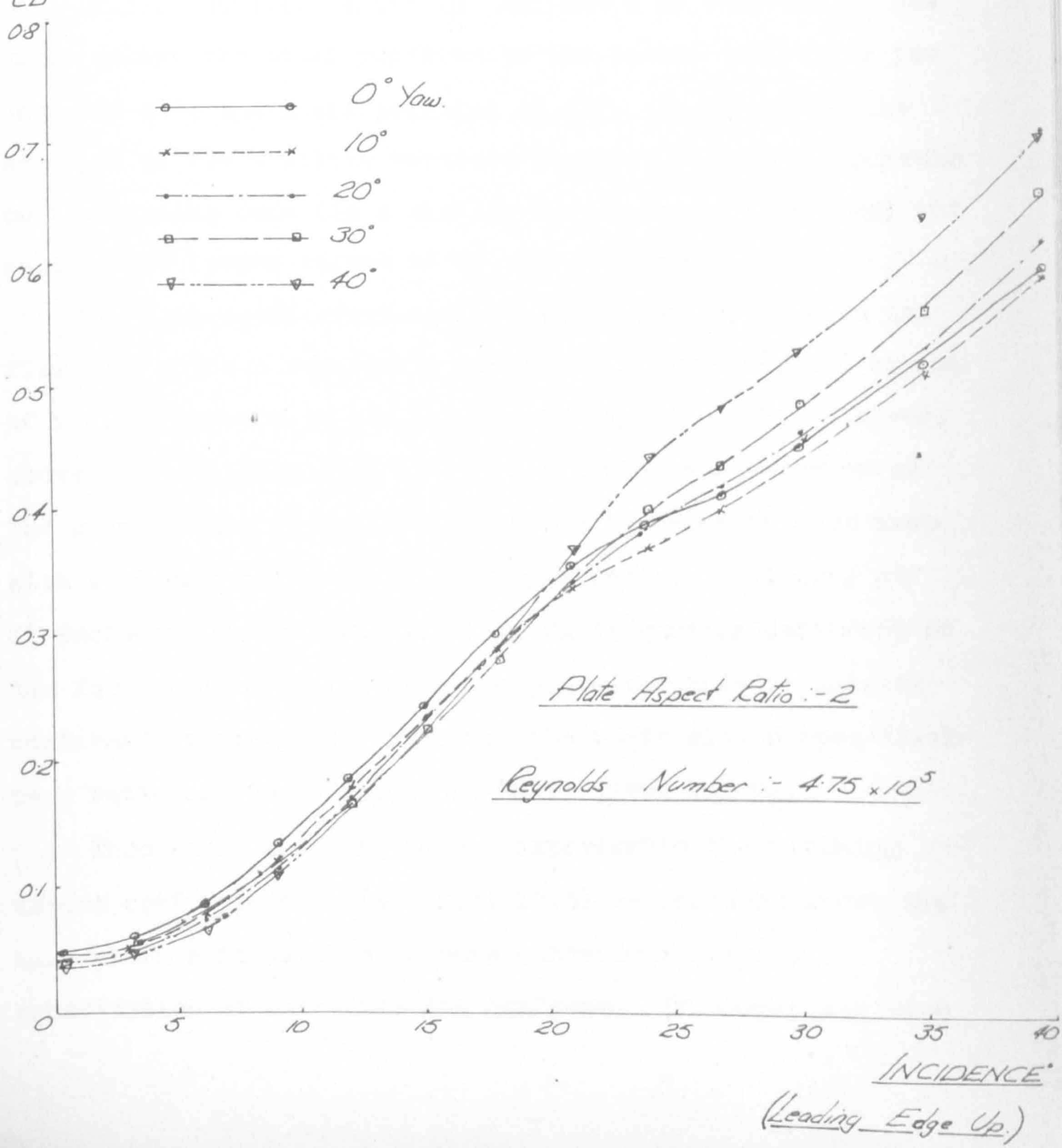

velocity range considered here.

The results for the yawed plate follow the anticipated trends, because the lift curve slope is only altered slightly in the incidence range 0 - 15° when the plate is yawed (see ref. 12.3). However, above 15° incidence an increase of yaw angle delays the stall position to the extent that for a yaw angle of 40°, the stall position is 26°. In addition, the strength of the trailing vortices suppress the flow separation on the leading edge (in a similar manner to a delta wing) and as a result larger values of C_L are obtained.

The drag coefficient against incidence curve shown in fig. 12.2 gives a remarkably constant C_D curve for all values of yaw, considered in the incidence range 0 - 20°. However, above the stall position there is a definite divergence of the curves which is mainly due to the increase of form drag with a corresponding increase in yaw angle. Similarly at 0° incidence and yaw the value of C_D is greatly dependent on the form drag resulting from the plate thickness. This is confirmed by ref. 9.2, where for the plate with a span/thickness ratio of 100, a value of ·02 is given for C_D.

Throughout the wind tunnel experiments the pitching moment coefficient C_m (see fig. 12.3) is measured about the half chord axis as this is more convenient for the substitution of data into the analyses. In comparison with

FIGURE 12.3.

GRAPH OF PITCHING MOMENT COEFFICIENT AGAINST INCIDENCE FOR VARIOUS YAW ANGLES.

Plate Aspect Ratio:-2.

Reynolds Number:- $4{\cdot}75 \times 10^5$

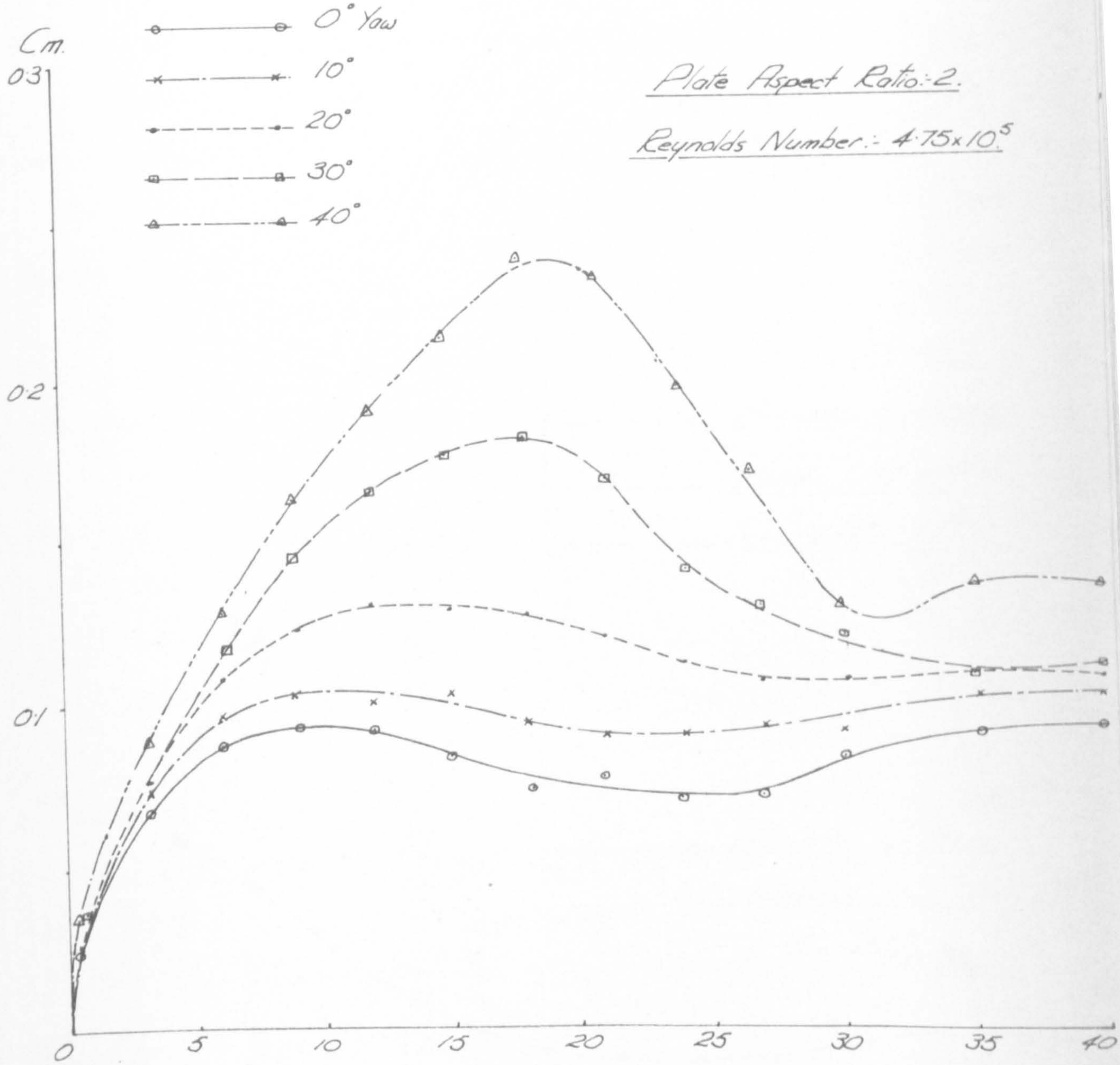

FIGURE 12.4

GRAPH OF NORMAL FORCE COEFFICIENT AND CENTRE OF PRESSURE AGAINST INCIDENCE.

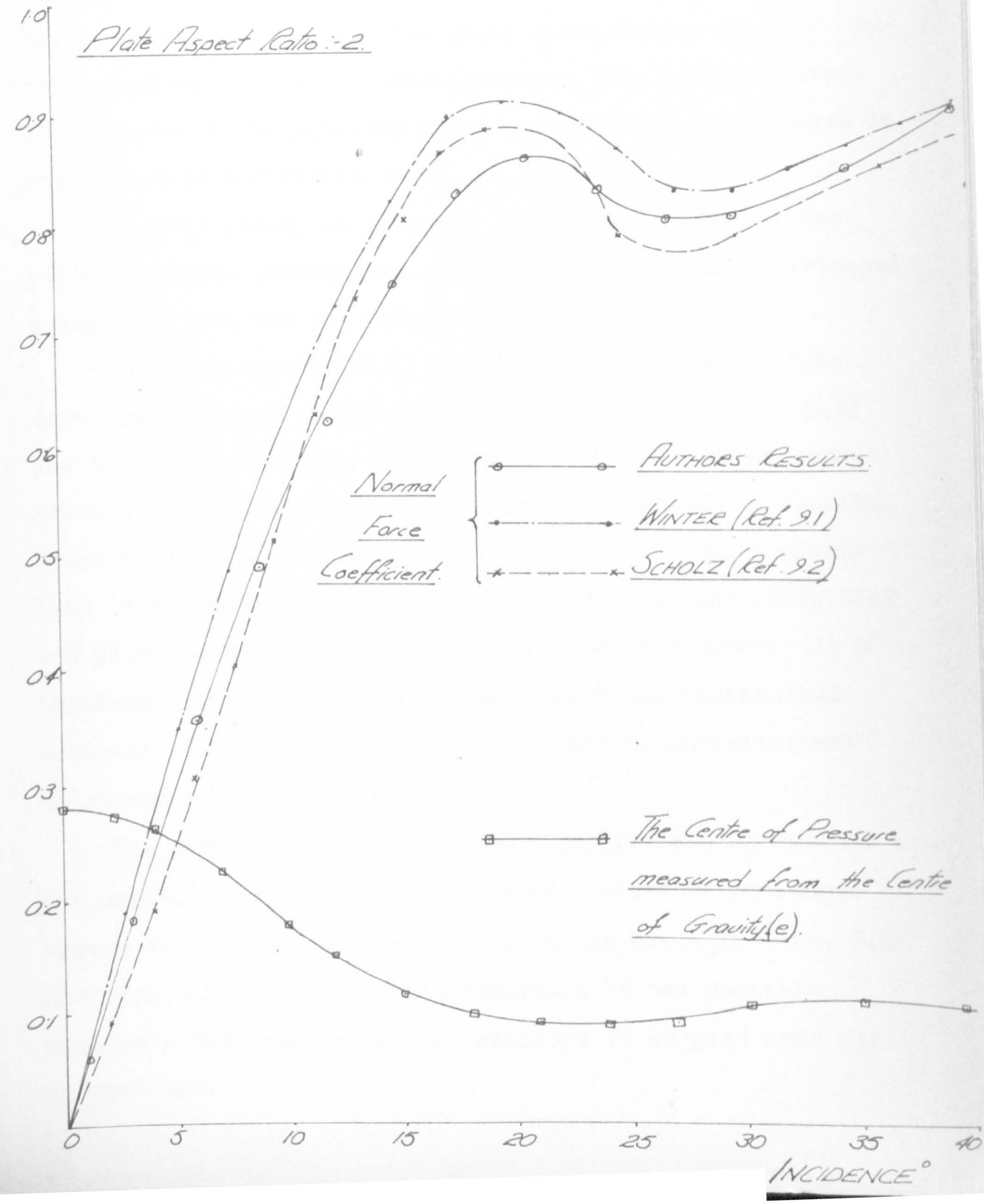

C_m measured about the quarter chord line, the results are very non-linear and open to criticism, even when directly used to determine derivative data for small perturbation theory. For these initial stability investigations, this point is overlooked because the pitching moment coefficient is not used in the important derivative terms.

As anticipated, an increase in yaw angle affects the pitching moment coefficient quite appreciably, as experienced previously with the lift coefficient.

Fig. 12.4 shows the C_N against incidence curves (for zero yaw) obtained by Winter (ref. 9.1), Scholz (ref. 9.2) and the present writer. The agreement is seen to be good. Also, a measure of the centre of pressure position (e) with respect to the plate centre of gravity at 0° yaw is given. This is estimated in the usual manner knowing the lift, drag and pitching moment coefficients at a set incidence. At 0° incidence, this compares favourably with the theoretical estimate of 0·22 - 0·25 for a flat plate of infinitesimal thickness (see ref. 12.1).

The results for the side force coefficient C_Y against yaw angle (see fig. 12.5) for various values of incidence appear to be of a similar order to those given in refs. 7.8 and 12.2, although a direct comparison is not possible because a different order of rotations is adopted here for convenience.

FIGURE 12.5.

GRAPH OF SIDE FORCE COEFFICIENT AGAINST YAW ANGLES FOR VARIOUS ANGLES OF INCIDENCE.

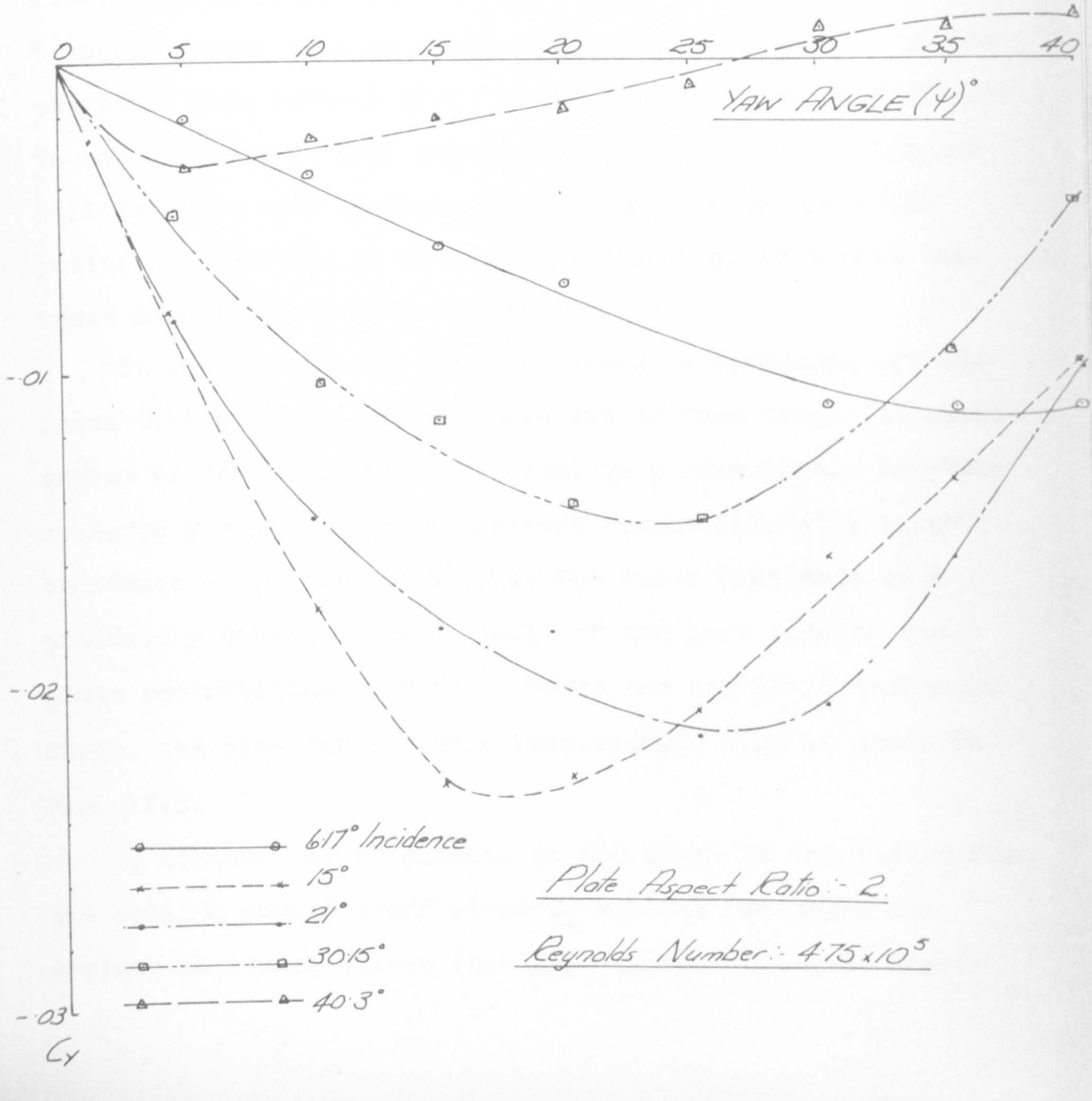

Plate Aspect Ratio :- 2.

Reynolds Number :- 4·75 x 10⁵

It is apparent that between 0° and 6° incidence the effects of yaw on the side force are not large, although a further increase of incidence to the stall point increases the side force appreciably. The C_Y term is clearly dependent on the induced flow over the plate tips (see ref. 12.3). At finite angles of yaw (in the usual positive sense) the induced effects will be greater on the port side than on the starboard side because of a 'shadow' effect. Hence side forces will result from this asymmetric induced loading and will increase with increase of incidence up to the stall position. However, it is apparent from fig. 12.5 that they break down at post stall incidences.

In addition to the induced forces, a component of side force will also act on the plate due to form drag. At small angles of yaw these act in a negative y direction. However, at large yaw angles it is apparent (especially at a large incidence - see fig. 12.5) that the force then acts in a positive y direction as a result of the port side of the plate contributing to force. Hence for the 40·3° incidence curve, the side force coefficient changes sign as shown in fig. 12.5.

A similar set of results to the above is determined for the rolling moment coefficient C_l against yaw angle for various incidence values (see fig. 12.6). Owing to the

FIGURE 12.6.

GRAPH OF ROLLING MOMENT COEFFICIENT AGAINST YAW ANGLES FOR VARIOUS ANGLES OF INCIDENCE.

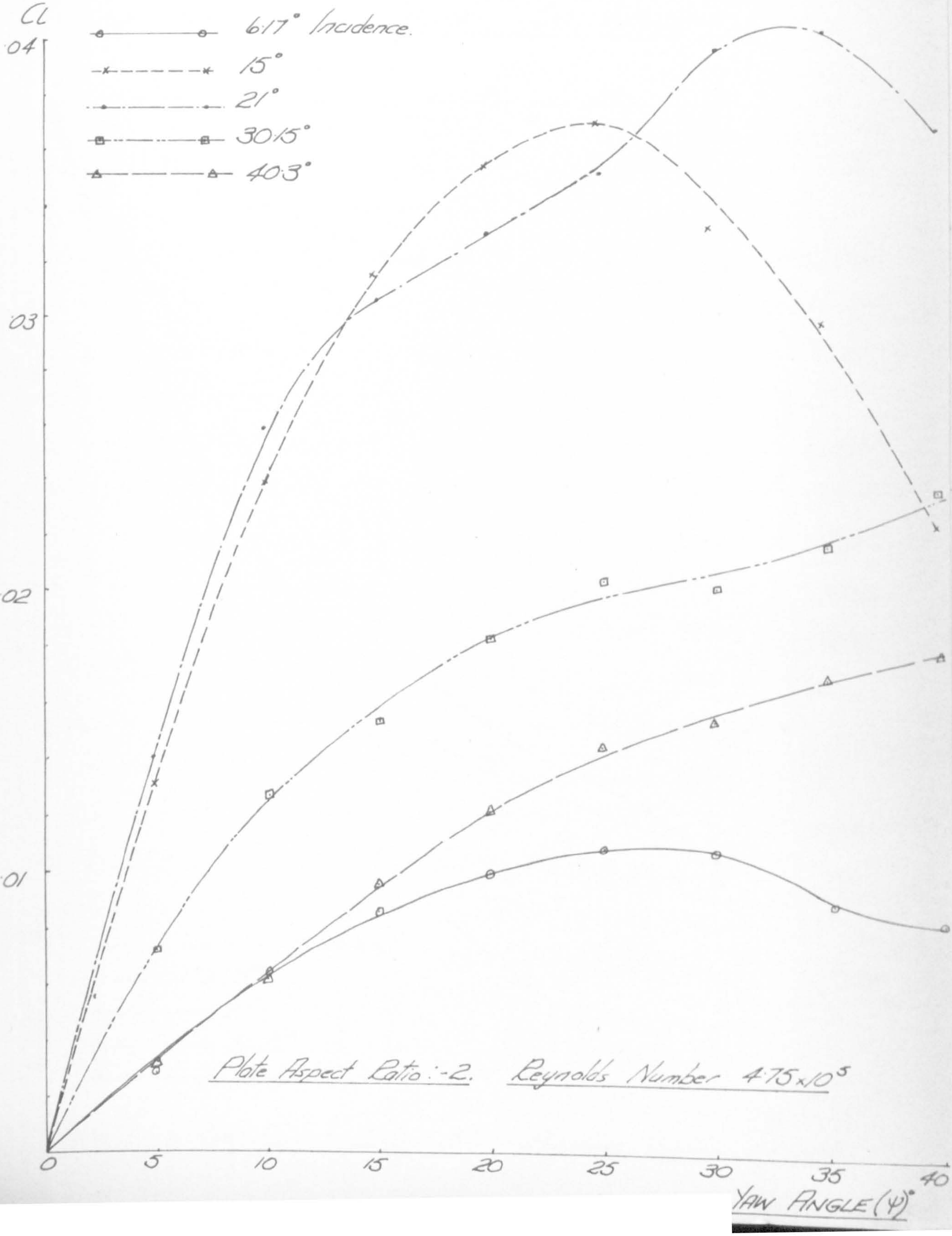

FIGURE 12.7

GRAPH OF YAWING MOMENT COEFFICIENT AGAINST YAW ANGLES FOR VARIOUS ANGLES OF INCIDENCE.

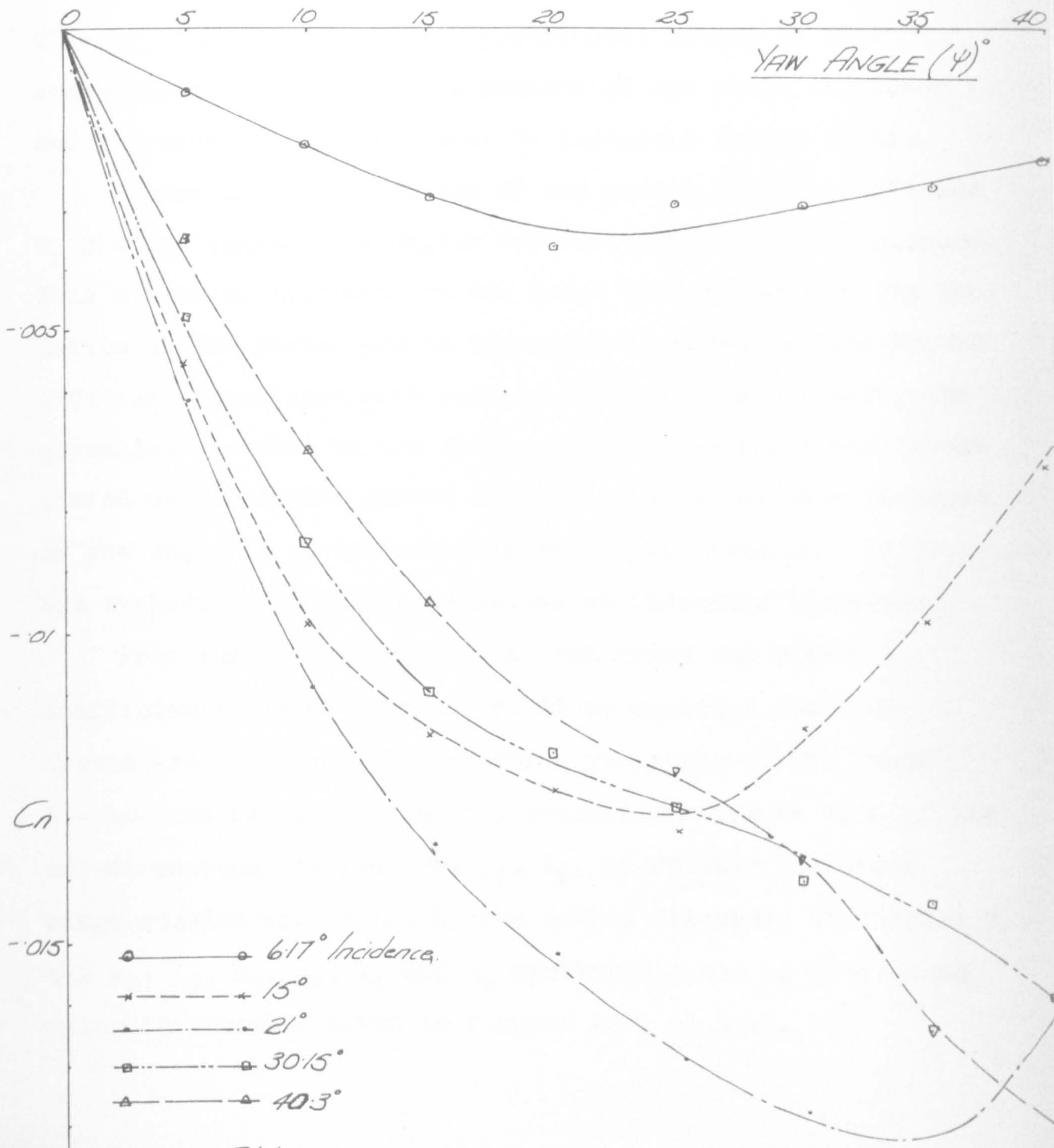

Plate Aspect Ratio :- 2. Reynolds Number 4·75×10⁵

asymmetric induced loading acting on the yawed plate at incidence, unequal lift is set up on the two halves of the plate. Thus a nett rolling moment occurs about a wind x-axis. Clearly, the induced loading contributes mainly to this component because it is at a maximum at the stall incidence and decreases as the incidence is increased beyond stall.

Figure 12.7 shows curves of the yawing moment coefficient C_n plotted against yaw angles for various values of incidence. This moment is dependent on the local induced drag on the two halves of the plate, and is therefore dependent on the induced lift (and associated with rolling moment). As a result, the asymmetric loading on the plate creates a yawing moment about a wind axis and this moment therefore increases with increase of yaw angle in an incidence range $0 - 21^{\circ}$ (see fig. 12.7), but thereafter generally decreases as incidence increases.

From the results of the lateral force and moment coefficients against yaw angle, it is apparent that the curves are reasonably linear for a yaw angle in the range $0 - 10^{\circ}$ and hence satisfactory estimations can be made of the non-dimensional derivatives y_ψ, l_ψ, n_ψ for the incidence range considered. Also, by the method discussed in Chapter 7, the y_v, l_v, n_v, y_ϕ, l_ϕ and n_ϕ derivatives can be determined using the results given in figures 12.1 to 12.7.

FIGURE 12.8.

PLOT OF STIFFNESS DERIVATIVES $X_\theta, Z_\theta, M_\theta$ AGAINST INCIDENCE (α_2)

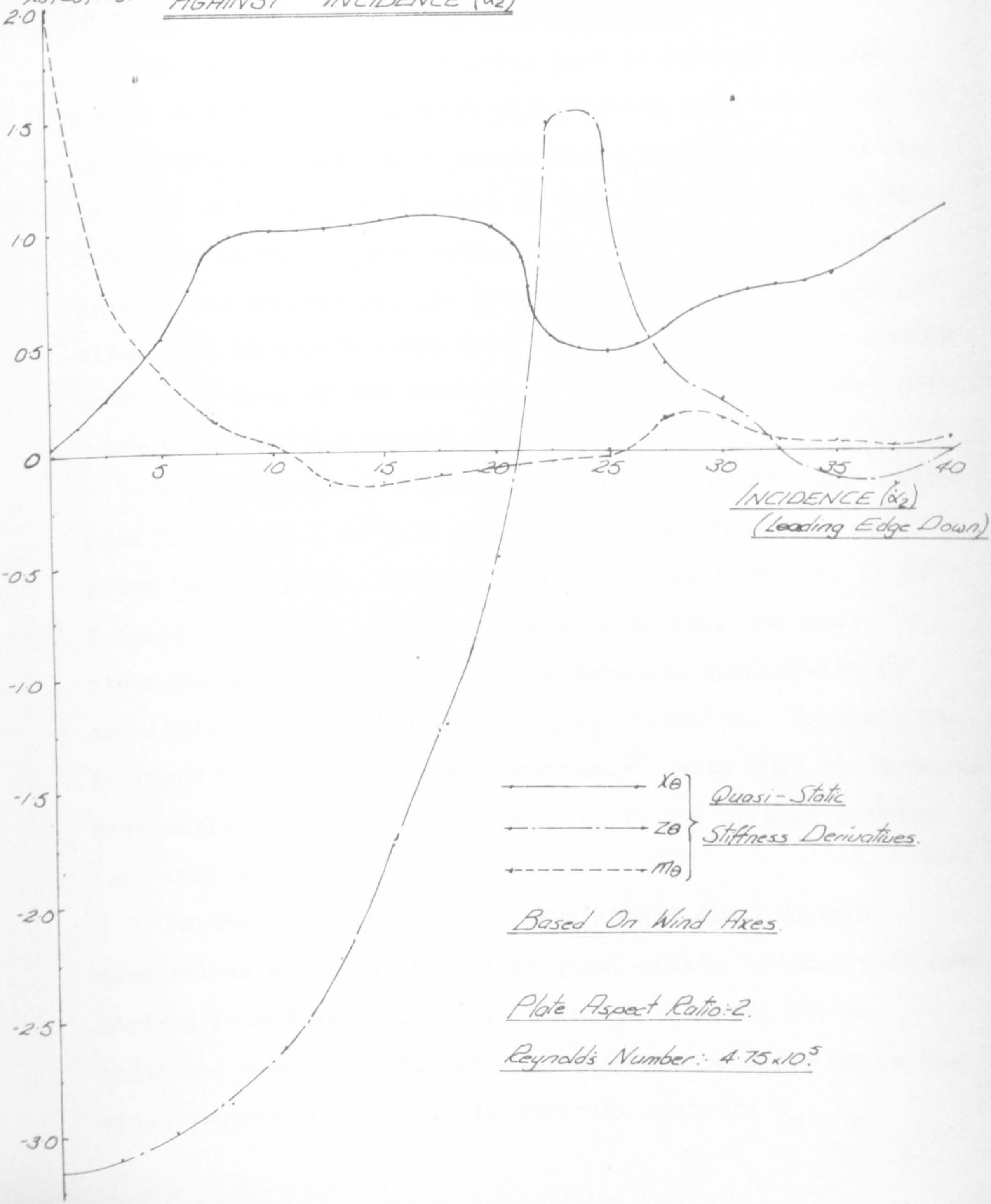

Based On Wind Axes.

Plate Aspect Ratio:-2.

Reynolds Number:- $4{\cdot}75 \times 10^5$.

12.3 The Aerodynamic Derivative Information

The derivative data included here is derived by experimental techniques, determined with lifting line theory or alternatively estimated on quasi-static assumptions. In the majority of cases (see Chapter 7) data are not available to make even an approximate comparison. This is undoubtedly because the derivatives are never estimated for rectangular wings with an aspect ratio less than four. Hence only a brief account of some of the derivatives is given here, since direct comparisons are not possible.

The longitudinal stiffness derivatives at 0^{o} yaw, derived from figures 12.1 to 12.3 and developed on wind axes, are shown in fig. 12.8. With an increase of incidence α_2 (i.e. leading edge down) below the stall condition, the non-dimensional z_θ and m_θ derivatives decrease appreciably in magnitude whilst at the same time x_θ increases. However, it is found in the 'derivative importance' tests that these terms have negligible effects on stability in the present problem (see Chapter 13).

Furthermore, in fig. 12.9 the longitudinal damping derivatives at 0^{o} yaw (based on quasi-static assumptions) are derived from figs. 12.1 to 12.3 and illustrated for an incidence range $0-40^{o}$, although they are required up to the stall incidence only. It is apparent that the x_w, z_w

FIGURE 12.9

GRAPH OF DAMPING DERIVATIVES X_u, Z_u, M_u, X_w, Z_w, M_w AGAINST INCIDENCE (α_2).

Plate Aspect Ratio 2.

Reynolds Number 4.75×10^5

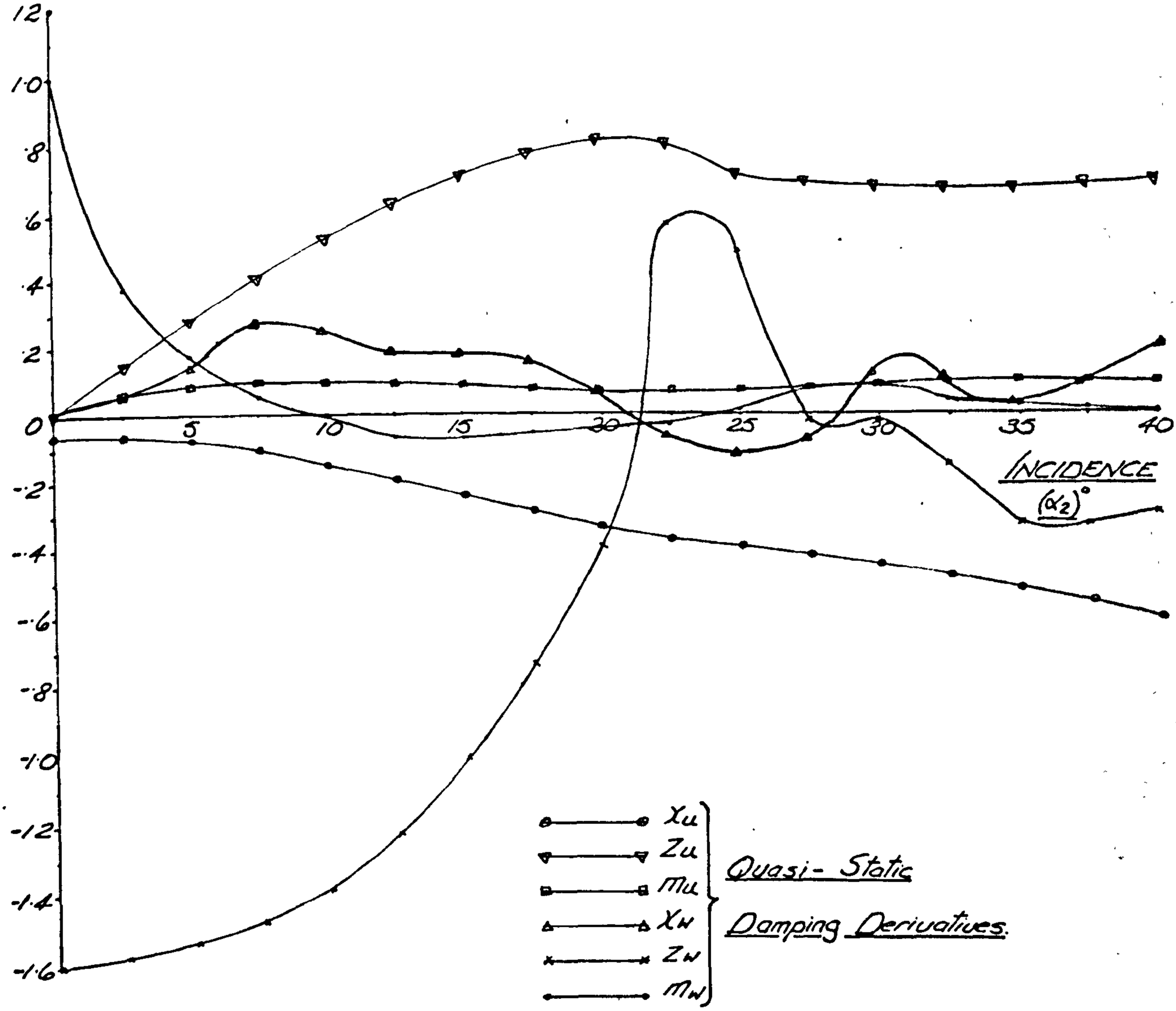

Based on Wind Axes.

derivatives, together with the m_w derivative above 10° incidence are negative below the stall position, whilst the remaining z_u, m_u and x_w terms are always positive. However, from the 'derivative importance' tests (see Chapter 13), the x_u derivative is, generally, far more important than the others in affecting the longitudinal stability of the system. Hence the m_u and m_w derivatives (determined from the non-linear curves in fig. 12.3) are of secondary importance in these initial stability investigations.

The importance of the non-dimensional m_q and z_q rotary damping derivatives at 0° yaw has been mentioned previously in Chapters 7 and 10. Curves of these terms are shown in fig. 12.10 for Strouhal and Reynolds' numbers approximating to the required values (given in Chapter 10).

For the m_q derivative two curves are available for comment:- The 'uncorrected' curve is obtained from experimental dynamic work carried out in the 3'6" open-jet wind tunnel, whilst the 'corrected' curve is similarly obtained from work carried out in an 18' x 12' closed working section. Although the two curves are determined at slightly different Strouhal and Reynolds' numbers, this is thought to have a negligible effect on the derivatives. Hence, for reasons unknown at present, the former tunnel imposed a premature stalling effect on the freely oscillating plate set at

FIGURE 12.10.

GRAPH OF THE DAMPING DERIVATIVES m_q AND z_q.

AGAINST INCIDENCE.

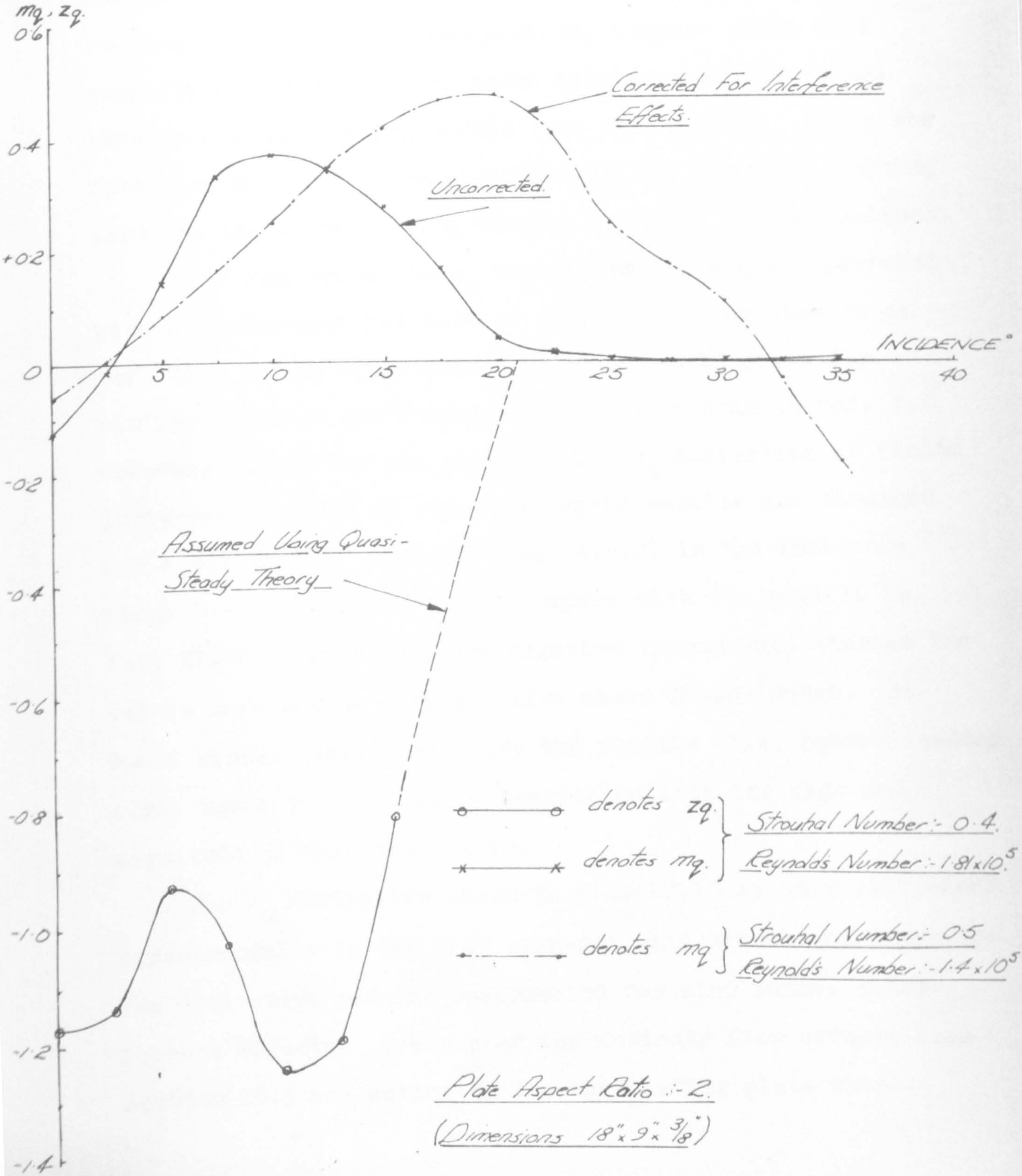

incidence. Unfortunately, this cannot be confirmed by recourse to previous investigations, because there is a scarcity of information on three dimensional wind tunnel effects for oscillating models (see ref. 10.11). Since the interference effects are negigible in the 18' x 12' working section, the corresponding results are used in the analyses.

At 0^{o} incidence the m_q derivative is in good agreement with a theoretical estimate of -0.101 given by Glauert in ref. 10.2 and an experimental value of -0.13 given for similar Strouhal and Reynolds' numbers by Acum in ref. 7.2. However, values are not given of the m_q derivative at finite incidences, except in ref. 10.5 where results are obtained for a rectangular cambered wing (A.R.2) in the incidence range $0 - 10^{o}$. These do not compare with the results in fig. 12.10 because they are negative throughout, whereas the values here become very positive above 2^{o} incidence. It would appear, therefore, that the profile (i.e. square leading edge) has a very important bearing on both the sign and magnitude of this derivative.

The z_q derivative shown in fig. 12.10 is only determined experimentally in the 3'6" open-jet wind tunnel and therefore the derivative remains uncorrected for wind tunnel interference effects. Because of the unsteady flow effects (see section 10.5.4c) acting on the oscillating plate when

FIGURE 12.11

GRAPH OF DAMPING DERIVATIVES AGAINST INCIDENCE (α_2)°

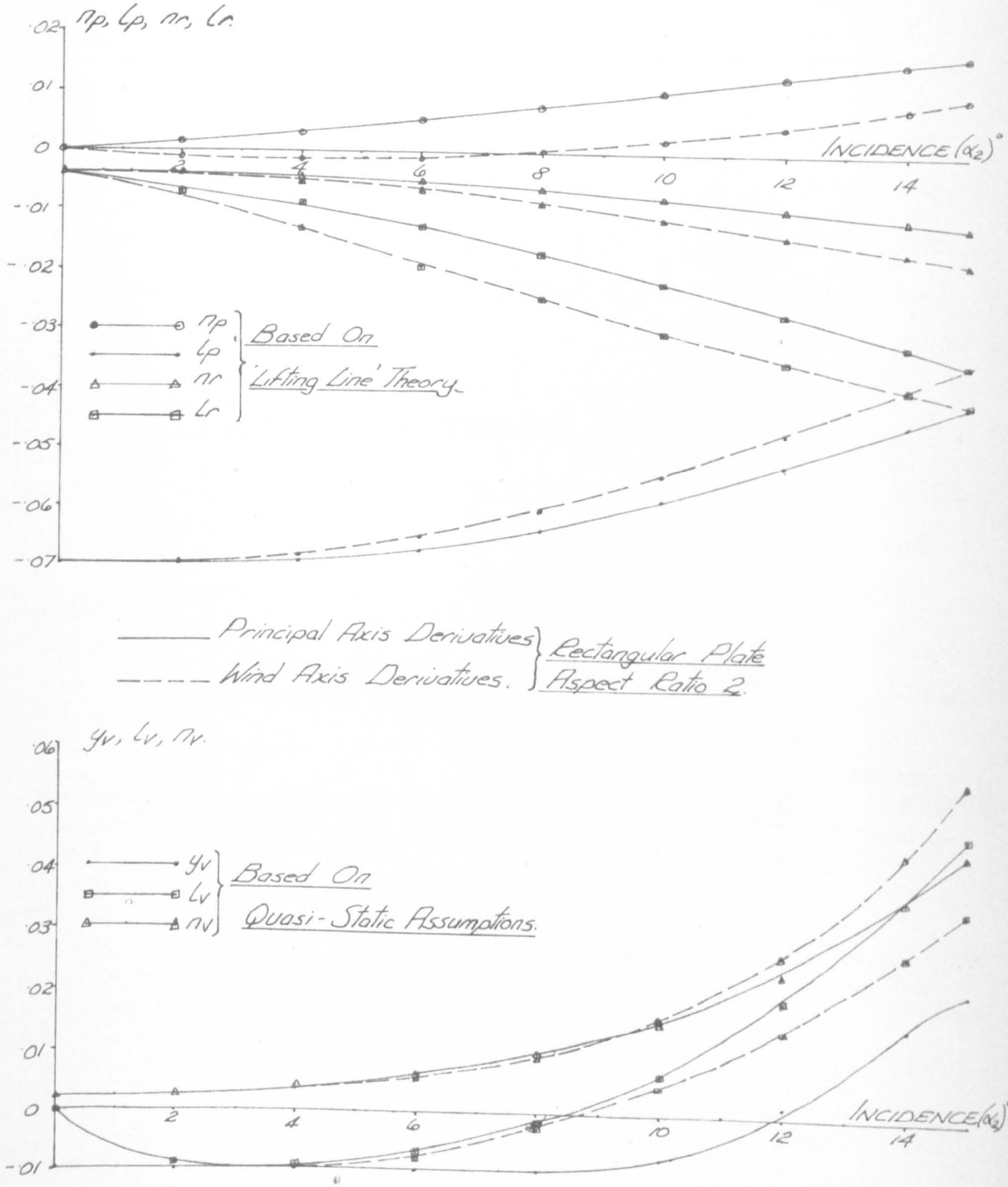

FIGURE 12.12.

GRAPH OF STIFFNESS DERIVATIVES AGAINST INCIDENCE (α_2)°

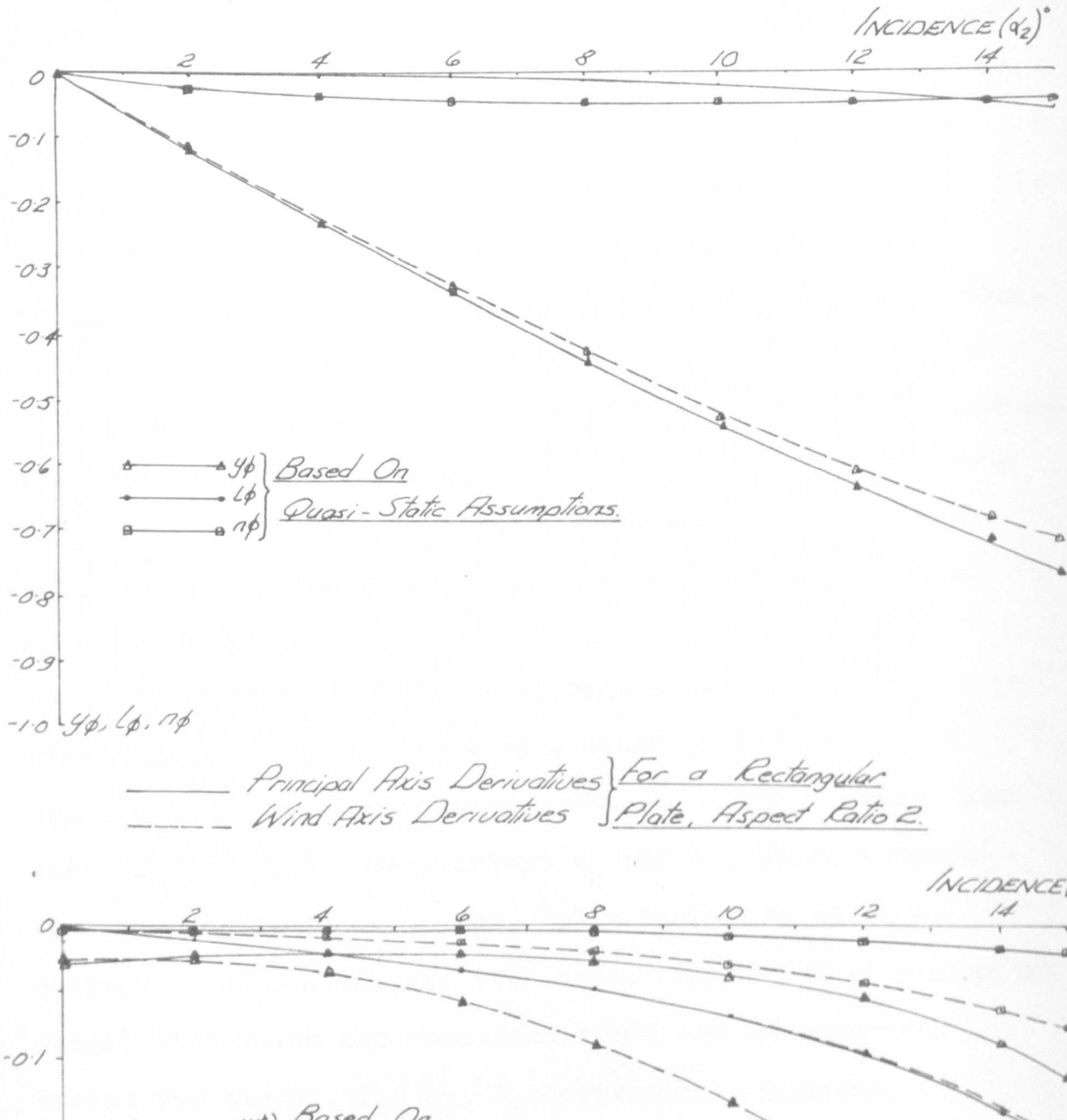

approaching the stall position, values of z_q are determined only for an incidence range of 0 - 15°. However, a line is continued to the stall point (based on quasi-static assumptions) where z_q would be zero (see Chapter 10). It can then be conveniently used for any incidence in the incidence range of the longitudinal stability investigations.

It is apparent in fig. 12.10 that z_q remains negative throughout the range of incidence investigated. Unfortunately this cannot be confirmed completely by recourse to previous investigations, although Glauert determined a theoretical value of -0·382 for z_q based on a steady rotation of the plate at 0° incidence.

The lateral damping and stiffness derivatives shown in figs. 12.11 and 12.12 are given, based on both wind and principal axes in the incidence range 0 - 15°. Except for the non-dimensional derivatives n_r and l_p, which compare favourably with those in ref. 7.10, there are no other derivative data available (for aspect ratio 2 flat plates or wings) with which the remaining terms can be compared. Except for the n_p, l_p, n_r, l_r derivatives, however, the remaining terms are derived from the static wind tunnel results given in figs. 12.1 to 12.7, where the general form of the latter is in agreement with previous investigations.

CHAPTER 13

RESULTS OF THE ANALYTICAL STUDIES

The results included in this chapter are derived from stability investigations for the three types of suspension of the pallet. An immense amount of data has been accumulated and, because of the limited space available, only typical results are shown.

In an effort to explain the mechanism of instability encountered with the single strop suspension of a pallet, discussions of the separate longitudinal and lateral analyses are presented. The results obtained for these two types of motion are discussed more simply when further separated into the various modes of oscillation. Subsequent brief discussions (similar to the above) are also included for the twin strop and trapezoidal configurations.

For the longitudinal and lateral analyses there are generally two and three modes of oscillation respectively. However, in some cases, subsidences and divergencies occur as substitutes for oscillatory modes.

13.1 The Single Strop Configuration

Longitudinal and lateral stability investigations have been carried out for the single strop configuration in a similar manner to that described in chapter 6. Furthermore the results were obtained for a variety of parameters (see

VELOCITY ft/sec.

0 20 40 60 80 100 120 140

SINGLE STROP AND TWIN STROP ARRANGEMENTS.

LONGITUDINAL MODE 1.

d_1 = 100ft.
d_1 = 50ft.
d_1 = 25ft.
d_1 = 10ft.

For $m_1 g$ = 5lbs

$m_2 g$ = 200lbs.

d_2 = 25ft.

d_2 = 100ft.

All Readings Below Stall Conditions.

-01 -02 -03 -04 -05

ζ_1

PLOT OF DAMPING FACTOR AGAINST FORWARD SPEED

FIGURE 13.1.

section 6.2.1). These parameters include the pallet weight ($m_2 g$), lifting hook weight ($m_1 g$), strop length (d_1), normal length between the hook and pallet (d_2) and the 'steady state' incidence (α_2) of the pallet.

13.1.1 The Longitudinal Modes

At this stage it must be mentioned that the longitudinal theories derived for the single and twin strop configurations (see chapter 4) are identical and therefore the results given here are applicable to both.

Two separate longitudinal modes of oscillations are obtained. These are (a) mode 1 - a low frequency 'pendulum' mode involving rotation about the helicopter attachment point(s), and (b) mode 2 - a high frequency 'flutter' mode involving rotary motion about the pallet centre of gravity with only a small translational movement of the pallet. No system displayed either a divergence or subsidence.

13.1.1a Mode 1

In this low frequency 'pendulum' mode of oscillation it is apparent from fig. 13.1 (where the non-dimensional damping factor r_1 is plotted against forward velocity V) that r_1 is negative and therefore for the velocity range considered the mode of oscillation is quite stable and small disturbances are damped out. It is also apparent that the degree of stability increases with velocity upto a point.

PLOT OF FREQUENCY PARAMETER AGAINST FORWARD VELOCITY

SINGLE AND TWIN STROP ARRANGEMENTS

LONGITUDINAL MODE 1.

$m_1 g = 50$ lbs, $d_1 = d_2 = 50$ ft

FOR VALUES OF PALLET WEIGHT INDICATED.

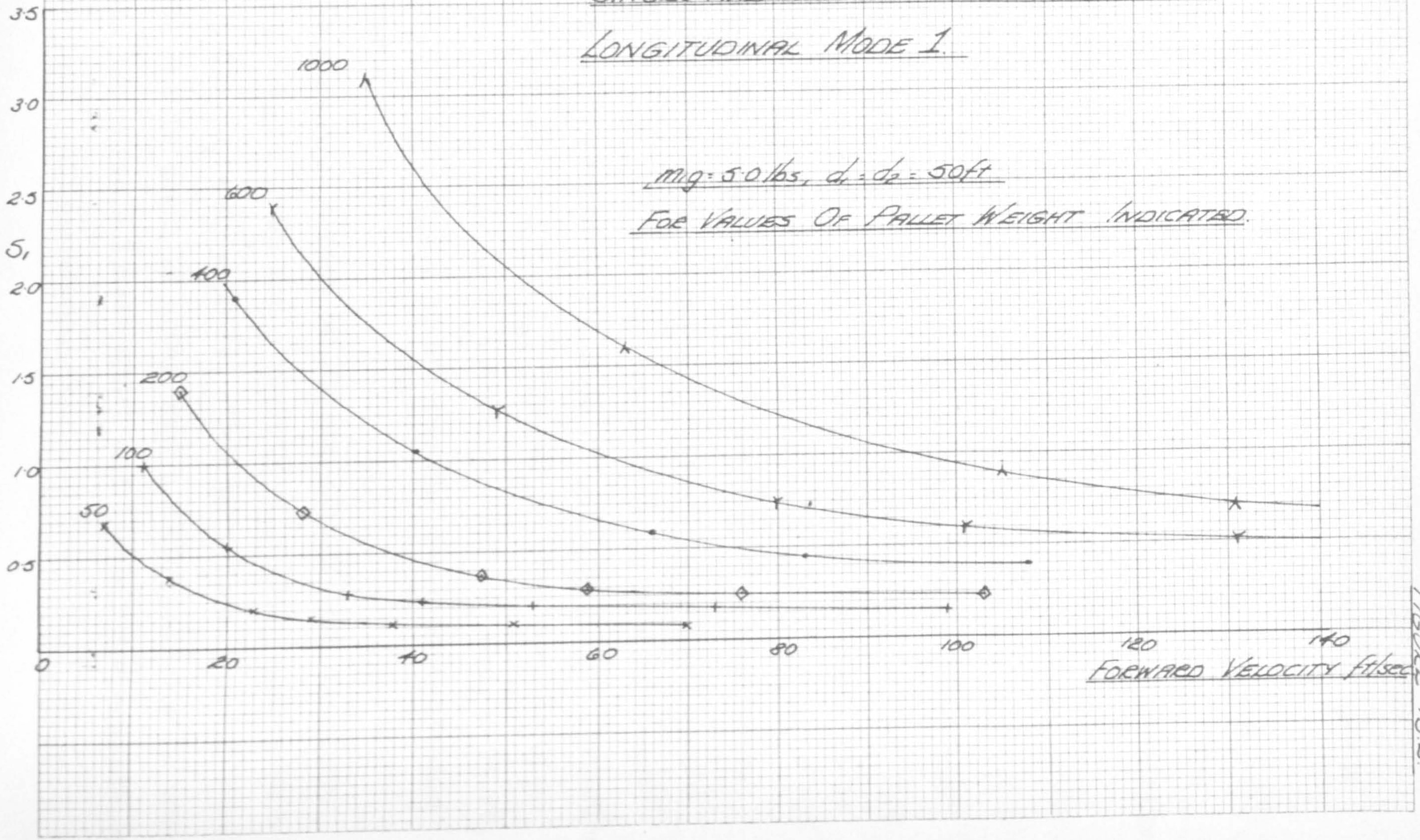

FIGURE 13.2.

It is shown in fig. 13.1 that for all forward speeds of the helicopter, an increase of d_1 appears to have a destabilising effect on the pendulum mode. The effect is more apparent for smaller lengths of d_2, i.e. 25 ft. The variation of the length d_2 has a similar effect on stability as the length d_1, although this is only noticeable at higher velocities (as shown in fig. 13.1).

Although illustrative data is not given, the results show that for a pallet weight $\geq$ 50 lbs the effects on the damping factor r_1 of varying the weight of the lifting hook (in the range 0.5 - 10 lbs) are negligible. However, it is likely that when the weights of the hook and pallet approach each other, the effects would not be negligible. Furthermore, an independent increase of the pallet weight between 50 and 1000 lbs appears to have an insignificant destabilising effect on the mode of oscillation in comparison with variations of d_1 or d_2. Therefore, the results show that the more stable configuration is with $d_1 = d_2 = 25$ ft, $m_1 g = 0.5$ lbs and $m_2 g = 50$ lbs for the range of variables considered.

In fig. 13.2 a plot of the non-dimensional frequency parameter s_1 is given for a variety of pallet weights when $m_1 g = 5$ lbs, $d_1 = d_2 = 50$ ft. This plot is a typical example and is given in order that a comparison can be made between the various longitudinal and lateral frequencies of the various configurations.

FIGURE 133.

PLOT OF THE RELATIVE DERIVATIVE IMPORTANCE AGAINST FORWARD VELOCITY.

All Readings Below Stall Conditions

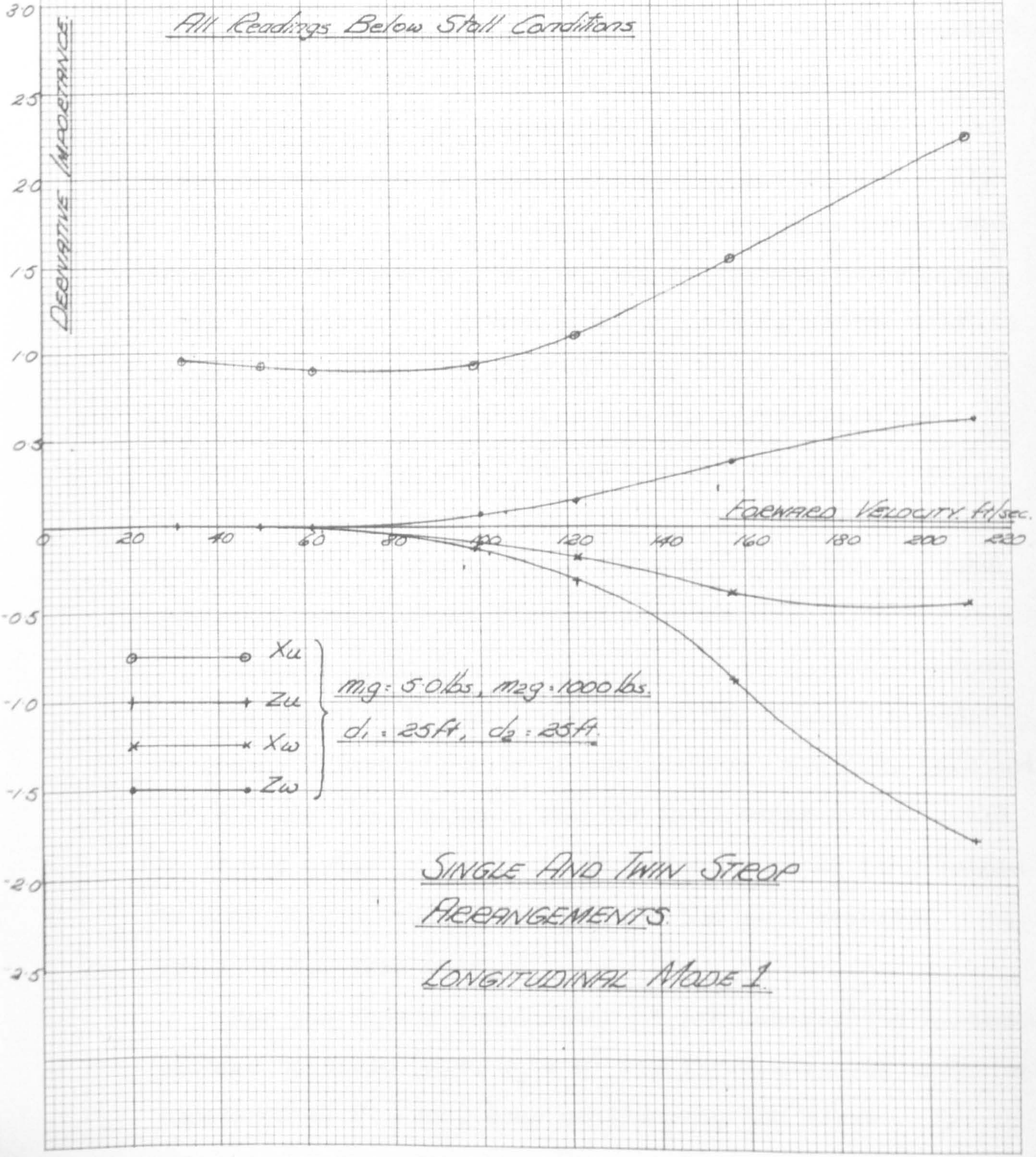

SINGLE AND TWIN STROP ARRANGEMENTS.

LONGITUDINAL MODE I.

An attempt is made to give a brief resumé of the important derivative terms for this oscillatory mode. Fig. 13.3 is given as a typical example, where the most important derivatives are illustrated. It must be realised that the figure gives only a relative (not absolute) representation of the derivatives for a particular combination of the physical parameters (see section 6.1).

From fig. 13.3 it is obvious that the non-dimensional damping derivatives x_u, z_u, x_w and z_w are the important terms for this mode, although z_u, x_w and z_w assume only minor importance in the low velocity regime. All other non-dimensional damping and stiffness derivatives are insignificant. Hence if the quasi-static assumptions are questioned when deriving x_u, z_u, x_w and z_w, it would be worthwhile to obtain their correct values for the true ranges of Reynolds and Strouhal numbers.

13.1.1b Mode 2

In relation to the 'pendulum' mode, this is a high frequency ('flutter') mode of oscillation (see fig. 13.2 and 13.6) and the frequency for the full scale system could be of the order of 1 c.p.s. Unfortunately, it is possible to show only a small proportion of the many results obtained for this mode.

For the chosen combination of parameters, the system becomes unstable (i.e. $r_2 > 0$) for forward speeds in excess of 24 ft./sec. when considering the worst

All Readings Below Stall Conditions.

——— $m_1 g$ = 0·5 lbs. $d_1 = d_2$ = 25 ft.

– – – – – $m_1 g$ = 0·5 lbs. $d_1 = d_2$ = 100 ft.

For Values of $m_2 g$ Indicated.

× 50 lbs
\+ 100 lbs
◇ 200 lbs
· 400 lbs
Y 600 lbs
λ 1000 lbs.

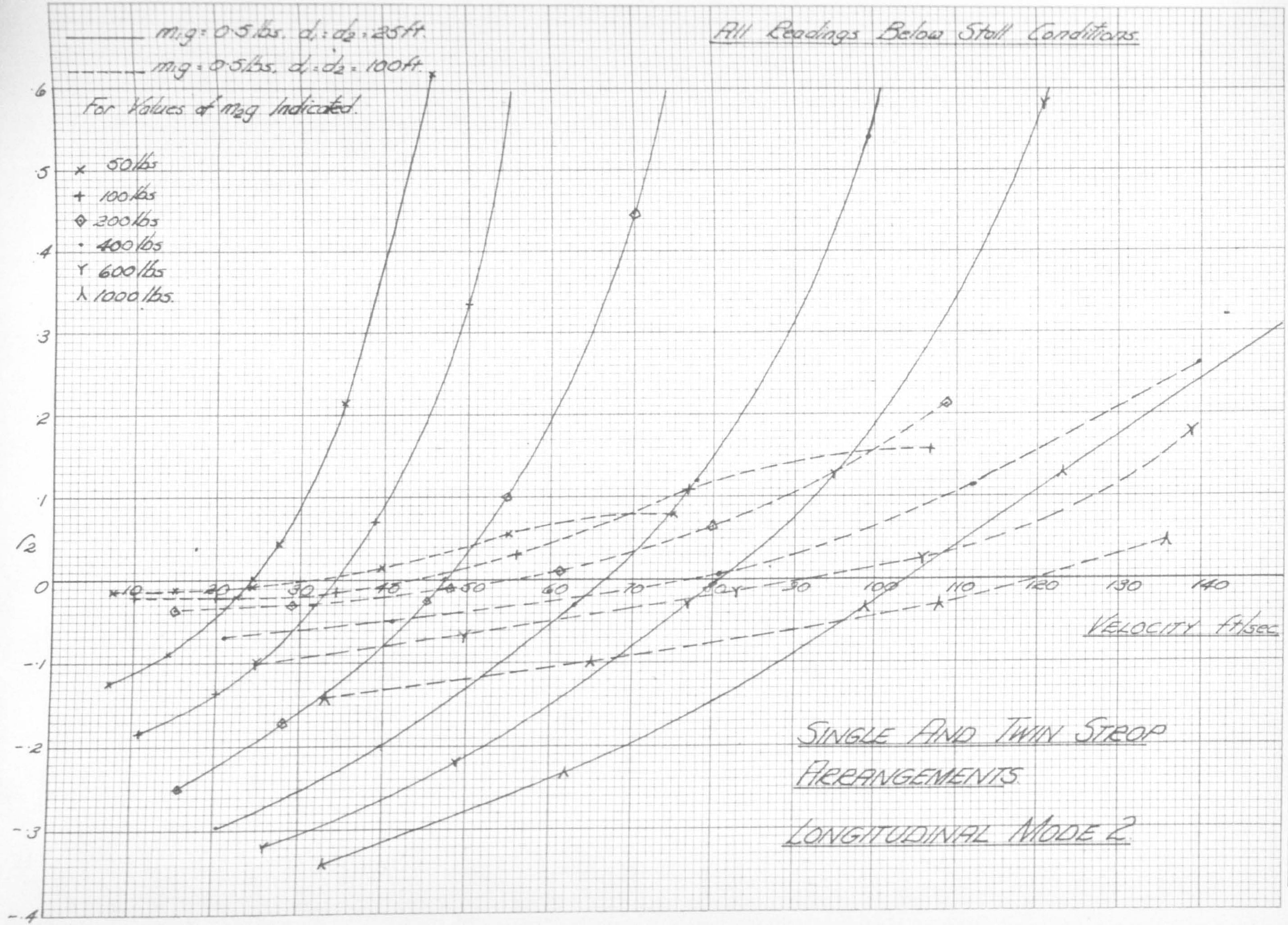

SINGLE AND TWIN STEOP ARRANGEMENTS

LONGITUDINAL MODE 2

FIGURE 13.4.

PLOT OF DAMPING FACTOR AGAINST FORWARD VELOCITY.

FIGURE 13.5.

PLOT OF CRITICAL VELOCITY AGAINST PALLET WEIGHT.

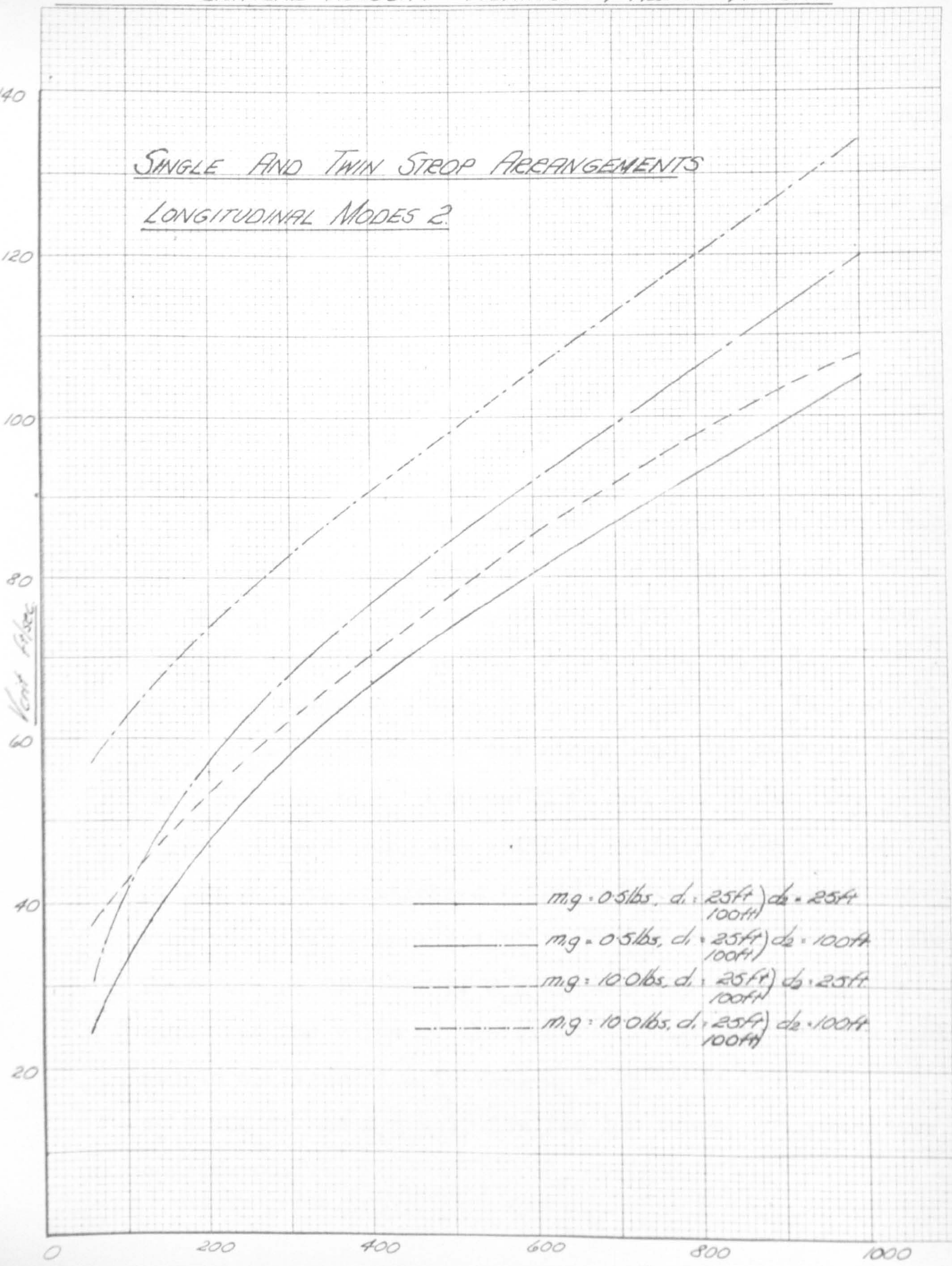

arrangement, i.e. m_1g = 0.5 lbs, m_2g = 50 lbs, d_1 = 25 ft, d_2 = 25 ft. This trend in the results is clearly confirmed in figs 13.4 where a plot of the non-dimensional damping factor, r_2, against forward velocity, V, is given. Furthermore, fig. 13.4 shows that for a general increase in the distance between the helicopter and pallet (in the range of 50 ft - 200 ft) there is a corresponding reduction in the damping factor r_2. An increase of the lifting hook weight, m_1g, from 0.5 lbs to 10 lbs also has a large reducing effect on r_2.

From the results given by the typical graph fig. 13.4, a graph of critical velocity (i.e. with r_2 = 0) against the pallet weight is given in fig. 13.5. This shows the critical velocity to be unaffected due to variations of the strop length d_1, when the pallet weight is in the range 50 - 1000 lbs. On the other hand, an increase in the strop length d_2 between 25 ft and 100 ft has the effect of increasing the critical velocity for all the pallet weights considered. This effect is more pronounced when the lifting hook weight is 10 lbs rather than 0.5 lbs. Therefore an increase of m_1g between 0.5 lbs and 10 lbs increased the value of the critical velocity, and the most stable configuration is with d_1 = 25 ft to 100 ft, d_2 = 100 ft and m_1g = 10 lbs for the ranges of parameters considered.

PLOT OF FREQUENCY PARAMETER AGAINST FORWARD VELOCITY.

SINGLE AND TWIN STEOP ARRANGEMENTS.

LONGITUDINAL MODE 2.

m_g = 5·0 lbs. $d_1 = d_2$ = 50ft

FOR VALUES OF PALLET WEIGHT INDICATED.

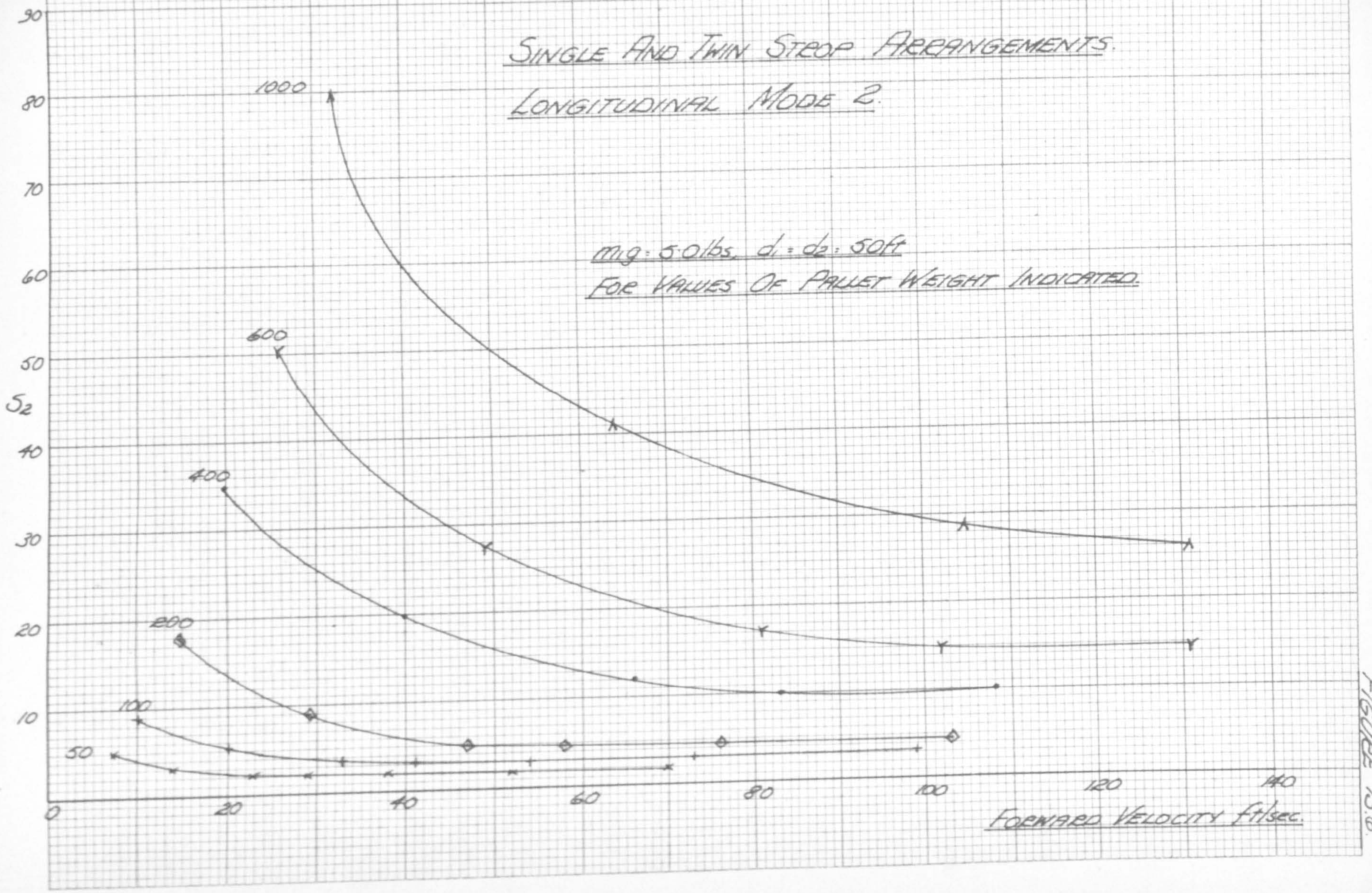

FIGURE 13.6.

As before, a plot of the non-dimensional frequency parameter s_s (see fig. 13.6) against forward velocity is given for comparison with other oscillatory modes.

Investigations have been made to ascertain the more important stability derivatives for the 'flutter' mode of oscillation. The complete set of longitudinal derivatives has been considered, but only the important terms are shown in fig. 13.7, where a plot of the relative derivative importance is given against forward velocity.

It is clear from the results obtained that the m_q damping derivative is extremely important in the stable and unstable regimes of velocity. For small velocities in the stable regime, only the m_q derivative is important. However, with increase of velocity up to and including the unstable regime of velocity it is generally apparent that the z_q damping derivative has an effect equally as important as the m_q term. It would seem therefore that justification has been given for deriving both the m_q and z_q terms for the correct ranges of Reynolds and Strouhal numbers.

In the various configurations investigated m_q and z_q are of prime importance, although as is shown in fig. 13.7 other derivatives of lesser importance also have strong stabilising and destabilising effects which cannot

FIGURE 13.7

PLOT OF THE RELATIVE DERIVATIVE IMPORTANCE AGAINST FORWARD VELOCITY

SINGLE AND TWIN STROP ARRANGEMENTS.

LONGITUDINAL MODE 2.

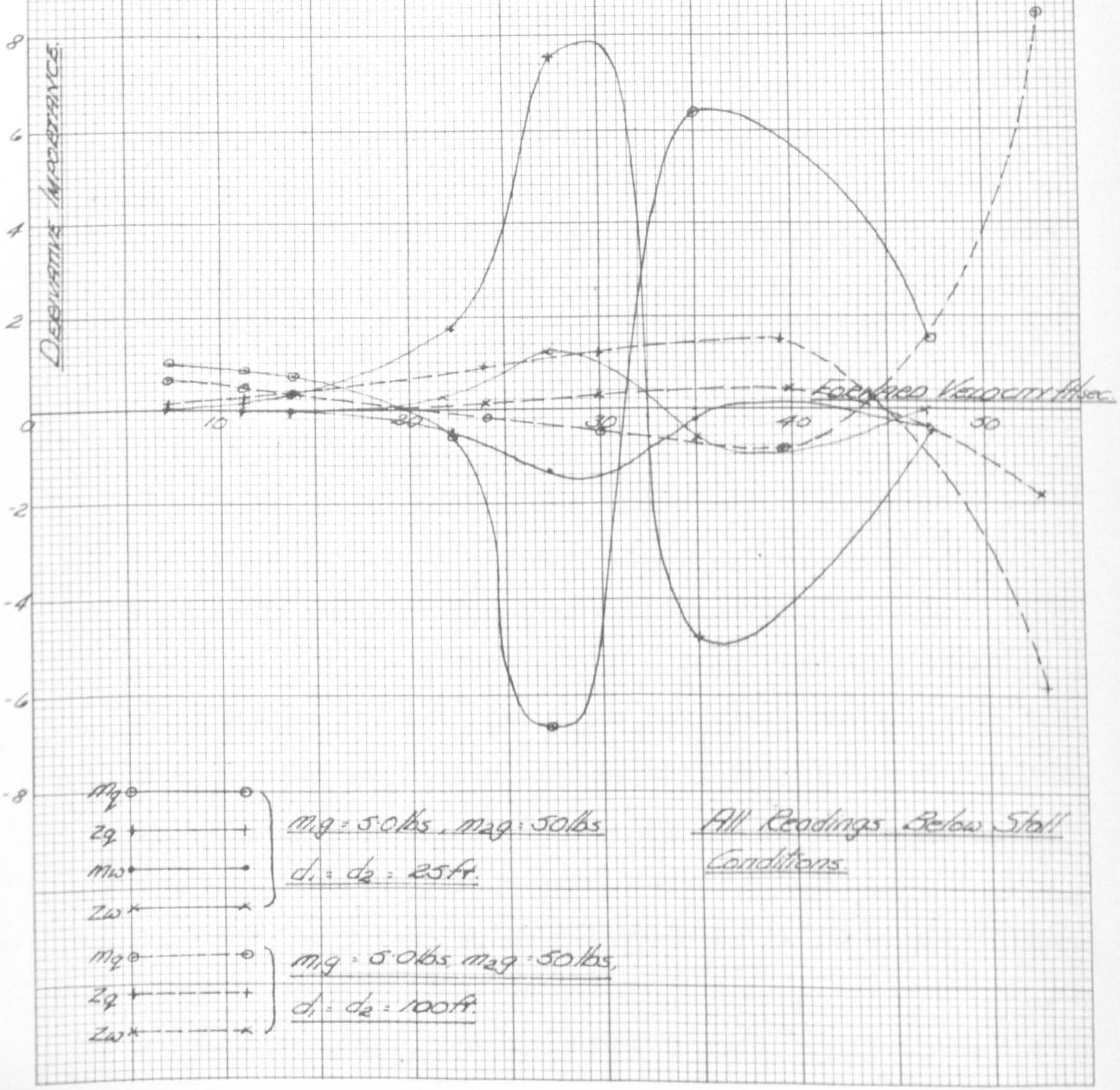

$m_1 g = 5{\cdot}0$ lbs, $m_2 g = 50$ lbs

$d_1 = d_2 = 25$ ft.

$m_1 g = 5{\cdot}0$ lbs $m_2 g = 50$ lbs,

$d_1 = d_2 = 100$ ft.

All Readings Below Stall Conditions

be neglected. This is illustrated for two configurations in fig. 13.7. However a closer study of the importance of the derivative effects on stability is ignored here because of the limited time available.

13.1.2 The Lateral Modes

There are usually three lateral modes of oscillation of the pallet. These are found to be (a) mode 1 - a low frequency yawing mode at low velocities which combines with a lateral pendulum displacement at higher velocities; (b) mode 2 - a moderate frequency lateral pendulum mode which changes to a combined yawing-pendulum mode at higher velocities, and (c) mode 3 - a short period lateral mode (comparable with the longitudinal flutter mode) with only a small translational movement of the pallet.

13.1.2a Mode 1

This mode of oscillation comprises a predominant yawing motion for all forward speeds, although at high values of incidence for each configuration (i.e. $\alpha_s > 10^o$) the yawing motion combines with a small pendulum sideslip displacement (of both masses). For small disturbances the mode remains completely stable, but for large disturbances instability is likely owing to the lack of structural constraint on the yawing displacement.

For the pallet weights considered in those investigations it appears that variations in the structural parameters $m_1 g$, d_1 and d_2 have negligible effects on the

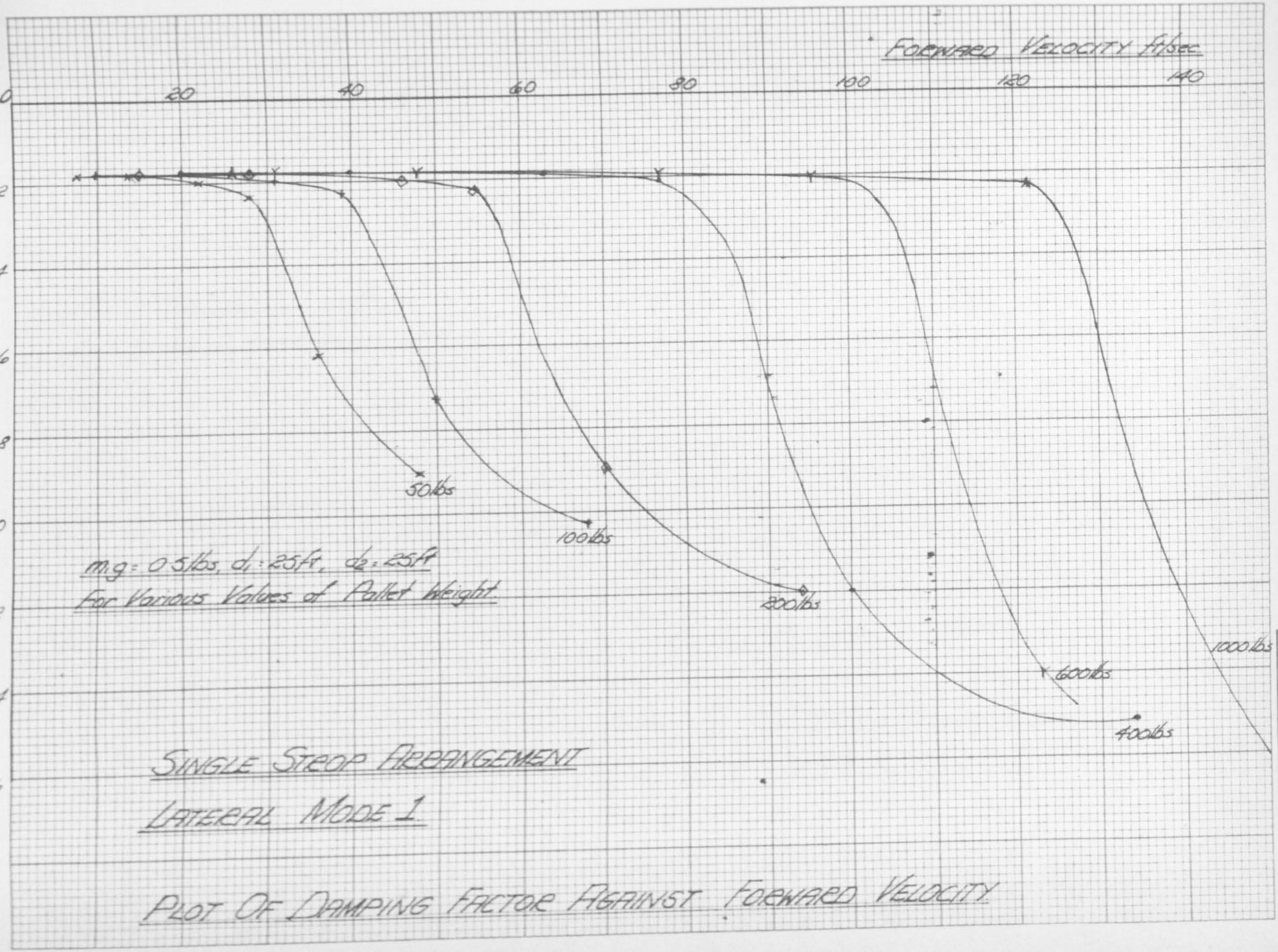
FORWARD VELOCITY ft/sec
0
20
40
60
80
100
120
140
-02
-04
-06
-08
-10
-12
-14
-16
50lbs
100lbs
200lbs
400lbs
600lbs
1000lbs
m.g = 0.5lbs, d1 = 25ft, d2 = 25ft
For Various Values of Pallet Weight.
SINGLE STEOP ARRANGEMENT
LATERAL MODE 1
PLOT OF DAMPING FACTOR AGAINST FORWARD VELOCITY

FIGURE 13.8

PLOT OF FREQUENCY PARAMETER AGAINST FORWARD VELOCITY

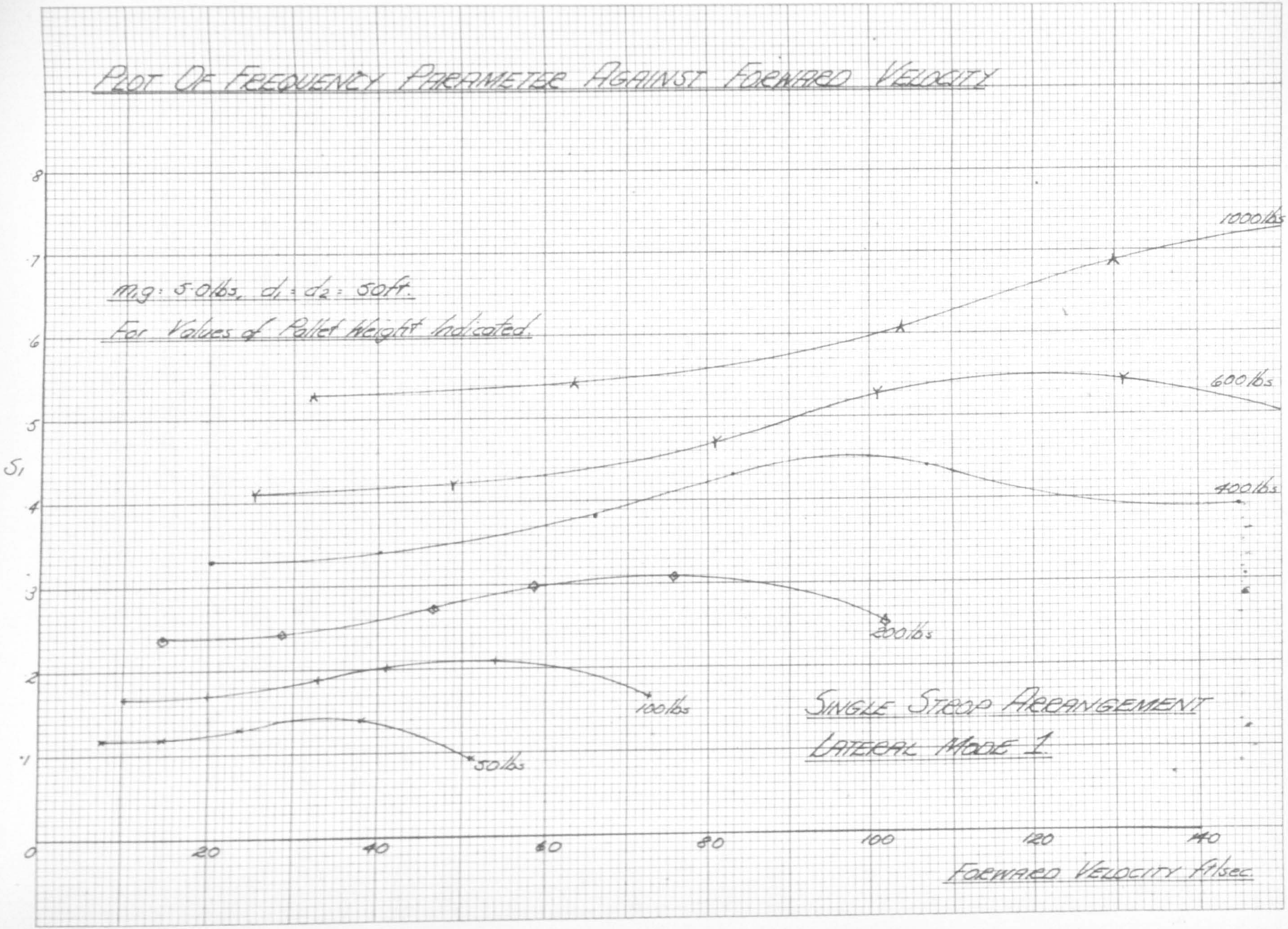

FIGURE 13.9.

damping in the system. It is necessary therefore to illustrate one set of stability curves for a configuration (see fig. 13.8). From this figure it is apparent that the minimum non-dimensional damping factor r_1 is -0.018 for all pallet weights. The damping factor for a pallet weight of 50 lbs tends to remain at this value for higher angles of incidence than does that for a pallet weight of 1000 lbs.

In addition to the previous figure, a graph is given of the non-dimensional frequency parameter s_1 against forward velocity (see fig. 13.9) for the typical structural arrangement when $m_1 g = 5.0$ lbs, $d_1 = d_2 = 50$ ft. A comparison with other graphs of frequency parameter shows this particular graph to be somewhat unusual. This would appear to be due to the dimensional frequency parameter's strong dependence on forward velocity as a result of the yawing constraint being purely aerodynamic.

A derivative importance investigation has been carried out on this mode of oscillation, and as shown in fig. 13.10 the expected result is obtained. That is, the lateral damping derivative n_r is predominantly important for the complete velocity range of all configurations considered. It is interesting to note, however, that at higher values of incidence (and, of course, velocity) where the modal form changes from a pure yawing motion to a combined

FIGURE 13.10.

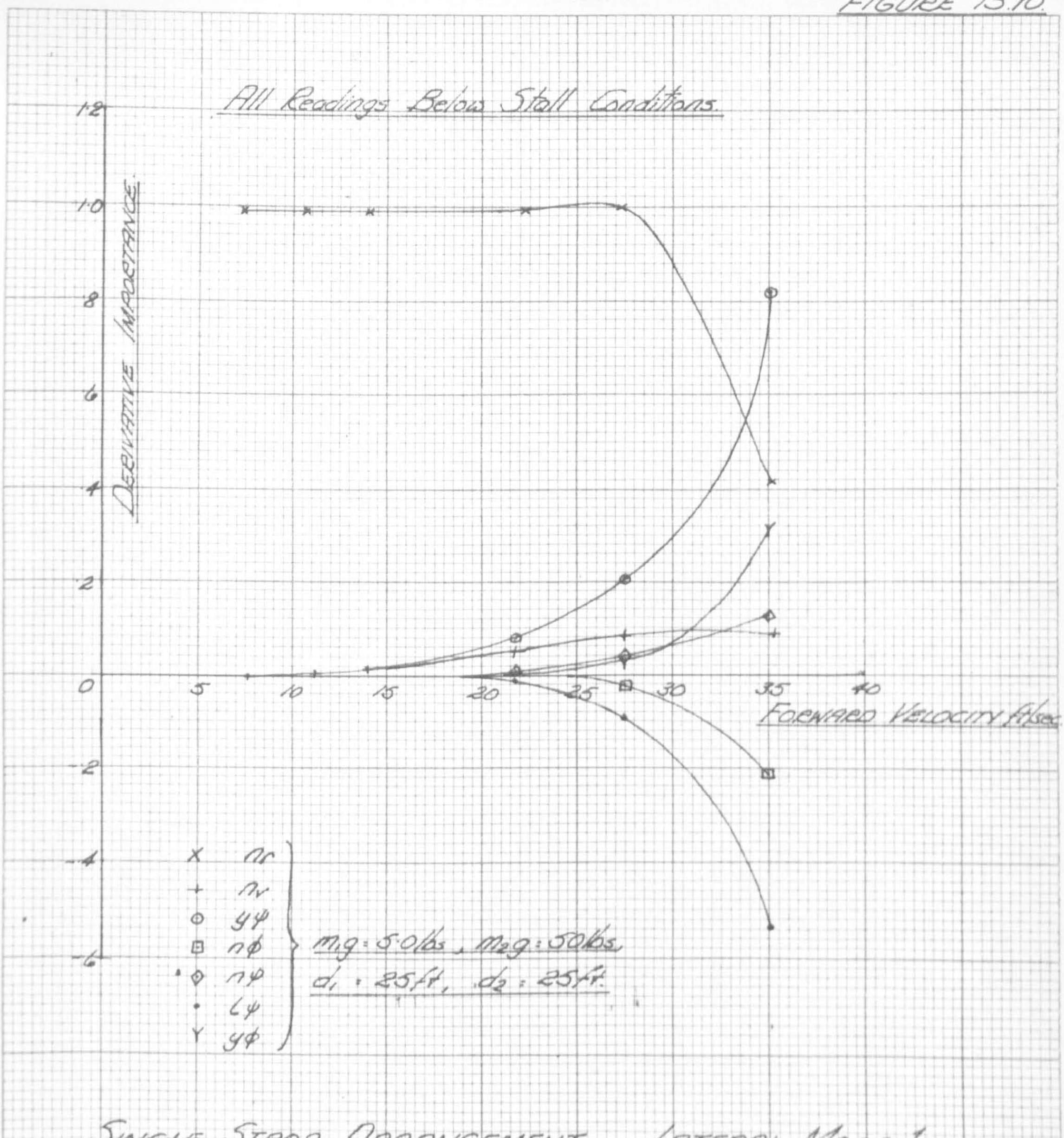

SINGLE STROP ARRANGEMENT LATERAL MODE I

PLOT OF THE RELATIVE DERIVATIVE IMPORTANCE AGAINST FORWARD VELOCITY.

PLOT OF DAMPING FACTOR AGAINST FORWARD VELOCITY.

SINGLE STROP ARRANGEMENT.
LATERAL MODE 2.

$m_1 g = 0.5$ lbs, $d_1 = 100$ ft, $d_2 = 100$ ft.
for Values of $m_2 g$ indicated.

- 50 lbs
- 100 lbs
- 200 lbs
- 400 lbs
- 600 lbs
- 1000 lbs

Γ_2

.10 .09 .08 .07 .06 .05 .04 .03 .02 .01 0 -.01

20 40 60 80 100 120 140

FORWARD VELOCITY ft/sec.

FIGURE 13.11.

yawing and small sideslip motion, the damping derivative n_v becomes important (see fig. 13.10). Furthermore, fig. 13.10 illustrates the importance of the stiffness derivatives y_ψ, n_ϕ, n_ψ, l_ψ and y_ϕ at higher forward velocities in this particular mode.

13.1.2b Mode 2

The mode of oscillation is found to be of an oscillatory lateral pendulum nature at small forward velocities, but changes to a combined yawing-pendulum mode at higher velocities. This transition seems to occur for all the pallet weights considered, when the 'steady state' incidence is in the range $1^\circ - 3^\circ$. For values of incidence greater than 3°, the yawing displacement is predominant over the sideslip displacement. Furthermore, except for small values of incidence, i.e. $< 1^\circ$ (see fig. 13.11), the mode is generally unstable for all the configurations considered.

The importance of the structural parameters $m_1 g$, $m_2 g$, d_1 and d_2 on the stability of this lateral mode are illustrated in fig. 13.12 where a plot of critical velocity (i.e. $r_2 = 0$) against the range of pallet weight is given. From a detailed comparison of the results it is found that the weight of the lifting hook ($m_1 g$) has a negligible effect on the damping in the system for the range of pallet weights considered. On the other hand, figs 13.11 and 13.12 show that an increase in the pallet weight

FIGURE 13.12.

PLOT OF CRITICAL VELOCITY AGAINST PALLET WEIGHT.

SINGLE STEOP ARRANGEMENT

LATERAL MODE 2.

120
100
80
60
40
20

V crit ft/sec.

m.g = 0.5 lbs, d_1 = 25 ft, d_2 = 25 ft.
m.g = 0.5 lbs, d_1 = 100 ft, d_2 = 25 ft.
m.g = 0.5 lbs, d_1 = 25 ft, d_2 = 100 ft.
m.g = 0.5 lbs, d_1 = 100 ft, d_2 = 100 ft.

0 200 400 600 800 1000

PALLET WEIGHT m.g lbs.

PLOT OF FREQUENCY PARAMETER AGAINST FORWARD VELOCITY

SINGLE STROP ARRANGEMENT

LATERAL MODES 2.

m_g : 5·0 lbs, $d_1 : d_2$: 50ft

For Values of Pallet Weight Indicated.

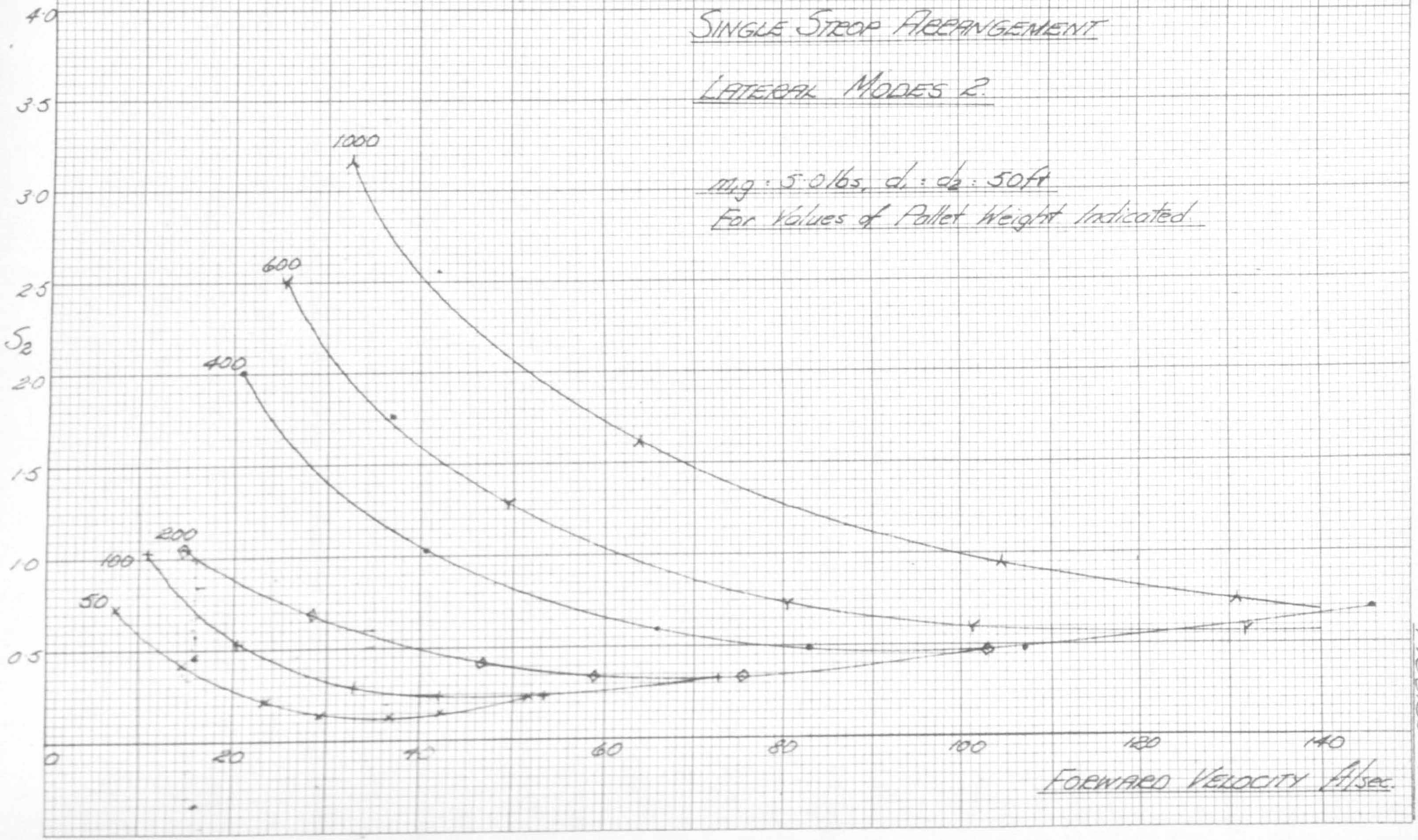

FIGURE 13.13

between 50 - 1000 lbs has a stabilising effect on the mode and correspondingly increases the value of critical velocity. Fig. 13.12 also shows that an increase in the strop lengths d_1 or d_2 have a moderately destabilising effect on the system.

In comparison with the previous mode it is found that (from fig. 13.9 and 13.13) the non-dimensional frequency parameter for mode 2 is generally larger, and the typical curves adopt the more usual shape found with other strop arrangements. In fact they compare quite favourably with those of the longitudinal mode 1 of the single and twin strop arrangements (fig. 13.2).

It is interesting to note from fig. 13.14, where a plot of relative derivative importance is given against forward velocity, that a large number of lateral damping and stiffness derivatives assume importance. Although one configuration only is shown, the curves given are typical of those for other configurations considered. The y_v, l_p, l_v and n_v damping derivatives are clearly the most important derivatives at small and moderate velocities. At higher velocities the damping derivative n_r becomes more important because of the combined yawing-sideslip motion. Its importance is secondary, however, in comparison with the stiffness derivatives, y_ϕ, n_ϕ, y_ψ, l_ψ.

FIGURE 13.14

All Readings Below Stall Conditions

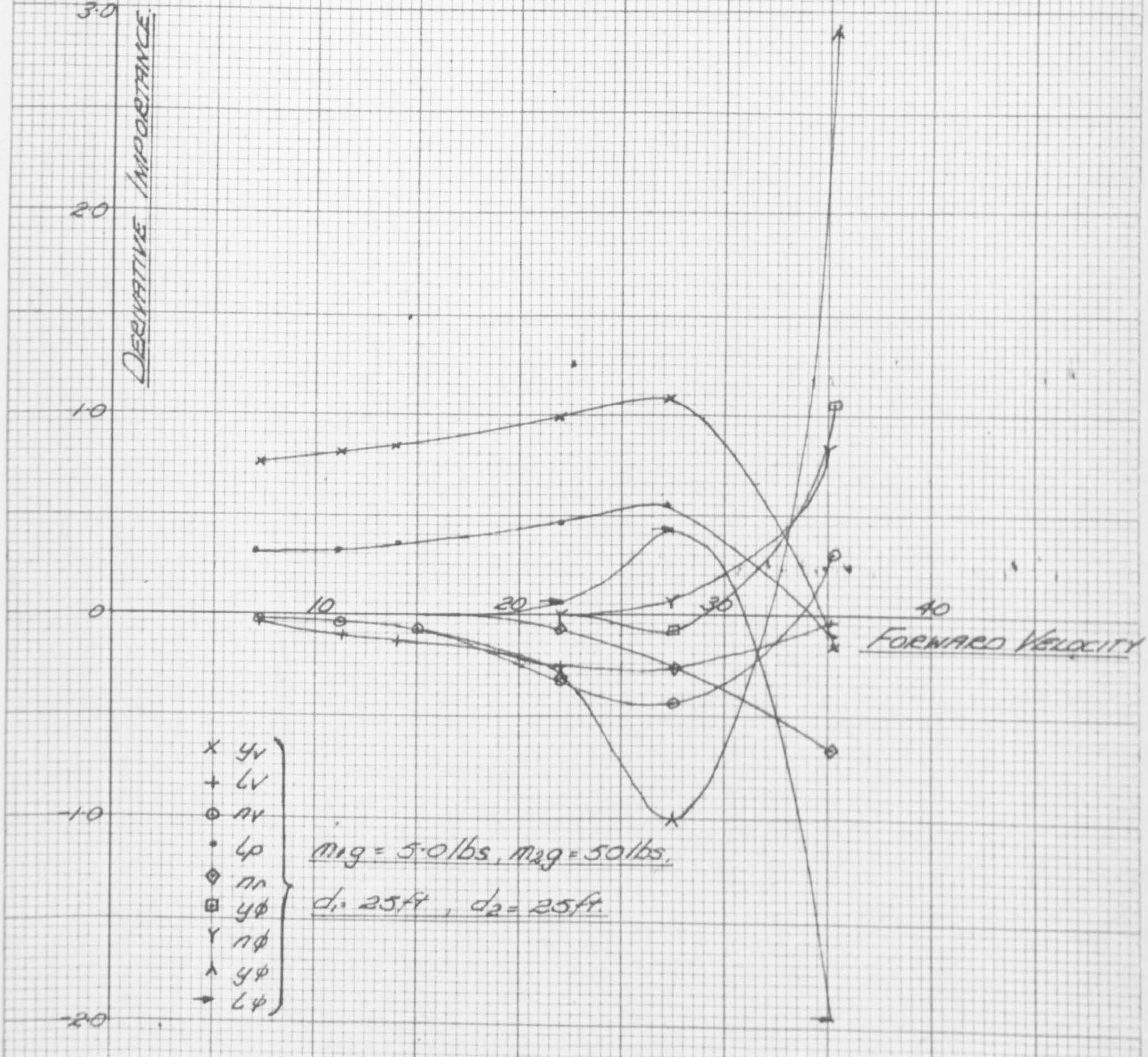

Single Stroop Arrangement Lateral Mode 2.

Plot Of The Relative Derivative Importance

Against Forward Velocity

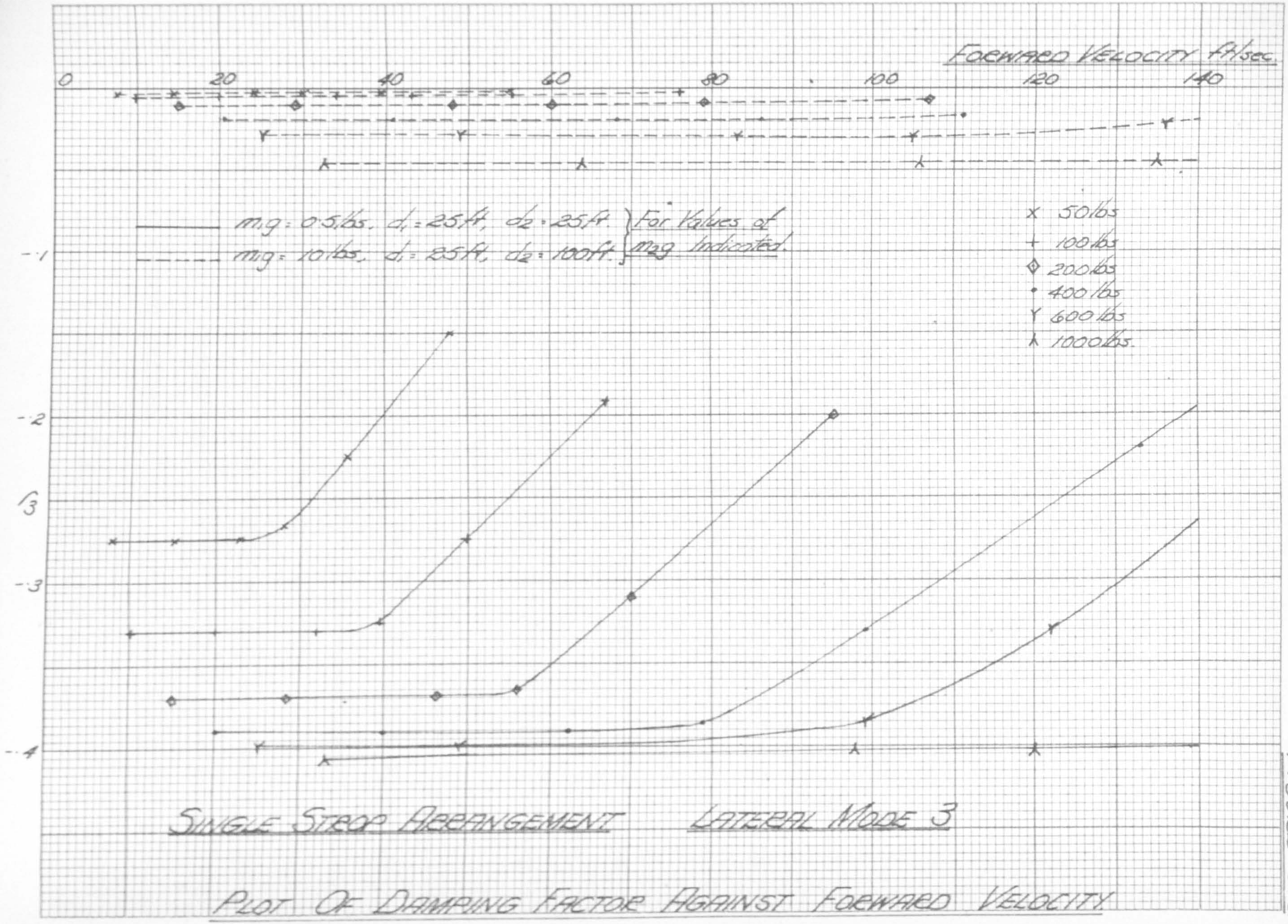

SINGLE STEP ARRANGEMENT LATERAL MODE 3

PLOT OF DAMPING FACTOR AGAINST FOREWARD VELOCITY

FIGURE 13.15

13.1.2c Mode 3

This mode of oscillation is a 'short-period' mode and is similar in form to the 'flutter mode' in the previous longitudinal studies, because it consists of a rotary motion about the longitudinal axis of the pallet (with only small translational movements of the pallet). In contrast to the two previous lateral modes, this modal form remains the same throughout the range of the investigations. Whilst the mode always remains stable, the degree of damping in the system depends greatly on most of the structural parameters. This is illustrated in fig. 13.15 where a comparison is made between the most stable and lightly damped arrangements.

Although detailed results are not shown, it is found that increases of both the lifting hook weight ($m_1 g$) and the strop length d_2 above 0.5 lbs and 25 ft respectively have strong destabilising effects on the mode. On the other hand variations in the strop length d_1 have negligible effects on stability. Also fig. 13.15 shows the increase of the pallet weight ($m_2 g$) to have a stabilising effect on the lateral mode.

Having analysed the importance of the derivatives on this mode it has proved unnecessary to give an illustration of their relative values. This is because the damping

FIGURE 1316.

Plot of Frequency Parameter Against Forward Velocity

Single Stage Arrangement

Lineal Mode 3

m_q = 6 lbs., $d_1 = d_2$ = soft

For Values of Pulley Weight Indicated

1000
600
400
300
200
100
80
70
60
50
53
40
30
20
10
0

derivative l_p is predominantly important throughout the investigations. All the other derivative terms are completely negligible.

Finally fig. 13.16 shows a typical form of the non-dimensional frequency parameter (s_3) against forward velocity curves for this particular mode of oscillation. As usual, the typical arrangement of $m_1 g$ = 5 lbs, $d_1 = d_2$ = 50 ft is considered.

The results obtained so far for the single strop configuration have been discussed separately for the longitudinal and lateral modes; assuming small disturbances throughout. However, for the unstable modes with oscillations of increasing amplitude, it is obvious that second order terms (previously neglected) increase in importance and coupling would most probably occur between the longitudinal and lateral oscillations, especially if the modes are of similar frequency. For these present investigations, modes of common frequency only are considered briefly, although it is realised that non-linear coupling could occur between two modes having frequencies related by integral multiplying factors.

From a comparison of the frequencies for the longitudinal and lateral 'short period' modes of oscillation (see fig. 13.6 and 13.16) it is apparent that the

PLOT OF FREQUENCY PARAMETER AGAINST FORWARD VELOCITY

SINGLE STROP ARRANGEMENT

LATERAL MODE 3.

$m_1 g = 5.0$ lbs, $d_1 = d_2 = 50$ ft

For Values of Pallet Weight Indicated

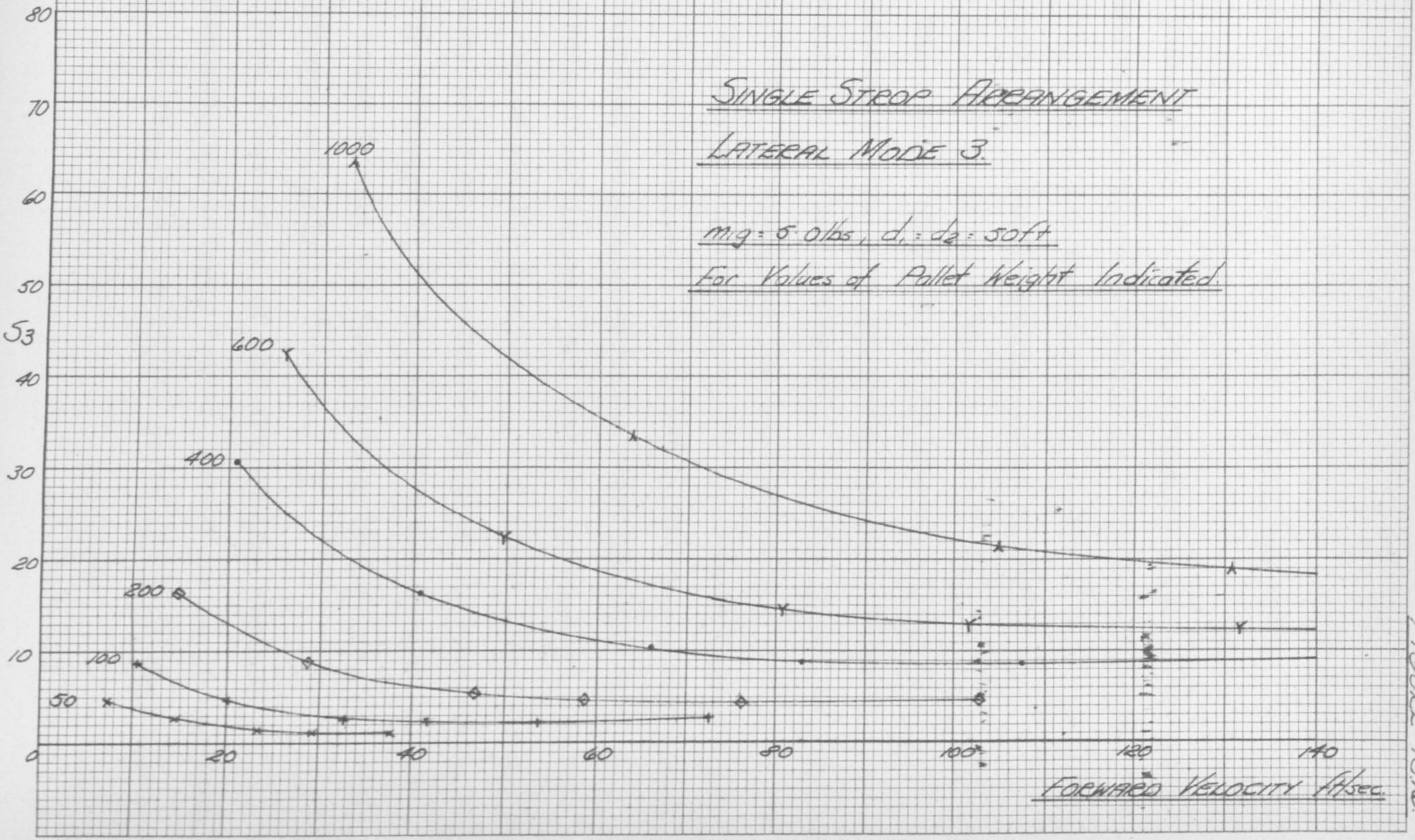

FIGURE 13.16.

derivative l_p is predominantly important throughout the investigations. All the other derivative terms are completely negligible.

Finally fig. 13.16 shows a typical form of the non-dimensional frequency parameter (s_3) against forward velocity curves for this particular mode of oscillation. As usual, the typical arrangement of $m_1 g$ = 5 lbs, $d_1 = d_2$ = 50 ft is considered.

The results obtained so far for the single strop configuration have been discussed separately for the longitudinal and lateral modes; assuming small disturbances throughout. However, for the unstable modes with oscillations of increasing amplitude, it is obvious that second order terms (previously neglected) increase in importance and coupling would most probably occur between the longitudinal and lateral oscillations, especially if the modes are of similar frequency. For these present investigations, modes of common frequency only are considered briefly, although it is realised that non-linear coupling could occur between two modes having frequencies related by integral multiplying factors.

From a comparison of the frequencies for the longitudinal and lateral 'short period' modes of oscillation (see fig. 13.6 and 13.16) it is apparent that the

longitudinal mode has unstable properties and both modes have very similar ranges of frequency. It is therefore likely that coupling would occur between the two modes. This would result in an oscillatory divergence that could be similar to the instability encountered with the full scale pallet.

Furthermore, non-coupling could occur between the longitudinal 'pendulum' mode and the unstable lateral mode 2 (see fig. 13.2 and 13.13), because both modes of oscillation are in a similar frequency range. Clearly, the extension of these initial investigations is beyond the scope of the work here, although these coupling effects should not be ignored when more detailed studies are carried out.

In an effort to eliminate the instabilities encountered in the lateral considerations of the single strop configuration, the twin strop configuration is considered because it imposes a constraint on the yawing and rolling displacements of the lifting bar and pallet.

13.2 The Twin Strop Configuration

A wide range of promising results has been obtained for the twin strop configuration using a similar method to that adopted for the single strop configuration (see chapter 6). In addition to the previous variables, the

lifting bar length (2a) is also considered in the range 6 ft to 18 ft. Furthermore, special attention is given to the particular case where the lifting bar length approximates to the span of the pallet, i.e. 12 ft. (The reason for this is given later in this chapter). As mentioned previously, the longitudinal modes of the single and twin strop configurations are identical - hence, the lateral modes only are studied here.

13.2.1 The Lateral Modes

As with the single strop, three lateral modes are evident here. No arrangement displays either a divergence or subsidence at any forward velocity considered. The three modes are:- (a) mode 1 - a low frequency stable mode which has a predominant lateral pendulum action for a range of small to moderate velocities (although at higher velocities the modal form is a combined sideslip - yawing displacement), (b) mode 2 - a low frequency stable or unstable yawing mode throughout the range of velocities investigated, (c) mode 3 - a high frequency stable mode of a similar form to the third lateral mode of the single strop configuration. In this the pallet rotates about a longitudinal axis in a rolling sense whilst executing only small translational movements.

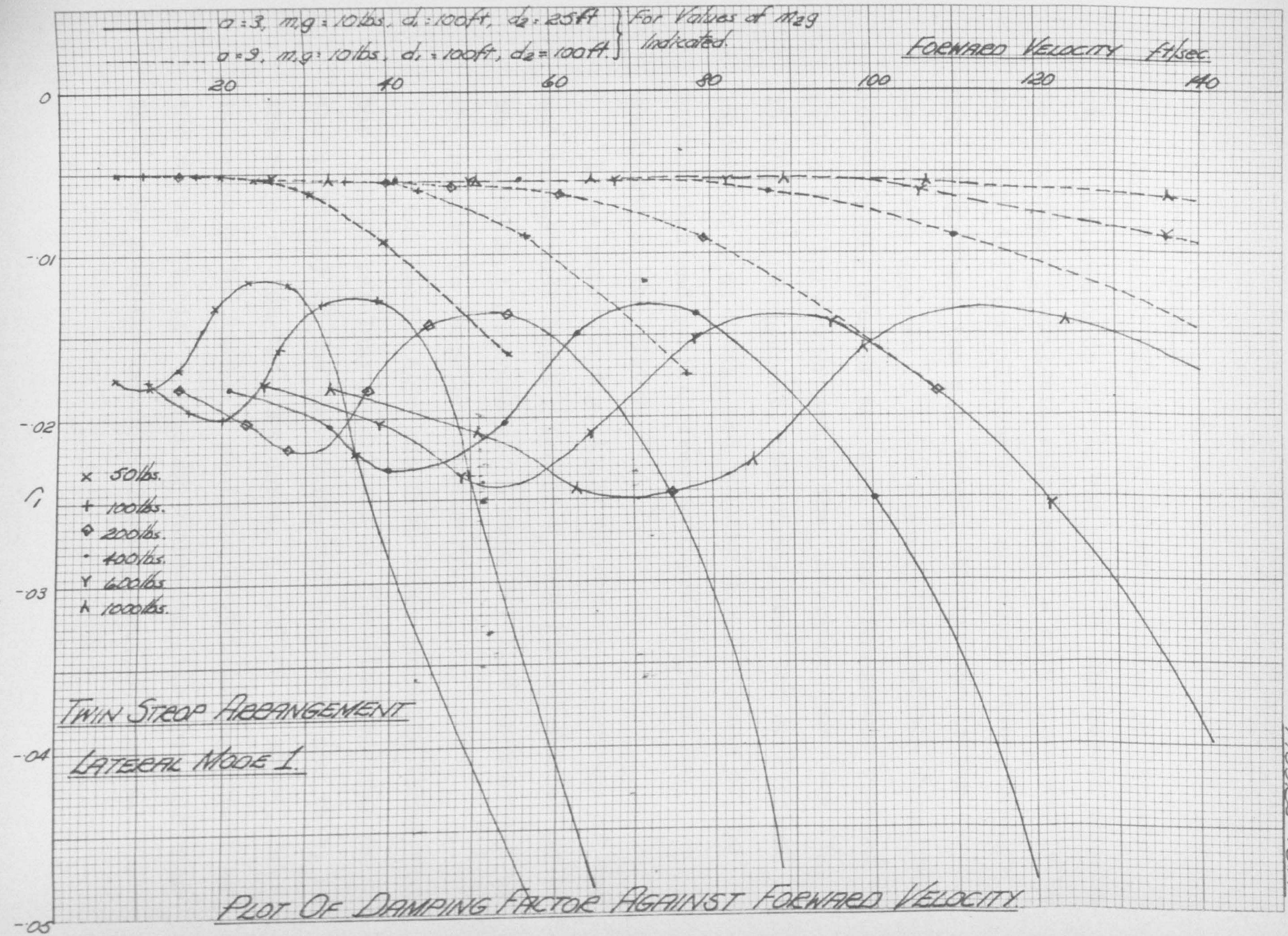

PLOT OF DAMPING FACTOR AGAINST FORWARD VELOCITY

FIGURE 13.17.

13.2.1a Mode 1

This lateral mode has a pendulum motion of 'steady state' incidences up to 3°, but above 3° the motion changes to a combined yawing-sideslip form. A comparison should be made with the lateral mode 2 of the single strop arrangement which shows the same trend. Whilst the latter arrangement appears to have a generally unstable form, the corresponding mode of the twin strop arrangement remains stable for the greater part of the investigations (see fig. 13.17). It is apparent, therefore, that the constraint imposed on both yawing and rolling displacements of the lifting bar and pallet gives an improvement in the stability of the system.

If we refer to fig. 13.17 we observe a measure of the non-dimensional damping factor r_1 and its dependence on the structural parameters. A more detailed examination of the results is therefore necessary.

It has become apparent from these investigations that the lifting bar length (2a) has an important bearing on the stability of the twin strop configuration and that, in the range of lengths considered, i.e. 6 ft to 18 ft, an increase in length has a distinct destabilising effect on the system at high values of incidence (i.e. greater than 10°). In fact the occasional configuration becomes

PLOT OF FREQUENCY PARAMETER AGAINST FORWARD VELOCITY

TWIN STEOP ARRANGEMENT

LATERAL MODE 1

$m_1 g = 5.0$ lbs, $a = 6$ ft, $d_1 = d_2 = 50$ ft

For Values of $m_2 g$ Indicated

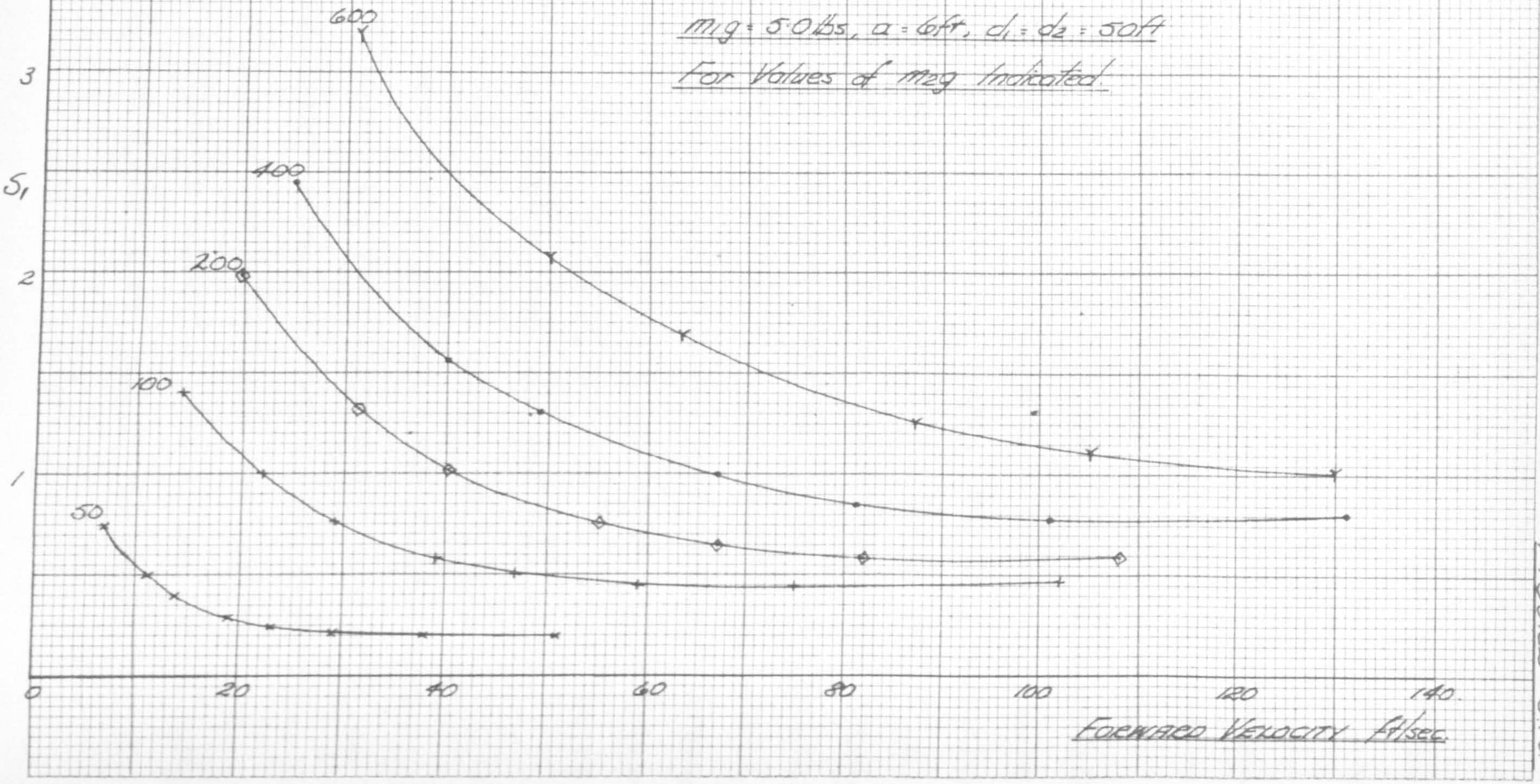

FIGURE 13.18.

unstable when the lifting bar length is 18 ft and the 'steady state' incidence 15°. Otherwise at incidences below 10°, an increase in length between 6 - 18 ft is not so markedly destabilising. It is clear, however, that further investigations must be made on this point to determine the optimum length between 0 and 18 ft where maximum damping occurs.

From fig 13.17 it is shown that the effect of increasing the pallet weight (m_2g) appears to shift a particular curve of damping into a higher velocity range. Further, variation of the lifting bar weight (m_1g) has a negligible effect on stability for the range of structural parameters considered. It has also been found that an increase in the strop length d_1 between 25 ft and 100 ft has a marked stabilising effect for all configurations. This is more apparent for a lifting bar length of 6 ft than for a bar of length 18 ft. Furthermore, an increase in the length d_2 between 25 ft and 100 ft has a destabilising effect on the mode and this effect increases with an increase in the strop length d_1. Reference to the corresponding mode of the single strop arrangement illustrates the fact that an increase of d_1 or d_2 has a destabilising effect. In conclusion, therefore, for the range of parameters considered, the most heavily damped system is that in which the lifting bar length and strop lengths d_1 and d_2 are 6 ft, 100 ft and 25 ft respectively.

FIGURE 13.19.

PLOT OF THE RELATIVE DERIVATIVE IMPORTANCE AGAINST FORWARD VELOCITY

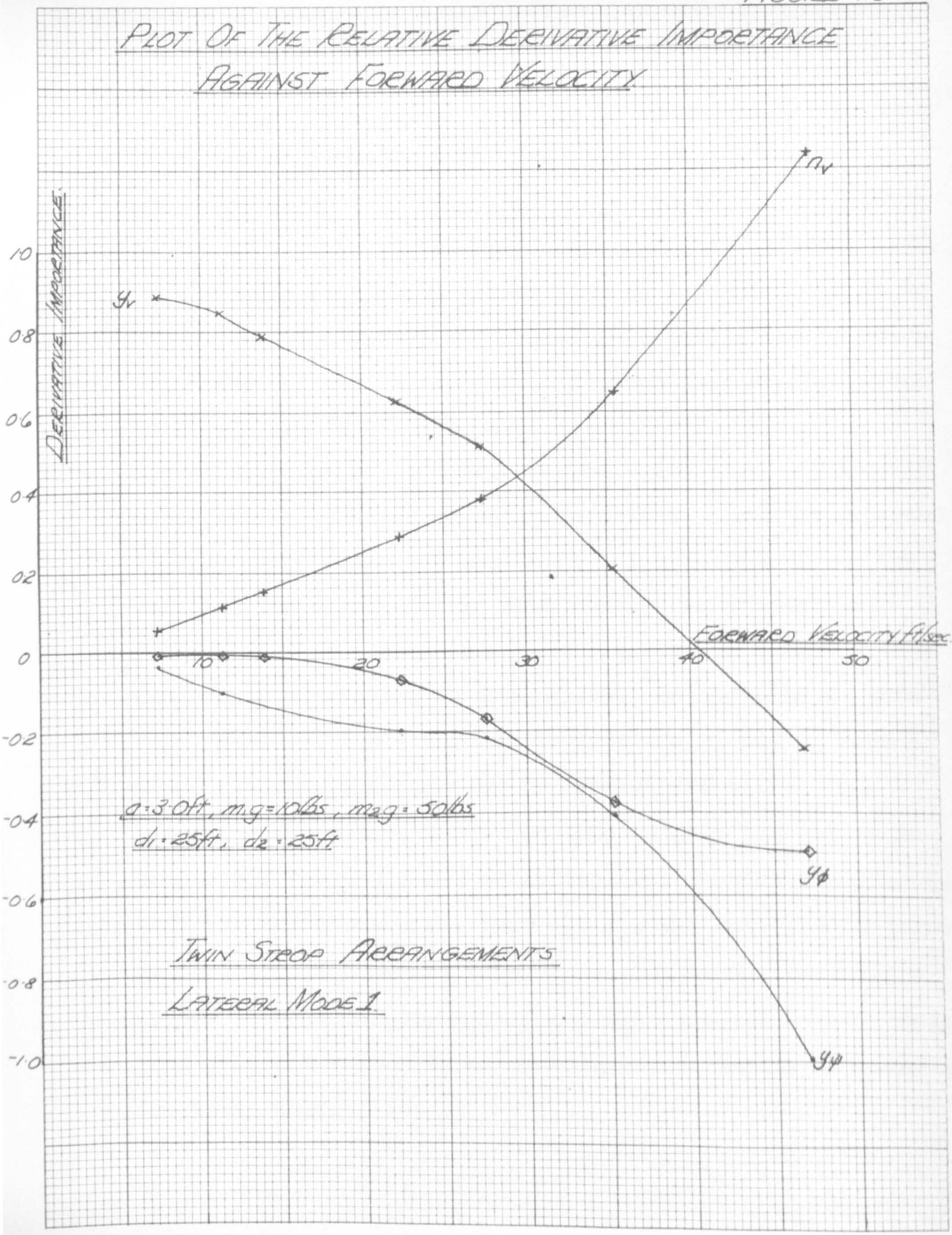

$a = 3.0$ ft, $m_1 g = 10$ lbs, $m_2 g = 50$ lbs

$d_1 = 25$ ft, $d_2 = 25$ ft

TWIN STEOP ARRANGEMENTS

LATERAL MODE I.

As previously, a plot of the non-dimensional frequency parameter (s_1) is given in fig. 13.18 for the case $m_1 g$ = 5 lbs, 2a = 12 ft and $d_1 = d_2$ = 50 ft. A discussion on the importance of the frequency parameter is given later.

Because of the importance of this lateral mode, it is worthwhile to make a brief investigation into the relative importance of the derivatives. A graph is therefore given in fig. 13.19 of the important terms. This shows the general case where at small forward velocities the damping derivative y_v is predominantly important. This is expected in view of the sideslip motion at low velocities. As the velocity increases, so the mode changes to a combined yawing-sideslip motion and the derivative n_v takes on importance - as shown in fig. 13.19. In addition to this term, however, the stiffness derivatives y_ϕ and y_ψ become important with the increase in forward velocity. The remaining derivative terms are consistently negligible in comparison for the range of lifting bar lengths considered. Although the derivatives (y_v, n_v, y_ϕ, y_ψ) have been obtained from static wind tunnel tests (see chapter 7) and would appear to be accurate, the y_v and n_v terms, at least, should really be determined by an oscillatory technique in order to ascertain their accuracy.

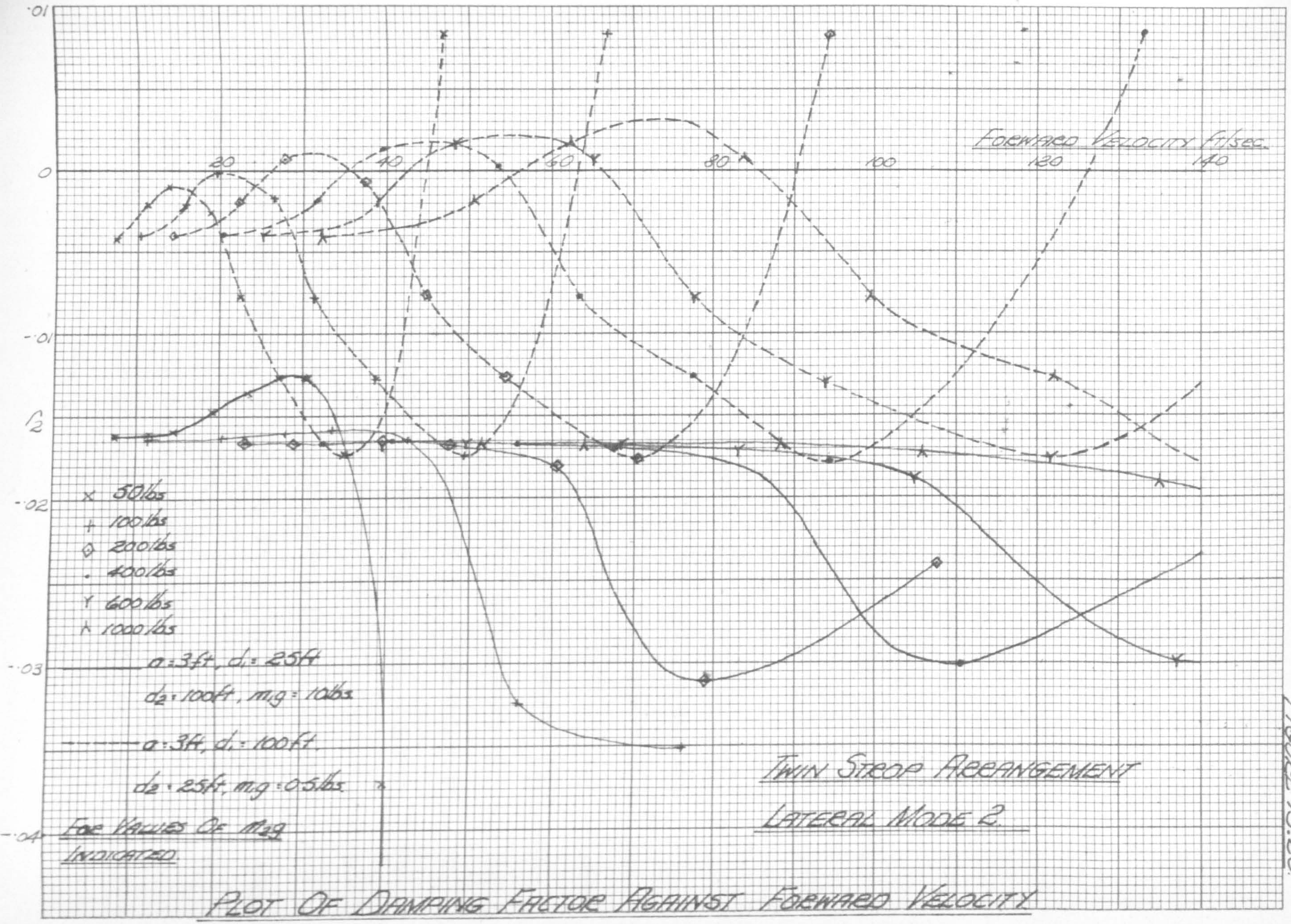

Twin Strop Arrangement

Lateral Mode 2.

Figure 13.20.

Plot Of Damping Factor Against Forward Velocity

13.2.1b Mode 2

This mode of oscillation takes the form of a pure low frequency yawing mode for all forward velocities and is quite stable for the majority of arrangements considered. It is noted, however, that certain arrangements do in fact become temporarily unstable at certain forward velocities. The similarity between the modal form of this mode and the lateral mode 1 of the single strop arrangement is very apparent, although there is no tendency for the latter to become unstable. Furthermore, the curves of fig. 13.8 and 13.20 are seen to be similar.

Whilst there is a distinct difference in terms of stability between the two typical examples shown in fig. 13.20, this is found to be the exception because the majority of results exhibit stability. In fact variations (in the usual ranges) in the lifting bar length (2a) and weight and length (d_2) appear to have only small effects on the non-dimensional damping factor r_2. Consideration of the increase in the lifting bar length (2a) between 6 ft and 18 ft shows an increase in the damping factor between lengths 6 ft and 12 ft. An increase in the lifting bar length between 12 ft and 18 ft, however, generally has the opposite effect. In addition to this, variations in the weight of the lifting bar have negligible effects on stability, except for pallet weights < 50 lbs where there is no definite trend.

PLOT OF FREQUENCY PARAMETER AGAINST FORWARD VELOCITY.

TWIN STROP ARRANGEMENT

LATERAL MODE 2.

$m_1 g$ = 50 lbs, a = 6 Ft, $d_1 = d_2$ = 50 Ft.

For Values of $m_2 g$ Indicated.

600

400

200

100

50

S_2

8 7 6 5 4 3 2 1

0 20 40 60 80 100 120 140

FORWARD VELOCITY Ft/Sec.

FIGURE 13.21

The variations in the structural parameter d_1 appear to have the greater effect on the damping factor r_2. It is found that an increase in d_1 between 25 ft and 100 ft has a strong destabilising effect on the system. This is especially marked when the lifting bar length (2a) is 6 ft. An increase up to 18 ft, however, shows this effect to fall off somewhat. In the particular case, for example, given in fig. 13.20 the unstable curves are obtained with 2a - 6 ft and d_1 = 100 ft. On the other hand, with 2a = 12 ft or 18 ft and d_1 = 100 ft, the mode remains stable.

Variations in the strop length d_2 are, in comparison to d_1, found to have only small stabilising effects on the configurations and this is only for lifting bar lengths less than 6.0 ft. For values greater than 6.0 ft, variations have no effect on the damping factor. Finally, an increase in the pallet weight between 50 - 1000 lbs has the effect of shifting the stability curves for lesser weights to higher velocity regions (see fig. 13.20). Whilst this is also the case for the isolated unstable instance given in fig. 13.20, it is apparent there that the increase in pallet weight has a destabilising effect.

In fig. 13.21 the usual plot of frequency parameter corresponding to mode 2 (with $m_1 g$ = 5 lbs, 2a = 12 ft, $d_1 = d_2$ = 50 ft) is given for comparison with various

FIGURE 13.22.

PLOT OF THE RELATIVE DERIVATIVE IMPORTANCE AGAINST FORWARD VELOCITY.

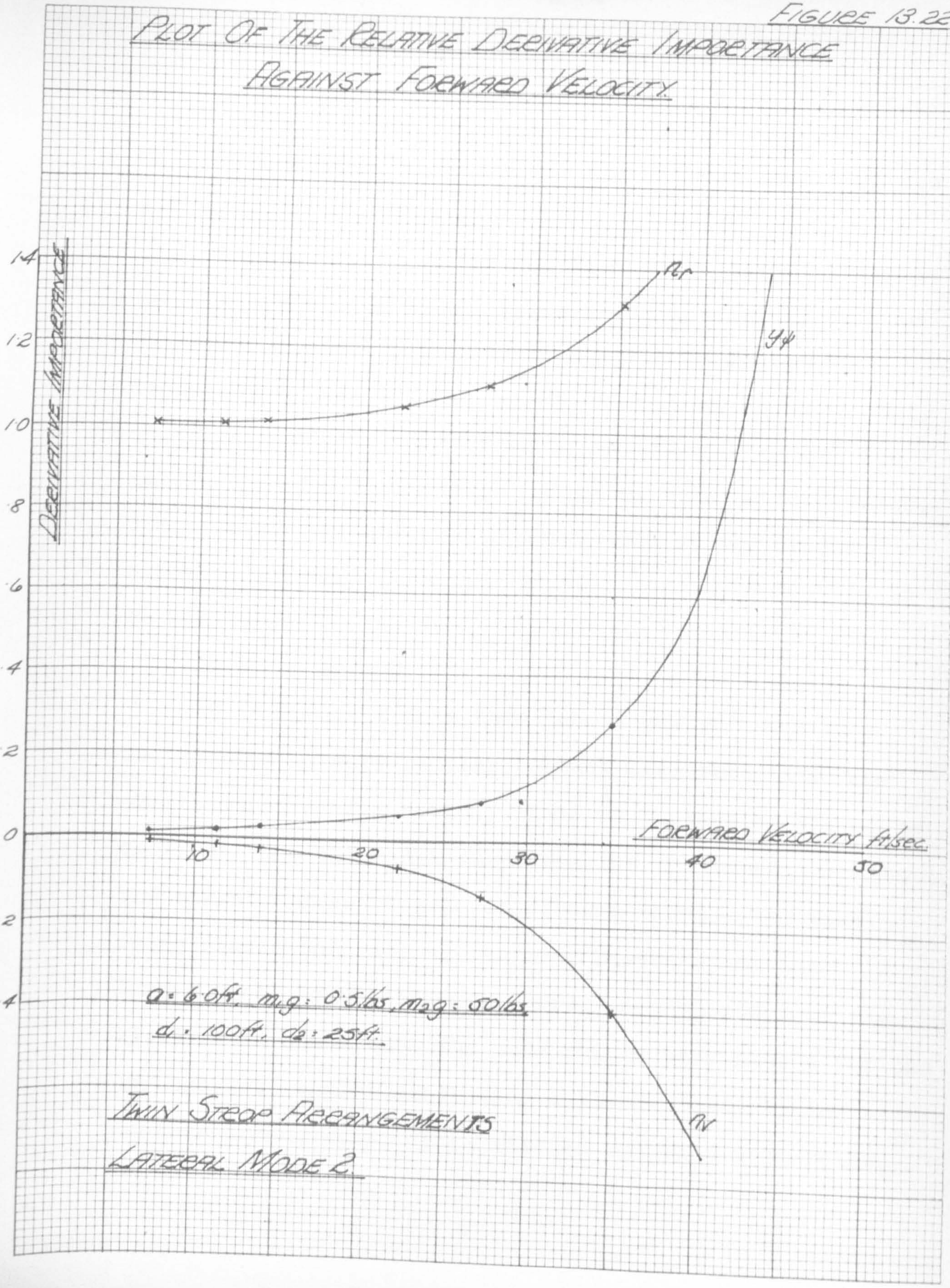

a = 6·0ft. $m_1 g$ = 0·5lbs. $m_2 g$ = 50lbs.
d_1 = 100ft. d_2 = 25ft.

TWIN STEOP ARRANGEMENTS
LATERAL MODE 2.

other modes of oscillation. The frequency range is understandably greater than for the lateral mode 1 of the single strop arrangement.

The usual plot of the relative derivative importance against forward velocity, V, is given in fig. 13.22. As expected, the damping derivative n_r is predominantly important up to moderate 'steady state' incidences. Only at incidences above 10° where higher forward speeds are attained do the derivatives n_v and y_ψ take on importance. Comparison with the corresponding mode of the single strop arrangement (see fig. 13.10) show these results to be similar.

13.2.1c Mode 3

It is apparent that this 'short period' mode of oscillation is very similar to that discussed with the single strop configuration. This is further confirmed by the fact that the modal shape remains unaltered throughout the range of forward velocities considered; the mode being stable and similar, in many respects, to the longitudinal "flutter" mode. From an inspection of fig. 13.23 it is shown that the mode can be very stable for one arrangement, whilst exhibiting neutral stability for another arrangement. This will be enlarged upon below.

FORWARD VELOCITY ft/sec.

0 20 40 60 80 100 120 140

ζ_3

-·1 -·2 -·3 -·4

a = 3·0ft, m.g = 0·5lbs, d_1 = 25ft, d_2 = 25ft.

a = 9·0ft, m.g = 10lbs, d_1 = 25ft, d_2 = 100ft.

× 50lbs
\+ 100lbs
◇ 200lbs
· 400lbs
Y 600lbs
Λ 1000lbs.

TWIN STEOP ARRANGEMENT
LATERAL MODE 3.

PLOT OF DAMPING FACTOR AGAINST FORWARD VELOCITY.

FIGURE 13.23

From a general study of the results obtained for various values of the lifting bar length, i.e. 6 ft, 12 ft and 18 ft, it is found that the extreme lengths lead to more stable systems than does the 12 ft length. However on comparison with the similar lateral mode 3 of the single strop arrangement it is found that the latter arrangement is more heavily damped. This trend was expected for the twin strop configuration because the lifting bar must constrain the rolling motion of the pallet, so that the rotary damping derivatives in roll have a smaller effect. For the particular case when the lifting bar length and the span of the pallet are equal, i.e. 12 ft, the mode is in a state of neutral stability, i.e. $r_3 = 0$. This is because the pallet remains level for this 'short period' mode and the rotary damping derivatives have a negligible effect on stability.

Except for the particular case when the lifting bar length is equal to the span of the pallet, it is found that an increase of d_2 greater than 25 ft (in the usual range) has a strong destabilising effect on the mode. On the other hand, variations in the strop length d_1 have virtually no effect on the stability of the mode.

As expected from the 'single strop' results, an increase in the weight of the lifting bar ($m_1 g$) in the usual range has a strong destabilising effect. In

PLOT OF FREQUENCY PARAMETER AGAINST FORWARD VELOCITY

TWIN STOOP ARRANGEMENT
LATERAL MODE 3.

$m_1 g$ = 5·0lbs, a = 6ft, $d_1 = d_2$ = 50ft.
For Values of $m_2 g$ Indicated.

600
400
200
100
50

S_3

100
90
80
70
60
50
40
30
20
10
0

0 20 40 60 80 100 120 140

FORWARD VELOCITY ft/sec.

FIGURE 13.24

comparison, the fig. 13.23 shows that an increase of the pallet weight above 50 lbs has a stabilising effect on the system. The investigations thus show that the most stable system considered for this mode is one with $m_1 g$ = 0.5 lbs, d_2 = 25 ft and d_1 taking a value between 25 ft and 100 ft.

In addition to the above graphs, fig. 13.24 gives a set of curves for the non-dimensional frequency parameter, s_3, plotted against forward velocity when $m_1 g$ = 5 lbs, 2a = 12 ft and $d_1 = d_2$ = 50 ft. On comparison with the similar mode for the single strop configuration, it is found that the constraint of the extra strop increases the frequency parameter - as expected. As a result the possibility of coupling (on a 1 : 1 frequency basis) between this lateral mode and the longitudinal flutter mode would be less likely, although not impossible for the smaller pallet weights.

A plot of the relative derivative importance against forward velocity is not necessary for this mode, because it has been found that the damping derivative l_p is predominantly important at all velocities. All other derivative terms are in fact negligible in comparison.

The results obtained for the lateral oscillations of the twin strop configuration are rather encouraging. Practical considerations notwithstanding, it is apparent

that a considerable improvement in stability can be obtained in comparison with the single strop configuration. Unfortunately the same cannot be said of the longitudinal stability of the twin strop configuration (which, of course, is precisely similar to that of the single strop configuration).

If the possibility of introducing aerodynamic surfaces (in order to improve the longitudinal stability of the twin strop configuration) is excluded, it is necessary to constrain the longitudinal movements of the pallet by structural means. Hence a bifilar arrangement in the form of the trapezoidal configuration appeared to be the type of suspension required, although it was realised that the necessary lateral constraints on the pallet would be partially removed. However, since the lateral and longitudinal modes are separable, it is possible, at this stage, to examine the possibility of conferring longitudinal stability, in the knowledge that (if a stable longitudinal configuration is achieved) a combined twin strop/trapezoidal suspension might well be designed to eliminate instability in both sets of modes.

13.3 <u>The Trapezoidal Configuration</u>

With the trapezoidal configuration it is apparent that, in comparison with the previous twin strop configuration, an extra parameter has to be included with the previous terms because the lower strops (d_2 and d_3) are of

unequal length. This unfortunately leads to a rather impractical investigation (see chapter 6) because incidence α_2 has to be chosen independent of velocity, V. In practice this is, of course, not the case. A satisfactory assessment of the stability of the configuration can be obtained, however, if initial integer values of d_3, α_2, V, m_1, m_2 and 2a are chosen.

13.3.1 The Longitudinal Modes

The longitudinal studies of the trapezoidal configuration are shown to be similar to those pertaining to the single and twin strop configurations. Furthermore, the results for this configuration show a vast improvement on previous symmetric considerations.

As anticipated, two modes of oscillation are obtained, as follows: (a) mode 1 - a low frequency pendulum mode, and (b) mode 2 - a high frequency 'flutter' mode. Both these forms are similar to those of the single and twin strop configurations.

13.3.1a Mode 1

This low frequency pendulum mode is found to be of an oscillatory form for the major part of the investigations, although for small pallet weights, i.e. in the order of 50 lbs, there is a definite trend towards the development of either a subsidence and divergence or two subsidences.

FIGURE 13.25.

PLOT OF DAMPING FACTOR AGAINST FORWARD VELOCITY.

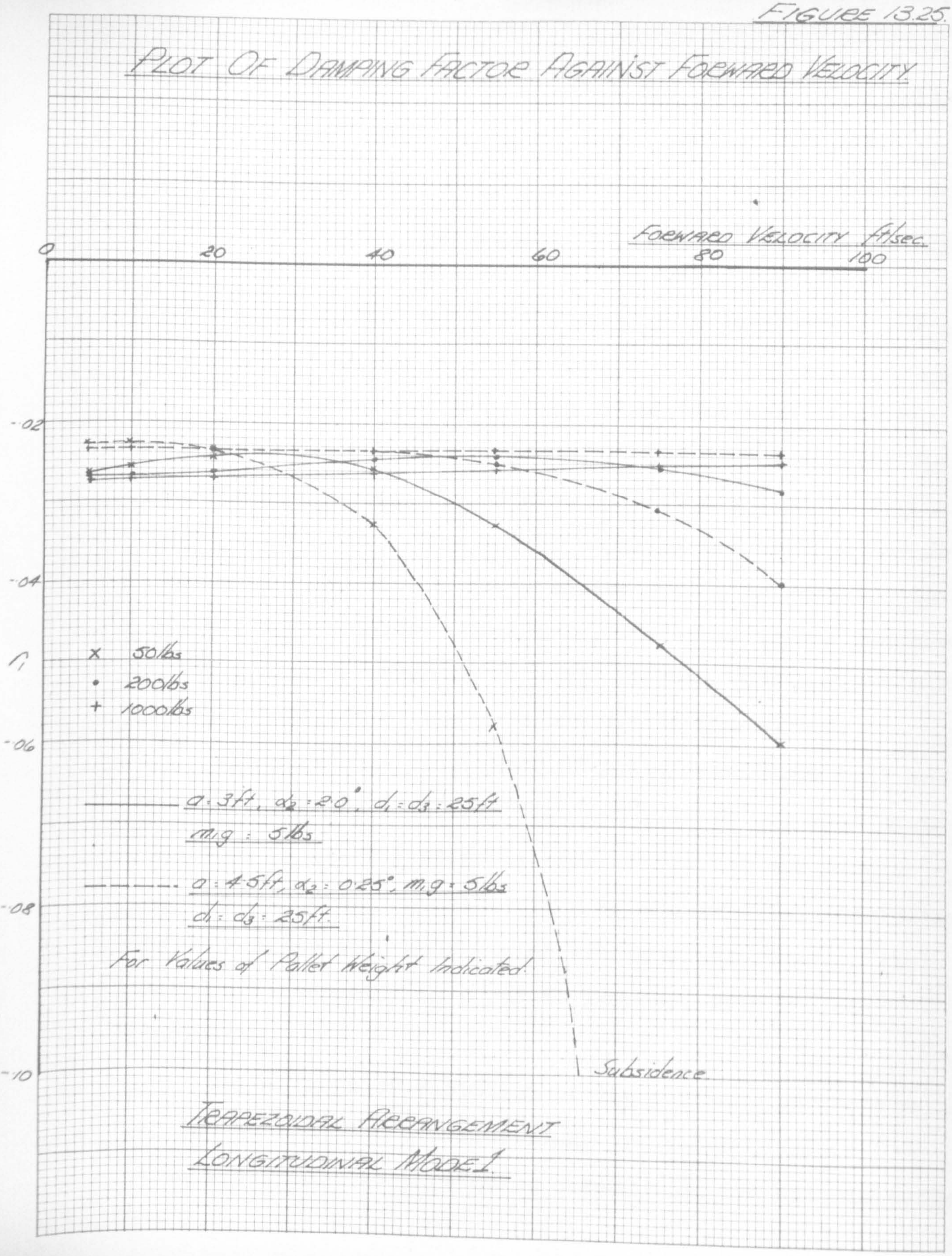

TRAPEZOIDAL ARRANGEMENT

LONGITUDINAL MODE I.

Otherwise, the mode remains stable for all the other pallet weights considered, i.e. $100 < m_2 g < 1000$ lb for all forward velocities. It is interesting to note that for the oscillatory modes, variations on the pallet weight between 100 and 1000 lbs have only small, indefinite, effects on the damping factor for all the configurations considered (see fig. 13.25).

In a similar manner, it is found that variations in the lifting bar length between 3 ft and 9 ft have very small effects on the damping and show no definite trend. Furthermore, variations in the weight ($m_1 g$) of the lifting bar in the usual range of 0.5 lbs - 10 lbs appear to have negligible effects on stability. Similarly, increases in the lengths d_1 or d_3 in the range 25 ft - 100 ft have very small effects on the stability of the mode and can be discounted.

Although only two values of pallet incidence (α_2) are considered here, i.e. 0.25° and 2.0°, it is apparent that the mode is usually slightly more stable for the larger incidence. From a consideration of the important derivatives pertaining to this mode (which are later discussed), the aerodynamic damping is found to increase with pallet incidence.

The effects of variation of the physical parameters in the trapezoidal configuration, are illustrated in fig. 13.25 for two particular cases, i.e. two extreme cases

FIGURE 13.26.

PLOT OF FREQUENCY PARAMETER AGAINST FORWARD VELOCITY.

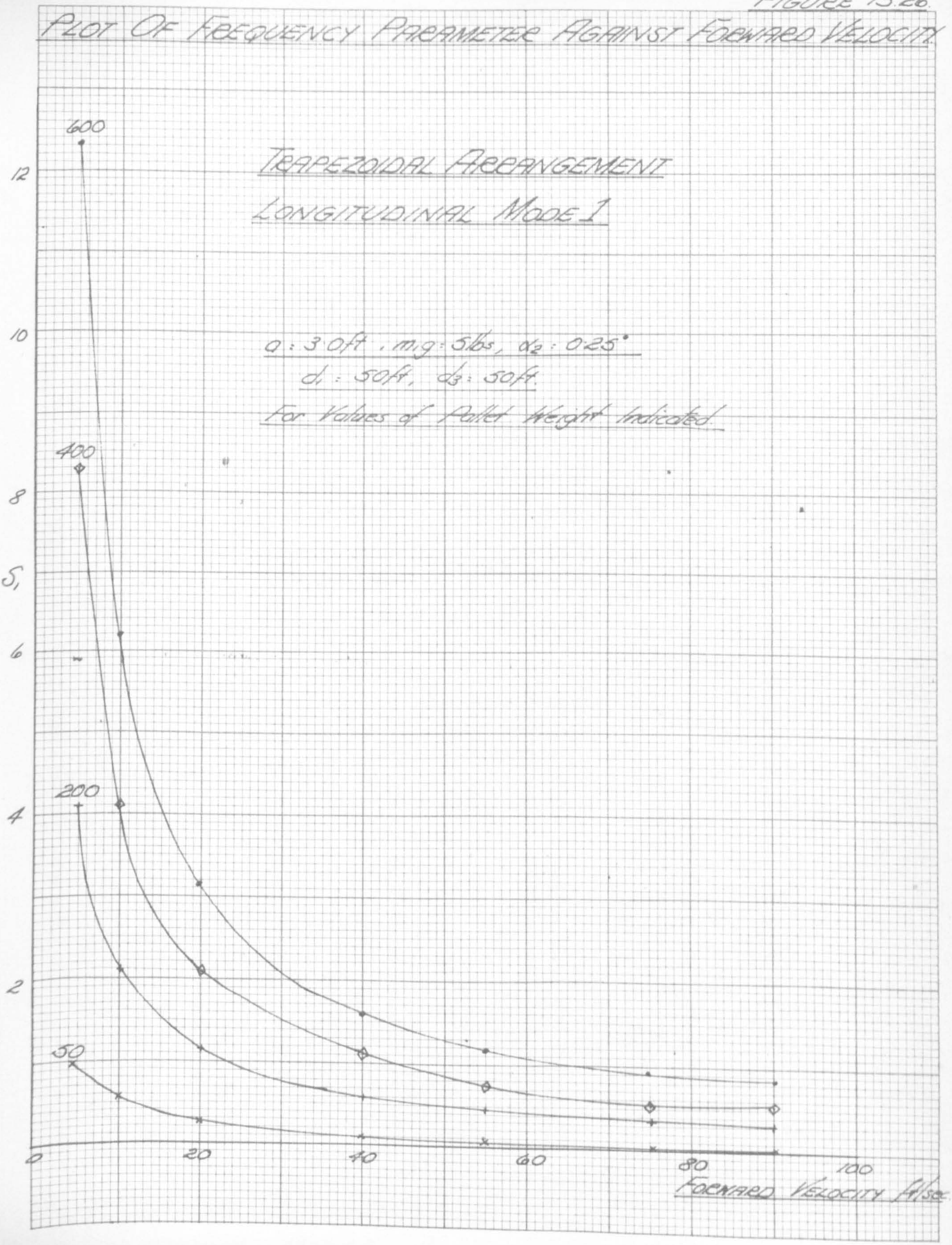

FIGURE 13.27.

PLOT OF DERIVATIVE IMPORTANCE AGAINST FORWARD VELOCITY

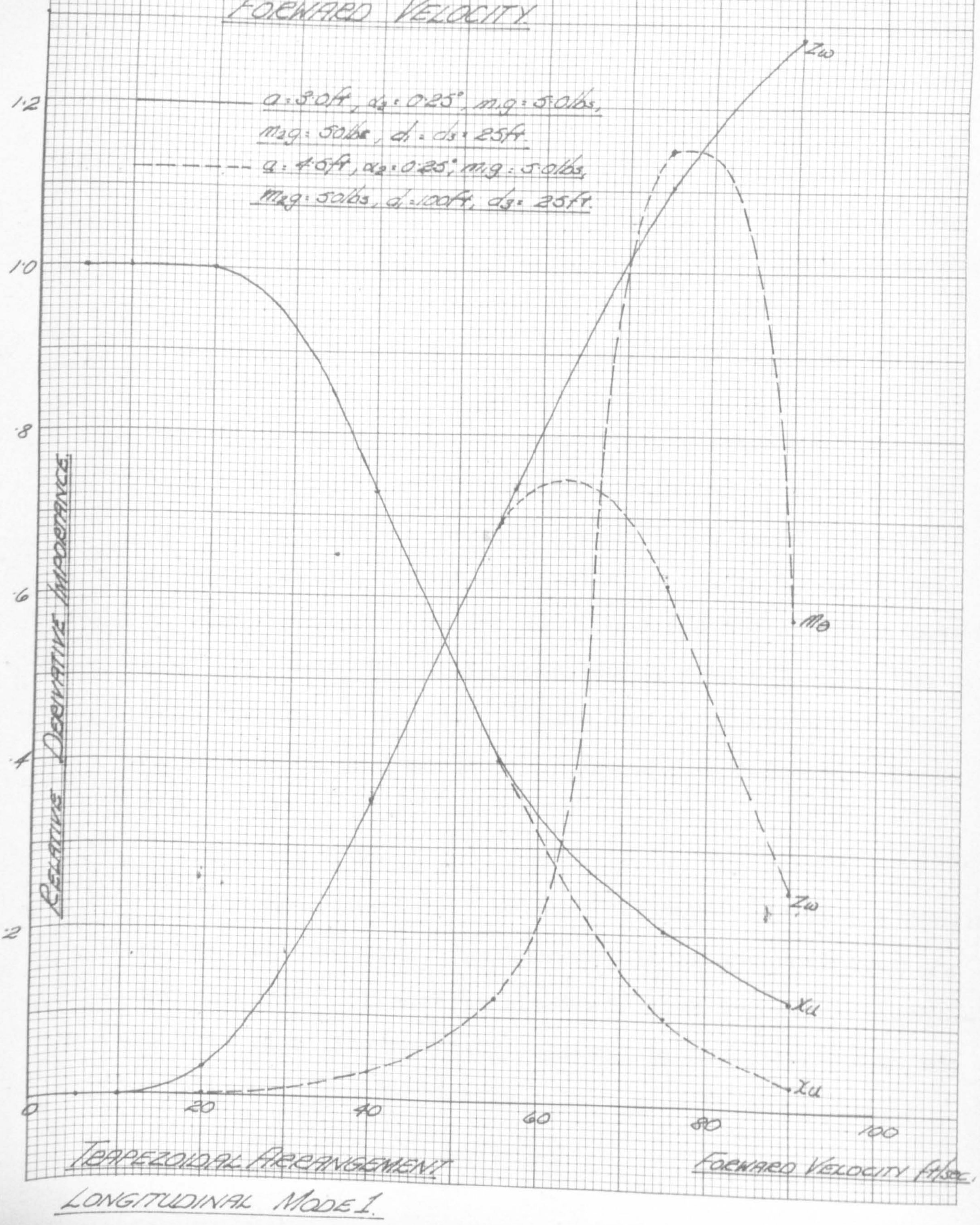

TRAPEZOIDAL ARRANGEMENT

LONGITUDINAL MODE I.

of damping. Clearly, the effect of varying the parameters has but a small overall effect on the damping factor. In addition to this figure, a graph is given of the non-dimensional frequency parameter s_1 against forward velocity (see fig. 13.26). This will be used later for comparison with other oscillatory modes of the trapezoidal configuration.

In order to illustrate the relative derivative importance for this mode, a typical graph is given (fig. 13.27) of the important terms plotted against forward velocity. For the two configurations considered, the damping derivative x_u is predominantly important at small forward velocities. However for an increase of velocity z_w takes on some importance, whilst the importance of the x_u term falls off. It is also found for the isolated case (and also when the lifting bar length does not equal the chord length of the pallet) that the stiffness derivative m_θ assumes major importance at the higher velocities (see fig. 13.27).

13.3.1b Mode 2

The mode is similar to the 'flutter' mode of the single strop configuration. Furthermore, it is apparent from the immense amount of results obtained, that a general improvement in stability has been achieved in comparison with the results given in section 13.1.1b. As with the previous

FIGURE 13.28

PLOT OF DAMPING FACTOR AGAINST FORWARD VELOCITY

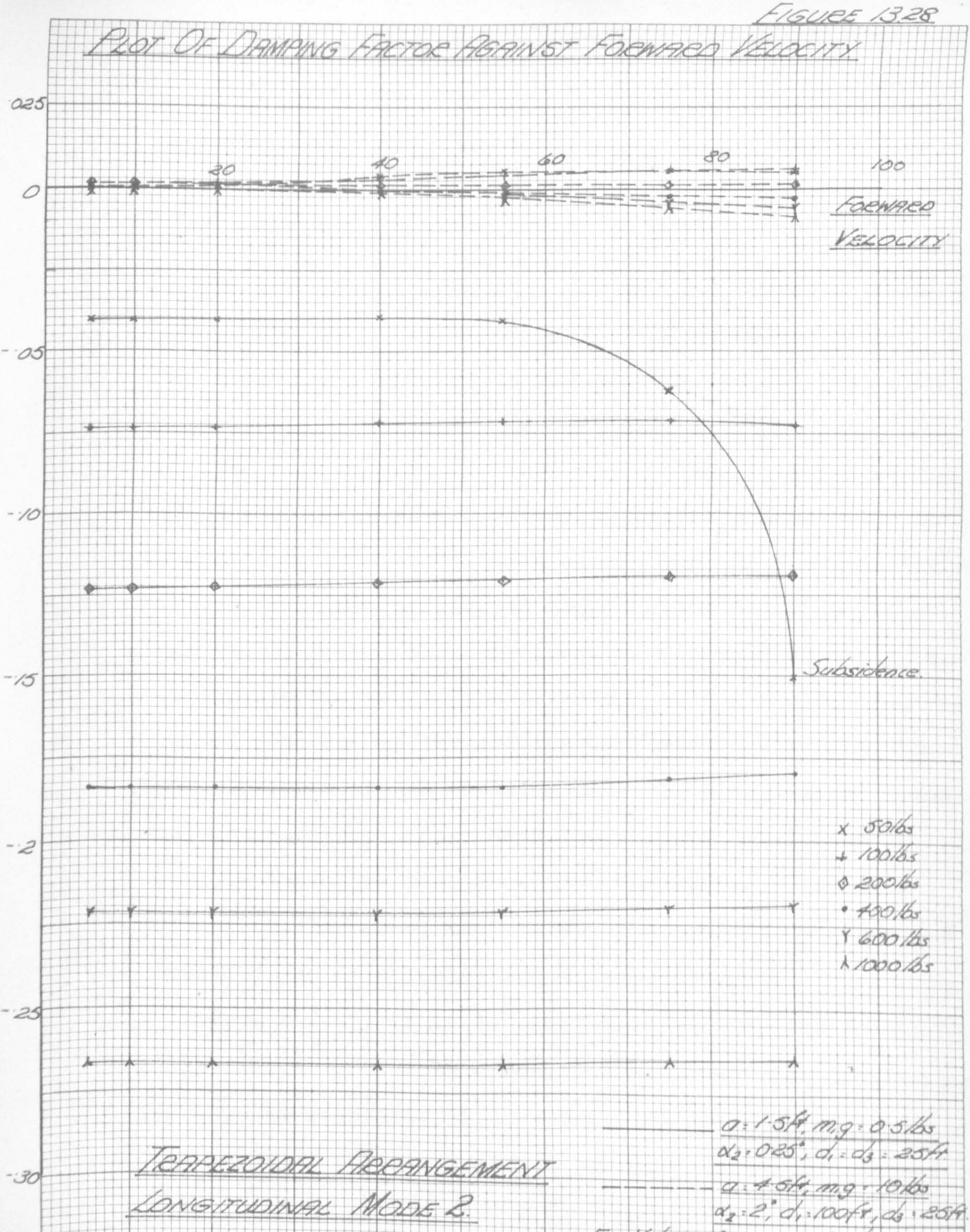

TRAPEZOIDAL ARRANGEMENT

LONGITUDINAL MODE 2.

For Values of m_2g Indicated.

mode, investigations are made with values of lifting bar length 3.0 ft and 9.0 ft, in addition to the particular case of 6.0 ft. Whilst the two former sets of results follow similar trends, different trends are found when the lifting bar length is 6.0 ft. In fig. 13.28 the extreme (stable and unstable) results, for the parameter ranges considered, are given as in illustration of the variation of stability in this mode of oscillation.

The results indicate that an increase in value of the 'steady state' incidence of the pallet (α_2) from 0.25° to 2° has a strong destabilising effect for all the variations of the parameters considered (see chapter 6). This is undoubtedly due to the corresponding decrease of the aerodynamic damping on the pallet.

An increase of the lifting bar weight above 0.5 lbs up to 10 lbs also has a strong destabilising effect on all the systems except those when the lifting bar length is equal to the chord length of the pallet, i.e. 6 ft. In this particular case, the systems all exhibit near neutral stability and no definite trends are apparent.

From fig. 13.28 it is shown that an increase in the pallet weight (for both arrangements) gives rise to an increase in stability of a system. It has been found, however, that this is not true for all the configurations.

FIGURE 13.29

PLOT OF FREQUENCY PARAMETER AGAINST FORWARD VELOCITY

TRAPEZOIDAL ARRANGEMENT

LONGITUDINAL MODE 2.

$a = 3.0$ ft, $m_1 g = 5.65$, $\alpha_2 = 0.25$

$d_1 = 50$ ft, $d_3 = 50$ ft.

For Values of Pallet Weight Indicated.

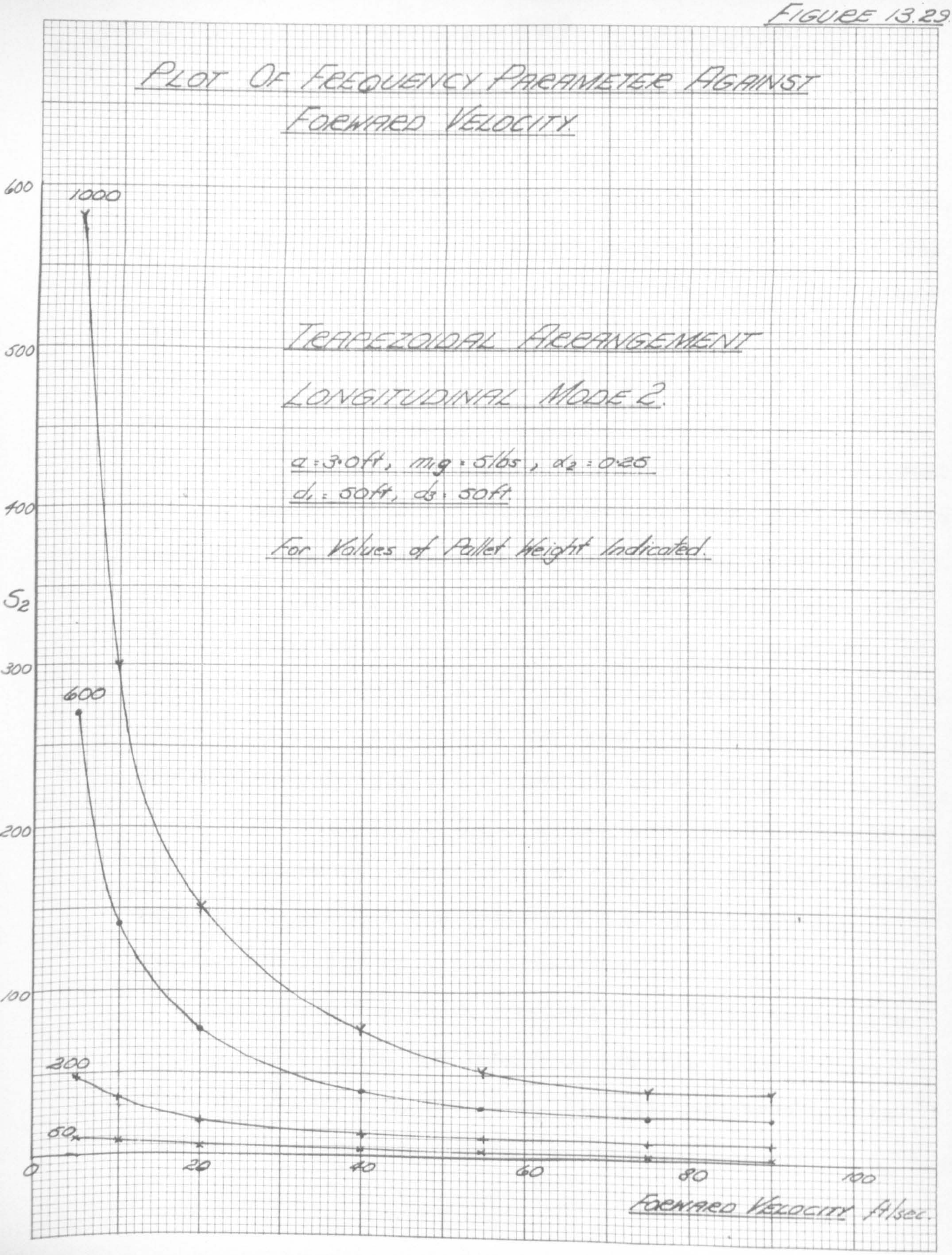

For example, when the lifting bar length is 3.0 ft, an increase in the pallet weight (in the usual range) has a strong stabilising effect as shown in fig. 13.28. However, for the two cases of lifting bar length 6.0 ft and 9.0 ft, it is found that no general trend is apparent. This could be due to the different 'steady state' positions the arrangements take up for such values of lifting bar length as 6.0 ft and 9.0 ft.

Variations in the lifting bar length (2a) have a great bearing on whether a system is stable or unstable. This is emphasised by the fact that for all the configurations considered (in their usual ranges), the arrangements are always stable when 2a = 3.0 ft or 6.0 ft, although the latter case always exhibits near neutral stability. On the other hand when 2a = 9.0 ft the mode does become unstable for certain configurations (usually when the incidence, α_2, is of 2^{o}). Because of these rather complicated effects it will be necessary, therefore, to carry out further investigations to predict the optimum value of 2a, for the maximum stability of a configuration.

Further to the above complexities, it is noticeable that an increase in the length d_3 greatly reduces the value of the damping factor r_2 for all the arrangements considered. However, variations of the strop length d_1 have

FIGURE 13.30.

PLOT OF DERIVATIVE IMPORTANCE AGAINST FORWARD VELOCITY.

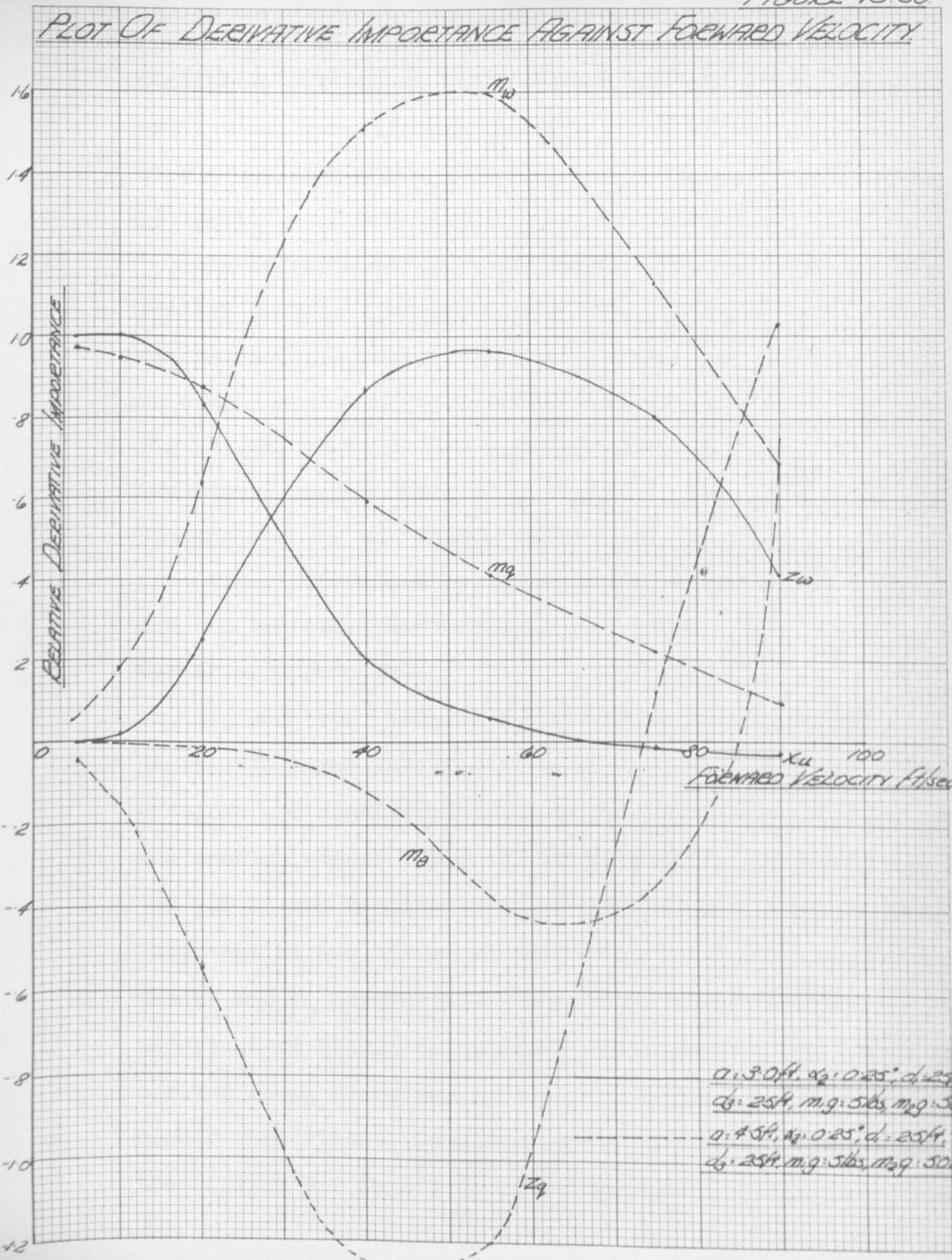

TRAPEZOIDAL ARRANGEMENT LONGITUDINAL MODE

negligible effects on stability and therefore these trends are indeed, very similar to those encountered with the single and twin strop in longitudinal mode 2 (see section 13.1.1b).

In addition to the usual plot of damping factor, a typical plot is also given (see fig. 13.29) of the non-dimensional frequency parameter against forward velocity. On comparison with the previous longitudinal mode (see fig. 13.26) there is a remarkable difference in the frequency ranges. Similarly, a comparison with the corresponding mode of the single and twin strop configurations (see fig. 13.6) shows an increase in the frequency range for the trapezoidal configuration compared with the two former arrangements.

An endeavour is made to establish the important derivative terms involved in this 'flutter' mode. Two configurations are considered for illustration in fig. 13.30. For the configurations where the lifting bar lengths are 3.0 ft and 9.0 ft the damping derivative m_q is always predominantly important at small forward velocities as shown. However, the z_q and m_w derivatives prove to be consistently important at higher velocities. Furthermore, the stiffness derivative m_θ occasionally takes on major importance at the higher velocities. Considering the particular case where the lifting bar length is equal to the chord length of the

pallet, i.e. 6.0 ft in this case, the above derivative terms have a negligible effect on stability because of the structural constraint imposed on the pitching of the pallet. Instead, it is found that the damping derivatives x_u and z_w are consistently important. As shown in fig. 13.30, the x_u term is predominantly important at small forward velocities, whereas at higher velocities the z_w term becomes primarily important. All other derivative terms appear to have a negligible effect on the damping of this particular configuration.

13.3.2 The Lateral Modes

The modes of oscillation obtained from the lateral studies of the trapezoidal configuration appear to be similar to those for the single and twin strop configurations. These are: (a) mode 1 - a stable mode of low frequency dominated by a yawing motion; (b) mode 2 - a low frequency stable mode with a combined sideslip - yawing motion, and (c) mode 3 - a 'short period' oscillatory mode which is similar to mode 3 of the single and twin strop configurations.

13.3.2a Mode 1

This mode of oscillation exhibits a stable yawing nature for the usual range of variables considered. On comparison with the single and twin strop configurations,

FIGURE 13.31

PLOT OF DAMPING FACTOR AGAINST FORWARD VELOCITY

FORWARD VELOCITY

0 20 40 60 80 100

·002 ·004 ·006 ·008 Γ_1 ·010 ·012 ·014 ·016 ·018 ·02

× 50 lbs
+ 100 lbs
◆ 200 lbs
• 400 lbs
Y 600 lbs
λ 1000 lbs

——— $a = 1.5$ ft, $m.g = 5$ lbs, $\alpha_2 = 0.25°$
$d_1 = 25$ ft, $d_3 = 25$ ft.

– – – – – – $a = 4.5$ ft, $m.g = 5$ lbs, $\alpha_2 = 0.25°$
$d_1 = 100$ ft, $d_3 = 100$ ft

TRAPEZOIDAL ARRANGEMENT

LATERAL MODE 1.

its shape conforms with the lateral modes 1 and 2 respectively, although certain other characteristics, e.g. frequency parameter, are dissimilar. A graph of the non-dimensional damping factor r_1 against forward velocity is shown in fig. 13.31 where curves for two different configurations are given. For the variations in the parameters, these are found to be the most stable and unstable arrangements. Variations in this small damping factor are minor for corresponding major changes in the values of the structural parameters.

On considering these structural parameters in more detail it is found that, for example, an increase in the lifting bar length (2a) between zero and 9.0 ft generally has a destabilising effect on the system. For the larger lengths, i.e. 9.0 ft, there are found to be a number of inconsistencies in this trend when the forward velocity is greater than 50 ft/sec. In a similar manner, it is found that an increase in the pallet weight between 50 lbs and 1000 lbs generally has a stabilising effect on a system, although for the larger lifting bar lengths this trend is not definite for forward velocities greater than 50 ft/sec (approximately). On the other hand, variations in the lifting bar weight ($m_1 g$) appear, as expected, to have a negligible effect on the damping factor r_1.

FIGURE 13.32.

PLOT OF FREQUENCY PARAMETER AGAINST FORWARD VELOCITY

TRAPEZOIDAL ARRANGEMENT

LATERAL MODE 1

$a = 4.5$ft, $m_g = 5$lbs, $\alpha_2 = 0.25°$

$d_1 = 50$ft, $d_3 = 50$ft

For Values of Pallet Weight Indicated

1000
600
400
200
100
50

S_1

28 26 24 22 20 18 16 14 12 10 8 6 4 2 0

20 40 60 80 100

FORWARD VELOCITY ft/sec.

The 'steady state' incidence of the pallet is found to have an important effect on the amount of damping of this mode. Clearly an increase in the overall effective damping of the important derivative terms n_r, n_v and y_v (see fig. 13.33) increases the stability of the mode. It should be noted, however, that these effects are more apparent at lower, rather than higher velocities in the usual range.

An increase in the strop length d_1 (in the range 25 - 100 ft) appears to have a small reducing effect on the damping factor. This effect is more prominent at larger values of the lifting bar length, i.e. 9.0 ft. Also, an increase in the strop length d_3 has a similar effect on the stability of the system, although this is not quite so definite for the longer lifting bars.

Figure 13.32 gives an illustration of the non-dimensional frequency parameter, s_1, plotted against forward velocity for the typical configuration of $2a = 9.0$ ft, $m_2 g = 5$ lbs, $\alpha_2 = 0.25^\circ$, $d_1 = d_3 = 50$ ft. On comparison with the curves (fig. 13.9 and 13.21) for the corresponding lateral mode of the single and twin strop arrangements, the frequency range given in fig. 13.32 is obviously greater than that for the single strop arrangement, and, rather surprisingly, less than that for the twin strop arrangement.

FIGURE 13.33

PLOT OF RELATIVE DERIVATIVE IMPORTANCE AGAINST FORWARD VELOCITY

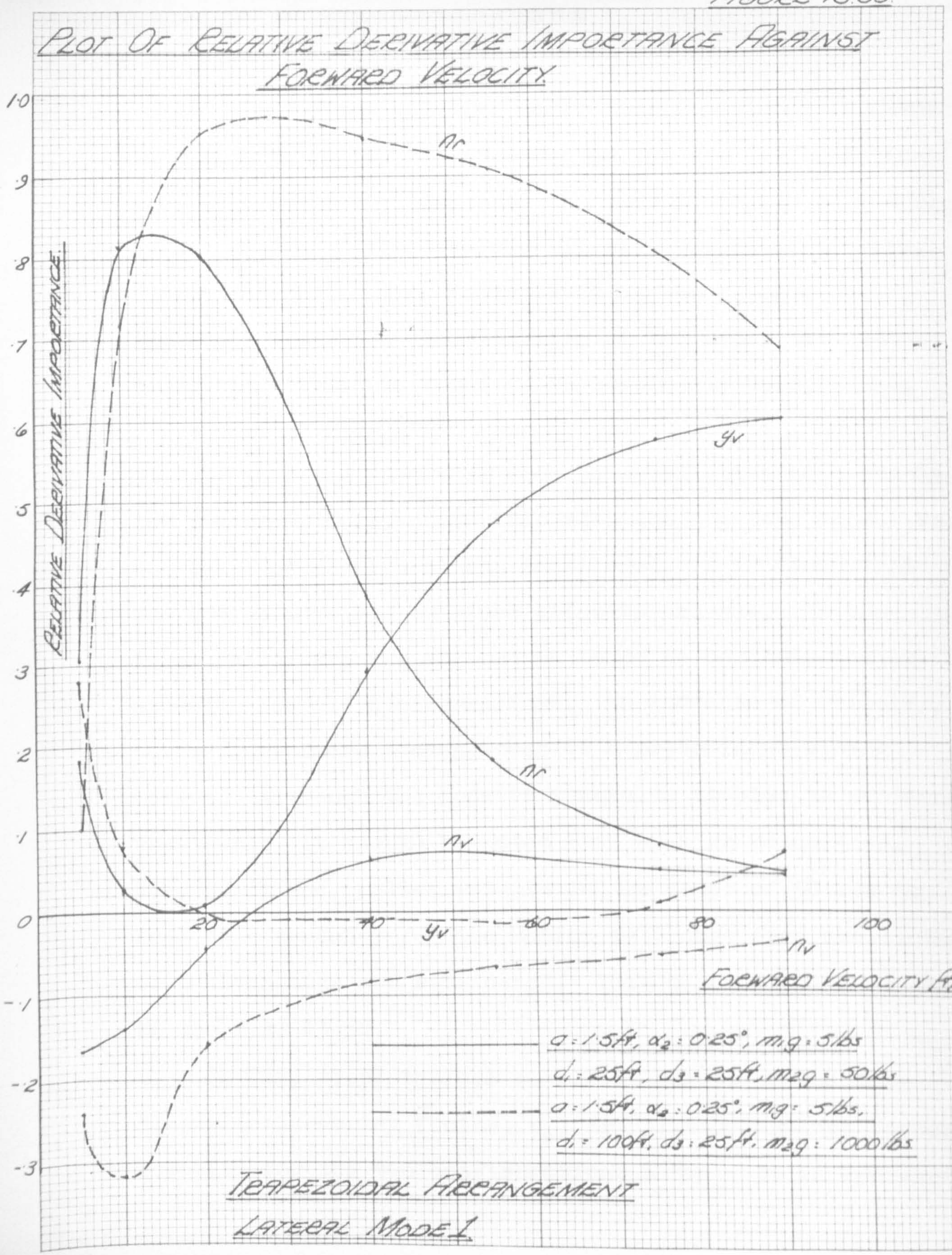

TRAPEZOIDAL ARRANGEMENT

LATERAL MODE I

A plot of the relative derivative importance is given for the mode in fig. 13.33. Curves for two configurations are given and both illustrate the importance (as expected) of the damping derivative n_r. It is interesting to note, also, that the damping derivatives n_v and y_v have an important effect on the stability of the mode. All other derivative terms are found to be completely unimportant.

13.3.2b Mode 2

It is found that this mode of oscillation is a stable low frequency mode, comparable with the previous mode. For the range of configurations considered, it is found that the motion involves combined sideslip and yaw. In the lower velocity range the motion tends to be dominated by sideslip for all configurations. An increase of velocity, however, produces a changeover to a predominant yawing motion. Although the mode is generally stable, as mentioned previously, it should be noted that at high velocities, i.e. 90 ft/sec, pallet weights in the order of 50 lbs do lead to a tendency for the motion to change from oscillatory to a divergence and subsidence. This change is illustrated in the fig. 13.34.

In fig. 13.34 typical stability curves of the non-dimensional damping factor, r_a, are plotted against forward velocity for the two configurations shown. It is apparent

FIGURE 13.34.

PLOT OF DAMPING FACTOR AGAINST FORWARD VELOCITY.

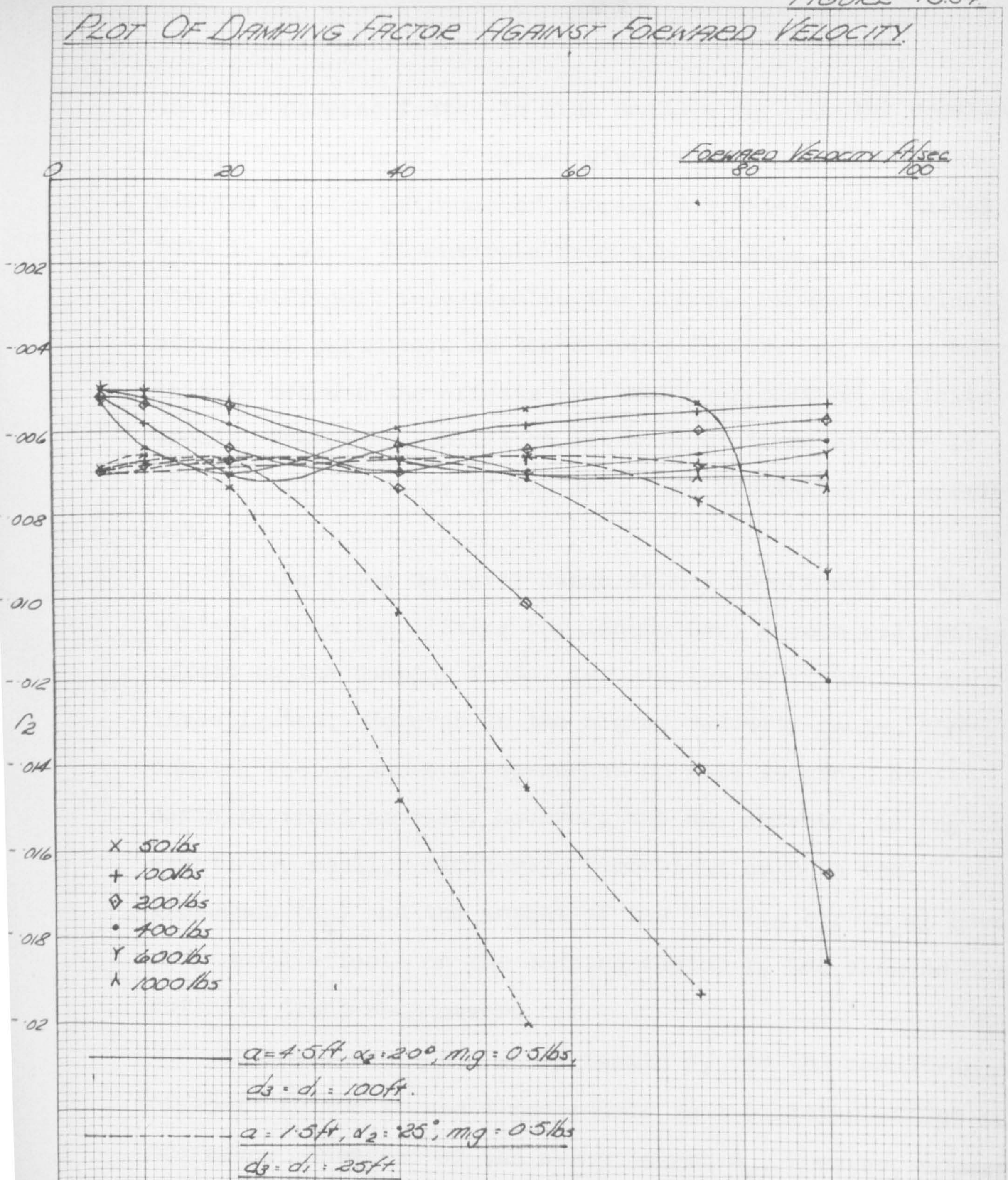

TRAPEZOIDAL ARRANGEMENT

LATERAL MODE 2.

that the damping factor is even smaller than in the previous mode. The two sets of curves given show the difference between the two extremes of damping for this mode. Whilst this is easy to demonstrate from the results, it has proved rather difficult to determine the effects of the individual structural parameters on the damping factor. As shown below, this is because the effects are small and show no definite trend. Therefore, whilst an estimate of these effects is given, a closer study of the mode must eventually be carried out.

In the lower velocity range it has been found that variations in the lifting bar length (2a) have a negligible effect on the damping factor for all the configurations investigated. However in the higher velocity range, the damping factor shows a dependence on this length. No definite trend emerges, however, but the effects, in any event, are small. Similarly, variations in both the incidence (α_2) and the weight of the lifting bar ($m_1 g$) have very small effects on the damping factor r_2 and show no definite trend whatsoever.

An increase in the strop length d_1 for the usual range of 25 ft to 100 ft has a moderately destabilising effect on the mode. Increase of the strop length d_3, however, appears to have a small, indefinite, effect on the damping factor r_2.

FIGURE 13.35.

PLOT OF FREQUENCY PARAMETER AGAINST FORWARD VELOCITY.

TRAPEZOIDAL ARRANGEMENT

LATERAL MODE 2.

$a = 4.5$ ft, $m_g = 5$ lbs, $d_1 = 50$ ft,
$d_3 = 50$ ft, $\alpha_2 = 0.25°$
For Values of Pallet Weight Indicated.

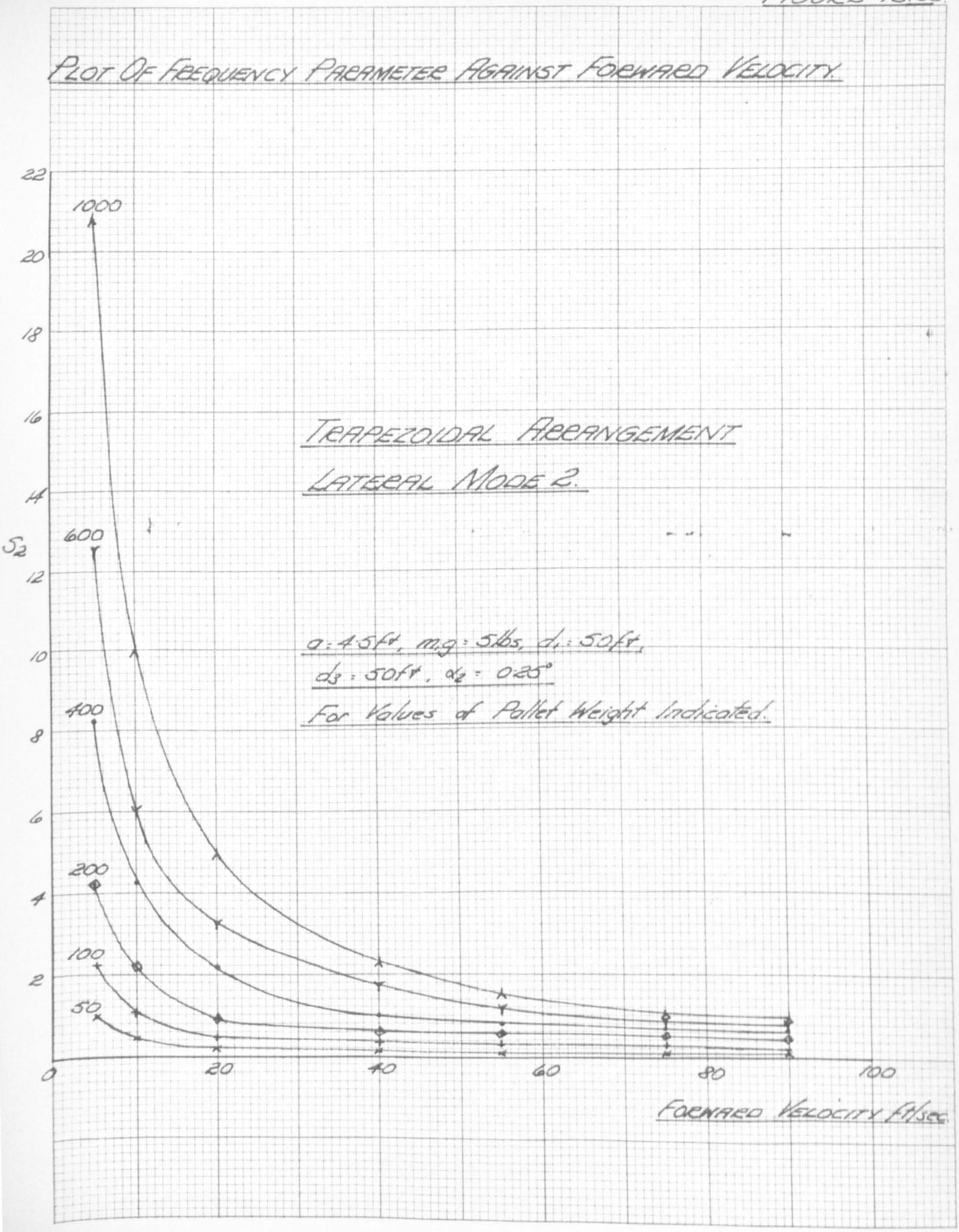

FIGURE 13.36

PLOT OF RELATIVE DERIVATIVE IMPORTANCE AGAINST FORWARD VELOCITY

——— a = 1.5 ft, m_1g = 5 lbs, d_1 = 25 ft, d_3 = 25 ft, m_2g = 50 lbs, α_2 = 25°

- - - - - - a = 4.5 ft, m_1g = 5 lbs, d_1 = 100 ft, d_3 = 100 ft, m_2g = 50 lbs, α_2 = 2°

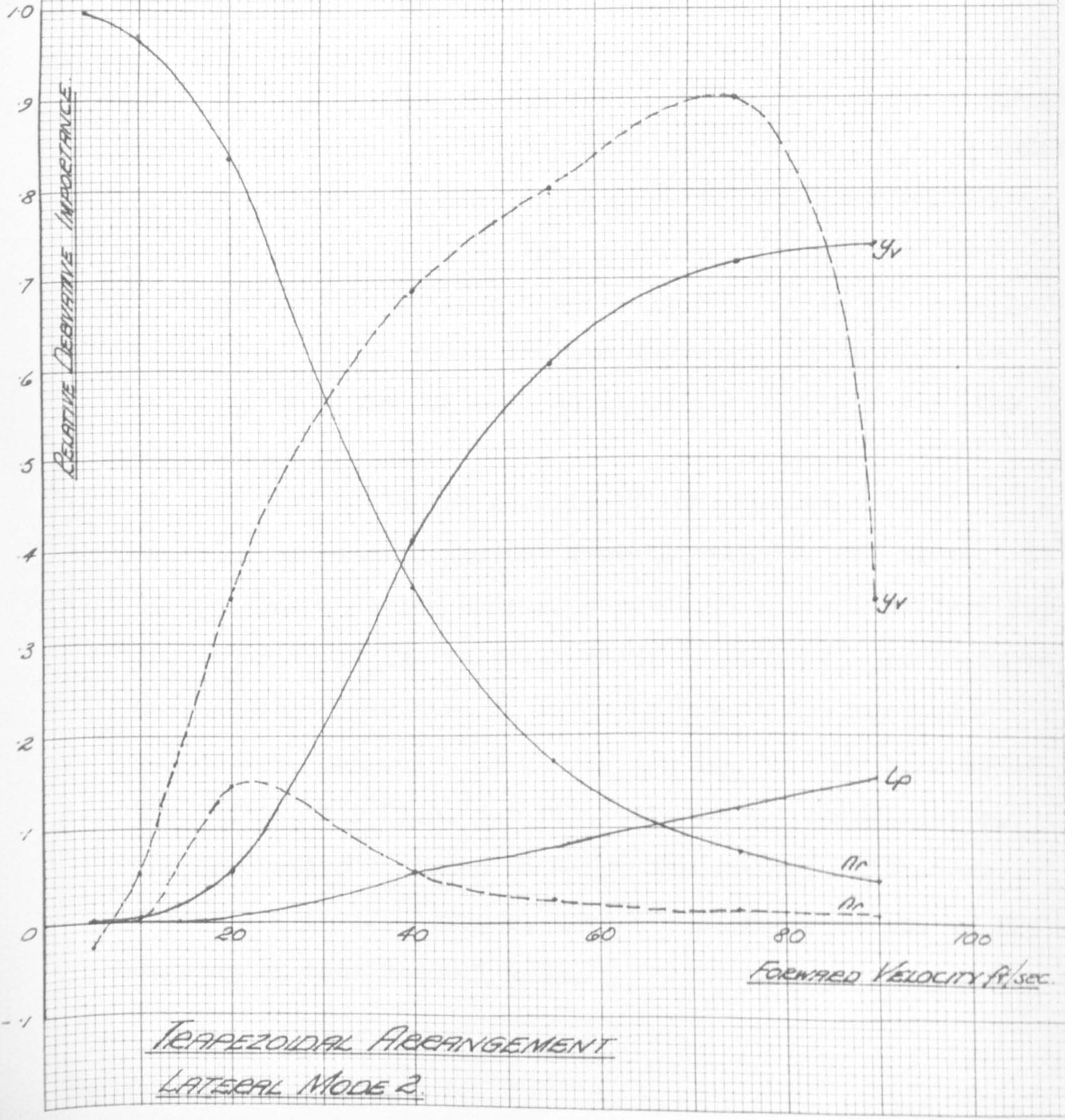

TRAPEZOIDAL ARRANGEMENT

LATERAL MODE 2.

Finally, the variations in the pallet weight between 50 lbs and 1000 lbs are shown in fig. 13.34 to exhibit no definite trend, although their effect on the damping can be quite strong for certain configurations.

As usual, a plot of the non-dimensional frequency parameter s_2 against forward velocity is given in fig. 13.35 for the configuration 2a = 9.0 ft, $m_1 g$ = 5 lbs, $d_1 = d_3$ = 50 ft and $\alpha_2 = 0.25^\circ$. On comparison with the two longitudinal modes of the trapezoidal configuration, it is found that the frequency range is similar to the longitudinal mode 1. Unless one of the modes becomes unstable, however, it is unlikely that the one mode could couple unstably with the other.

In fig. 13.36 the results of the most important derivatives plotted against forward velocity are given. It is apparent that the damping derivative y_v is important for the majority of the velocity range considered. Furthermore, the damping derivative n_r is important at low forward velocities, but only, as shown, for the smaller lengths of the lifting bar (i.e. 3.0 ft). Also, very occasionally, the derivative l_p takes on minor importance. All other derivative terms, however, have a negligible effect on the damping of this lateral mode.

FIGURE 13.37.

PLOT OF DAMPING FACTOR AGAINST FORWARD VELOCITY

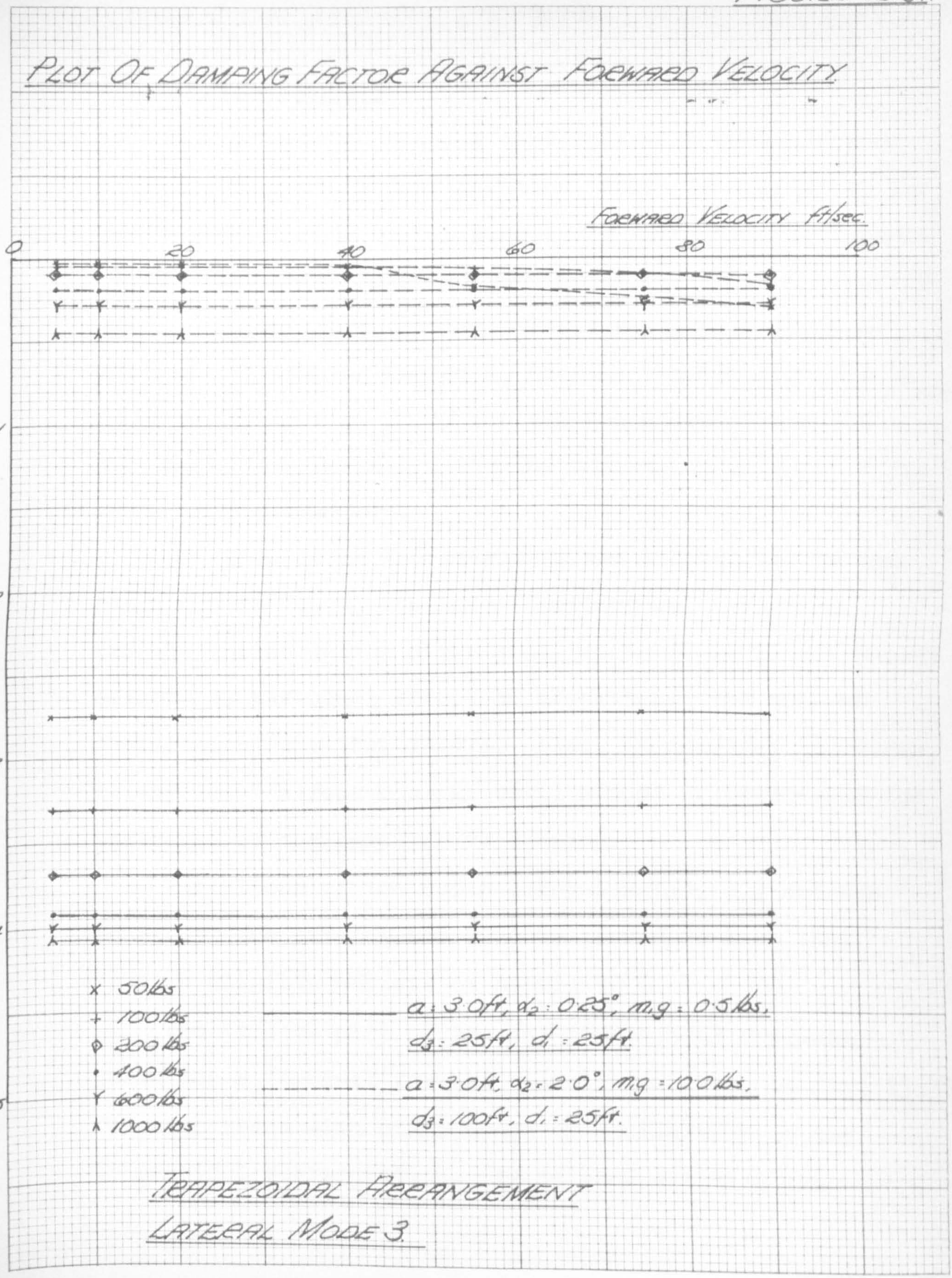

TRAPEZOIDAL ARRANGEMENT

LATERAL MODE 3.

13.3.2c Mode 3

A short period mode of oscillation is obtained here for the trapezoidal configuration, which is similar to the corresponding mode of the single and twin strop configurations. The mode therefore remains stable for the range of configurations investigated. The variation in the non-dimensional damping factor r_3 against forward velocity is illustrated in fig. 13.37 for the two extreme cases of damping; thus demonstrating the importance of some of the structural parameters.

An increase in the weight of the lifting bar in the range 0.5 lbs to 10 lbs has a distinct destabilising effect, whilst on the other hand, an increase in the pallet weight has the usual effect of stabilising the mode of oscillation (see fig. 13.37). Also, an increase in length of the lower strops has the usual effect of decreasing the influence of the aerodynamic damping.

Variations of the upper strop lengths, d_1, and the length of the lifting bar (2a) are found to have their usual negligible effects on stability.

The typical plot of the non-dimensional frequency parameter s_3 against forward velocity is given in fig. 13.38 for comparison with other modes of oscillation of the trapezoidal configuration. It is apparent that the

FIGURE 13.38.

PLOT OF FREQUENCY PARAMETER AGAINST FORWARD VELOCITY

TRAPEZOIDAL ARRANGEMENT

LATERAL MODE 3.

a: 4.5ft. $m.g$: 5lbs, α_2: 0.25°

d_1 = 50ft, d_3 = 50ft.

For Values of Pallet Weight Indicated.

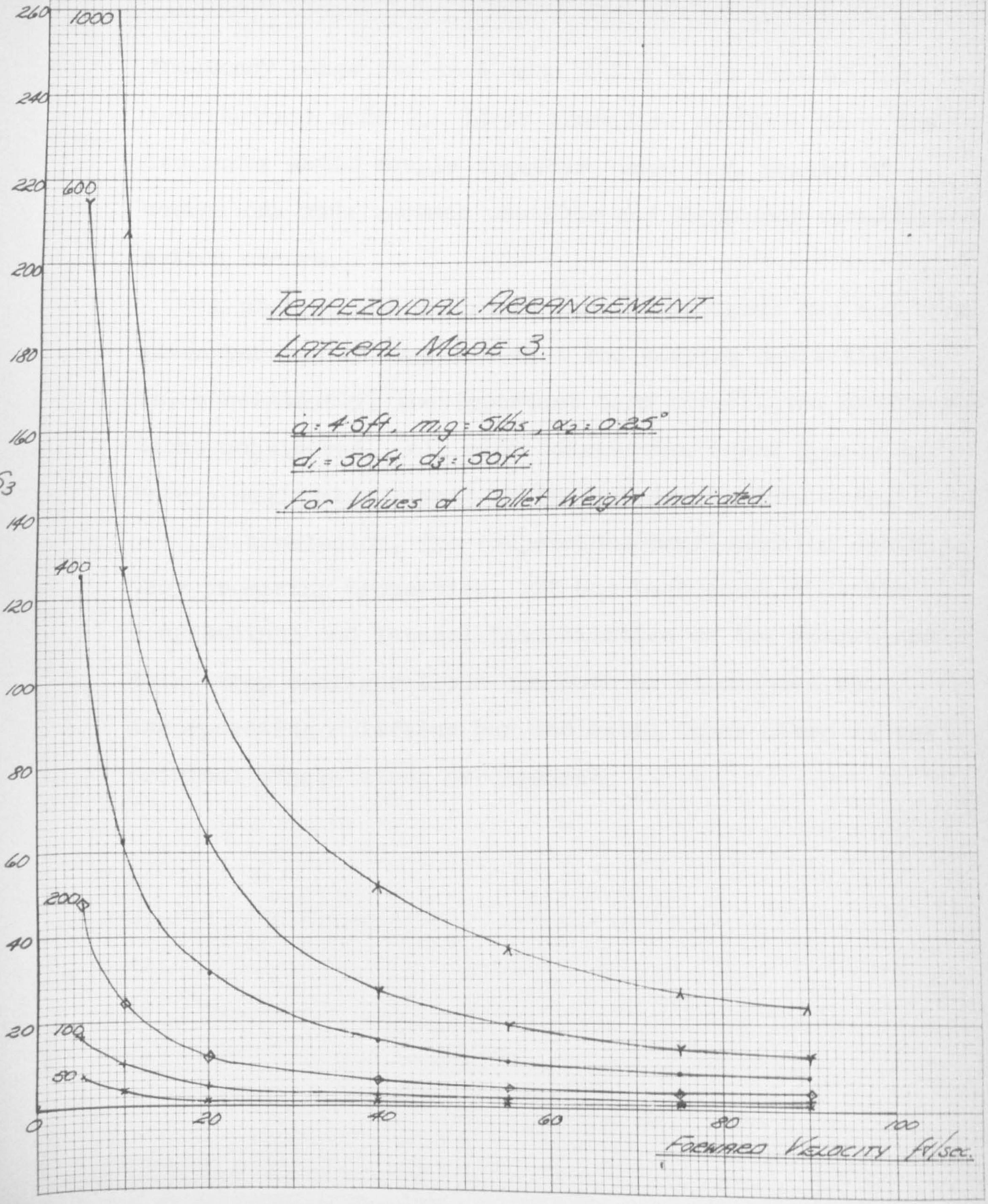

frequency range for this mode falls below that of the longitudinal mode 2. It is therefore unlikely that the two modes would couple together unstably, unless of course one mode becomes unstable and frequency demultiplication occurs.

A plot of the important derivative terms has not been given because it is found that the damping derivative l_p is, consistently, the important term for all the configurations considered. All other derivative terms appear to have a negligible effect on the damping in this mode.

In conclusion, the trapezoidal configuration exhibits very promising properties. It has been shown that the longitudinal and lateral instabilities of the single and twin strop configurations can both be eliminated by incorporating a lifting bar and extra upper strop in the original single strop arrangement.

CHAPTER 14

CONCLUSIONS

By use of the linearised equations of motion and the resulting stability equations, it has been possible to investigate the nature and stability of the motions of a pallet, suspended via various strop configurations, beneath a moving helicopter.

From the investigations of the single strop configuration, it was concluded that, even for small disturbances, both longitudinal and lateral instabilities can be encountered for a practical range of forward velocities. Two modes (one longitudinal and one lateral) were found to be unstable over the complete range of speeds investigated - the remaining modes all being stable. It was not surprising, therefore, that the full scale pallet (suspended by a single strop arrangement beneath a helicopter) became unstable, in practice, at all reasonable forward speeds. Although the frequency ranges of the unstable longitudinal and lateral modes were found to be dissimilar, it is possible that non-linear coupling of the two modes occurred to give the combined instability exhibited.

The severe longitudinal instability of the pallet occurred for forward speeds of the helicopter greater than 24 ft/sec (depending on the weight of the pallet) and

appeared to be due to insufficient aerodynamic damping in pitch on the pallet (i.e. a deficiency of the m_q damping derivative). Whilst it might be difficult to change effectively the damping by alteration of the aspect ratio of the pallet, it is possible that the addition of a tail section or some equivalent aerodynamic surface could increase the aerodynamic damping in pitch sufficiently to obviate the instability.

The severe lateral instability was found to occur for forward speeds greater than 18 ft/sec (depending on the pallet weight) and the corresponding mode was found to consist of a sideslip-yawing motion of the complete arrangement. It was apparent, therefore, that either (a) a constraint should be imposed on the sideslip or yawing displacement of the pallet, or (b) the aerodynamic damping must be improved for such yawing - sideslip displacements - for example, by provision of a 'fin'.

Throughout the theoretical investigations, the aim was to keep the profile of the pallet and the geometry of the strop arrangement as simple as possible. Therefore, before pursuing more complicated and less practical arrangements, it was necessary to investigate the twin strop and trapezoidal configurations.

Adoption of the twin strop configuration to support the pallet obviously had no effect on the longitudinal motions. However, a vast improvement was made on the stability of the severely unstable lateral mode encountered with the single strop configuration. In fact, one result of providing a twin strop configuration was to confer complete stability on the combined yawing - sideslip mode for all practical forward speeds. One other result, unfortunately, was to reduce the stable range of the yawing mode, although the instabilities were found to occur when the length of the lifting bar was of the same order as the chord length of the pallet. Clearly, further investigations were required in order to determine the unstable velocity range for this case.

The trapezoidal configuration had the advantage over the single and twin strop configurations of improving considerably the stability of the unstable longitudinal mode of oscillation of the pallet. Such was the extent of the improvement, that for certain values of the structural parameters (see chapter 13) the configuration was longitudinally stable for forward speeds between 0 and 100 ft/sec. The structural constraint imposed a limitation on the 'steady state' incidence (α_s) and pitching displacement of the pallet and, as a result, the aerodynamic damping was sufficient to promote stability.

In a similar manner, it was found that the trapezoidal configuration conferred complete stability on the three lateral modes of oscillation for all practical forward speeds of the helicopter, and for all the various configurations considered. Neither of the three modes showed any tendency to become unstable.

Whilst the longitudinal and lateral studies on the trapezoidal configuration have given encouraging results for the limited range of investigations, it is apparent that more studies are necessary to gain a fuller understanding on the stability of the configuration (see chapter 13).

If for a practical reason, the trapezoidal configuration proves to be an unsuitable means of suspending loads beneath a helicopter (e.g. because the longitudinal stability of the helicopter plus pallet is inadequate) then the twin strop arrangement could quite possibly be adopted. A droque chute could then be used as a possible means of conferring stability on the troublesome longitudinal mode. Clearly, further investigations would be required to confirm this.

The aerodynamic derivative data obtained by the static and dynamic wind tunnel experiments have proved to be satisfactory for use in the stability investigations and

have contributed to the existing aerodynamic derivative data for flat plates at large angles of incidence and yaw. It is unfortunate, however, that the few rotary damping derivatives (obtained by the 'lifting line' theory) could not have been determined by the more accurate experimental methods. However, this would have been very time consuming in the limited time available.

From the wind tunnel dynamic tests it is interesting to note the dependence of the damping derivative m_q on the mean incidence of the pallet and especially the transition to the unexpected values of negative damping. Further investigations are clearly warranted here. Similarly, the effect of the wind tunnel interference on the m_q derivative requires further study, as this is a relatively unexplored field of investigation.

These initial studies on a pallet suspended beneath a helicopter have shown the importance of the theoretical approach when ad hoc full scale tests have failed to produce satisfactory results. With further investigations into the trapezoidal configuration, it would appear to be possible to obtain a stable form of external transportation via a helicopter, for even a larger range of forward speeds than those investigated. If a more stable arrangement than the trapezoidal configuration were required, it is possible

that investigations into a triple strop configuration, i.e. a combination of the twin strop and trapezoidal arrangement would give promising results. Also, in a similar manner, further theoretical studies could be made on the suspension of bulkier loads (provided derivative data were available) which have shown (see ref. 14.1 and 14.2) certain instabilities in full scale tests.

CHAPTER 15

SUGGESTED FURTHER RESEARCH

The work described herein forms a significant part of a large field of investigation which has, until quite recently, remained virtually unexplored (see chapter 1). As a result a considerable amount of research can be carried out, which could contribute to the encouraging results already obtained with the trapezoidal configuration. An elucidation of some of the more important extensions of the present work are now given:-

From an examination of the results obtained for the trapezoidal configuration studies (see chapter 13), it is apparent that the length and weight of the lifting bar have a most important effect on the overall stability of the configuration (especially in the short period longitudinal mode). It is therefore desirable that a more thorough investigation into the significance of these two parameters be undertaken. Furthermore, a wider range of 'steady state' incidences of the pallet should be investigated to confirm whether an improvement on the present results can be obtained.

Stability investigations on the trapezoidal configuration have so far taken the form of ascribing fixed values to the strop lengths d_1 and d_3, the pallet incidence, α_2

and the weights of the pallet and lifting bar for chosen values of forward velocity. A simple computation has then given the required strop length d_3 (see chapter 6). Now that a completely stable range of results has been obtained, it will be more practical to fix the structural parameters (for the maximum apparent stability), allow the incidence, α_2 to vary with forward velocity and confirm the stability of the fixed configuration over a suitable range of velocity.

For reasons given in chapter 1, attention here has been focused on a rectangular pallet of aspect ratio 2. However, it might be conceivable that a more stable trapezoidal configuration could exist with a pallet of different aspect ratio. This would, of course, involve further experimental measurements of the stiffness and damping derivatives.

As already mentioned in the previous chapter, it is possible that for certain practical reasons, the trapezoidal configuration might prove unsatisfactory. An arrangement in the form of a triple strop configuration could well prove a good alternative form of suspension (owing to a greater stiffness in roll). This is a compromise between the twin strop and trapezoidal configurations and would consist of the pallet suspended by the

usual four lower strops - these strops being attached to a cruciform lifting bar. (The two front strops would be attached at one point on the main beam of the bar, whereas the two rear strops would be attached on either end of the cross beam of the bar.) By means of three upper strops, the configuration can then be suspended from three attachment points on the helicopter. Unfortunately, time did not allow a theoretical study of this configuration.

The importance of the rotor downwash effects on the suspended pallet is outlined in chapter 8. It is apparent that the downwash impingements on the pallet would affect the aerodynamic forces acting on the pallet. Therefore, with a fuller understanding of the rotor downwash effects at forward velocities of the helicopter, it might be possible to incorporate a representation of these into the equations of motion. Now that an intrinsically stable configuration has been found for uniform conditions, this is clearly the next most important field of investigation.

With the aid of the 'derivative importance' technique it has been possible to ascertain the important derivatives for a particular mode of oscillation. In the present work, however, the derivatives were assumed to be linearly dependent on displacement and velocity. Therefore, it could well prove useful to introduce certain non-linearities

(pertaining to the important derivatives) into the theoretical investigations and analyse the effects, maybe on a large analogue computer.

In the present work it has been assumed in all the studies, that the strops are of a rigid form and massless. Further extensions of these initial assumptions should be made so that the effects on stability could be observed, when say the mass of the strops is introduced into the analysis. The hypothetical configuration on which the theory is based would then approximate more closely to the actual physical situation.

Finally, now that a stable configuration has been obtained, it will be necessary to evaluate the combined stability of the helicopter and pallet, although it would involve a considerable amount of additional theory. However, it may be feasible to 'patch' the equations on a large analogue computer.

BIBLIOGRAPHY

1.1	L. Bairstow, R. Jones and E.F. Rolf.	The Stability of Kite Balloons : Mathematical Investigation. A.R.C. R. & M. 208 (1915)
1.2	A.R. McLeod	On the Action of Wind on Flexible Cables, with Applications to Cables Towed below Aeroplanes and Balloon Cables. A.R.C. R. & M. 554 (1918)
1.3	H. Glauert	The Stability of a Body Towed by a Light Wire. A.R.C. R. & M. 1312 (1930)
1.4	H. Glauert	The Form of a Heavy Flexible Cable used for Towing a Heavy Body below an Aeroplane. A.R.C. R. & M. 1592 (1934)
1.5	L.W. Bryant, W.S. Brown and N.E. Sweeting.	Collected Researches on the Stability of Kites and Towed Gliders. A.R.C. R. & M. 2303 (1942)
1.6	M. Pitkin and M.O. McKinney, Jr.	Theoretical Analysis of the Lateral Stability of a Glider Towed by Twin Parallel Towlines. N.A.C.A. A.R.R.3K17 (WRL-372), (1943)
1.7	M. Pitkin and M.O. McKinney, Jr.	Flight Tests of a Glider Model Towed by Twin Parallel Towlines. N.A.C.A. R.B.3030 (WRL-498), (1943)
1.8	B. Etkin and J.C. Machworth.	Aerodynamic Instability of Non-Lifting Bodies Towed Beneath an Aircraft. U.T.I.A. T.N. 65 (1963)

1.9 W.P. Reid — Stability of a Towed Body. U.S. N.O.L. T.R. 64 - 116 (1964)

1.10 E.H. Law — The Longitudinal Equations of Motion of an Airborne Towed Vehicle Incorporating an Approximation of Cable Drag and Inertia Effects. Princetown University Aero. Eng. Report 687 (1964)

1.11 Superintendent of R.A.F. — The Use of a Fin Surface to Stabilise a Weight Towed from an Aeroplane. A.R.C. R. & M. 184 (1914)

. . . . . .

2.1 A.W. Babister — Aircraft Stability and Control. Pergamon Press (1961)

2.2 R.A. Frazer, W.J. Duncan and A.R. Collar. — Elementary Matrices. Cambridge University Press (1960)

. . . . . .

3.1 S. Neumark — Equilibrium Configurations of Flying Cables of Captive Balloons and Cable Derivatives for Stability Calculations. A.R.C. R. & M. 3333 (1961)

3.2 C.H. Bryan — Stability in Aviation, an Introduction to Dynamic Stability as Applied to the Motion of an Aeroplane. Macmillan Press (1911)

3.3 B. Etkin — Dynamics of Flight. J. Wiley and Sons (1959)

3.4 A.R. Collar — On the Stability of Accelerated Motion : Some Thoughts on Linear Differential Equations with Variable Coefficients. Aero. Quarterly, Vol.8. (1957)

6.1	P.C. Parks	Analytical Methods for Investigating Stability - Linear and Non-Linear Systems. Inst. of Mech.Eng., Vol.178 - Part 3M Proceedings 1963 - 64.
6.2	D.L. Woodcock	The Rates of Change of the Eigen-values of a Lambda Matrix and their use in Flutter Investigations. Journal Royal Aero.Society, Vol.70 (1966)
6.3	W.H. Wittrick	Rates of Change of Eigenvalues with Reference to Buckling and Vibration Problems. Journal Royal Aero.Society, Vol.66 (1962)
6.4	C.G.J. Jacobi	Über ein leichtes Verfahren die in der Theorie der Säcularstörungen Vorkommenden Gleichungen numerisch aufzulösen. Crelle's Journal, Vol.30 (1846)
6.5	W. Hahn	Theory and Application of Liapunov's Direct Method. Prentice-Hall (1963)

. . . . . .

7.1	H.H.B.M. Thomas	Estimation of Stability Derivatives (State of the Art). R.A.E. Tech.Note No. Aero.2776 (1961)
7.2	W.E.A. Acum	Comparison of Theory and Experiment for Oscillating Wings. A.R.C. C.P. 681 (1962)
7.3	H. Ashley, G. Zartarian and H.C. Neilson.	Investigation of certain Unsteady Aerodynamic Effects in Longitudinal Dynamic Stability. U.S.A.F. Tech. Report 5986 (1951)

7.4	S. Neumark	Two Dimensional Theory of Oscillating Aerofoils, with Application to Stability Derivatives. (Unpublished)
7.5	A.S. Halliday, L.W. Bryant and C.H. Burge	The Experimental Determination of Pitching Moment of an Aeroplane due to Rotation in Pitch. A.R.C. R. & M. 1556 (1933)
7.6	H. Glauert	The Lift and Pitching Moment of an Aerofoil due to a Uniform Angular Velocity of Pitch. A.R.C. R. & M. 1216 (1928)
7.7	C. Scruton, L. Woodgate and A.J. Alexander	Measurements of the Aerodynamic Derivatives for Swept Wings of Low Aspect Ratio describing Pitch and Plunge Oscillations in Incompressible Flow. A.R.C. R. & M. 2925 (1957)
7.8	J.P. Campbell, J.L. Johnson, Jr. and D.E. Hewes	Low-Speed Study of the Effect of Frequency on the Stability Derivatives of Wings Oscillating in Yaw with Particular Reference to High Angle-of-Attack Conditions. N.A.C.A. R.M.L55H05 (1955)
7.9	L.R. Fisher	Experimental Determination of Effects of Frequency and Amplitude on the Lateral Stability Derivatives for a Delta, Swept and Unswept Wing Oscillating in Yaw. N.A.C.A. Report 1357 (1958)
7.10	J.L. Johnson, Jr.	Low-Speed Measurements of Static Stability, Damping in Yaw, and Damping in Roll of a Delta, Swept and Unswept Wing for Angles of Attack from 0° to 90°. N.A.C.A. R.M. L56B01 (1955)

7.11 M. Lofts — Note on the Calculation of the Wing Contribution to the Lateral Stability Derivatives l_p, n_p, l_r, n_r with special reference to Rectangular and Elliptical Wings. R.A.E. Report No. Aero 2189 (1947)

7.12 C.W. Clenshaw and J.G. Hayes — Curve and Surface Fitting. Jour. Inst. of Maths and its Applications. Vol. 1. (1965)

. . . . . .

8.1 W. Castles, Jr. and J.H. de Leeuw. — The Normal Component of the Induced Velocity in the Vicinity of a Lifting Rotor and some Examples of its Application. N.A.C.A. T.N. 2912 (1953)

8.2 P.L. Michel — The Sikorsky Crane Helicopter. Jour. Royal Aero. Soc., Vol. 66 (1962)

8.3 E.A. Fradenburgh — Flow Field Measurement of a Hovering Rotor near the Ground. American Helicopter Society Western Forum (1958)

8.4 R.G. Austin — Helicopter Performance (Unpublished)

. . . . . .

9.1 H. Winter — Flow Phenomena on Plates and Aerofoils of Short Span. N.A.C.A. T.M. 798 (1936)

9.2 V.N. Scholz — Kraft-und Druckverteilungsmessungen an Tragflächenkleiner Streckung. Inst. of Mechs. Braunschweig (1949)

9.3 R.C. Pankhurst — Orientation Angles and Axis Transformations in Wind Tunnel Testing. N.P.L. Aero. Note 1003 (1962)

9.4	P. Rebuffet	Some Strain Gauge Balances used in French Wind Tunnels. (English Translation from French). AGARD Report 6T (1956)
9.5	R.M. Hausen	Evaluation and Calibration of Wire Strain Gauge Wind Tunnel Balances under Load. AGARD Report 13 (1956)
9.6	T.A. Cook	A Note of the Calibration of Strain Gauge Balances for Wind Tunnel Models. R.A.E. T.N. Aero 2631 (1959)
9.7	R.C. Pankhurst and D.W. Holder	Wind Tunnel Technique. Pitman Press (1952)
9.8	A. Pope	Wind Tunnel Testing. Pitman Publishers (1958)
9.9	J.E. Adamson	An Experimental Investigation of Wind Tunnel Interference in the R.A.E. 5 ft. Open-Jet Circular Tunnel. A.R.C. R. & M. 1897 (1941)

. . . . . .

10.1	S. Neumark and A.W. Thorpe	Theoretical Requirements of Tunnel Experiments for Determining Stability Derivatives in Oscillatory Longitudinal Disturbances. A.R.C. R. & M. 2903 (1950)
10.2	H. Glauert	The Force and Moment on an Oscillating Aerofoil. A.R.C. R. & M. 1242 (1929)
10.3	J.B. Bratt	Wind Tunnel Techniques for the Measurement of Oscillatory Derivatives. A.R.C. R. & M. 3319 (1960)

10.4	S.C. Scruton	Some Experimental Determinations of the Apparent Additional Mass Effect for an Aerofoil and for a Flat Plate. A.R.C. R. & M. 1931 (1941)
10.5	J.B. Bratt and K.C. Wight	The Effect of Mean Incidence, Amplitude of Oscillation, Profile and Aspect Ratio on Pitching Moment Derivatives. A.R.C. R. & M. 2064 (1945)
10.6	W.J. Duncan	Control and Stability of Aircraft. Cambridge University Press (1959)
10.7	W.G. Molyneux	Measurement of the Aerodynamic Forces on Oscillating Aerofoils. AGARD Report 35.
10.8	H. Glauert	The Lift and Pitching Moment of an Aerofoil due to a Uniform Angular Velocity of Pitch. A.R.C. R. & M. 1216 (1928)
10.9	D.L. Birdsall	The Effect of Structural Non-Linearities on Flutter. Ph.D. Thesis, University of Bristol (1965)
10.10	P. Hunt	Ph.D. Thesis, University of Bristol (1968)
10.11	W.G. Molyneux	Wind Tunnel Interference in Dynamic Measurement. R.A.E. Tech. Report 64069.
		. . . . .
11.1	R.G. Austin and J. Flower	Investigation of the Stability of Flat-Plate Loads using a Wind Tunnel Model (Unpublished) 1963.

11.2	S.E. Kitchen and S.D. Thomas	The Aerodynamic Behaviour of Flat-Plate Type Loads Suspended beneath a Helicopter as Determined by Model Tests. University of Bristol B.Sc. Thesis (1963)
12.1	E.L. Houghton and A.E. Brock	Aerodynamics for Engineering Students Arnold Publishers (1960)
12.2	W.D. Wolhart and D.F. Thomas, Jr.	Static Longitudinal and Lateral Stability Characteristics at Low Speed of Unswept-Midwing Models having Wings with an Aspect Ratio of 2, 4 or 6 N.A.C.A. T.N. 3649 (1956)
12.3	S. Hoerner	Forces and Moments on a Yawed Aerofoil N.A.C.A. T.M. 906 (1939)
14.1	R.G. Austin and J. Nokes	Stability of Rectangular Box-Shaped Loads Suspended Beneath a Helicopter, (Unpublished) 1961.
14.2	A. Schlesinger	The Towing Behaviour of a near-hemispherical Shell as Determined by Tests on a Model, (Unpublished) 1960.

APPENDIX I

A TYPICAL STABILITY INVESTIGATION

As an aid to the understanding of the stability investigations discussed in chapter 6, it is worthwhile to consider a typical solution for, say, the longitudinal motions of the single strop arrangement.

Take, for example, the following system

$m_1 g = 0.5$ lbs, $m_2 g = 200$ lbs, $d_1 = 25$ ft., $d_2 = 25$ ft. and assume a pallet incidence of $0{\cdot}25°$. For this incidence the following data are obtained from predetermined polynomial equations:-

$x_u = -{\cdot}048$, $z_u = -{\cdot}0123$, $m_u = {\cdot}014$, $x_w = +{\cdot}037$, $z_w = -1{\cdot}63$, $m_w = 1{\cdot}36$, $x_q = 0$, $z_q = -1{\cdot}17$, $m_q = -{\cdot}117$, $x_\theta = +{\cdot}087$, $z_\theta = -3{\cdot}2$, $m_\theta = 2{\cdot}72$, $C_D = {\cdot}048$, $C_L = -{\cdot}0123$, $C_m = {\cdot}014$ and $e = 0{\cdot}27$. In addition $c = 6$ ft., $S = 6 \times 12 = 72$ ft^2, $k_1 = 1{\cdot}732$ ft. and $\rho = 23{\cdot}8$ slugs/ft.^{3}

Now the forward velocity V can be determined from eqn. 6.5.

Hence

$$V = \sqrt{\frac{2 \times 200 \times 25 \times 10^4}{23{\cdot}8 \times 72\left(\frac{{\cdot}048 \times 25 + {\cdot}0123 \times {\cdot}27 \times 6}{\tan(0{\cdot}25°)} - 25 \times {\cdot}0123 + {\cdot}048 \times {\cdot}27 \times 6\right)}}$$

$$= 14{\cdot}49 \text{ ft/sec.}$$

Also, from eqn. 6.6

$$\alpha_1 = \tan^{-1}\left(\frac{\cdot 048}{\frac{2(0.5 + 200) \times 10^4}{23.8 \times 14.49^2 \times 72} + \cdot 0123}\right) = 0.245^\circ$$

and from chapter 3.0 the relative density parameter and Froude number are thus

$$\mu_1 = \frac{200 \times 10^4}{32.2 \times 23.8 \times 72 \times 25} = 1.45 \quad \text{and} \quad F = \frac{14.49^2}{25 \times 32.2} = 0.2574$$

With the above values substituted into the longitudinal non-dimensional equations (see chapter 4.0) it can be shown that

$\underline{A}s_{11} = 0.6914$, $\underline{A}s_{12} = 0.6897$, $\underline{A}s_{21} = 0.6897$, $\underline{A}s_{22} = 0.693$

$\underline{B}s_{11} = 0.0331$, $\underline{B}s_{12} = 0.0297$, $\underline{B}s_{21} = 0.0298$, $\underline{B}s_{22} = 0.0297$

$\underline{C}s_{11} = 5.654$, $\underline{C}s_{12} = 0.0502$, $\underline{C}s_{21} = 0$, $\underline{C}s_{22} = 5.3636$.

Now the expansion of the determinant $|S_S|$ gives the characteristic equation $p_4\lambda_S^4 + p_3\lambda_S^3 + p_2\lambda_S^2 + p_1\lambda_S + p_o = 0$, whereupon using $\underline{A}s_{11} \ldots\ldots \underline{C}s_{22}$:-

$$p_4 = \underline{A}s_{11}\,\underline{A}s_{22} - \underline{A}s_{12}\,\underline{A}s_{21} = 0.00348$$

$$p_3 = \underline{A}s_{11}\,\underline{B}s_{22} + \underline{A}s_{22}\,\underline{B}s_{11} - \underline{A}s_{12}\,\underline{B}s_{21} - \underline{A}s_{21}\,\underline{B}s_{12} = 0.00181$$

$$p_2 = \underline{A}s_{11}\,\underline{C}s_{22} + \underline{A}s_{22}\,\underline{C}s_{11} + \underline{A}s_{12}\,\underline{C}s_{21} - \underline{A}s_{21}\,\underline{C}s_{12} + \underline{B}s_{11}\,\underline{B}s_{22} - \underline{B}s_{12}\,\underline{B}s_{21} = 7.491$$

$$p_1 = \underline{B}s_{11}\,\underline{C}s_{22} + \underline{B}s_{22}\,\underline{C}s_{11} = 0.3342$$

$$p_o = \underline{C}s_{11}\,\underline{C}s_{22} - \underline{C}s_{12}\,\underline{C}s_{21} = 29.525$$

The roots of the characteristic equation are found to be

$$r_1 + is_1 = -\cdot0223 + 2\cdot00005i$$

$$r_2 + is_2 = -\cdot4449 + 46\cdot67i$$

Because both roots have negative real parts, the system has two oscillatory damped modes of oscillation.

The modal form pertaining to the particular root, say $r_2 + is_2$ is determined by substitution of the root into $\text{adj}[S_S]$, where $\text{adj}[S_S]$ is given by

$$\begin{bmatrix} \underline{A}_{S_{22}}(r_2^2 - s_2^2) + \underline{B}_{S_{22}}\cdot r_2 + \underline{C}_{S_{22}} , & -\underline{A}_{S_{12}}\cdot(r_2^2 - s_2^2) - \underline{B}_{S_{12}}\cdot r_2 - \underline{C}_{S_{12}} \\ + i(2\underline{A}_{S_{22}}\cdot r_2\cdot s_2 + \underline{B}_{S_{22}}\cdot s_2) & - i(2\underline{A}_{S_{12}}\cdot r_2\cdot s_2 + \underline{B}_{S_{12}}\cdot s_2) \\ -\underline{A}_{S_{21}}(r_2^2 - s_2^2) + \underline{B}_{S_{21}}\cdot r_2 + \underline{C}_{S_{21}} , & \underline{A}_{S_{11}}(r_2^2 - s_2^2) + \underline{B}_{S_{11}}\cdot r_2 + \underline{C}_{S_{11}} \\ - i(2\underline{A}_{S_{21}}\cdot r_2\cdot s_2 + \underline{B}_{S_{21}}\cdot s_2) & + i(2\underline{A}_{S_{11}}\cdot r_2\cdot s_2 + \underline{B}_{S_{11}}\cdot s_2) \end{bmatrix}$$

giving

$$\begin{bmatrix} -1503.9 - 27.4i , & 1502.1 + 27.26i \\ 1502.1 + 27.39i , & -1500.1 - 27.17i \end{bmatrix}$$

or $\{1 , -\cdot9988 + \cdot000035i\}$ $[-1503.9 - 27.4i, 1502.1 + 27.26i]$

i.e. $\{q_s\}[p_s\ ]$

where the column matrix $\{q_s\}$ is the modal column pertaining to the root $r_2 + is_2$. Similarly, the above procedure is repeated for the root $r_1 + is_1$.

With the roots and their corresponding $\{q_s\}$ and $[p_s\ ]$ terms determined, it is a straightforward procedure to obtain the relative importance of the derivatives on the

stability of the system (using eqn. 6.4). Consider, for example, the importance of the m_q derivative. This derivative is contained in $\underline{B}_{S_{22}}$ only and therefore $\frac{d\underline{A}_S}{d\delta}$ and $\frac{d\underline{C}_S}{d\delta}$, in addition to $\frac{d\underline{B}_{S_{11}}}{d\delta}$, $\frac{d\underline{B}_{S_{12}}}{d\delta}$ and $\frac{d\underline{B}_{S_{21}}}{d\delta}$ are zero (m_q is denoted by δ when the other derivatives are maintained constant). Hence for the root $r_2 + is_2$ considered above, the rate of change of this root with respect to m_q is given by

$$\frac{d\lambda_S}{d\delta} = \frac{-\begin{bmatrix}1503.9 - 27.4i\\ 1502.1 + 27.26i\end{bmatrix}'\left\{(-.4449 + 46.67i)\begin{bmatrix}0 & , & 0\\ 0 & , & \frac{6^2}{25^2 \times 1.45}\end{bmatrix}\right\}\begin{bmatrix}1\\ -.9988 + .000035i\end{bmatrix}}{\begin{bmatrix}1503.9 - 27.4i\\ 1502.1 + 27.26i\end{bmatrix}'\left\{2(-.4449 + 46.67i)\begin{bmatrix}.6914, & .6897\\ .6897, & .693\end{bmatrix} + \begin{bmatrix}.0331, & .0297\\ .0298, & .0297\end{bmatrix}\right\}\begin{bmatrix}1\\ -.9988 + .000035i\end{bmatrix}}$$

This simplifies to $\frac{d\lambda_S}{d(m_q)} = 3.9411 + .0374i$ for the m_q derivative. In a similar manner $\frac{d\lambda_S}{d\delta}$ may be obtained for the other derivatives. For, say, a 100% change in each derivative, it can then be determined on comparison of the $\frac{d\lambda}{d\delta}$ x (derivative value) for each derivative, which has the greater effect on the root $r_2 + is_2$. A similar technique is then adopted for the remaining root $r_1 + is_1$.

APPENDIX 2

WIND TUNNEL CALIBRATIONS

As a result of work carried out in the 3' 6" open-jet closed circuit wind tunnel it was found in the preliminary investigations (see section 9.9) that finite values of lift force and rolling moment acted on the flat plate when set at 0° incidence and yaw in the wind tunnel. These terms were not small enough to be ignored and therefore investigations into their causation were made.

Swirl of the wind flow along the tunnel axis was considered to be the major contribution to the unusual loading on the plate. Therefore it was necessary to measure the angle of the wind flow on the lateral axis of the plate (with the plate and support arrangement removed).

A calibrated yawhead (similar in principle to the yawmeter) was used to measure the downwash angle of the wind. This yawhead was built into a long tube mounted across the tunnel working section on the plane of the flat plate. The yawhead itself consisted of two pressure tappings mounted in line (i.e. circumferentially) on the machined periphery of the tube and directed into the wind. With the two tappings connected to a sensitive manometer it proved possible to rotate the tube about its axis until the manometer gave a

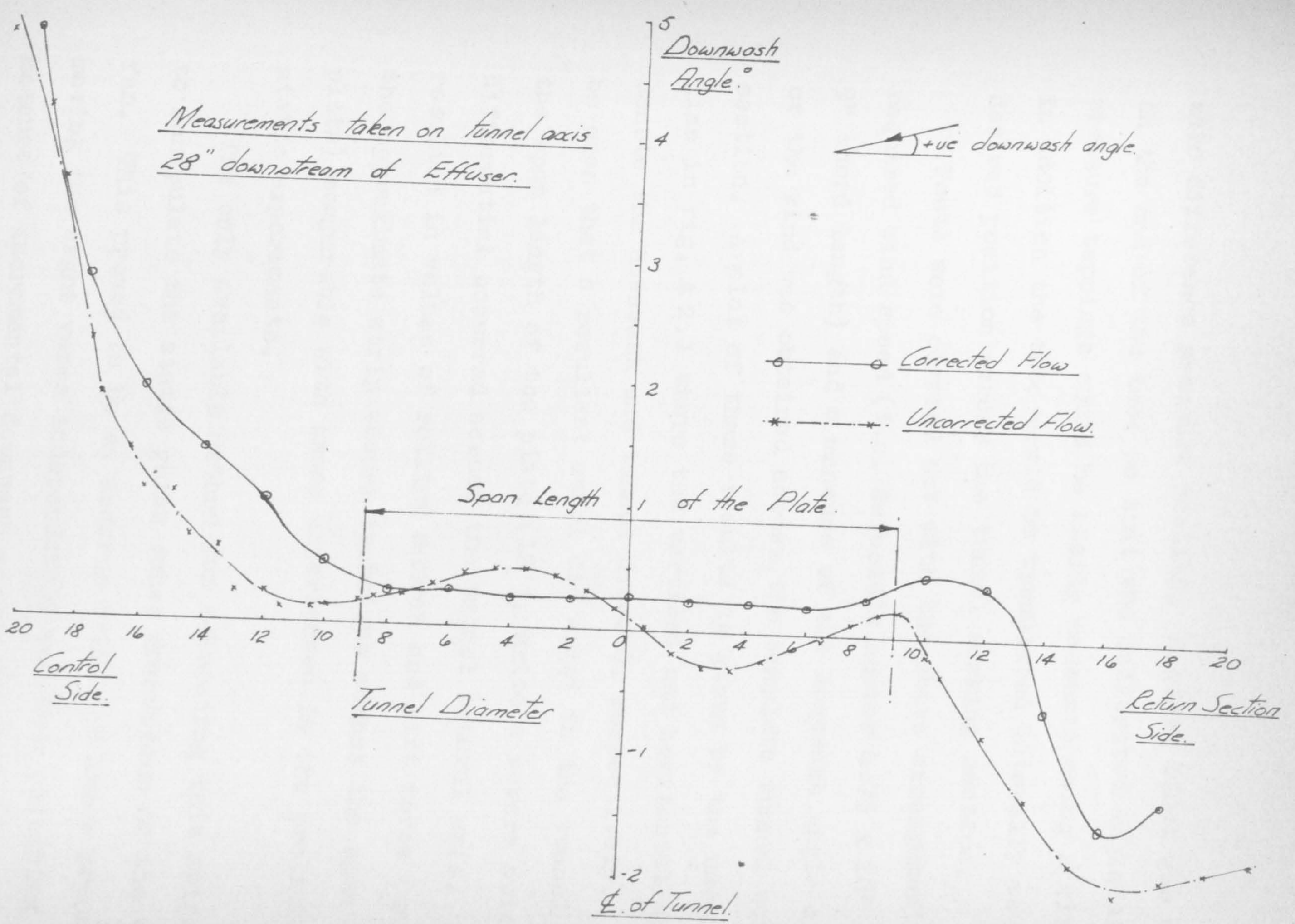

SWIRL CORRECTION IN THE 3'-6" DIA OPEN-JET WIND TUNNEL.

Fig. A2.1.

zero difference pressure reading. A steel block was mounted on the end of the tube so that the calibrated angle of the pressure tappings could be easily measured using a clinometer. In addition the tube could be translated laterally to any desired position across the tunnel working section.

Tests were carried out with the above arrangement for the required wind speed (i.e. Reynold's number 4.75×10^5 for a 9" chord length) and a measure of the downwash angle of flow of the wind was obtained across the complete tunnel working section. A plot of these results is given by the uncorrected line in fig. A 2.1 where the vertical and horizontal axes denote the downwash and tunnel diameter respectively. It can be seen that a resultant swirl did exist in the tunnel and for the span length of the plate (18"), quite a severe swirl differential occurred across the tunnel lateral axis. This resulted in values of rolling moment and lift force (using the approximate strip theory technique across the span of the plate) comparable with those experienced in the preliminary static experiments.

The only available method for correcting this swirl was to manipulate the static guide vanes downstream of the tunnel fan. This proved to be an arduous trial and error process, moving the eight vanes independently and then obtaining a measure of incremental downwash across the tunnel working

section. After two months work a satisfactory downwash distribution was obtained (as shown by the corrected line in fig. A 2.1). Although the downwash was severe at the extremes of the tunnel diameter, it was virtually constant over the majority of the plate span (i.e. 18"). Again simple strip theory was used to obtain the rolling moment and lift force, with the result that rolling moment was negligible whilst the lift force was 0.19 lbs. (i.e. for a downwash angle of 0.247°, assuming a $\frac{dC_L}{d\theta}$ value of 0.69 lb/degree from chapter 12). This unwanted downwash angle was taken into account in the wind tunnel corrections (see chapter 9).

With the tunnel corrections made for swirl, it proved necessary to recalibrate the tunnel mean velocity against the tunnel manometer using an external pitot-static tube (connected to an external manometer) in the empty tunnel section.

APPENDIX 3

A TYPICAL TRANSFORMATION OF THE WIND TUNNEL RESULTS

The wind tunnel (static) results obtained with the apparatus described in chapter 9, must be processed to give longitudinal and lateral derivative data based on principal and wind axes of the plate. The results are such that the forces and moments are measured on wind axes (at the centre of gravity of the plate) regardless of the orientation of the plate in tunnel (plate position is defined by a θ rotation followed by a ψ rotation as described in chapter 9). The results are therefore in a suitable form whereby certain wind axis derivatives can be obtained directly, i.e. N_{ϕ}. To obtain other derivatives, i.e. Y_v certain force, moment and angular displacement transformations have to be performed on the wind tunnel results in order that displacements and corresponding forces and moments are measured on the same axes. A typical transformation is now given to illustrate the determination of the principal axes derivatives Y_v, L_v and N_v. The transformation is considered in two parts for convenience, (i) angular displacement transformation, and (ii) force and moment transformations.

In order that the component of sideslip velocity v (see section 7.3.2) can be obtained, the plate should be yawed

through an angle β $(-\psi)$ followed by an angle θ. This final plate position can only be obtained in the wind tunnel, however, if the plate is assumed to have a degree of freedom, ϕ, in roll preceding the θ and ψ rotations respectively. With θ_1 and β_1 denoting negative rotations of the plate in the wind tunnel, in addition to ϕ measured in a positive direction and β_2 and θ_2 denoting the required rotations (both measured in negative directions) the following relationships can be developed using simple vector algebra:-

$$\begin{bmatrix}\bar{i}\\ \bar{j}\\ \bar{k}\end{bmatrix} = \begin{bmatrix}\cos\beta_1 & -\sin\beta_1 & 0\\ \sin\beta_1 & \cos\beta_1 & 0\\ 0 & 0 & 1\end{bmatrix}\begin{bmatrix}\cos\theta_1 & 0 & \sin\theta_1\\ 0 & 1 & 0\\ -\sin\theta_1 & 0 & \cos\theta_1\end{bmatrix}\begin{bmatrix}1 & 0 & 0\\ 0 & \cos\phi & \sin\phi\\ 0 & -\sin\phi & \cos\phi\end{bmatrix}\begin{bmatrix}\bar{i}_o\\ \bar{j}_o\\ \bar{k}_o\end{bmatrix} \quad ..A3.1$$

for the tunnel rotations and

$$\begin{bmatrix}\bar{i}\\ \bar{j}\\ \bar{k}\end{bmatrix} = \begin{bmatrix}\cos\theta_2 & 0 & \sin\theta_2\\ 0 & 1 & 0\\ -\sin\theta_2 & 0 & \cos\theta_2\end{bmatrix}\begin{bmatrix}\cos\beta_2 & -\sin\beta_2 & 0\\ \sin\beta_2 & \cos\beta_2 & 0\\ 0 & 0 & 1\end{bmatrix}\begin{bmatrix}\bar{i}_o\\ \bar{j}_o\\ \bar{k}_o\end{bmatrix} \quad \ldots\ldots\ldots \quad A3.2$$

for the required rotations, where $\{\bar{i}, \bar{j}, \bar{k}\}$ are unit vectors. $\{\bar{i}, \bar{j}, \bar{k}\}$ and $\{\bar{i}_o, \bar{j}_o, \bar{k}_o\}$ denote the final and initial positions of the plate axes Ox, Oy, Oz respectively. When both transformations are assumed to give identical final positions of the plate axes, the following identities are obtained from equations A3.1 and A3.2.

$$\cos\beta_1 \cos\theta_1 = \cos\theta_2 \cos\beta_2$$

$$\cos\beta_1 \sin\theta_1 \sin\phi + \sin\beta_1 \cos\phi = \cos\theta_2 \sin\beta_2$$

$$\cos\beta_1 \sin\theta_1 \cos\phi - \sin\beta_1 \sin\phi = \sin\theta_2 \qquad \ldots\ldots \text{A3.3}$$

$$\sin\beta_1 \cos\theta_1 = \sin\beta_2$$

$$\cos\beta_1 \cos\phi - \sin\beta_1 \sin\theta_1 \sin\phi = \cos\beta_2$$

$$\cos\beta_1 \sin\phi + \sin\beta_1 \sin\theta_1 \cos\phi = 0$$

$$\sin\theta_1 = \sin\theta_2 \cos\beta_2$$

$$-\cos\theta_1 \sin\phi = \sin\theta_2 \sin\beta_2$$

$$\cos\theta_1 \cos\phi = \cos\theta_2$$

From these identities it can be shown that

$$\theta_1 = \sin^{-1}\left\{\frac{\sin\theta_2}{(\cos^2\theta_2 \tan^2\beta_1 + 1)^{\frac{1}{2}}}\right\} \qquad \ldots\ldots\ldots \text{A3.4}$$

$\phi = \tan^{-1}(\tan\beta_1 \sin\theta_1)$ and $\beta_2 = \sin^{-1}(\sin\beta_1 \cos\theta_1)$.

However it is apparent that one set of rotations (say β_2 and θ_2) cannot be chosen in order that ϕ, θ_1 and β_1 can be determined. Therefore θ_2 and β_1 must be chosen and used in equation A3.4 to give θ_1, ϕ and β_2. Use of the above equivalent angular displacements can now be made to transform the wind tunnel forces and moments to principal forces and moments for the final plate position.

The wind tunnel forces and moments (X, Y, Z, L, M, N) acting on the plate are known for values of θ_1 and β_1 respectively. Because the angle ϕ precedes θ_1 and β_1 it is necessary to consider these forces and moments rotated

through an angle ϕ on the tunnel axis. Unfortunately, this does not position the terms on the final principal axes of the plate. Thus it is found to be necessary to transform the forces and moments to wind tunnel axes when the angles ϕ, θ_1 and β_1 respectively are applied to the plate. This transformation is given by

$$\begin{bmatrix} Z_1 \\ X_1 \\ Y_1 \\ M_1 \\ L_1 \\ N_1 \end{bmatrix} = \begin{bmatrix} \cos\phi & 0 & \sin\phi & 0 & 0 & 0 \\ 0 & 1 & 0 & 0 & 0 & 0 \\ -\sin\phi & 0 & \cos\phi & 0 & 0 & 0 \\ 0 & 0 & 0 & \cos\phi & 0 & \frac{2b\sin\phi}{c} \\ 0 & 0 & 0 & 0 & 1 & 0 \\ 0 & 0 & 0 & -\frac{2b\sin\phi}{c} & 0 & \cos\phi \end{bmatrix} \begin{bmatrix} Z_o \\ X_o \\ Y_o \\ M_o \\ L_o \\ N_o \end{bmatrix} \quad \ldots\ldots \text{A3.5}$$

where Z_o .... N_o are the wind tunnel results and Z_1 ....N_1 are the forces and moments measured on wind axes for the plate position denoted by ϕ, θ_1 and β_1. Because ϕ, θ_1 and β_1 are equivalent to β_2 and θ_2, it is now a simple matter to transform the forces and moments to the principal axes of the plate using direction cosines for the rotations β_2 and θ_2 respectively. Hence

$$\begin{bmatrix} Z_2 \\ X_2 \\ Y_2 \\ M_2 \\ L_2 \\ N_2 \end{bmatrix} = \begin{bmatrix} 1 & 0 & 0 & 0 & 0 & 0 \\ 0 & \cos\beta_2 & -\sin\beta_2 & 0 & 0 & 0 \\ 0 & \sin\beta_2 & \cos\beta_2 & 0 & 0 & 0 \\ 0 & 0 & 0 & \cos\beta_2 & -\frac{2b}{c}\sin\beta_2 & 0 \\ 0 & 0 & 0 & \frac{c}{2b}\sin\beta_2 & \cos\beta_2 & 0 \\ 0 & 0 & 0 & 0 & 0 & 1 \end{bmatrix} \begin{bmatrix} Z_1 \\ X_1 \\ Y_1 \\ M_1 \\ L_1 \\ N_1 \end{bmatrix} \quad \ldots\ldots \text{A3.6}$$

and

$$\begin{bmatrix} Z_3 \\ X_3 \\ Y_3 \\ M_3 \\ L_3 \\ N_3 \end{bmatrix} = \begin{bmatrix} \cos\theta_2 & \sin\theta_2 & 0 & 0 & 0 & 0 \\ -\sin\theta_2 & \cos\theta_2 & 0 & 0 & 0 & 0 \\ 0 & 0 & 1 & 0 & 0 & 0 \\ 0 & 0 & 0 & 1 & 0 & 0 \\ 0 & 0 & 0 & 0 & \cos\theta_2 & -\sin\theta_2 \\ 0 & 0 & 0 & 0 & \sin\theta_2 & \cos\theta_2 \end{bmatrix} \begin{bmatrix} Z_2 \\ X_2 \\ Y_2 \\ M_2 \\ L_2 \\ N_2 \end{bmatrix} \quad \ldots\ldots \text{A3.7}$$

where $\{Z_3 \ldots . N_3\}$ are the forces and moments measured on the principal axes of the plate. For the lateral derivatives it is necessary to consider Y_3, L_3 and N_3 and therefore from eqns. A3.5, A3.6 and A3.7 these can be shown as:-

$$\begin{bmatrix} Y_3 \\ L_3 \\ N_3 \end{bmatrix} = \begin{bmatrix} -\sin\phi\cos\beta_2, & \sin\beta_2, & \cos\phi\cos\beta_2, & 0 & , & 0 & 0 \\ 0 , & 0 , & 0 , & \frac{c}{2b}\begin{pmatrix}\cos\theta_2 \sin\beta_2\cos\phi \\ +\sin\alpha_2 \sin\phi\end{pmatrix}, & \cos\beta_2\cos\theta_2, & \begin{pmatrix}\sin\phi\cos\theta_2 \sin\beta_2 \\ -\cos\phi\sin\theta_2\end{pmatrix} \\ 0 , & 0 , & 0 , & \frac{c}{2b}\begin{pmatrix}-\sin\phi\cos\theta_2 \\ +\sin\theta_2\sin\beta_2\cos\phi\end{pmatrix}, & \sin\theta_2\cos\beta_2, & \begin{pmatrix}\sin\phi\sin\theta_2\sin\beta_2 \\ +\cos\theta_2\cos\phi\end{pmatrix} \end{bmatrix} \begin{bmatrix} Z_o \\ X_o \\ Y_o \\ M_o \\ L_o \\ N_o \end{bmatrix}$$

$$\ldots\ldots \text{A3.8}$$

With the above transformation built into an ALGOL computer programme and the wind tunnel results fitted with polynomials (using a curve fitting procedure), it is

now a relatively simple matter to obtain plots of Y_3, L_3 and N_3 against v (i.e. V $\sin\beta_2$) for various angles of incidence. For a range of β_2 (-5° to $+5^\circ$) the slopes of the lines (assumed linear) are measured and the Y_v, L_v and N_v derivatives derived relative to the principal axes of the pallet (see chapter 12).

The Orientation Of Wind And Principal Axes.

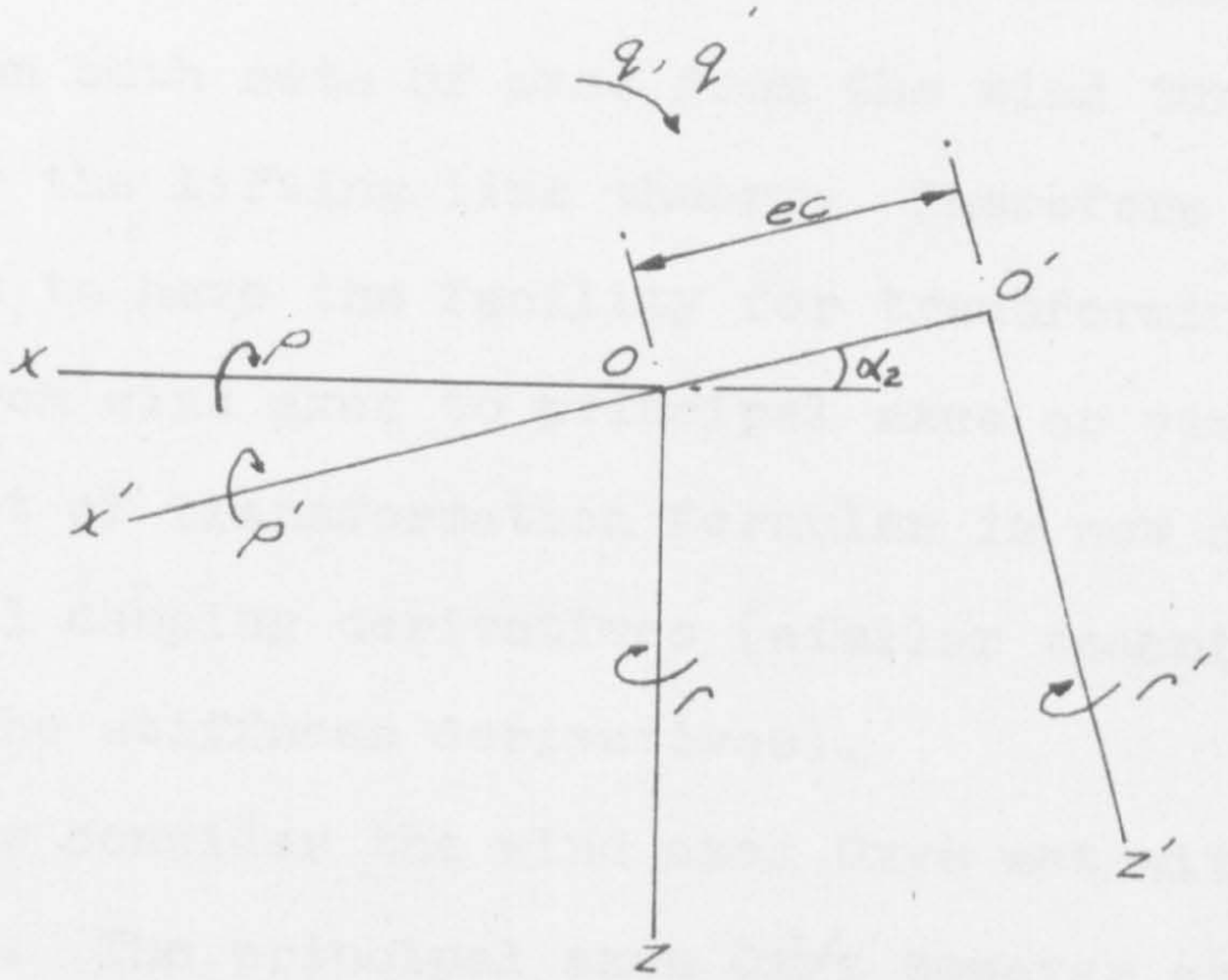

Oxyz - Wind Axes.

Ox'y'z' - Principal Axes.

Fig. A4.1.

APPENDIX 4

TRANSFORMATION FORMULAE

In the stability investigations the lateral derivative data is required on principal and wind axes of the plate. However, not all the derivative information can be obtained directly on both sets of axes from the wind tunnel static results or the lifting line theory. Therefore it is convenient to have the facility for transforming the derivatives from wind axes to principal axes or vice-versa. A typical set of transformation formulae is now derived for the lateral damping derivatives (similar techniques are also used for the stiffness derivatives).

We now consider the wind axes Oxyz set with the Ox axis horizontal. The principal axes $Ox'y'z'$ however are set at an angle α_2 (i.e. leading edge down) and displaced by a distance ec as shown in Fig. A4.1 (this represents the distance between the centres of pressure and gravity on the plate for a known value of α_2). In order that the principal axes derivatives can be obtained from wind axes derivatives, the following relationships are derived using Fig. A4.1.

$$\begin{bmatrix} \underline{U}+u \\ v \\ \underline{W}+w \\ p \\ q \\ r \end{bmatrix} = \begin{bmatrix} \cos\alpha_2 & 0 & -\sin\alpha_2 & 0 & ec\sin\alpha_2 & 0 \\ 0 & 1 & 0 & 0 & 0 & ec \\ \sin\alpha_2 & 0 & \cos\alpha_2 & 0 & -ec\cos\alpha_2 & 0 \\ 0 & 0 & 0 & \cos\alpha_2 & 0 & -\sin\alpha_2 \\ 0 & 0 & 0 & 0 & 1 & 0 \\ 0 & 0 & 0 & \sin\alpha_2 & 0 & \cos\alpha_2 \end{bmatrix} \begin{bmatrix} \underline{U}'+u' \\ v' \\ \underline{W}'+w' \\ p' \\ q' \\ r' \end{bmatrix} \quad \ldots A4.1$$

and

$$\begin{bmatrix} X' \\ Y' \\ Z' \\ L' \\ M' \\ N' \end{bmatrix} \begin{bmatrix} \cos\alpha_2 & 0 & \sin\alpha_2 & 0 & 0 & 0 \\ 0 & 1 & 0 & 0 & 0 & 0 \\ -\sin\alpha_2 & 0 & \cos\alpha_2 & 0 & 0 & 0 \\ 0 & 0 & 0 & \cos\alpha_2 & 0 & \sin\alpha_2 \\ ec\sin\alpha_2 & 0 & -ec\cos\alpha_2 & 0 & 1 & 0 \\ 0 & ec & 0 & -\sin\alpha_2 & 0 & \cos\alpha_2 \end{bmatrix} \begin{bmatrix} X \\ Y \\ Z \\ L \\ M \\ N \end{bmatrix} \quad \ldots A4.2$$

Consider now the rotary derivatives L_p, N_p, L_r, N_r (Y_p and Y_r are ignored on wind and principal axes) determined (on wind axes at the plate centre of pressure) from lifting line theory. These can be expressed in a partial derivative form (for the variables v, p and r) based on principal axes as follows:-

$$\begin{aligned} L'_{p'} &= \frac{\partial L'}{\partial p'} = \frac{\partial L'}{\partial v}\frac{\partial v}{\partial p'} + \frac{\partial L'}{\partial p}\frac{\partial p}{\partial p'} + \frac{\partial L'}{\partial r}\frac{\partial r}{\partial p'} \\ N'_{p'} &= \frac{\partial N'}{\partial p'} = \frac{\partial N'}{\partial v}\frac{\partial v}{\partial p'} + \frac{\partial N'}{\partial p}\frac{\partial p}{\partial p'} + \frac{\partial N'}{\partial r}\frac{\partial r}{\partial p'} \\ L'_{r'} &= \frac{\partial L'}{\partial r'} = \frac{\partial L'}{\partial v}\frac{\partial v}{\partial r'} + \frac{\partial L'}{\partial p}\frac{\partial p}{\partial r'} + \frac{\partial L'}{\partial r}\frac{\partial r}{\partial r'} \\ N'_{r'} &= \frac{\partial N'}{\partial r'} = \frac{\partial N'}{\partial v}\frac{\partial v}{\partial r'} + \frac{\partial N'}{\partial p}\frac{\partial p}{\partial r'} + \frac{\partial N'}{\partial r}\frac{\partial r}{\partial r'} \end{aligned} \quad \ldots\ldots A4.3$$

With $\frac{\partial L'}{\partial v}$ .....$\frac{\partial N'}{\partial r}$ determined from eqn.A4.2 i.e. $\frac{\partial L'}{\partial v} = L_v \cos\alpha_2 + N_v \sin\alpha_2$

and $\frac{\partial v}{\partial p'}$ .....$\frac{\partial r}{\partial r'}$ determined from eqn. A4.1 i.e. $\frac{\partial p}{\partial p'} = \cos\alpha_2$

then the above eqns. A4.3 can be reduced to the following non-dimensional form:-

$$l'_{p'} = l_p \cos^2\alpha_2 + (n_p + l_r) \sin\alpha_2 \cos\alpha_2 + n_r \sin^2\alpha_2$$

$$n'_{p'} = n_p \cos^2\alpha_2 + (n_r - l_p) \cos\alpha_2 \sin\alpha_2 - l_r \sin^2\alpha_2 \quad \text{..... A4.4}$$

$$l'_{r'} = l_r \cos^2\alpha_2 + (n_r - l_p) \cos\alpha_2 \sin\alpha_2 - n_p \sin^2\alpha_2 + (l_v \cos\alpha_2 + n_v \sin\alpha_2)\frac{ec}{2b}$$

$$n'_{r'} = n_r \cos^2\alpha_2 - (l_r + n_p) \sin\alpha_2 \cos\alpha_2 + l_p \sin^2\alpha_2 + (n_v \cos\alpha_2 - l_v \sin\alpha_2) \frac{ec}{2b} + y_v\left(\frac{ec}{2b}\right)^2$$

The principal axes derivatives are now in the form whereby wind axis derivatives (measured about the centre of pressure) can be used. If the transformations are required for a positional change on wind axes only (i.e. the ec displacement), then the $\cos\alpha_2$ and $\sin\alpha_2$ terms are 1 and 0 respectively in eqn. A4.4.

The y_v, l_v and n_v sideslip velocity derivatives are determined from experimental work based on the principal axes of the plate. In order that they may be used in eqn. A4.4, it is necessary for these terms to be derived on wind axes (at the plate centre of pressure). A similar transformation

technique to the above, but in the opposite sense gives

$$y_v = y'_v,$$

$$l_v = l'_v \cos\alpha_2 - n'_v \sin\alpha_2 + y'_v \frac{ec}{2b} \sin\alpha_2 \qquad \ldots\ldots \text{A4.5}$$

$$n_v = n'_v \cos\alpha_2 + l'_v \sin\alpha_2 - y'_v \frac{ec}{2b} \cos\alpha_2$$

Alternatively, y_v l_v and n_v can be determined on wind axes (at the plate centre of gravity) when ec is made zero in eqn. A4.5.

With the above simple transformations available, the lateral damping derivatives can be used for analyses based on wind axes or principal axes of the plate.